UNIVERSITY OF NOTTINGHAM

DEPARTMENT OF CIVIL ENGINEERING

MECHANICAL PROPERTIES OF GRANULAR MATERIALS FOR USE IN THERMAL ENERGY STORES

by

MICHAEL PATRICK O'REILLY B.Eng

Thesis submitted to the University of Nottingham
for the degree of Doctor of Philosophy

May 1985

CONTENTS

ABSTRACT

As part of an Advanced Compressed Air Storage System (ACAS), heat is to be extracted from high temperature compressed air and stored in a Thermal Energy Store (TES). The storage medium will be a granular material with ceramic particles. During a heating cycle large stresses will be generated within the TES due to the differential thermal expension of the pebble bed and the container.

The principal aim of this research was to carry out laboratory testing in order to investigate the properties of the granular materials for use in a quantitative structural analysis of the TES.

Two pieces of uniaxial triaxial apparatus were used. A large range of tests, from simple monotonic failure tests, to repeated loading tests with thousands of cycles, were performed. Resilient models based on the formulation by Pappin (1979) were derived. A series of modifications to this model have been discussed. In particular, a new form of volumetric strain model, and a method for taking hysteresis into account has been proposed.

Analyses of the TES problem revealed that principal stress rotation would occur. In order to determine its effect upon granular material properties, a large Hollow Cylinder Apparatus was designed and built. Unfortunately, lack of time prevented testing.

A simple design method for TES was developed based on a "worst case" analysis. Using this, a parametric study was carried out.

ACKNOWLEDGEMENTS

I wish to thank all those in the Department of Civil Engineering who, over the last three years, have provided help, advice and, most importantly, friendship.

I would like to thank Professors Rex Coates and Peter Pell who, in their turn, put all the facilities of their Department at my disposal.

A special vote of thanks is due to Professor Stephen Brown who guided this project, not only with wisdom and foresight, but also with great patience.

Many people helped with the equipment and testing: Jim Moody not only maintained and built apparatus with great skill, but provided advice in its design. Graham Handly and Norman Hardy also provided expert assistance. Thanks are also due to both Barry Brodrick and Simon Loach, who, despite their own heavy workloads, were always willing to provide assistance and advice.

The preparation of this dissertation has also involved a number of people. Beverly Watson must be thanked for the hours she spent at the word processor. Despite her ability to get it "right first time", she exhibited exemplary equanimity when I couldn't, especially on those occasions when my insistence that a sentence be changed necessitated the complete reprint of a chapter. Thanks must also be offered to Caroline Brayley for preparing the figures, and especially to Elisabeth Simcock who spent many hours correcting my English.

I would like to thank the technicians, lecturers and research workers in the Department for their friendship, especially those involved with the Pavement Research Group, the now demised Black and White Tie Club and the editors of "Rat and Svengali" - whoever they may be.

Finally, the financial assistance of the CEGB and the SERC is gratefully acknowledged.

ABBREVIATIONS

ACAS	Advanced Compressed Air Storage
CAS	Compressed Air Storage
CEGB	Central Electricity Generating Board
CSSA	Cambridge Simple Shear Apparatus
DSC	Directional Shear Cell
EPRI	Electric Power Research Institute
HCA	Hollow Cylinder Apparatus
LVDT	Linear Variable Differential Transformer
NTR	Normalised Temperature Rise
TES	Thermal Energy Store
RVDT	Rotary Variable Differential Transformer

SYMBOLS

D	Rate of Dilation ($d\epsilon_v/d\epsilon_s$)
G	Shear modulus
K	Bulk modulus
S	Normalised shear modulus (η/ϵ_s)
V	Normalised bulk modulus (η/ϵ_v)
M_R	Resilient modulus of elasticity
C	cohesion, constant
b	intermediate principal stress parameter = $(\sigma_2 - \sigma_3) / (\sigma_1 - \sigma_3)$
e	voids ratio = volume of voids/volume of solids
g	gravitational acceleration
l	shear path length in (p,q) stress space
p	normal stress. In triaxial test $p = \sigma_a+2\sigma_r$.
q	deviator stress. In triaxial test $q = \sigma_a-\sigma_r$.
v	specific volume = 1 + e
$\epsilon_1, \epsilon_2, \epsilon_3$	principle strains
ϵ_a	triaxial axial strain
ϵ_r	triaxial radial strain
ϵ_s	shear strain. In triaxial test $\epsilon_s = \frac{2}{3}(\epsilon_a-\epsilon_r)$
ϵ_v	volumetric strain. In triaxial test $\epsilon_v = \epsilon_a+2\epsilon_r$
η	Shear stress to volumetric stress ratio
Θ	sum of the principal stresses
μ	coefficient of material friction
ν	Poisson's ratio
$\sigma_1, \sigma_2, \sigma_3$	principal stresses
σ_a	triaxial axial stress
σ_v	triaxial radial stress
τ	shear stress

Φ	angle of internal friction

Suffices

f	at failure
r	repeated (stress) or resilient (strain)
o	denotes a reference stress or strain
cv	constant volume
μ	material property
vo	change from compressive to dilatant behaviour

Conventions

All compressive stresses and strains are positive

All stresses referred to are effective stresses unless otherwise indicated: hence $p = p'$.

CHAPTER ONE

INTRODUCTION

With rising fuel prices and heightened awareness of the problem of conserving energy, it has become increasingly necessary to provide efficient conversion from natural fuels to electricity.

The demand for electric power varies with time in a generally predictable manner, but the maximum efficiency at which a power station may operate is at constant output. This problem may be resolved by storage of energy during periods of low demand, with 'topping-up' of the supply system when demand exceeds output. Pumped hydro-storage is one example of the way in which this has been achieved: however, this requires the power stations to be located in a mountainous region where major construction problems are likely and where other factors, due to the remoteness of the site, may add extra difficulties.

Energy storage in the form of compressed air is considered to provide a possible alternative, and with the construction of the 290 MW Compressed Air Storage (CAS) installation at Huntorf in West Germany, CAS has become the first commercially available storage technology to compete with pumped hydro-storage. The main advantages of the CAS system are its flexibility of siting and its relatively low capital cost, but in its present form (i.e. as constructed at Huntorf) it has the major disadvantage of requiring combustion fuel for operation. The reason for this is that when a gas is adiabatically compressed, its temperature rises significantly. Heat is removed to prevent inefficient storage, and this means that the compressed air must be pre-heated in order to operate the turbines effectively. This drawback did suggest that the CAS system had limited applicability. In 1979 the Central Electricity Generating Board (CEGB) sponsored by the Electric Power Research Institute (EPRI) published a report (Glendenning et

al, 1979) outlining proposals for an Advanced Compressed Air Stogage (ACAS) system. The main development would be the incorporation of a Thermal Energy Store (TES) into the system. This would enable the heat energy to be stored separately from the compressed air, recombination taking place before energy retrieval.

Following the publication of the Glendenning report, a preliminary study of the mechanical problems likely to be encounterd in this type of structure was undertaken by Bridgewater and Wroth (1980). They examined possible modes of behaviour and likely problem areas: they suggested that the "determination of basic mechanical properties of a mass of pebbles e.g. Φ' as a function of stress etc., and of stress-strain relationships under cyclic conditions in a triaxial apparatus of suitable size "be carried out".

The research described in the present dissertation was commissioned in response to the recommendations of Bridgewater and Wroth, and the primary aim was therefore to investigate the types of material behaviour suggested by them. As the research progressed, however, it became apparent that a wider aspect was required. Consideration of the mechanisms operating within a TES during the heating/cooling cycle revealed that the preliminary investigations had failed to grasp the full complexity of the interactions between the granular material and the container. Certain aspects of the stress conditions likely to be experienced by the granular material (e.g. principal stress rotation) had been completely overlooked. These findings led to an increased emphasis on literature survey in order to ascertain the effect of the various types of behaviour: in some instances, no published report could be found which dealt with certain vital aspects (e.g. the effect of principal stress rotation on resilient stiffness). This led in one case to the construction of a major new piece of apparatus (the Hollow Cylinder Apparatus) which, it was intended, would help fill in some of the

lacunae.

Although not part of the initial project brief, it was thought worthwhile to develop a preliminary design procedure to provide a rough estimate of the stress levels to be expected within a TES. The finite element method appeared at first to offer the last opportunity for obtaining realistic design data, but for a variety of reasons (see Chapter 7) it was not used. It was decided eventually to approach the problem from a completely different angle; the method described in Chapter 7 is the result.

Because of the change in emphasis from the original narrow requirement to a much more comprehensive perspective, it is impossible to isolate a research philosophy existing ab initio, except in the very broad sense that anything which appeared to be relevant was investigated. Detail was often sacrificed for a panorama. In retrospect, the research programme can be categorised under four general headings:

1. A Study of TES Behaviour (Container/granular material interaction)
2. Literature Survey
3. Testing of Materials
4. Preliminary Design Work

Although the aims changed considerably during the course of the research, the nature of the project has remained largely experimental. As work progressed, the number of types of behaviour which it was thought necessary to investigate increased, and towards the end of the research period the following list could be compiled:

1. the physical properties of particles
2. comparison between different materials

3. comparison between aggregates with different size particles
4. behaviour at large strains (> 5%)
5. pre-resilient repeated load behaviour
6. resilient behaviour
7. the effects of principal stress rotation; and
8. the influence of the intermediate principal stress

Item 1 is covered in Chapter 3. Tests carried out dealt with the physical properties of individual particles as well as the en masse properties. Items 2 to 6 were investigated using two main pieces of apparatus; these were both of the uniaxial triaxial variety. They are discribed in Chapter 5 and the results from the tests carried out in them are described and discussed in Chapter 6.

The limitations of the uniaxial triaxial apparatus meant that it could not be used to study either items 7 or 8. The Hollow Cylinder Apparatus (HCA), on the other hand, does permit such investigation. When the project had been underway for approximately 20 months, it was decided to build an HCA. It was hoped that it may have been possible to design, construct and use the equipment to obtain results in the remaining 16 months. Unfortunately, this did not prove to be so, though the development of the HCA is far from being wasted effort. It will undoubtedly be used for testing within the near future and will provide general information about granular material behaviour under conditions of rotating principal stress, non-constant intermediate stress ratios and so on - information which will be directly applicable to the problem of TES design.

The position at the end of the project as far as the experimental work is concerned is not truly satisfactory. The testing which has been carried out in the uniaxial triaxial apparatus should, however, provide a basic fund of data which can be modified by subsequent tests in the HCA. If it

were found, for example, that the resilient shear stiffness was reduced during principal stress rotation by a factor which could be related to the amplitudes of stress rotation angle and stress path length, then it would be possible to use this result directly in TES design.

In addition to its rôle in pebble bed TES research, this project also formed part of a long-running research programme being carried out at Nottingham into the behaviour of granular materials under repeated loading. This latter programme, itself, forms part of a wider investigation into pavement material properties, the object of which is to rationalise highway design by using basic structural engineering principles.

Following the completion of large and sophisticated repeated load triaxial apparatus in 1974, investigations have been carried out into the behaviour of a range of granular materials, both graded (Boyce 1976, Pappin 1979) and single size (Shaw 1980). With each project, new aspects of granular material behaviour have been observed and the general understanding of these materials under repeated loading has increased. The research presented herein, although primarily directed at the TES design problem, is also concerned with continuing this tradition.

CHAPTER TWO

PEBBLE BED THERMAL ENERGY STORES

2.1 THE CHOICE OF T.E.S. CONFIGURATION

The CEGB report (Glendenning et al 1979) mentioned in Chapter 1, discusses the technical and economic feasibility of TES. The main conclusions which were drawn concerning the choice of TES configuration are summarised below in 2.1.1.

2.1.1 Direct and Indirect TES

The envisaged TES would have two main components; the material, which is thermally cycled, and the containment vessel with its associated insulation, cooling, foundations, etc. Two basic configurations can be identified.

1. Indirect TES systems in which the compressed air transfers heat to and from the storage material via a heat exchanger.
2. Direct TES in which the cycled air is directly in contact with the storage material matrix.

It was decided that indirect TES sytsems have a limited applicability to ACAS due to excessive containment costs and the problems of phase change or chemical change over the expected temperature range (30°C to 1000°C was considered to be a likely maximum range). The direct contact TES was, therefore, considered the cost-optimum design.

2.1.2 Thermal Energy Store Matrix Material

The requirements for the matrix materials to be used in the direct contact TES are:

1. Ability to withstand an oxidizing atmosphere over the whole expected temperature range (up to 1000°C).
2. High resistance to thermal shock.

3. Ability to withstand condensation and evaporation of water.
4. High density, specific heat capacity and thermal conductivity.
5. High creep strength.
6. Low coefficient of thermal expansion.
7. Low capital cost.

Fortunately, refractory materials exhibit many of these properties and, in the CEGB Report, their use was considered to be appropriate.

Within practical and financial limitations, the TES matrix should ideally be arranged so as to offer the largest heat transfer surface to volume ratio, and the smallest void ratio possible. Two configurations were considered.

1. Checker Bricks. These are stacked to form a stable structure in which the heat transfer surface consists of a large number of parallel flow passages.
2. Pebble Beds. These consist of randomly packed ceramic pebbles.

It was suggested that with the large tonnages that would be required for the TES, the design of commercially available checker bricks could be modified in order to increase the transfer surface to volume ratio. However, gap passage size would have to be significantly reduced and no production process has currently been identified which could manufacture such checkers.

Pebble beds have a further advantage in that the heat transfer coefficient is greater due to the disturbed flow condition which they cause, and so at this stage it was decided that the optimum matrix material would be a granular aggregate of rounded ceramic pebbles.

2.2 PROPOSED DESIGNS FOR PEBBLE BED THERMAL ENERGY STORES

Several preliminary thermal storage facility designs have been

advanced.

The design of a thermal energy store will be influenced by economic and thermodynamic as well as structural considerations. It is therefore to be expected that as economic conditions change and research progresses, the optimum design will change. It is consequently necessary to discuss a range of possibilities.

2.2.1 Underground Thermal Energy Store

Fig. 2.1 shows a typical proposal for an 80 bar pressure system (Glendenning et al, 1979). The TES is housed in an underground cavern at a depth of 670m. The cavern is lined and pressurized so that the pressure difference across the container walls is minimal. This system has the obvious advantage that the pebble bed container does not have to satisfy the requirements of a pressure vessel. The main disadvantage of the design is that it must be constructed at a considerable depth with consequent accessibility and cost problems.

2.2.2 Surface TES

Fig. 2.2 shows the surface TES design advocated by United Engineers and Constructors (1982). The pebble bed is contained within a "basket". The internal fluid pressure is contained by a pre-stressed concrete vessel which is separated from the pebble bed by a layer of insulation. The maximum inlet pressure is 16 bar. This particular arrangement separates the effect of pressures due to the pebble bed (carried by the "fill basket") and the effect of the fluid pressure carried by the prestressing tendons. Other proposed designs envisage the granular material being contained by the walls of the pressure vessel itself so that the pressure on the vessel wall at any time will arise from both sources.

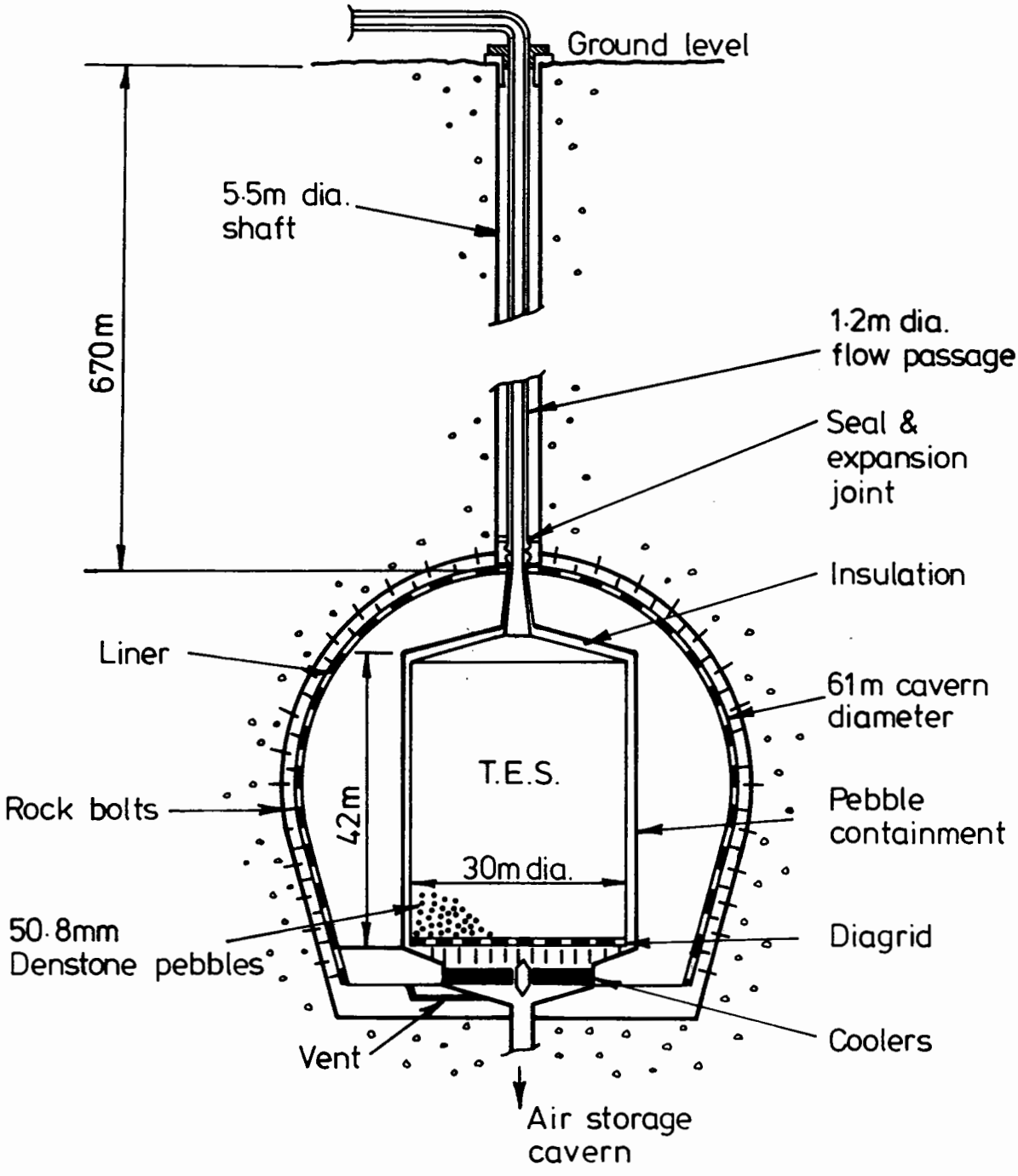

Fig. 2·1 Underground Thermal Energy Store (80 bar)

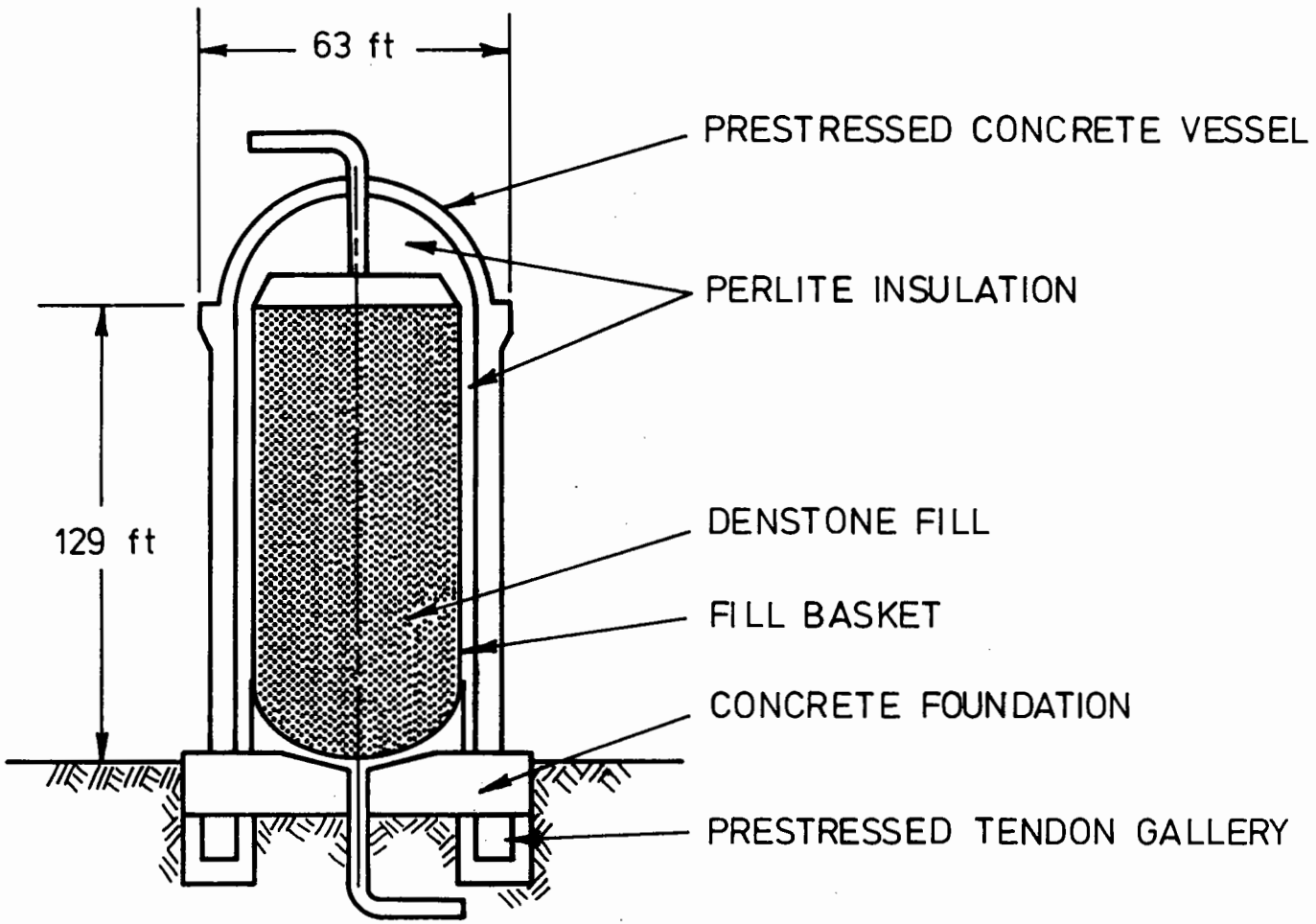

Fig. 2.2 Hybrid ACAS Thermal Energy Storage Unit Design (United Engineers & Constructors)

2.2.3 Underground Versus Surface TES

As has been noted, each arrangement has both advantages and disadvantages vis à vis the other. The CEGB study (Glendenning et al, 1979) shows that for low pressure systems (e.g. 16 bar) the net advantage is with surface storage. At very high pressures (e.g. 80 bars) the underground system may be economically competitive. The advantages, however, are marginal and the recommendation in the CEGB study is clearly that surface storage is preferable since this is a proven technology. A further suggestion is that a semi-submerged TES may be the most acceptable design on environmental and aesthetic grounds.

2.2.4 Vessel Materials

The CEGB study (Glendenning et al, 1979) clearly shows that concrete pressure vessels are cheaper than steel vessels for pressures greater than 10 bars. The high cost of steel containers is mainly attributable to fabrication costs when dealing with thick plate.

2.3 STRUCTURAL ASPECTS OF PEBBLE BED THERMAL ENERGY STORES

Stresses will be generated within the granular medium and the containment vessel due to their interaction under static self-weight and cyclic thermal loads. It is useful at this stage to discuss the ways in which these stresses may originate and the likely effect of various container and process configurations .

2.3.1 The Sources of Stress Generation

Self-Weight: The mass of the granular material will cause stresses due to self weight. The general distribution of these stresses is well-known to silo engineers, but present knowledge about real mechanisms and behaviour

within silos is so incomplete that an exact determination is not possible.

Differential Thermal Expansion: Most materials, when subjected to a temperature rise, undergo expansion unless restrained. Where two materials of unequal coefficients of expansion are components of the same structure, a differential expansion will occur, thereby resulting in a change in the stress state.

In the case of a TES, it is unlikely that both container and granular material will have the same coefficient of thermal expansion. Even where the coefficients are only slightly different, the wide range of temperature to be applied (up to 1000°C) will cause large stress changes.

Shear Stresses along the Container Walls: These stresses are not independent of the two sources outlined above. More correctly they are a consequence of them. They are the result of friction between particles attempting to move relative to the wall in response to the stress field. The predicted directions of these shear stresses are shown in Fig. 2.3.

1. Fig. 2.3(a) shows the shear stresses expected to occur along the container wall due to self-weight alone. As the fill material settles under its own weight, friction stresses along the wall will resist settlement.
2. Fig. 2.3(b) shows the shear stresses expected to occur along the wall due solely to thermal expansion. As the fill material expands relative to the container, it will tend to rise in the vessel. Friction stresses will resist this tendancy.

Note that although it has been assumed when discussing Fig. 2.3(b) that the coefficient of expansion of the granular material is higher than that of the container, similar stress conditions would also ensue if the converse were true. If the fill material had a lower coefficient, a

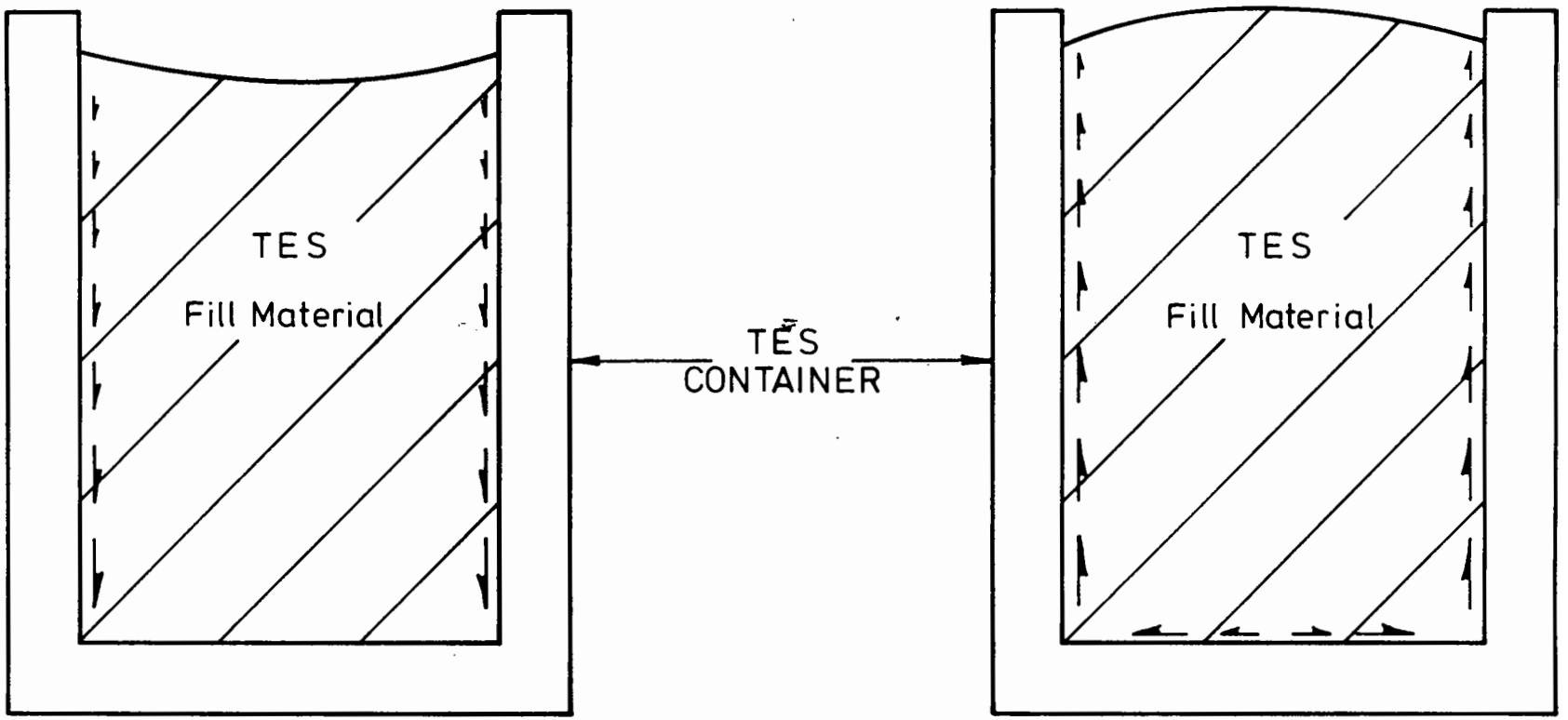

(a) Shear Stresses due to Self Weight and Settlement

(b) Shear Stresses due to Relative Expansion of TES Fill Material

Fig. 2.3 Shear Stresses Along the TES Container Wall

"shrink-fit" situation would arise during the heat extraction phase.

Combinations of Stress: It has been convenient to discuss the sources of stress in isolation. Indeed in many aspects of structural design it is useful to deal with separate sources independently and to use the theory of superposition to calculate the behaviour of the structure under a combination of loads.

This, however, is only applicable to structures made from simple linear elastic materials. Granular materials on the other hand exhibit a considerable degree of non-linearity and are also elasto-plastic and stress history dependent. When dealing with these complex materials,the principle of superposition, therefore, ceases to be of use and it is necessary to calculate the total stress at all stages.

An important point to note is that the stress field will vary in a generally cyclic manner as the TES is subjected to a cyclic thermal load. The stress-history dependence of granular materials means that its mechanical properties will change from cycle to cycle. Furthermore, hysteresis effects will result in a difference between behaviour during loading and unloading. Thus, to calculate the response of an element of granular material to a change in stress, it is necessary to know the stress history of that element of material.

2.3.2 Principal Stress Rotation in TES

An aspect of behaviour which is not usually considered, is the effect of principal stress rotation. This occurs whenever an increment of stress is not co-axial with the total stress. Because the contributions of stress from self-weight and differential thermal expansions will not be coaxial in the TES (see Fig. 2.3), and since the properties of the total stress that each contributes will not be constant throughout the thermal cycle, principal stress rotations must occur.

Where the material is anisotropic (either as a result of its deposition or its subsequent stress history) the direction of the principal stresses will be important. In addition to this, it is likely that the response of the material will be dependent not only upon the stress path followed in principal stress space, but also upon the orientation of those stresses relative to a fixed direction in the granular material. This is confirmed by work recently conducted at Imperial College, London (Hight 1983, Symes 1983).

2.3.2.1 A Simple Computer Simulation

In order to provide a demonstration of the phenomenon of principal stress rotation in a simple granular material heat store, a finite-element computer simulation was performed. The basic mesh is as shown in Fig. 2.4. The container and granular material were given the properties shown, including different coefficients of thermal expansion. Both materials were assumed to be linear elastic. Fig. 2.5 shows the rotation of major principal stress direction for five elements as the structure is heated. The rotation of stress direction is seen to be a major feature during the initial stages of heating.

2.3.2.2 Thermoclines

The transfer of heat to and from the TES would give rise to high temperature gradients or "thermoclines" within the granular materials. If, for example, hot compressed air was fed into a uniform temperature TES, the thermocline would begin at the hot air inlet and progress towards the air outlet. During the extraction of heat from the TES by passing cool air through the pebble bed, the thermocline would again travel from the fluid source to the sink, although the temperature gradient would be in the opposite direction. Fig. 2.6(a) shows a typical thermoclinic system.

Material	E (Pa)	ν	γ (kg/m^3)	α (/°C)
1	5×10^{10}	0·2	$2\cdot4\ 10^3$	8×10^{-6}
2	$1\cdot5\times10^{10}$	0·4	$1\cdot6\times10^3$	10×10^{-6}

Elements A to E are considered in Fig. 2·5

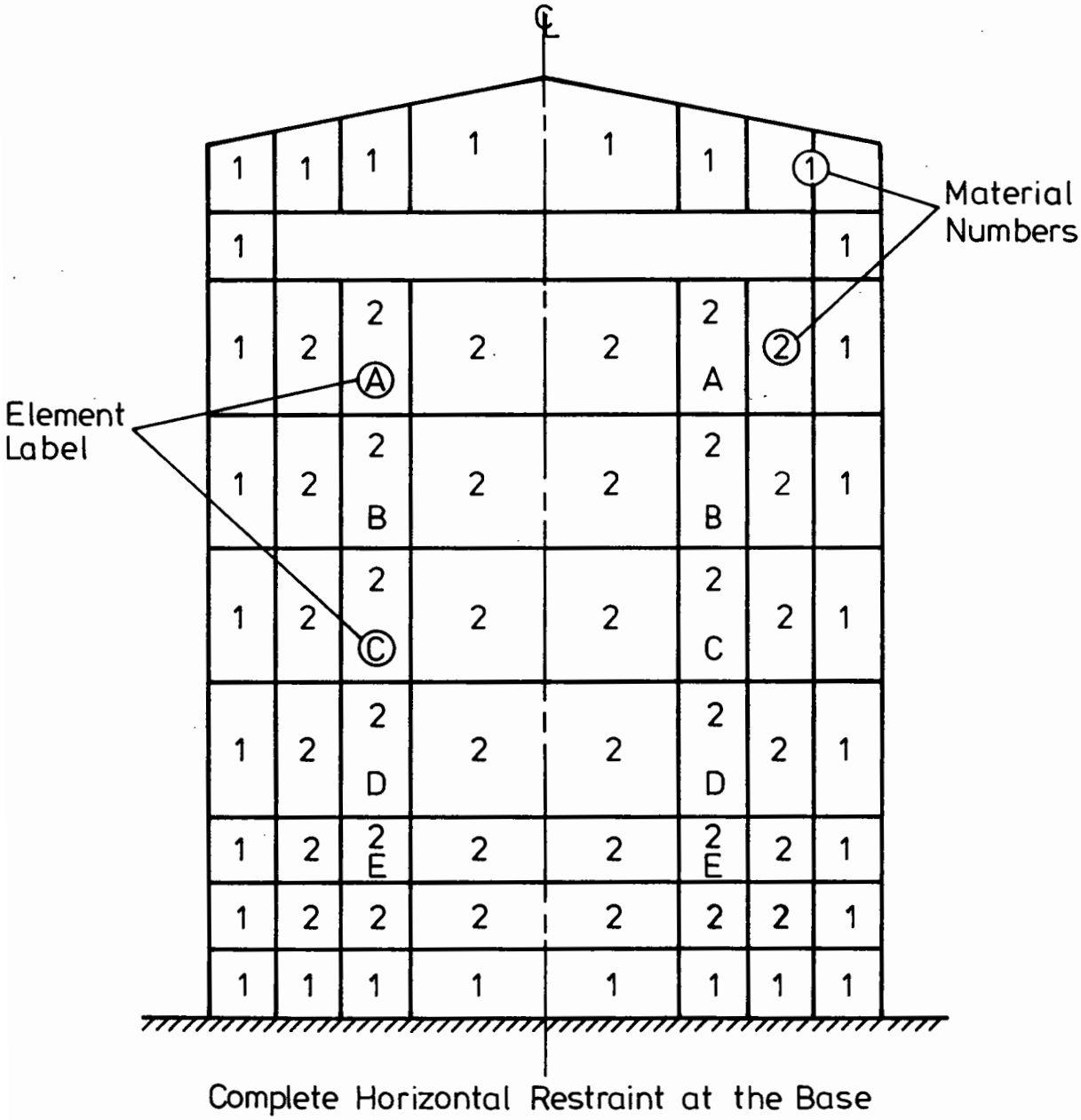

Fig. 2·4 Mesh Used in Finite Element Simulation

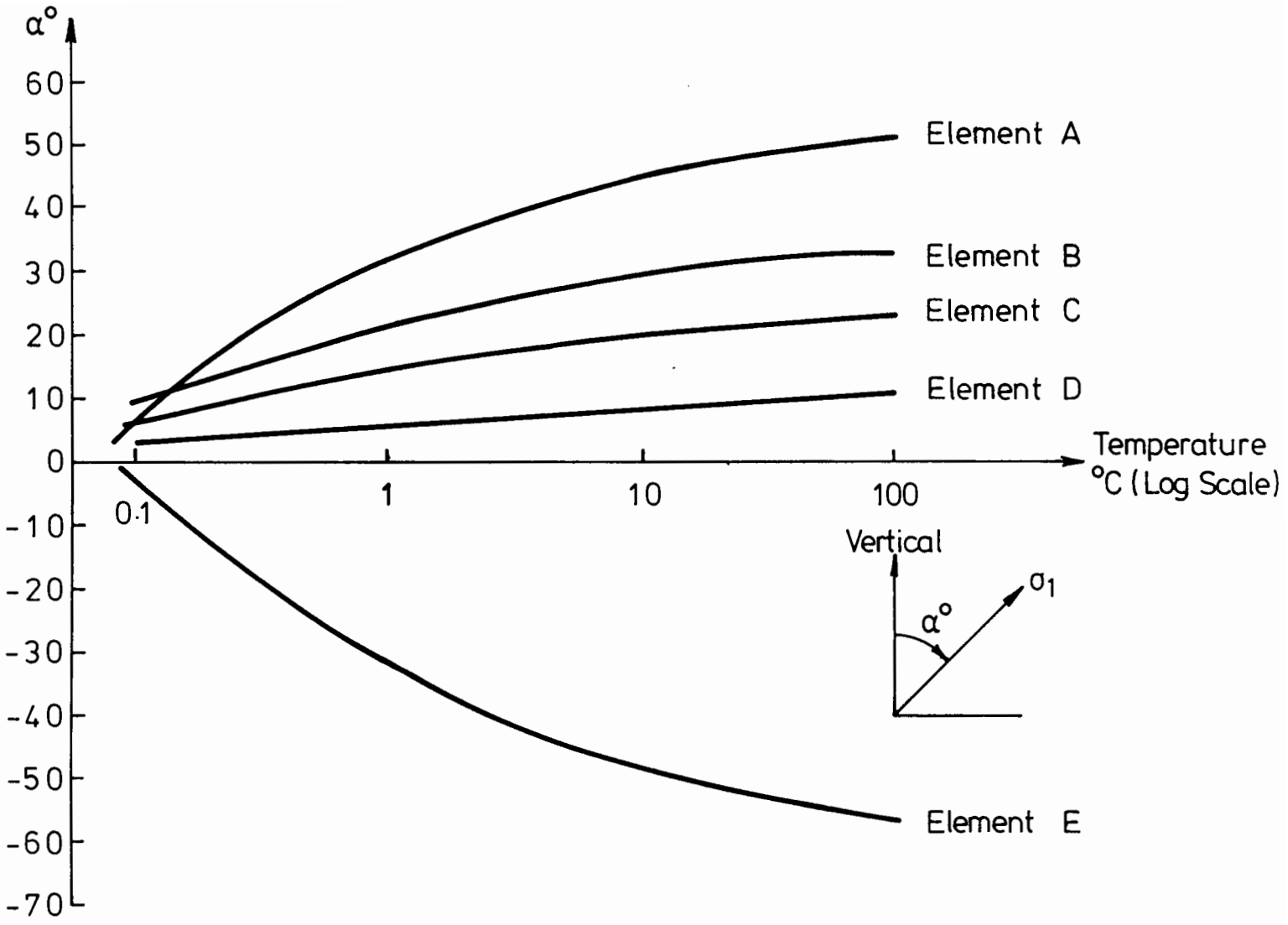

Fig. 2.5 Principal Stress Rotation During Finite Element Simulation

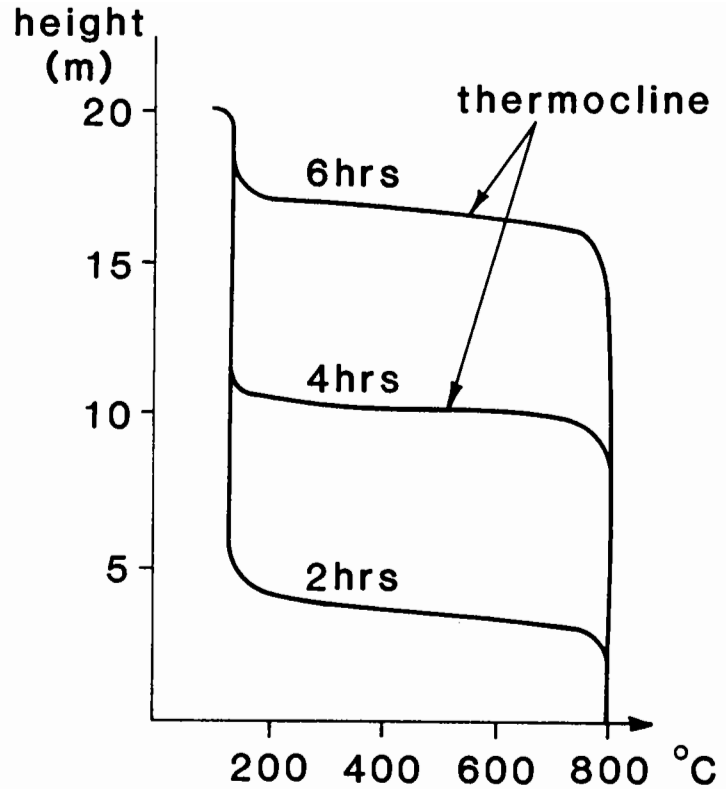

(a) Typical thermocline system with heat source at base of the heat store

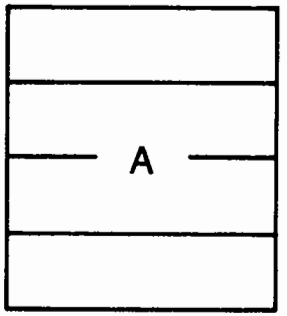

(i) remote from thermocline

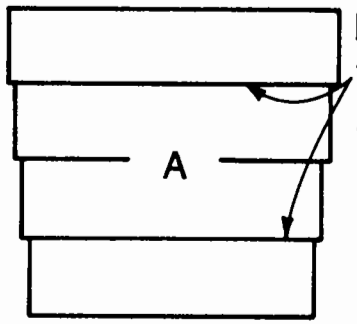

(ii) at the thermocline

(b) The effect of a thermocline pass on an element of granular material

Fig. 2.6 THERMOCLINES AND STRESS ROTATION

In Fig. 2.6(b), the stresses on an element within a TES are considered. When the pebble bed is at constant temperature, the stresses arise from the three main sources outlined in 2.3.1 above (self-weight, differential thermal expansion and shear stresses along the TES wall). When a thermocline is passing through the pebble bed, however, the situation is more complicated; one of the main effects is principal stress rotation. In Fig. 2.6(b)(i), a small section (A) of material in a uniform temperature TES is shown. For the sake of simplicity it is assumed that the major principal stress in A is approximately vertical. This will make it possible to divide A into horizontal slices with frictionless interfaces without changing its shape (because there are no shear stresses acting in directions perpendicular to a principal stress). When the thermocline is passing, the layers of A towards the top are much warmer than those at the bottom and expand relative to them unless restrained. If A is now sliced in the same way as before, the configuration shown in Fig. 2.6(b)(ii) will be observed. In reality, of course, shear stresses will be mobilised along horizontal surfaces in order to resist the mode of deformation shown. Shear stresses in the horizontal direction mean that the direction of principal stress can no longer remain vertical, and so principal stress rotation must have occurred.

During the cooling phase, the stress rotation due to the thermocline pass will occur yet again. If, for some reason, it is decided that the air-flow must always be in the same direction through the TES, the temperature gradient will be in the opposite sense during cooling. The direction of the shear stresses induced in an element during the thermocline pass in that case will be reversed. The stress rotation will therefore be in the opposite direction. The effect of this will be to halve the number of stress rotations (from two to one per complete temperature cycle) but to approximately double their amplitude.

The magnitude of the principal stress rotation occurring as a result of the thermocline pass will depend on factors such as the geometry of the pebble bed, the stiffness of the container and the relative coefficients of expansion of the container and pebble bed. For any given TES, the major factor will be the slope of the temperature gradient across the thermocline.

2.3.2.3 The Likely Effect of Principal Stress Rotation

The experience of research into this field (see Chapter 4) tends to indicate that the major effects of principal stress rotation will be (a) increases in the build-up of both permanent shear and (b) volumetric (contractant) strains.

2.3.3 Combination of Fluid Pressure and Granular Material Loads

In a direct TES configuration (i.e. one where the hot air transfers its heat directly to the granular material without using an intermediate medium), it is necessary that the TES should be internally pressurized. This pressure may be counteracted by an external pressure (as in cavern TES) or carried by the container itself (as in surface TES). During normal operation this internal pressure would probably not be lowered considerably between charging and discharging. If, however, it was decided to reduce the pressures for any reason, new design complications might arise (unless a separate "fill basket" was used). For example, it may be found necessary to lower pressures, except during charge or discharge, in order to reduce material creep. Should this be the case, the resulting wall pressure regimes will further complicate the loading pattern .

It will be necessary to provide for contingencies such as a lowering of pressure due to associated system malfunction etc., even if the pressure is to be maintained during normal operation.

2.3.4 The Possibility of Racheting

If the granular material undergoes a permanent settlement in each cycle, the phenomenon of "racheting" is said to take place.

When the coefficient of thermal expansion of the granular material is greater than that of the container, settlement will occur during the discharge phase. At the highest temperature, the granular material will experience a high magnitude of stress. As the temperature falls, the radial stress will decrease and if plastic straining has occurred during the heating process, then the final stress in the radial direction will be lower than it was at the same point during the previous cycle. Two effects will become important:

1. As the radial stress diminishes, so will the mean normal stress. Since granular materials are frictional, the shear strength and stiffness of the TES fill will also decrease.
2. The reduced radial stress will mean that a lower wall friction may be mobilized, and so a higher overburden stress will be transmitted vertically through the granular material.

   The combined effect of these will be that the vertical to radial stress ratio will increase; this will cause settlement to occur.

In the case where the granular material has a lower coefficient of thermal expansion than the container, racheting may be observed during the heating cycle.

The problem of racheting may be reduced in several ways. Firstly, if the container wall is very rough, it will be more difficult for the material to settle, as the movement will be strongly resisted by wall friction. Secondly, if the granular material is highly dilatent, it will increase its volume when it undergoes a shearing strain and this will cause the mean normal stress to increase, so reducing the stress ratio and consequently the propensity to settle. Unfortunately, it must be noted

that a highly dilatant material in a rough lined container will cause higher stresses during that part of the cycle where the highest magnitude of stresses are experienced.

Racheting may be accompanied not only by a reduction in bed volume but more importantly by steadily increasing stresses. This problem is discussed in Chapter 7.5.

2.3.5 The Formation of Equilibrium Conditions

It will be seen, both in the literature review (Chapter 4) and in the test results (Chapter 6), that granular materials, when subjected to constant cycling (whether stress or strain controlled) tend towards a resilient equilibrium. When this stage is reached, all strains are recoverable, and an elastic analysis may be carried out.

In any structure with a granular component which is subjected to a cyclic loading regime, resilient conditions for the whole structure will only be reached if the plastic strains which occur before resilient equilibrium is achieved, tend to make the structure more stable. As has been shown above, racheting may occur (see 2.3.4). If it does, it will be accompanied (in the case of a well-designed container) by increasing average stresses and reduced shear stress. This reduced stress ratio will result in increased stability in the granular material. As long as the TES wall is capable of withstanding the internal pressure without yielding, therefore, the TES will tend towards resilient equilibrium conditions with increasing number of cycles. If the TES wall itself begins to deform plastically, however, the situation may become one in which the plastic strains that occur in the granular material make the structure less stable, and incremental collapse may follow.

2.3.6 The Relative Magnitude of the Intermediate Principal Stress

The relative magnitude of the intermediate principal stress is usually given in terms of the ratio b, where:

$$b = (\sigma_2 - \sigma_3)/(\sigma_1 - \sigma_3)$$

In a TES, the value of b will alter during a thermal cycle. Consider a vertical-walled granular material store in which there is no friction between the fill and the wall. Under normal conditions, the only forces acting upon the granular material are due to self-weight. In the absence of wall-friction, the principal stresses are clearly the vertical stress (Yh) and the horizontal stress (k_oYh), the major principal stress being vertical. The granular material is thus subject to a stress system similar to that experienced by a uniaxial triaxial sample in compression, i.e. b = 0.

If a change in temperature is now uniformly applied to the container system such that the fill, unless restrained, expands relative to the container, the horizontal stress will increase relative to the vertical. At some stage, isotropic stress conditions are reached, and if the temperature change is increased still further, the major principal stress now lies in the horizontal plane. The fill experiences a stress state similar to that within a uniaxial triaxial sample in extension, i.e. b = 1.

In a real TES, wall friction and non-uniform heating (eg. the passing of a thermocline) will cause the principal stresses to rotate so that they will no longer be in the vertical and horizontal directions. This will destroy the stress-symmetry about the vertical axis and consequently the intermediate principal stress will be equal to neither the major nor the minor principal stress, i.e. $0 < b < 1$. During a temperature cycle, the principal stress directions will rotate continuously; the value of b may

also be expected to change continuously.

The effect of b upon granular material properties is discussed in Chapter 4 and also in Chapter 6C.3.4.

CHAPTER 3

CHARACTERISTICS OF THE TEST MATERIALS

3.1 THE MATERIALS

In Chapter 2 the reasons for the choice of direct TES as the cost-optimum arrangement and the selection of refractory materials as being the most suitable for the present application was discussed. In this chapter, the properties of these materials are examined.

Denstone 57: This is a completely vitrified ceramic material manufactured by the Norton Chemical Co. Various sizes ae available in both sphereical and cylindrical form. At present, the primary use of this material is as a catalyst support medium in the chemical engineering industry.

The use of cylindrical particles may lead to close-packed non-homogeneous and anisotropic regions within the TES, resulting in inefficient transfer of heat from the compressed air to the pebble bed. The CEGB considered it advantageous, therefore, to use spherical particles for the present application. The following sizes have been tested: 6mm, 9mm and 19mm diameter.

The particles are not, in fact, true spheres and a survey was undertaken in order to quantify the deviation from the spherical shape. For a randomly chosen sample of 50 particles from each size range, the maximum and minimum dimensions were measured using a micrometer. The results presented in Table 3.1(a) show a significant departure from the nominal shape. It was observed that the particles were generally ellipsoidal in shape. It is considered, therefore, that a more accurate description of the particle shape is an ellipsoid with a major to minor axis ratio of 1.14.

From Table 3.1(a) it can also be seen that the measured particle size

TABLE 3.1(a) THE MEASURED DIMENSIONS OF 'DENSTONE 57' PARTICLES

Nominal Size (mm)	Mean Max. Dimension (mm)	Std. Dev. of Max. Dim. (mm)	Mean Min. Dimension (mm)	Std. Dev. of Min. Dim. (mm)	Ratio of Max. to Min. Dimension
6	7.79	0.996	6.56	0.386	1.19
6 (a)	7.38	0.456	6.45	0.355	1.14
9	11.03	0.778	9.73	0.484	1.13
19	22.90	0.880	19.90	0.620	1.15

Note Size 6mm (a) refers to the portion of the 6mm sample which was made from 'singles'. 'Doubles', which are particles formed when two pieces of raw clay joined before firing, composed 28% of the 6mm sample.

is in excess of the nominal dimension. However, the use of existing nominal dimensions will be retained throughout in order to avoid confusion.

Iron Oxide Pellets: In the manufacture of this material, raw iron ore powder is mixed with a bentonite slurry. The resulting mixture is pre-heated to drive off most of the water and then fired in a kiln.

The samples which have been supplied consist of randomly sized and shaped particles. An accurate investigation into their deviation from a spherical shape would involve measuring many parameters, and in the present case, it was considered impractical. Information supplied by the manufacturer via the CEGB, indicates that there is a mixture of sizes in the range 6mm to 16mm, with 80% in the range of 9mm to 12mm diameter. On inspection, this appears to be the case.

Modified Denstone: In response to the requirement for a medium suitable for TES, Norton Chemicals have developed a Modified Denstone material. In order to produce this material, iron oxides are added to the unfired Denstone slurry. This increases the density of the material, and more importantly, its specific heat density. The modified clay slurry is then fired in a similar way to the normal Denstone product, thus producing approximately spherical ceramic particles. Table 3.2 gives material details (as supplied to Nottingham University by Norton Chemicals). It should be noted that the composition of this product is likely to vary, and that this will lead to variations in the properties of the material.

A size and "shape" survey was performed on the particles using a micrometer. The results of this survey are presented in Table 3.1(b).

The main difference in particle shape between the Modified and Standard Denstones is the reduction in symmetry of the Modified Denstone material about the long axis; it is not clear whether this is attributable

TABLE 3.1(b) SIZE AND SHAPE SURVEY OF MODIFIED DENSTONE (ALL DIMENSIONS IN MM)

Dimension	Mean	Standard Deviation
Maximum	14.40	1.154
Intermediate	12.02	0.457
Minimum	10.67	0.804

TABLE 3.2 PROPERTIES OF MODIFIED DENSTONE

Size and Shape	$\frac{1}{2}$" spheres (see Table 3.1(b)
Apparent porosity, %	4.36
Water Absorption, Wt %	1.51
Apparent Specific Gravity	3.03
Particle Density, gm/cc	2.09
Packing Density, kg/m^3	1688
Crush Strength, FPCS, kg	116

to the fact that the sample was produced as a small batch rather than in a full-scale commercial manufacture operation, or if the addition of the iron oxide affects the slurry properties so as to cause this phenomenon. The ratio of maximum to minimum mean dimension is 1.35 which is greater than the 1.19 value measured for 6mm Denstone. If the average of the intermediate and minimum dimensions is used instead of the minimum, the ratio for modified Denstone becomes 1.27. This is much closer to the 1.19 Standard Denstone value.

3.2 MATERIAL TESTS

A range of tests were performed upon the above materials (except the modified Denstone, the sample of which arrived at a very late stage in the project), in order to determine their basic material properties. These are discussed below.

3.2.1 Specific Gravity

Samples of each size of Denstone and of iron oxide pellets were weighed. The volumes occupied by the samples was measured by water displacement and the specific gravity calculated. The mean results from these tests on each material are presented in Table 3.3.

3.2.2 Water Absorption Tests

Samples of each material were cleaned by air-blasting and weighed. They were allowed to stand in water for 24 hours. They were then surface dried, first using a paper towel, following by placing the sample in an oven at 135°C for 5 minutes. The samples were then re-weighed in the surface-dry condition, and percentage absorptions were calculated. The results are presented in Table 3.4.

TABLE 3.3 THE OBSERVED SPECIFIC GRAVITY OF DENSTONE AND IRON OXIDE

Material	Mean Specific Gravity
6mm denstone	2.280
9mm denstone	2.363
19mm denstone	2.363
Iron Oxide	3.843

TABLE 3.4 THE OBSERVED WATER ABSORPTION OF DENSTONE AND IRON OXIDE

Material	Water Absorbed (% by weight)
Iron Oxide	3.92
6mm denstone	0.13
9mm denstone	0.23
19mm denstone	0.30

The results for the Denstone are surprising, because the absorption decreases with increasing surface area to volume ratio. A possible explanation is that smaller particles are more completely vitrified and, hence, are less absorptive.

3.2.3 Packing Tests

Tests were performed to determine the packing densities which may be obtained. The apparatus used for this investigation is shown in Fig. 3.1. It consists of a steel container 355mm in diameter, and 500mm high, resting on rubber pads and tied to a vibrating table. The vibratory method of compaction has been used for many years. The table operated at 100 Hz and the accelerometer measured the applied acceleration. The accelerometer output did not display the expected sinusoidal shape but indicated severe harmonic interference was present. This was not considered to be highly detremental to the investigation, as Kolbuszewski and Alyanak (1964) had shown that as the frequency of vibration increased, the range of accelerations which would produce the maximum density also increased.

The volume of the particulate mass in the container was found by measuring the average height of the plywood platen from the top of the container, the system having been initially calibrated using known volumes of water. The weight of the particles enabled the determination of the volume of solids; hence, the specific volume, ν, where:

$$\nu = 1 + \frac{\text{volume of voids}}{\text{volume of solids}}$$

Material was placed using a small container and pouring from 'zero height' in order to obtain the minimum possible density. It had initially been intended to perform tests at different accelerations. It became apparent,

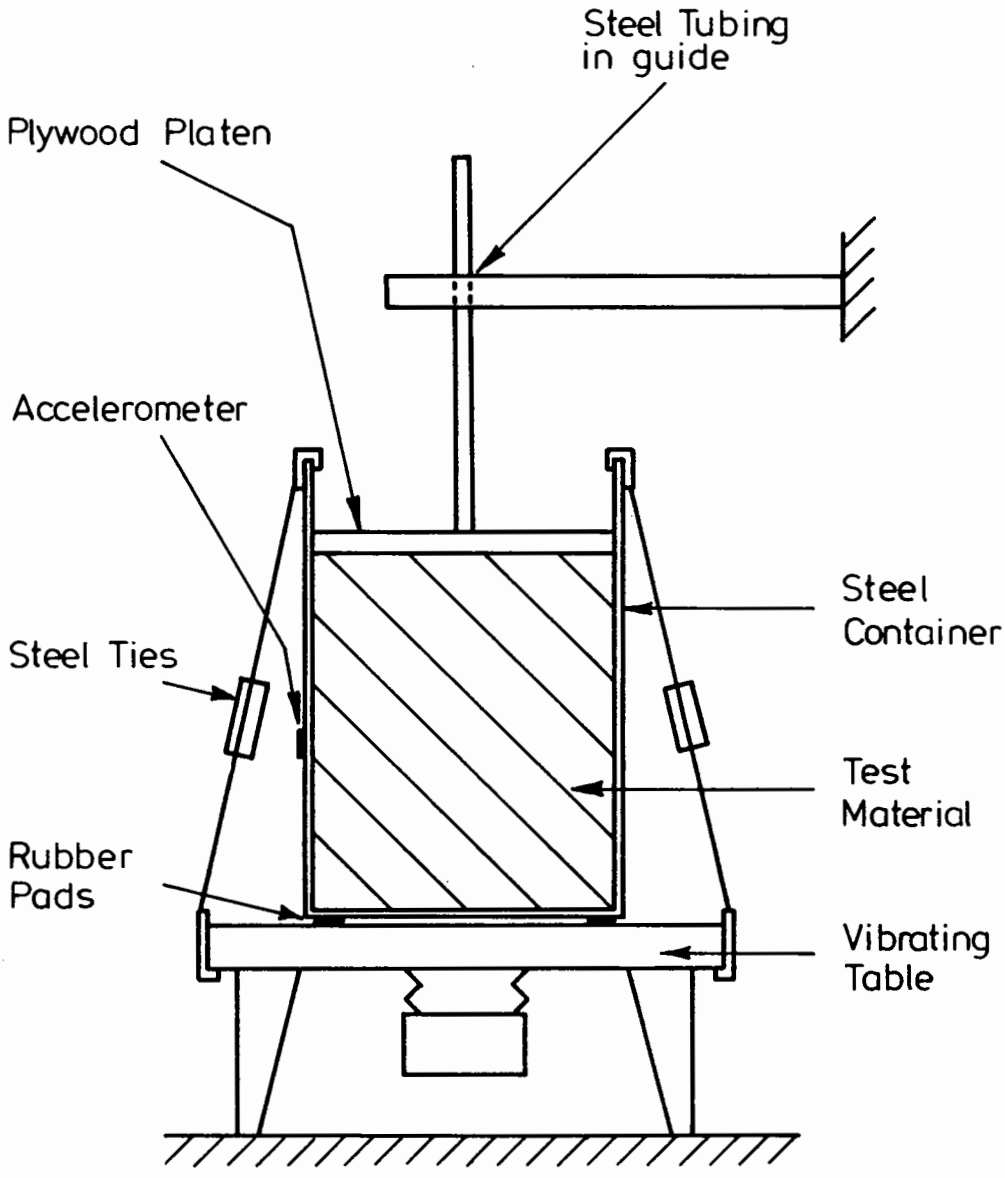

FIG. 3.1 VIBRATORY COMPACTION TEST APPARATUS

however, that due to the harmonic interference described above, the application of any isolated magnitude of acceleration was impossible using the available equipment. The accelerometer output showed that a range of accelerations were applied and therefore the accurate identification of critical values was not possible. However, it appeared that there existed a 'threshold value' below which little or no compaction occurred, and above which a high density was achieved within ten to fifteen seconds. The accelerometer appeared to register a mean value of about 4g for this threshold, but it should be noted that the instrument was attached to the container rather than being embedded in the material. There is no way of knowing whether the acceleration registered in the external location was the same as the acceleration experienced by the material. Indeed, 4g seems very high for a threshold of this kind; Kolbuszewski and Alyanak achieved maximum densities using accelerations of approximately 2g.

The values of low and high density obtained in these tests appeared to be constant for any given material. This is in agreement with the findings of Scott (1960), who suggested that the only stable random configurations for an aggregate of spheres, are the maximum and minimum random densities, and that intermediate densities are difficult to achieve and maintain. The results of these tests, presented in Table 3.5, show that the packing density increases as the particle size decreases. Scott observed considerable boundary effects and the measured differences in specific volume for the present material may be attributed to this phenomenon.

Three further tests, A to C, were conducted on 9mm Denstone as follows:

A: 10 layers, each of 5 kg with 5 minutes vibration per layer

B: 5 kg batches poured in from the level of the container top

C: 5 layers, each of 10 kg being subjected to five hand tamps

The results of these tests are presented in Table 3.6.

TABLE 3.5 OBSERVED SPECIFIC VOLUMES ACHIEVED DURING PACKING TESTS

Material (Nominal Size)	Initial Specific Volume	Final Specific Volume
19mm denstone	1.742	1.618
9mm denstone	1.695	1.575
6mm denstone	1.667	1.555
Iron Oxide	1.776	1.667

TABLE 3.6 RESULTS FROM FURTHER PACKING TESTS; A,B,C

Test	Final Specific Volume
A	1.511
B	1.672
C	1.684

TABLE 3.7 THE VARIATION ON FRICTIONAL PROPERTIES OF MINERALS WITH SURFACE MOISTURE (HORN AND DEERE, 1962)

Mineral	Coefficient when dry	Coefficient when saturated
Quartz	0.13	0.45
Feldspar	0.12	0.77
Calcite	0.14	0.68

Tests B and C show densities only slightly higher than the minimum density. Test A, however, shows that a considerable increase in density is achieved by prolonged vibration. It is considered that this may be due to the formation of regular packing, as observed by Wroth (1958).

In order to estimate the specific volume observed in a container of any size, the results of the tests on denstone were plotted against the ratio of particle diameter to container surface area (d/A) as shown in Fig. 3.2. An estimate of the maximum and minimum specific volumes which may be obtained in very large containers, is obtained by extrapolation. These are found to be 1.58 and 1.49 respectively.

3.2.4 Friction Tests

The average contact forces in a uniform particulate mass are proportional to the square of the particle size. For example, in a mass of 20mm diameter particles, likely average values are of the order of 40 N/100 kPa (using figures quoted by Penman (1978)). The research work of Konishi and Oda (see Chapter 4) has revealed that stresses within granular materials are transmitted through heavily loaded contiguous chains of particles. This means that the idea of a "mean contact force" is not very meaningful unless the contact force distributions are also known.

A machine was designed in order to apply such forces across a sliding interface. This apparatus, shown in Fig. 3.3, enabled friction tests to be performed. Tests to investigate both inter-particulate friction and friction between particles and the loading platens (see Chapter 5) were carried out.

Investigation into the Material Friction Properties of Denstone

50mm denstone particles were obtained for this test. These were sawn up and arranged in the test apparatus as shown in Fig. 3.4(a). A normal

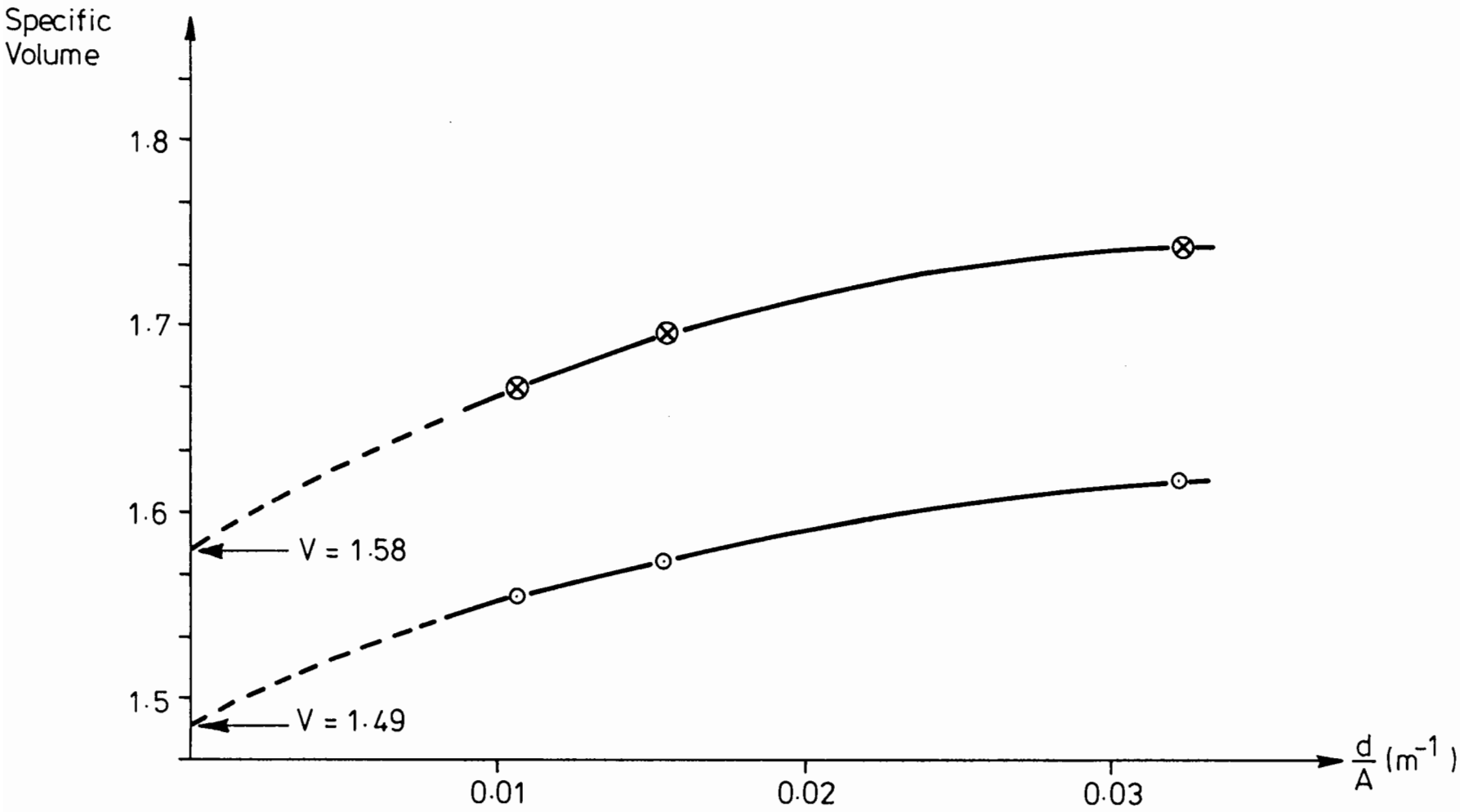

FIG. 3.2 THE EFFECT OF SURFACE AREA ON OBSERVED SPECIFIC VOLUMES

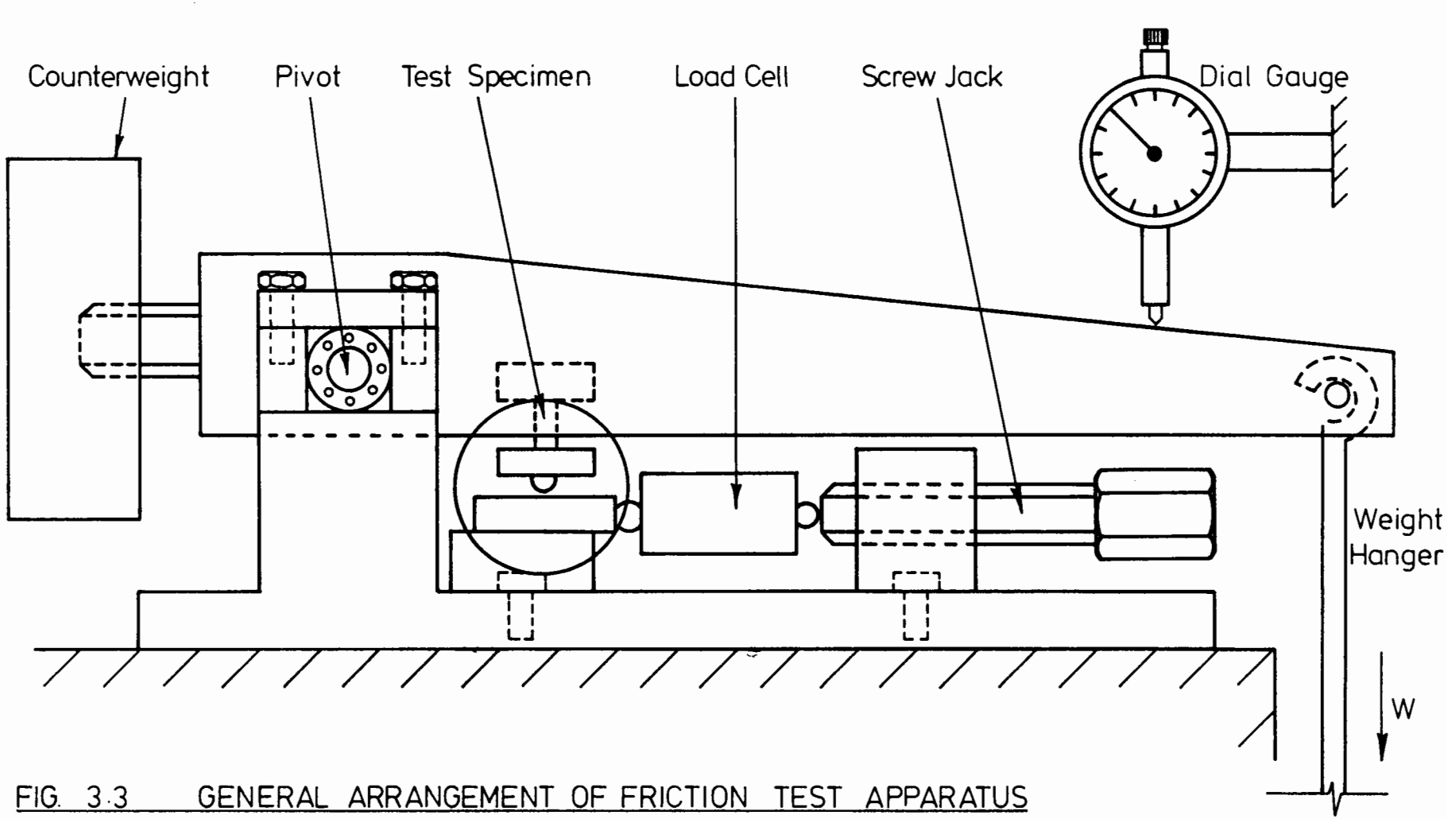

FIG. 3.3 GENERAL ARRANGEMENT OF FRICTION TEST APPARATUS

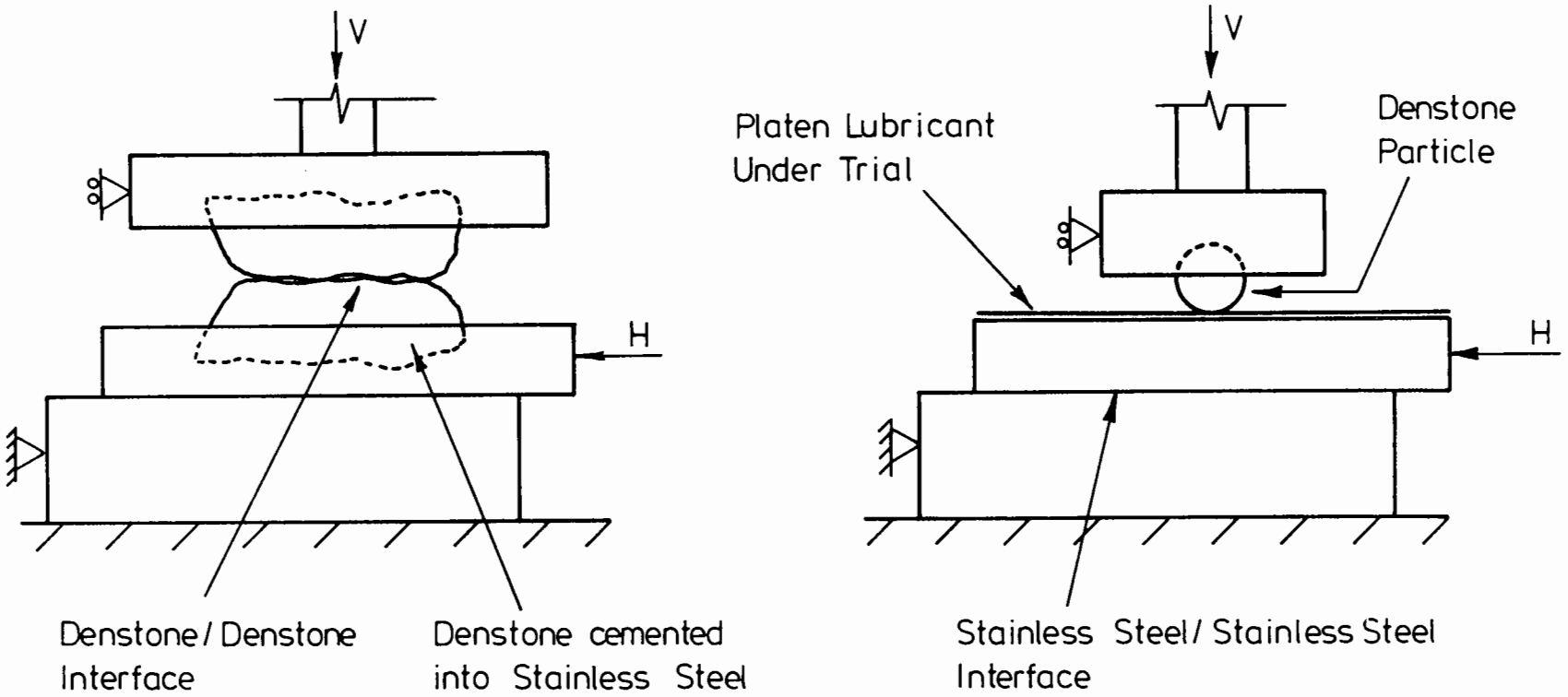

FIG. 3.4 DETAILS OF LOADING ARRANGEMENT FOR FRICTION TESTS

load was applied across the two interfaces, i.e. Denstone to Denstone and stainless steel to stainless steel. The horizontal force required to overcome the friction provided by the stainless steel to stainless steel interface was calculated using the previously measured coefficient of friction (μ = 0.235). The value of applied horizontal load in excess of this value was attributed to the friction between the two Denstone surfaces.

Since these tests were performed, consideration about the validity of this last assumption, has led to the conclusion that it is probably wrong. The reason for this is the "stick-slip" hypothesis (Boden and Tabor 1945) in which an apparently smooth sliding interface is, on the microscopic scale at least, a series of sticks and slips. The method of calculation outlined above, of course, assumes that both interfaces were sliding simultaneously and continuously, an assumption which is not supported by experimental evidence. It has, however, been decided to include the data on the grounds that it provides some interesting comparative results.

The dial gauge, shown in the general arrangement of Fig. 3.3, was used to check that no vertical displacements occurred. In fact, very little vertical movement was observed. But, as an added precaution, the lower Denstone surface was turned through 180° and the test was repeated.

The Denstone to Denstone interface was tested in both the oven dry and surface saturated conditions under a range of normal loads. The material interface was maintained in a saturated condition by the injection of water to the contact area throughout the test. The results presented in Fig. 3.5 show that, despite the misgivings about tht accuracy of this test, the value of interparticle friction is dependent upon the surface moisture conditions and the normal load.

It is well established that surface moisture increases the surface friction of minerals, as Table 3.7 from Horn and Deere (1962) shows. Rowe

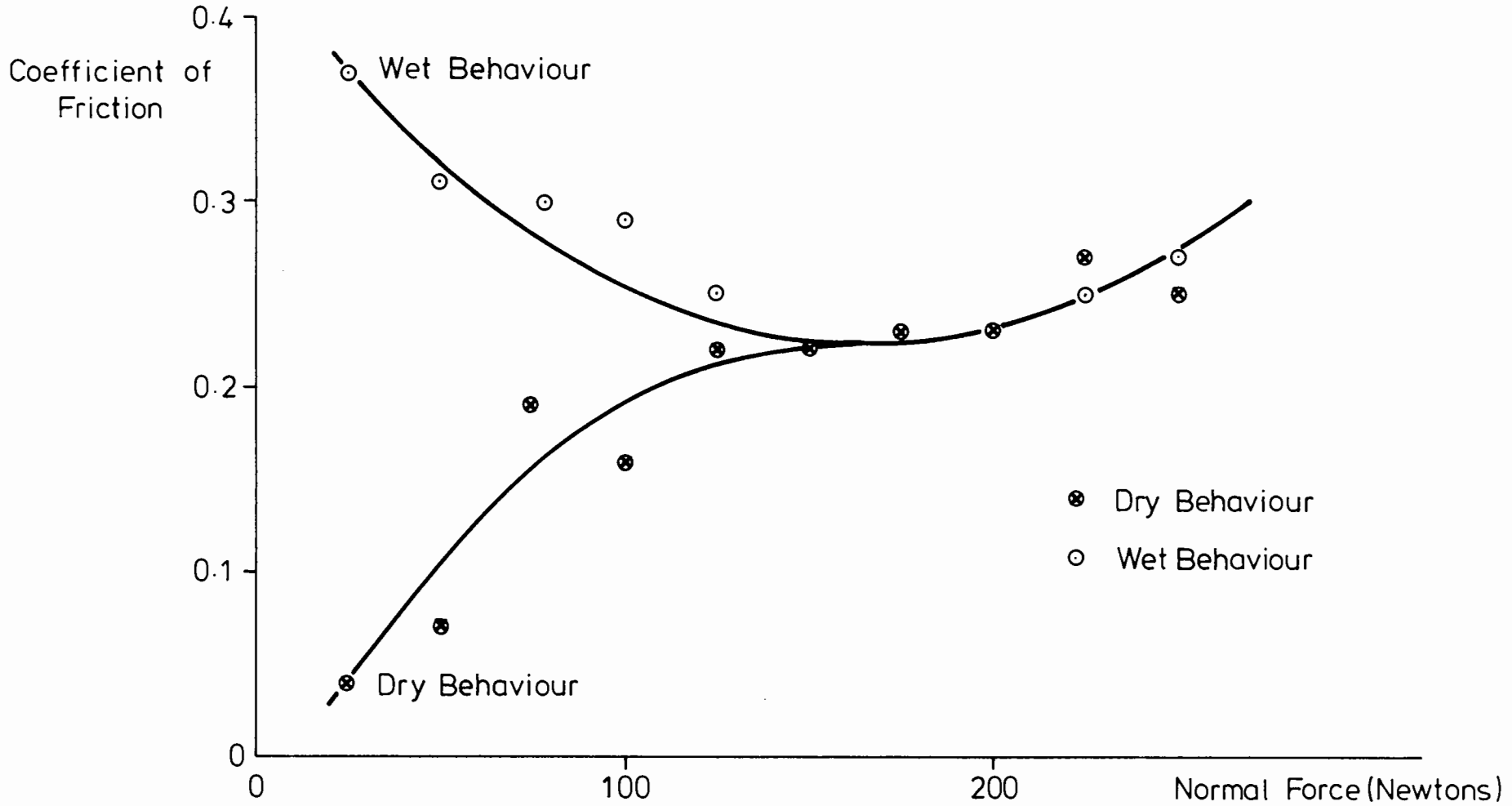

FIG. 3·5 FRICTION PROPERTIES OF DENSTONE IN WET AND DRY CONDITIONS

(1962) performed friction tests using the apparatus shown in Fig. 3.6(a). The results for a quartz sand are presented in Fig. 3.6(b). These show that the friction angle is dependent on particle size with large particles providing less resistance to shear.

If the models of Caquot (1934) and Bishop (1954) (which assume that strength is derived solely from resistance to sliding at particle contacts - see Chapter 4), are correct, the observed friction properties of the Denstone would lead to the prediction of a large disparity in the shear resistance of dry and saturated samples deforming at the critical state. This hypothesis does not appear to be borne out by experiment. Neither the monotonic strength (Proctor and Barton 1974) nor resilient properties (see Chapter 6) appear to be affected by the surface conditions of the material.

3.3 DEFORMATION AND STRENGTH TESTING

Hertz (1981) gave the solution for the deformation of perfectly elastic spheres in contact. The solution assumes extremely high stresses which, in practice, materials under working conditions cannot withstand without yielding. A simple loading test was set up to investigate the effect of loading a denstone sphere. A simple modification was made to the friction test apparatus (Fig. 3.3) so that a Denstone particle could be loaded between two plates (see Fig. 3.7(a)). The deformations were measured by the dial gauge (having calibrated out the deflections of the loading frame). Only two tests (both using 19mm denstone) were performed as it was considered that the practical value of the results was limited. The deformations recorded in each test were found to be similar, and these are presented in graphical form in Fig. 3.7(b).

Strength tests were also performed on 9mm and 19mm particles using the same apparatus but loading to failure. The results are presented in Table 3.8.

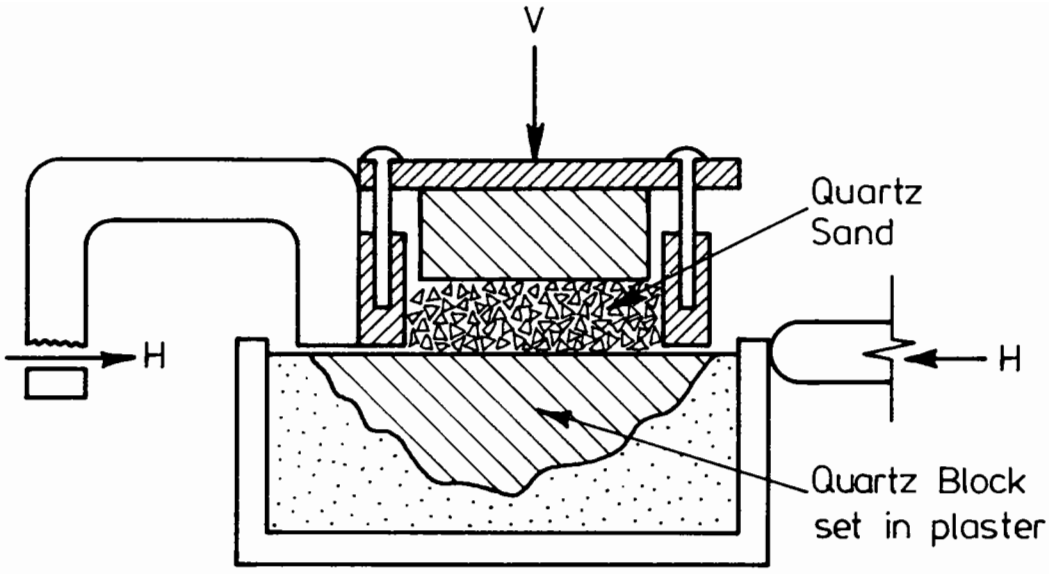

(a) Friction Testing Machine (Rowe 1962)

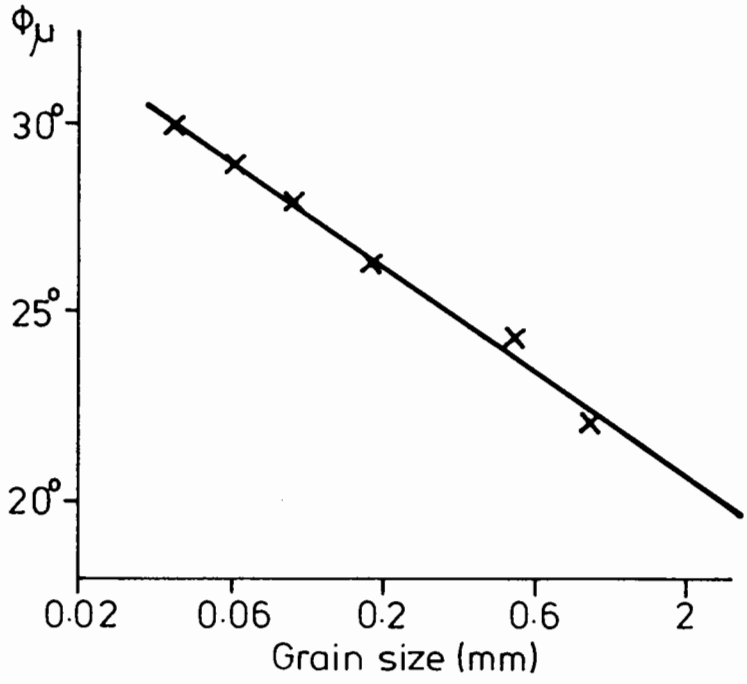

(b) Friction Angle of Quartz Sands as a function of Grain Size (Rowe 1962)

FIG. 3.6 FRICTION TESTING OF QUARTZ SANDS (ROWE 1962)

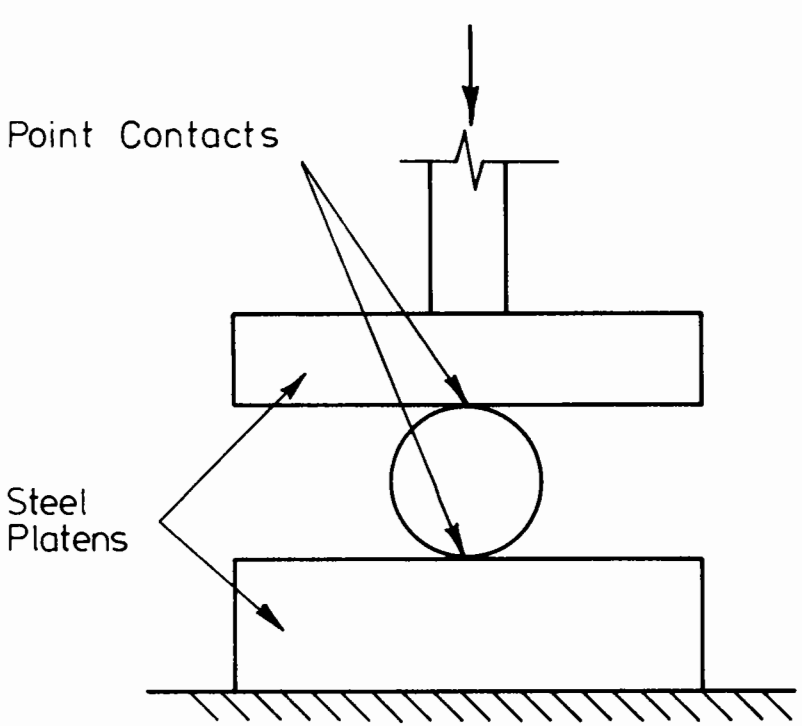

(a) Modification to friction test apparatus for deflection testing.

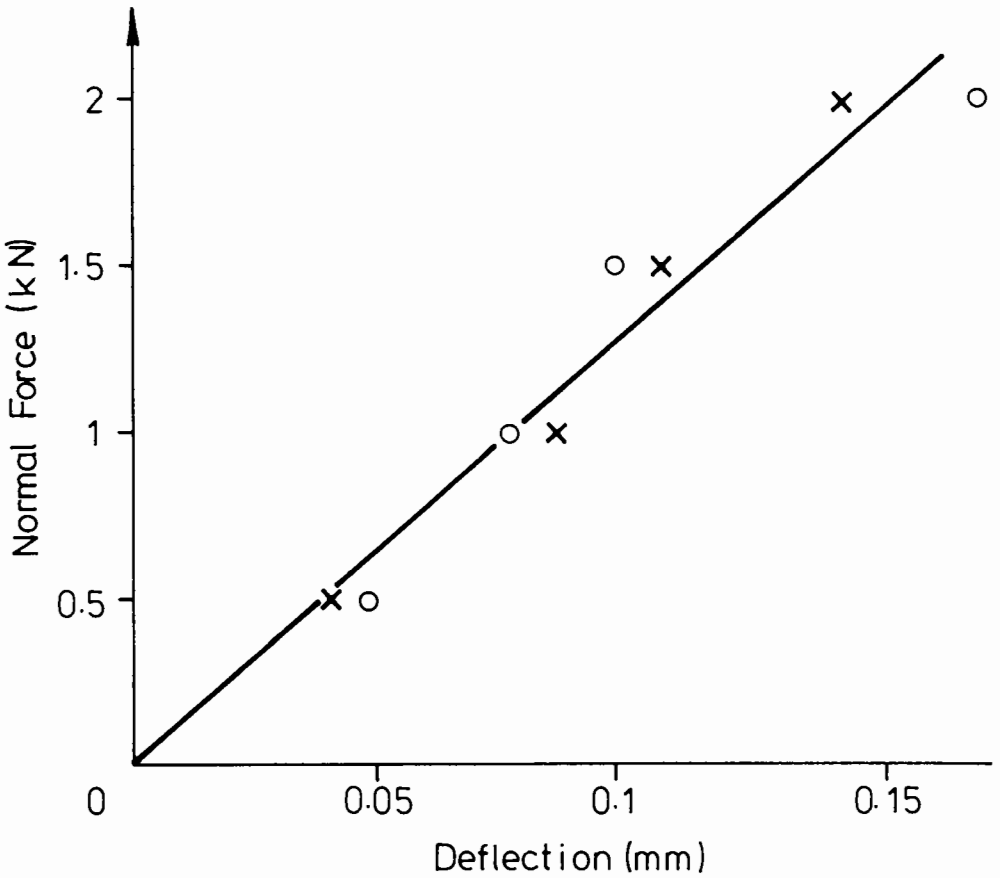

(b) Results of Deflection Test.

FIG. 3.7 DEFLECTION TEST DETAILS AND RESULTS

TABLE 3.8 RESULTS OF POINT LOADING FAILURE TESTS ON DENSTONE

Material Size	No. of Tests	Mean Failure Load (N)	Std. Dev. of Failure Load (N)
10mm	8	1561	628
19mm	8	4272	669

CHAPTER FOUR

A LITERATURE REVIEW

4.1 INTRODUCTION

In 4.2 the traditional continuum approach to mechanics of granular media is outlined and its inadequacy when dealing with sophisticated design problems is discussed. A review of theories which have been derived from a consideration of behaviour at the particle level is presented. Following this, a review of fundamental experimental work is given. This deals with the mechanisms which have been observed within particulate media and their effect on the mechanical properties of granular media. The concept of fabric is also discussed.

A review of experimental work is presented in 4.3. This includes work on the cyclic loading of granular materials and tests which feature principal stress rotation. 4.4 provides, firstly, a brief survey of silo design, and secondly, a review of vertical walled silo behaviour with reference to cycled thermal conditions.

4.2 ANALYTICAL DERIVATIONS AND FUNDAMENTAL EXPERIMENTATION

4.2.1 The Inadequacy of a Continuum Approach

In 1776 Coulomb produced an equation to quantify the shear strength of a soil:

$$s = c + \sigma \tan \Phi \qquad \text{(Eqn. 4.1)}$$

where s is the shear strength

c is the cohesion (zero for an ideal granular material)

σ is the normal stress across an incipient failure plane

Φ is the 'angle of friction'

Coulomb's equation gives an indication of the factors of safety that might be expected in an earth stability situation and in this context has been used successfully right up to the present day. However, the assumptions in this formulation are that a soil behaves as a rigid continuum until failure (i.e. rigid-plastic behaviour). Thus, it ignores many important aspects of granular material behaviour.

The ability of a granular medium to increase its volume (dilate) when sheared was first recognised by Reynolds (1885). This is one aspect of granular soil properties which invalidates Coulomb's hypothesis when soils are subject to high stresses close to their ultimate shear strength and after 'failure' has taken place. This was recognised by Terzaghi (1920), who said of Coulomb's law:

> "...it developed into an obstacle against further progress as soon as its hypothetical nature came to be forgotten by Coulomb's successors."

From then on, a number of investigations have attempted to describe the behaviour of granular media using a discrete particle approach involving the equilibrium of particles and their compliance to external forces. These models aim to reproduce the ability, of a particulate material to undergo volume changes and to accept strain discontinuities.

4.2.2 The Discrete Particle Approach

Caquot (1934) and Bishop (1954) both derived relationships between the effective angle of shear during constant volume shearing (Φ_{cv}) and the interparticle angle of friction ($\Phi\mu$). In 1957 Newland and Allely adopted a new approach by considering sliding in directions other than in the plane of failure and this idea was extended by Rowe (1962, 1963) in his Stress-Dilatancy theory. Rowe was sceptical about the validity of previous

approaches and stated in his paper to the Royal Society:

> "..a fresh start has been made based on a consideration of the forces between particles. In the following work, relations are derived between the applied stress ratio to an assembly, the true physical angle of friction Φ_μ, the geometry of the particle arrangement and the rate of change of unit volume relative to the longitudinal strain for given particle arrangements."

Rowe tested various regular packings and explained their behaviour in theoretical terms, introducing the concept of minimum energy. The equation which he derived may be written:

$$\frac{\sigma_1}{\sigma_3 \ (1+d\dot{V}/V\dot{\epsilon}_1)} = \tan^2 \ (45 + \frac{1}{2} \Phi_\mu) \qquad \text{(Eqn. 4.2)}$$

where, σ_1 = major principal stress

σ_3 = minor principal stress

$d\dot{V}/V$ = rate of unit volume change

$\dot{\epsilon}_1$ = rate of strain in the direction of σ_1

Rowe also tested random packings of non-uniform material and in view of the discrepancies which arose between their behaviour and that predicted by theory, he suggested replacing the material friction value Φ_μ in (Eqn.4.2) by a value of Φ_f which is related to Φ_μ but also takes into account the effects of remoulding and the associated energy loss.

The concept of the energy principle and other devices used by Rowe were heavily criticised by Gibson and Morgenstern (1963), Trollope and Parkin (1963), Scott (1964) and Roscoe and Schofield (1964). In answer to these criticisms Rowe (1964) explained that this solution simply gave a

lower bound solution, a view endorsed by Horne (1965, 1969) who produced proofs for those parts of Rowe's Stress-Dilatancy theory which were criticised as mathematically invalid or simply intuitive. Horne also rederived the Stress-Dilatancy equations using the more general case $\sigma_2 \neq \sigma_3$. Again it was suggested that to generalise the equations, Φ_μ must be replaced by Φ_f, giving the general relation proposed by Rowe in 1962, viz.:

$$\tan \Phi_f = k \tan \Phi_\mu \qquad \text{(Eqn.4.3)}$$

where k increased with the degree of remoulding. Procter (1974) derived an equation for plane strain deformation conditions which gives an analytical value for the upper bound of Φ_f, thus complementing the lower bound solution given by Rowe (1962) and Horne (1965).

Josselin de Jong (1976), while questioning the minimum energy ratio principle, was attracted by the existence of apparently supporting experimental data. He showed that the result derived by Rowe is obtained by considering the same model of toothed separation planes as that treated by Rowe and applying to that model the laws of friction only. He states that his analysis is only appropriate given that a particular mode of deformation occurs, and that in certain circumstances (e.g. stress reversals and behaviour after peak) the behaviour will be different. Finally, Josselin de Jong states that the coincidence of the two results is not a proof of the minimum energy ratio principle and that it is a fortuitous consequence of the assumptions underlying the model behaviour.

Matsuoka (1976), in connection with his stress-dilatancy work, proposed the use of a "Spatialized Mobilized Plane" which is the stress plane in which soil particles are, on average, mobilized the most in 3-D space. It is coincident with the octahedral plane under isotropic stress

but moves when shear stresses are applied. Symes (1983) points out that, amongst the questionable features of this model is the prediction that no changes in strain will occur during principal stress rotation provided that the magnitudes of the principal stresses remain constant. Tokue (1979) proposed a three-dimensional stress dilatancy model which does not assume that the minimum energy ratio principle is observed. He describes results in a true triaxial apparatus which support his theory.

The relationships outlined above all asssume that sliding at particle contacts is the controlling factor in relation to the shear strength (at constant volume). However, after numerous experimental attempts to correlate Φ_μ with Φ_{cv}, for example by Skinner (1969) and Proctor and Barton (1974). It must be concluded that the overall strength of real granular materials is not greatly dependent on interparticle friction. Skinner (1969) postulated that, in the light of this result, the primary deformation process was one of particle rotation rather than sliding at contacts. Sharma (1976), using an x-ray technique, showed that this was in fact the case. Round (1976) and Cundall et al (1982), both using computer models based on discrete particle mechanics, show that rotations should be observed. These findings must cast doubt on the validity of certain aspects of the stress-dilatancy theories outlined above.

4.2.3 Computer Analyses

Computer methods have been developed in which the behaviour of an assembly of particles is calculated by considering the behaviour and inter-relation of individual contacts. Round (1976) prepared a programme where particle movements are obtained from the solution of equilibrium equations. Cundall and Strack (1979) have prepared a programme 'Ball' which used the 'Distinct Element Method' which considers particle dynamics. It is time dependent and models the slow progressive particle movements. The main

advantage of the latter type of solution is that necessary storage space is relatively small and, in the future, may become a major geomechanical research tool.

4.2.4 Fabric and the Mechanism of Load Transfer in Granular Materials

The mechanism of load transfer: Dantu (1957) demonstrated with the aid of photo-elastic models that stresses in granular materials were not uniformly distributed but were concentrated along load-carrying particle chains. In 1974 Oda described an experiment performed by Konishi (1972) in which photo-elastic rods were loaded biaxially. Forces across individual particle contacts were monitored by counting the resulting interference fringes. From these results several important phenomena may be observed.

Stresses are not transferred in a uniform manner but are concentrated along contiguous columns of particles. The particles in between the columns carry relatively little load but act to stabilise the columns, that is they provide lateral support. At some critical point a column will fail and the internal structure will be rearranged. This may result in the formation of new columns if particles in that region are favourably orientated. In this way the deformation of a particulate mass under increasing load is seen to be the continual collapse and generation of contiguous chains of load-bearing particles.

The predominant orientation of particle contacts was in the direction of the major principal stress.

Following this work up, Oda and Konishi (1974) tested photo-elastic rods in a simple shear apparatus and showed that as the principal stresses rotated, so too did the direction of the preferred contact direction. Konishi (1982) demonstrated a similar effect using oval rods.

Cundall et al (1982) describe numerical experiments in which the phenomena described above are observed.

Fabric: In the context of particulate mechanics, "fabric" is understood to mean the structure of the soil at the particle level - that is the mean and deviation of contact numbers and directions. Void-ratio is the most common measure of structure. It is, however, a non-directional quantity and experimental evidence shows (e.g. Darwin 1883, Oda 1972 and Symes 1983) that the mechanical properties of a granular material may be significantly changed by altering the method of compaction or deposition (without affecting the void ratio) Oda et al (1980), however, suggest that the orientation of the particles is not a good measure of granular fabric since it is insensitive to external disturbances as compared to a fabric quotient based on contact distributions only. The changes in particle orientation appear to be more dependent on the magnitude of strains rather than the intensity of stress. It is, therefore, incapable of taking stress-history into account adequately. It should consequently be regarded as a factor which will affect the future contact formation rather than the instantaneous mechanical properties.

Bernal and Mason (1960) determined the number of contacts (co-ordination number) that randomly packed spheres made with their neighbours. Oda (1977) investigated the effect of co-ordination number on the strength of particulate masses. He found that , on its own, the co-ordination number was not sufficient to predict the strength but that the standard deviation of the co-ordination number was required also. The relationship is as indicated in Fig.4.1.

A more comprehensive and meaningful quantification of fabric will include the distribution of the number and directions of contact points in a granular mass. Satake (1982) proposes the use of a fabric tensor derived from a statistical count of contact normals in a particle mass. In practise the problems both in obtaining the data and analysing it are awesome. Oda et al (1980) decided to adopt an approach based on empirical

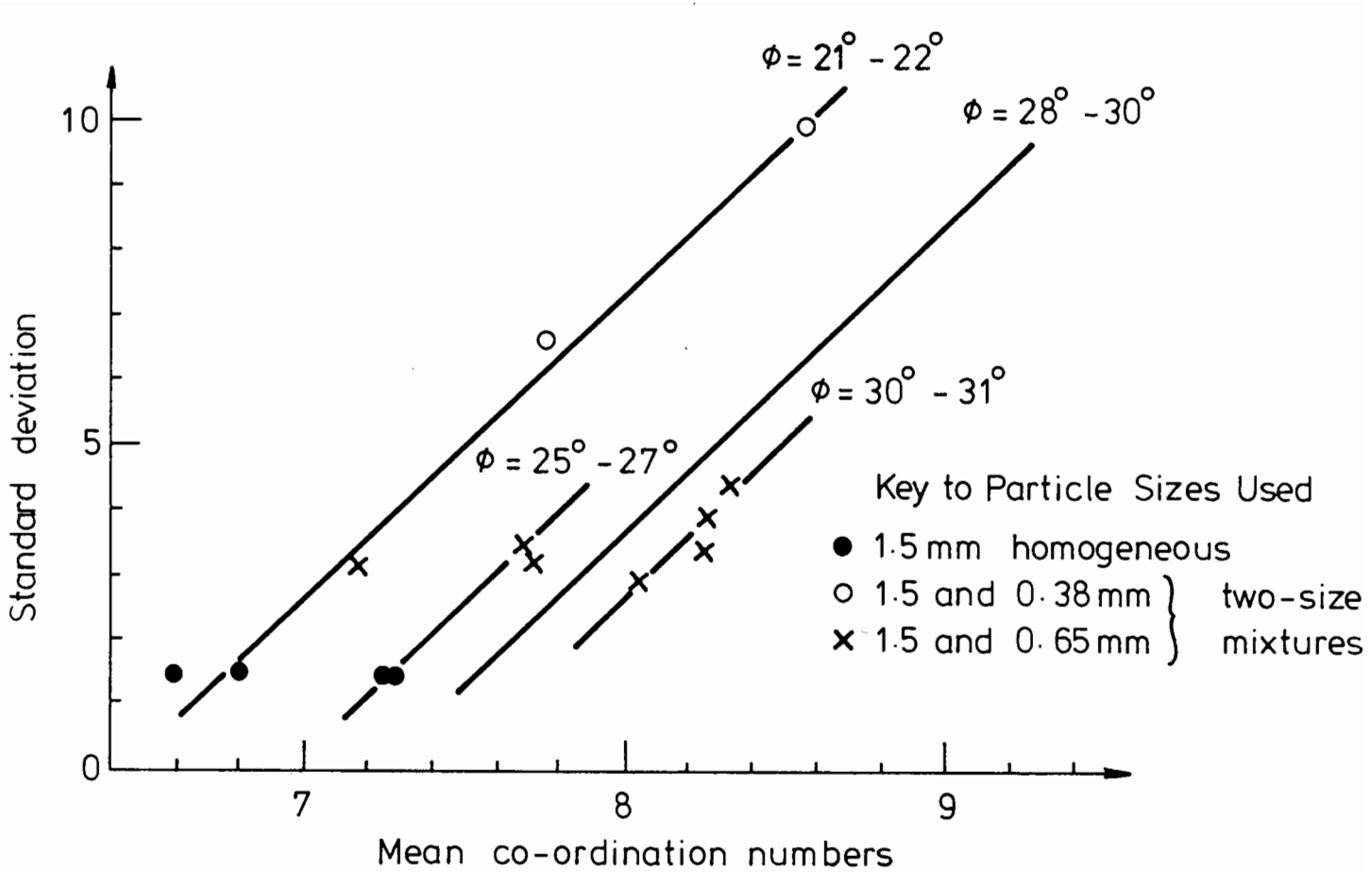

Fig. 4.1 Relationship Between Strength and Mean and Standard Deviation of Particle Co-ordination Numbers (from Oda 1977)

relationships between the applied principal stress ratio and the fabric index (the ratio of contact normals parallel to the major and minor principal stresses). Using this and assuming co-axiality between the stress and fabric tensor, a fabric ellipsoid (which represents a second order tensor) is derived.

Anisotropy: The behaviour of a granular medium depends at any point on the fabric. If particle contacts are randomly distributed so that there is no preferred orientation the material is isotropic - if not, then some degree of anisotropy will exist.

It is possible to separate two components of anisotropy:

(a) Inherent anisotropy: The effect of compaction or deposition: Oda (1972 a) showed that samples formed by pluviation were considerably stronger and stiffer (in the direction of pluviation) than those formed by rodding. The explanation of this is that, on reaching the surface, the pluviated particles are relatively unrestrained and so may fall in the most stable position, i.e. long-axis in the horizontal plane. Rodding, on the other hand, disruptes the anisotropic structure formed by pluviation.

(b) Induced anisotropy: This is the effect of stress history. Oda (1972 b,c) showed, by taking thin sections, that when the stress state is altered the fabric changes will be the result of both the magnitude and directions of the principal stresses and the inherent anisotropy. For example, if an isotropic stress state exists, and this is increased in magnitude then the number of particle contacts formed will be greatest in directions of inherent anistropy. If on the other hand an inherently isotropic material is subject to a shear stress, the number of particle contacts formed will be greatest in the direction of the maximum principal stress. It is thus possible for a material to be inherently anisotropic but, at any instant, to have an isotropic fabric because of its stress

history.

4.2.5 Particle Contact Deformations

Although particle contact deformations are not normally considered as being important, their magnitude is likely to become significant when strains are small. When a particle mass under repeated load reaches an "equilibrium" resilient condition, i.e. when all strains are recoverable, particle contact deformations will become a major factor. The case of elastic spheres in contact was first solved by Hertz (1881). He derived the deformation equation for normal forces only. The case of oblique contact between elastic spheres was first considered by Mindlin (1949), who calculated the effect of a relative tangential displacement of the spheres' centres superimposed upon a normal Hertzian compression. Using a similar analysis, Mindlin and Deresiewicz (1953) investigated the behaviour of elastic spheres in contact under varying oblique forces. Walton (1978) showed that if the normal and tangential displacements occur simultaneously then the resultant configuration differs significantly. It must be noted, however, that the above analyses assume perfect sphericity and elastic behaviour, all of which are oversimplifications likely to result in erroneous solutions when applied to a real problem. However, in the field of mechanical engineering, Hertzian solutions are used with considerable success.

4.3 REVIEW OF EXPERIMENTAL WORK

A large amount of experimental data from triaxial tests on granular material has been published. The majority deals with behaviour under monotonic loading and is primarily concerned with material failure. A proportion involves repeated loading, which is mainly concerned with the

determination of elastic stiffness in applications such as highway engineering. Data from tests on sand by Lau (1975) (Fig. 4.2) shows the way in which a granular material behaves during repeated loading. An equilibrium condition is reached after a number of load applications even when the applied deviator stress is a high proportion of the failure value (in the case of Fig. 4.2(b), 90% of the failure value). At the equilibrium, strains are predominantly recoverable (elastic) and the behaviour is termed resilient. It is also important to note the large irrecoverable (plastic) strains which occur (particularly during the first cycle). This early development of plastic strain is not normally considered to be important in the field of highway engineering as compaction is achieved by repeated loading. Therefore the majority of published results concern only resilient behaviour and the development of long term plastic strain.

4.3.1 Triaxial Cyclic Loading - Resilient Strain:

That part of the strain caused by a load application which is recoverable, is termed the resilient strain. The majority of available data is concerned with the resilient behaviour of crushed rock and gravel materials used in highway and railway construction, although the behaviour of sands has also been studied. All published results show that the stiffness of a granular medium increases with mean normal stress (p). The stiffness is usually expressed as the resilient modulus M_R which is analogous to Young's modulus for a linear elastic continuum. A simple non-linear model developed by Hicks (1970) is given by:

$$M_R = k_1 \Theta^{k2} \qquad \text{(Eqn. 4.4)}$$

where Θ is the sum of the principal stresses ($\Theta = 3p$) and k_1 and k_2 are

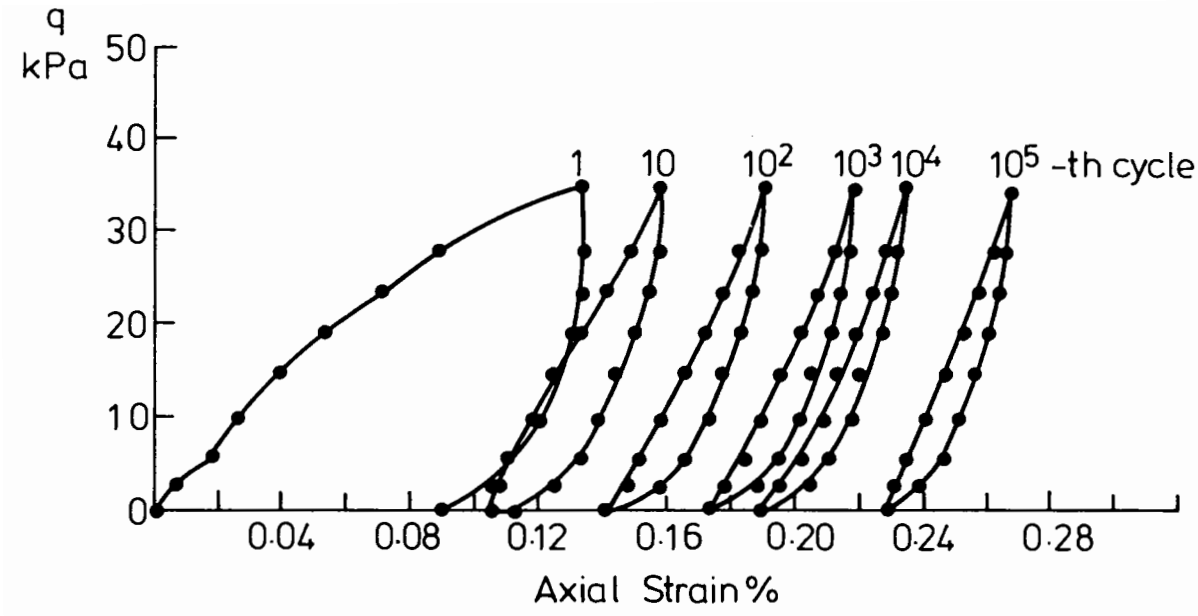

(a) Maximum Deviator Stress at 25% of Failure Value

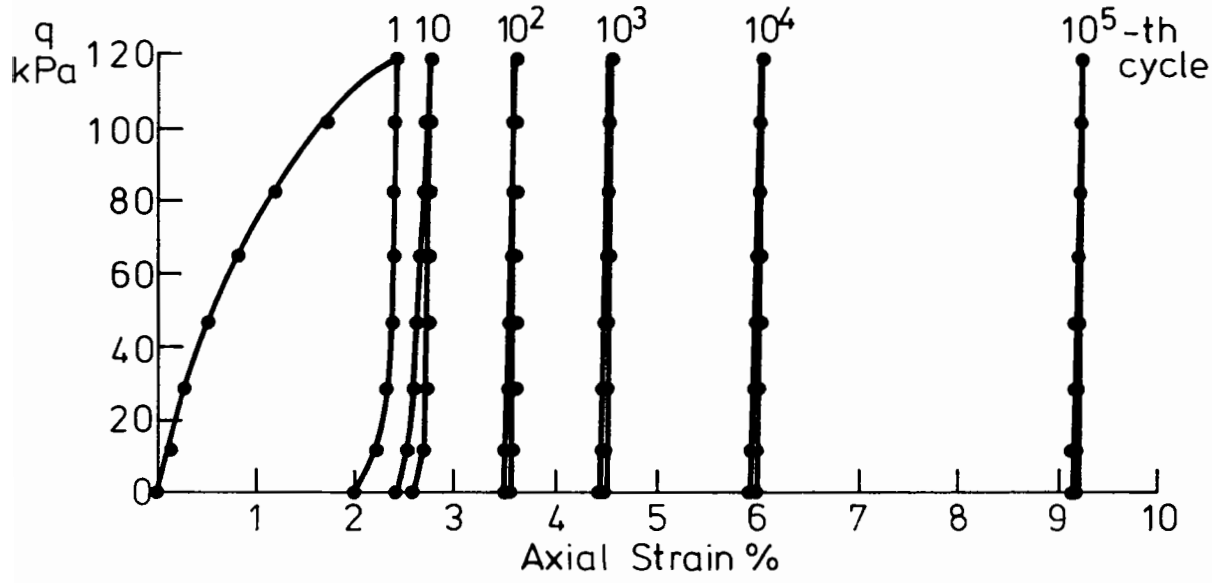

(b) Maximum Deviator Stress at 90% of Failure Value

Fig. 4.2 Behaviour of Sand During Repeated Loading (from Lau 1975)

material constants. Most researchers have reported relationships of this type, e.g. Biarez (1962) who tested a uniform sand and Robinson (1974) who tested a dry uniform sand. Biarez gives k_2 as $0.5 < k_2 < 0.6$ and Robinson gives k_2 as $0.48 < k_2 < 0.6$.

Boyce (1976), Pappin (1979) and Shaw (1980) all carried out repeated load triaxial tests at the University of Nottingham. They tested well-graded and uniform granular media with confining stress both constant and cycled, measuring both axial and radial deformations. The following stress and strain invariants were used to present test results:

$$\begin{aligned} &\text{normal stress} && p = (\sigma_a + 2\sigma_r)/3 \\ &\text{deviator stress} && q = \sigma_a - \sigma_r, \\ &\text{volumetric strain} && \epsilon_v = \epsilon_a + 2\epsilon_r, \\ &\text{shear strain} && \epsilon_s = 2/3\ (\epsilon_a - \epsilon_r) \end{aligned} \qquad \text{(Eqn. 4.5)}$$

where, σ_a and σ_r are the stresses in the axial and radial directions respectively, and ϵ_a and ϵ_r are the strains in those directions. For the complete derivation of these invariants see Schofield and Wroth (1968) and for a useful introduction to their application to soil mechanics see Atkinson and Bransby (1977).

The results of the above tests tend to indicate that the k - theta model, while useful for tests in which the magnitude of cycled stress is constant, is not sufficiently accurate when used to predict strains due to stress paths with considerable variation in length. Boyce proposed a model which took into account the stress state at the limits of a cycled stress path and this idea was extended by Pappin who used (as a graphical representation of his model) contours of resilient strain superimposed on a plot of p–q stress space to predict the values of shear and volumetric strains (see Figs. 4.3(a), 4.3(b)). The model predicts:

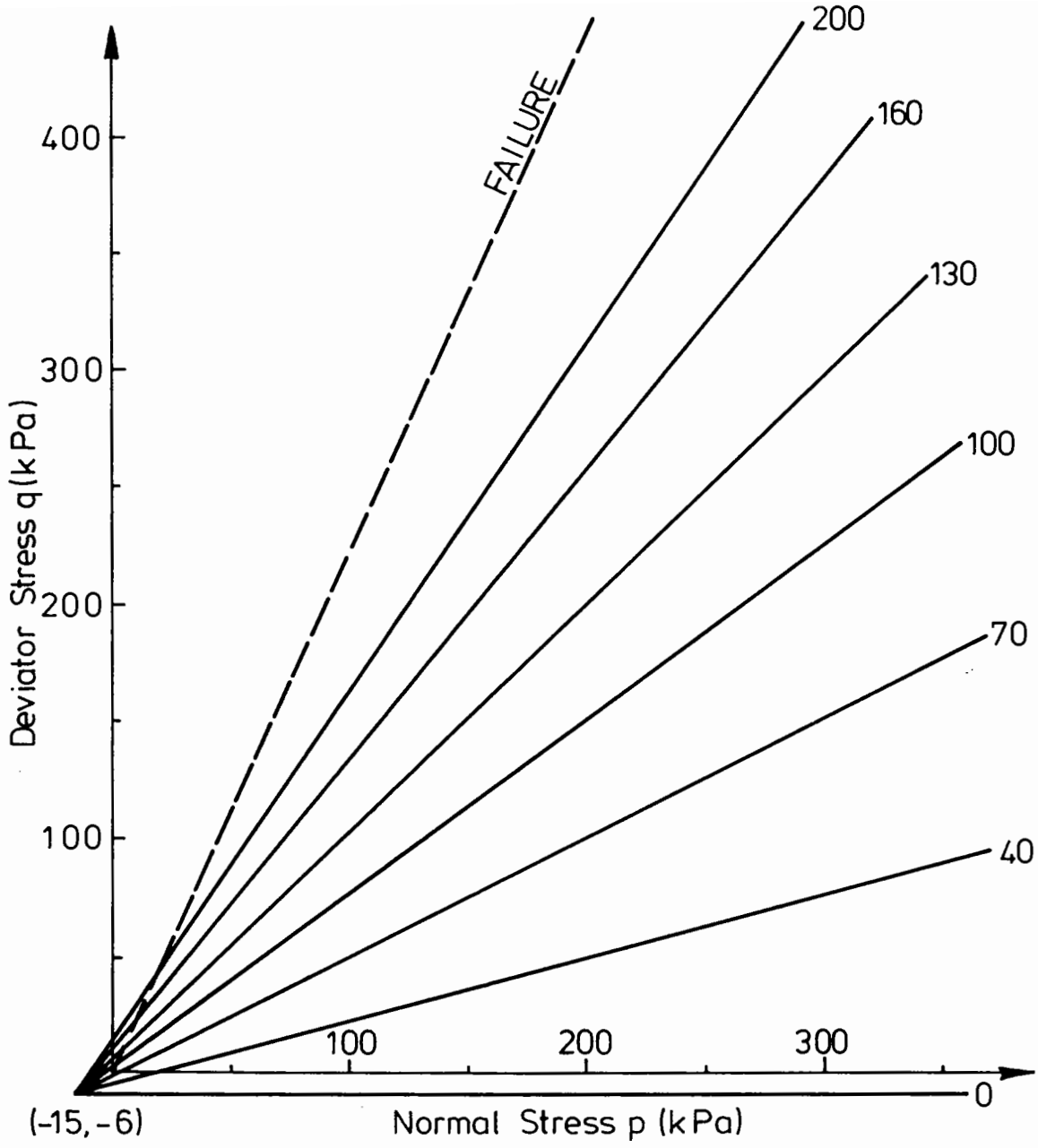

FIG. 4.3(a) NORMALISED SHEAR STRAIN CONTOURS ($\mu\varepsilon$) IN p-q STRESS SPACE

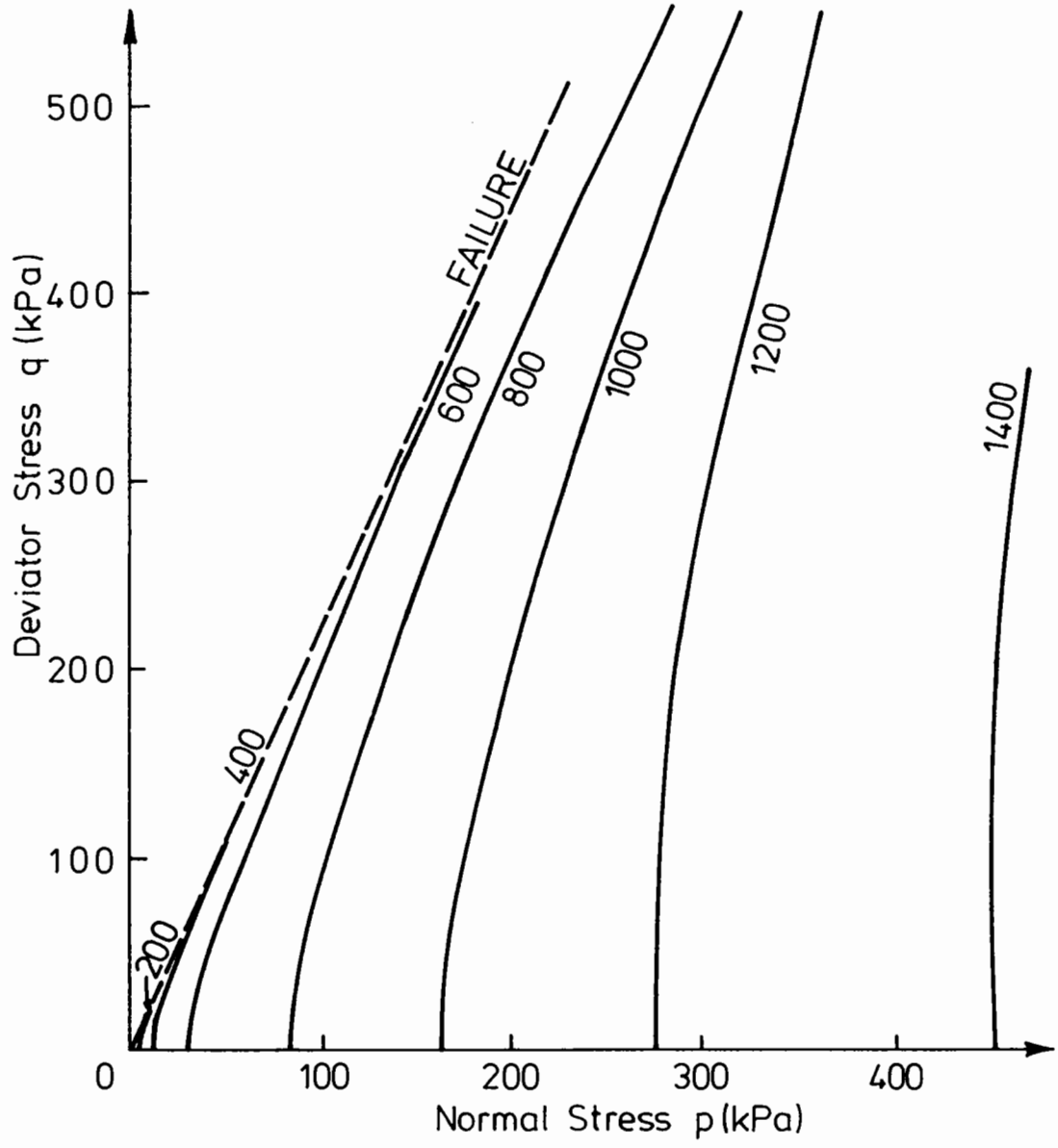

FIG. 4.3(b) CONTOURS OF VOLUMETRIC STRAIN ($\mu\varepsilon$) IN p-q STRESS SPACE

(a) that the magnitude of volumetric resilient strains is independent of stress path length and is basically dependent on p, with q/p becoming a significant factor as the stress path approaches the failure condition.

(b) that resilient shear strains were dependent on stress path length.

Shaw tested a single-sized crushed limestone and found that it obeyed the same relationship as for the well-graded crushed limestone although the constants were different.

Effects of loading frequency: Attempts have been made to determine the effect of the frequency of loading on the stiffness of a granular material, (e.g. Robinson (1974) and Boyce (1976)), but results lead to the conclusion that in the range of 0.1 Hz to 20 Hz there is little or no effect. Hardin (1965) reports that during low strain repeated loading tests stiffness is independent of frequency of loading in the range from slow monotonic up to 600 Hz. At larger strains, an increase in loading rate leads to higher stiffnesses. This is usually attributed to dilational inertia. There is, however, no data available relevant to cycle times of very long duration.

Influence of Density: Trollope et al (1962) reported slow repeated load tests on a uniform sand, and found that the resilient modulus of a dense sample was up to 50% greater than that for loosely compacted samples. Hicks (1970) reported the results of an extensive test programme on a graded material. He observed a general trend that resilient modulus increased with dry density, although he was unable to establish a consistent mathematical relationship between them.

Influences of Grading and Particle Shape: Hicks (1970) compared results of a crushed and a partially crushed aggregate and found that the resilient

behaviour was similar at comparable relative densities (relative density is here defined as the sample density relative to the maximum and minimum density that could practically be achieved).

Shaw (1980) compared the results which he obtained using a single-sized material with those obtained by Pappin (1979) using a graded material. It was reported that the uniform material gave greater volumetric strains for a given increase in normal stress. The shear strains for the uniform material were almost twice those obtained for the graded material for equivalent stress paths. Shaw suggested that the difference in behaviour was due to the increased voids ratio and reduced particle contact in the single-sized material. The voids ratio (e) of the graded material was 0.19 whereas that of the single-size material was 0.68.

Robinson (1974) postulated that k_2 (see Eqn. 4.4) was dependent on the angularity of the sands which were tested with a value ranging from 0.48 for angular sands, to 0.60 for rounded sands. This indicates that the stiffness of a medium composed of rounded particles is more sensitive to mean normal stress conditions than an angular assembly.

Influence of Moisture: Hicks (1970), reviewing previous work in America, stated that the resilient modulus of a totally saturated sample of graded material differs only slightly from that of a dry sample, but that for a partially saturated material the stiffness increases substantially. This effect, probably due to suction which alters the pore pressure and therefore the effective stress (i.e. that part of the load carried by the soil skeleton or matrix), is unlikely to make any significant contribution to the behaviour of an assembly of large uniform particles.

4.3.2 Stress History

The properties of a granular material at any instant are dependent both upon the deposition and the subsequent stress history. This may be explained by the concept of fabric, as discussed in Section 4.2.

Examples of the Effect of History on Behaviour include:

(a) When a granular material is subjected to a repeated load of constant amplitude, the fabric and structure change so that the material becomes stiffer, and the proportion of plastic to elastic strain decreases during each successive cycle (e.g. see Fig. 4.2 from Lau 1975).

(b) When monotonic tests are performed on virgin samples at constant stress ratio (η), large shear strains occur (e.g. see Fig. 4.4(a)) which show the constant η tests on Fuji River sand by Tatsuoka 1972). Under resilient conditions, however, the model proposed by Pappin (1979) suggests that no shear strain should occur during loading along those stress paths.

Six unloading tests were carried out during this project (on sample D-4 - see Chapter 6) after a considerable amount of resilient testing. The stresses were reduced so that no change in shear strain occurred. The results (see Fig. 4.4(b)) clearly vindicate Pappin's model. The disparity between Tatsuoka's and those presented herein result from the differing stress histories of the materials being tested.

4.3.3 Plastic Strain - A Review of current Models

Yield: Taylor and Quinney (1931) investigated the triaxial yield of annealed copper tubes. They observed that behaviour was elastic until the stress state predicted by Von Mises arises, i.e.,

$$(\sigma_1 - \sigma_2)^2 + (\sigma_2 - \sigma_3)^2 + (\sigma_3 - \sigma_1)^2 = 2\sigma_y^2 \qquad \text{(Eqn. 4.6)}$$

where σ_y is the yield stress in a simple tension test.

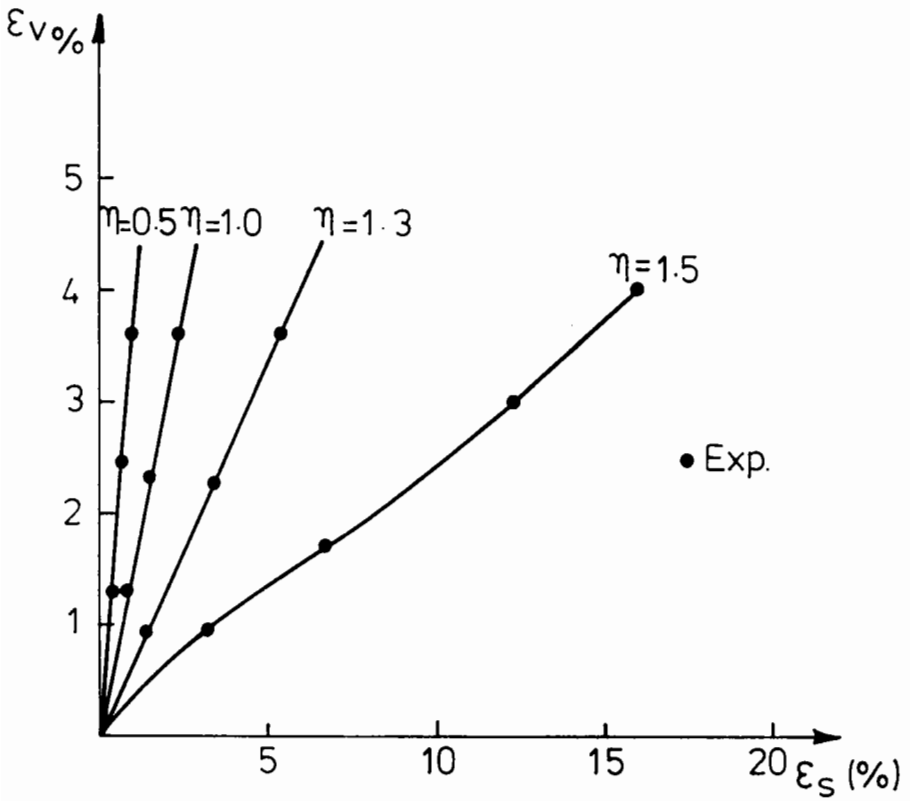

Fig. 4.4(a) Constant η Tests on Virgin Samples of Fugi River Sand (Tatsuoka 1972)

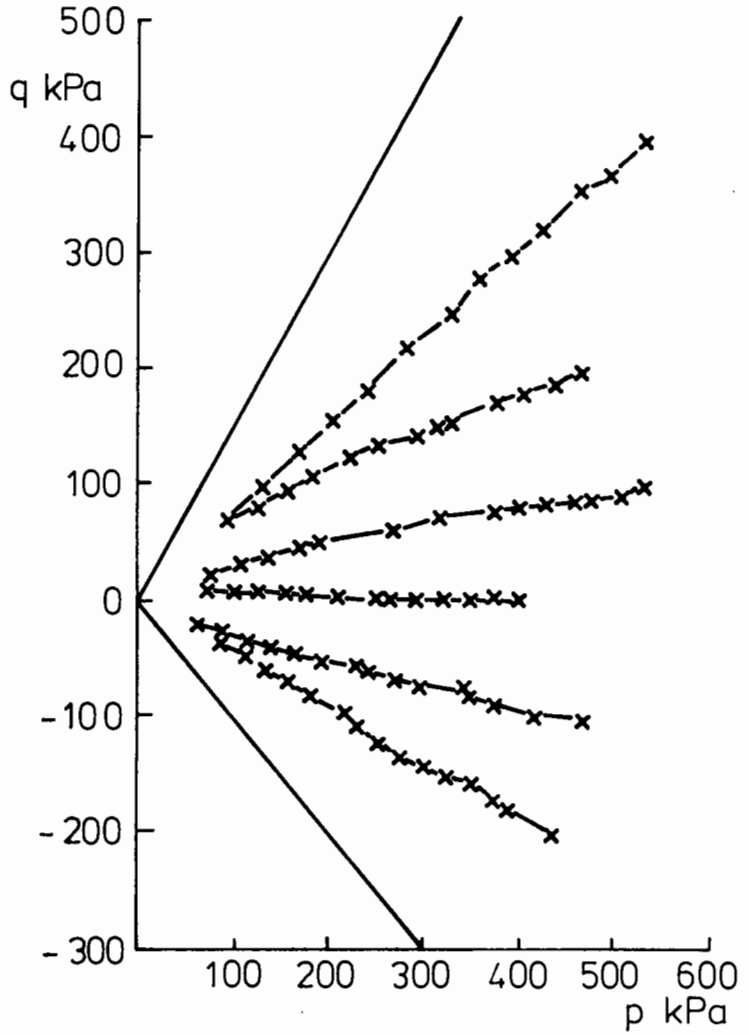

Fig. 4.4(b) Zero Shear Strain Tests on Denstone After Extensive Test Programme

They noted, furthermore, that when the material reached the yield locus (i.e. the set of points at which the yield criterion is met), further increments of stress always resulted in increments of plastic strain which had a direction normal to the yield locus.

Granular materials, like copper, exhibit strain hardening. The Critical State Theory postulates that the yield locus in q-p' stress space is given by an ellipse (major axis along q = 0) which passes through the origin and the "highest" effective stress which the material has experienced during its history. In Fig. 4.5(a), the yield loci for a sample of soil as predicted by Critical State Theory are shown as the soil is loaded from stress states 1 to 4. It is predicted that when the stres path is inside the current yield locus only elastic deformations can occur. When a stress path traverses the locus, strain increments occur at right angles to the yield locus (as observed during Taylor and Quinney's tests on copper), as shown in Fig. 4.5(b). Soils actually behave differently. In particular they exhibit non-associated flow (i.e. they do not obey the normality condition) and they strain plastically despite remaining within the yield locus. These differences between the model and reality are especially important during repeated loading.

Elasto-Plastic Behaviour during Repeated Loading: In order to model the experimental phenomenon of plastic strains occurring during repeated loading while the stress path remained within the "yield locus", Carter et al (1978) proposed a modification to the Critical State Theory (see Fig. 4.5(c)). They suggested that during unloading, the yield locus (which intercepts the p' axis at p'_c) would contract towards the origin so that:

$$\frac{dp_c'}{p_c'} = \Theta \frac{dp_s'}{p_s'} \qquad \text{(Eqn. 4.7)}$$

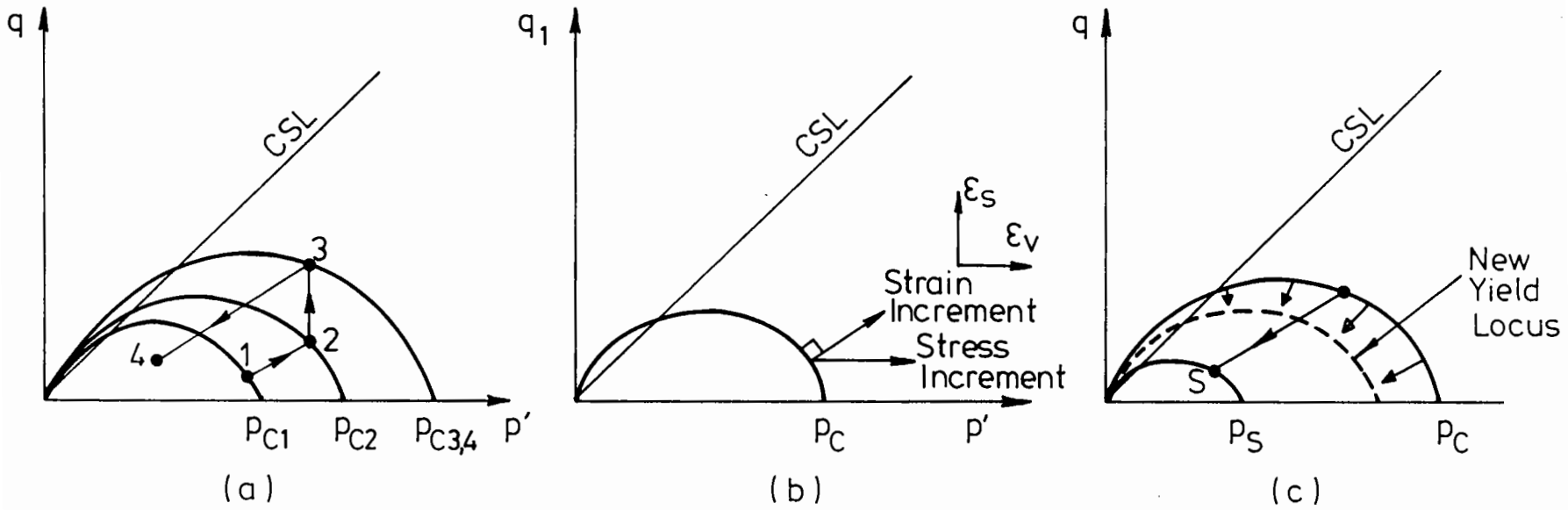

Fig. 4.5 Yield in Critical State Theory

where, p_s represents the intercept of a similar ellipse through the unloaded stress S, and where Θ is a material constant ($\Theta << 1$).

The model predicts that during repeated loading along stress paths, normally treated as being within the yield locus, plastic strains and (when drainage is allowed) densification will occur. This reduction in specific volume results in the material hardening law being changed so as to stiffen the soil during yielding.

A host of other cyclic loading models of varying sophistication have been advocated. Ghabousi and Momen (1982), in their model, propose a yield locus which need not be symmetrical about the isotropic stress line, but which can account for anisotropy due to kinematic hardening. Their flow rule is non-associated (in fact, only plastic shear strains are accounted for by the flow rule). Permanent volumetric strains are calculated subsequently using an energy method, which treats consolidation and dilation effects separately. The hardening law involves a plastic modulus which takes into account an experimentally derived function relating plastic stiffness to plastic strain, as well as parameters accounting for the behaviour during stress reversal.

Pappin (1979) and Shaw (1980) produced models to predict the long-term development of plastic strains in granular materials under constant amplitude repeated load. These models were designed specifically for pavement and highway engineering purposes. The materials in these structures have very different stress histories from most soils since during compaction and construction loading, they will have experienced much higher stresses than are to be expected during service conditions. The models for these materials must, therefore, be concerned with very high numbers of stress applications, all of which remain substantially below the "yield locus".

Habib and Luong (1978) recognised the importance of volumetric strains for granular material mechanics. They produced an impressive series of results from tests on Fontainbleam sand (see Fig. 4.6). These show the importance of η_D, the stress ratio at which volumetric behaviour changes from compressive to dilatant. When the stress ratio is greater than this value the plastic volumetric strains will be dilatant. This has important consequences for plastic shear strains as well, since the ratio η_D represents a state at which the soil fabric is ruptured. Unfortunately, their results are not presented in terms of shear strain, and consequently no marked difference between permanent shear strain development above and below the ratio η_D is obvious from the $q-\epsilon_a$ graph. The shear strains when $\eta > \eta_D$ are, however, greater than for those paths below η_D by a significant amount.

4.3.4 The Influence of the Intermediate Principal Stress

4.3.4.1 Introduction

In general, theories of material properties are based on the assumption that behaviour is dependent only upon the scalar quantities q (the shear stress) and p (the mean normal stress). For ductile metals, for example, both elastic strains and proximity to yield can be accurately calculated using q and p alone. Researchers have long been aware that where granular materials are concerned, however, other parameters must be ascertained before strains and proximity to yield can be calculated. One of these parameters, the directions of the principal stress, will be discussed below in 4.3.5.

A second important parameter describes the magnitude of the intermediate principal stress relative to the major and minor principal stresses. One quantification of this is Lodes parameter μ which is defined

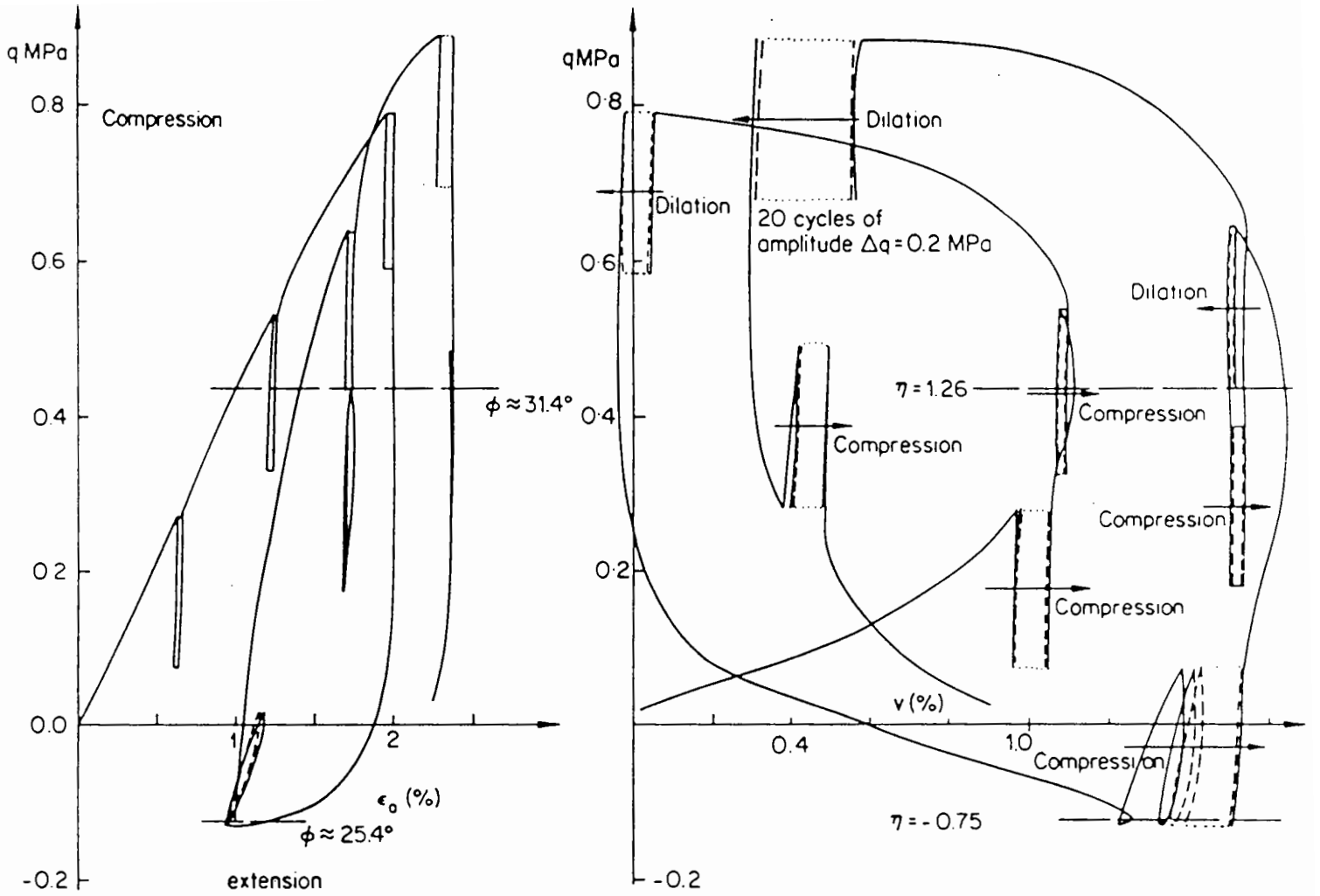

Fig. 4.6 Triaxial Test on Fontainebleau Sand (Habib and Luong 1978)

as:

$$\mu = (2\sigma_2 - \sigma_1 - \sigma_3) / (\sigma_1 - \sigma_3) \qquad \text{(Eqn. 4.8)}$$

But the more commonly used parameter in soil mechanics is b, defined as:

$$b = (\sigma_2 - \sigma_3) / (\sigma_1 - \sigma_3) \qquad \text{(Eqn. 4.9)}$$

Investigations into the influence of b on failure and stress-strain behaviour have been reported in a number of articles. The majority of these have involved the "true triaxial apparatus", although several early investigations made use of the hollow cylinder arrangement (eg. Kirkpatrick 1957). The literature shows that the value of b significantly affects behaviour.

4.3.4.2 Influence of b on Failure Conditions

(a) Shear Strength

Reades and Green (1976) carried out a comprehensive test programme in order to investigate the influence of b on the failure conditions. Their results show that as the value of b changes from 0 to 1 the value of the shear strength parameter Φ (= arcsin $[(\sigma_1 - \sigma_3) / (\sigma_1 + \sigma_3)]$) increases by 6-7°. This is shown in Fig. 4.7. As can be seen, the increase in Φ is most dramatic in the range $0 < b < 0.14$ and least pronounced in the range $0.14 < b < 0.5$.

A comprehensive survey of the effect of b on Φ was performed by Ladd et al (1977). They collected information on the relationship between b values and experimental Φ values from the available literature. Fig. 4.8 shows their compilation. Every report to date indicates that Φ rises sharply as the value of b increases from 0 to 0.15 - 0.2. There does

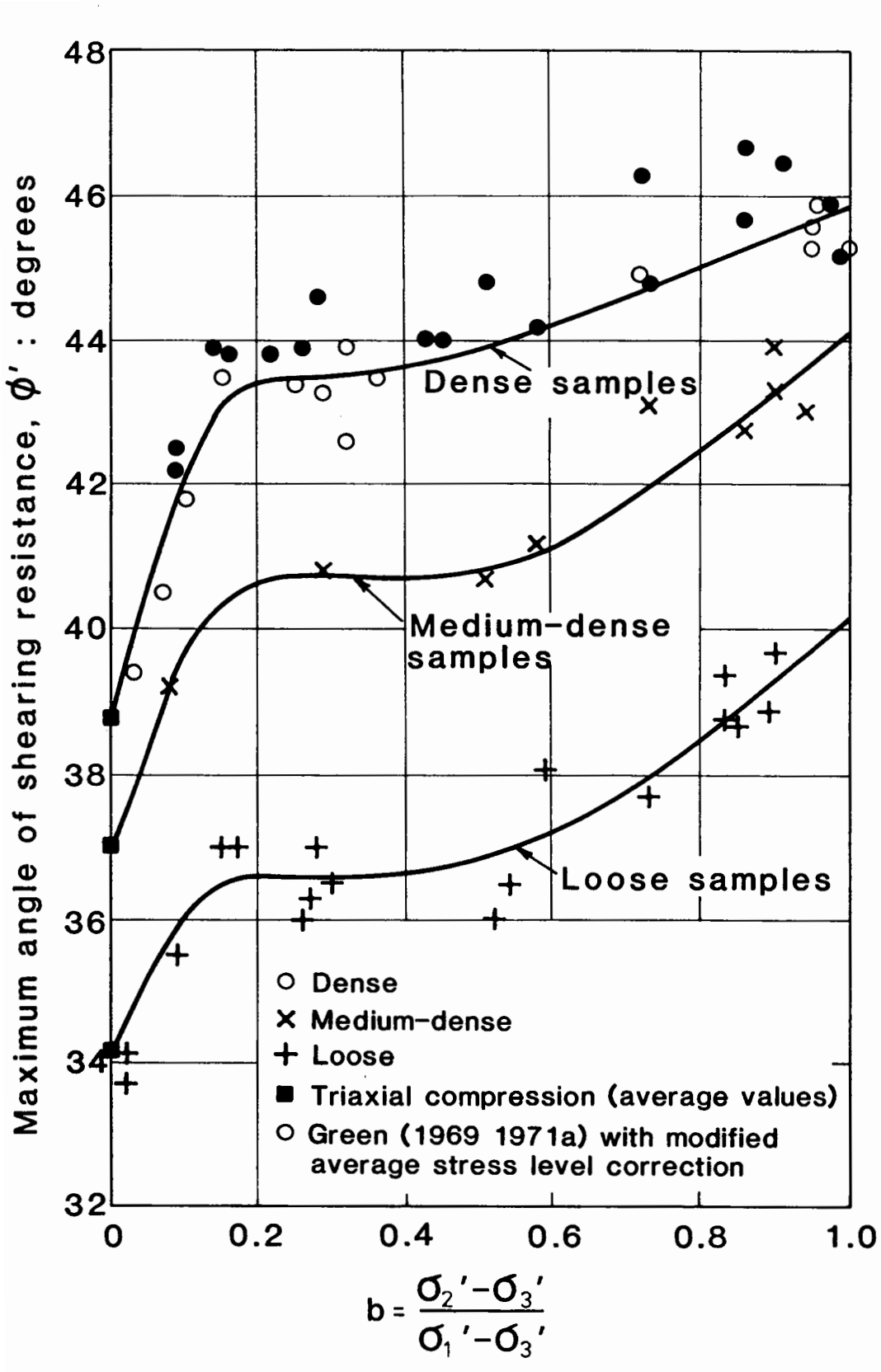

Fig. 4.7 THE EFFECT OF THE INTERMEDIATE STRESS PARAMETER b ON THE STRENGTH PARAMETER ϕ (FROM READES AND GREEN 1976)

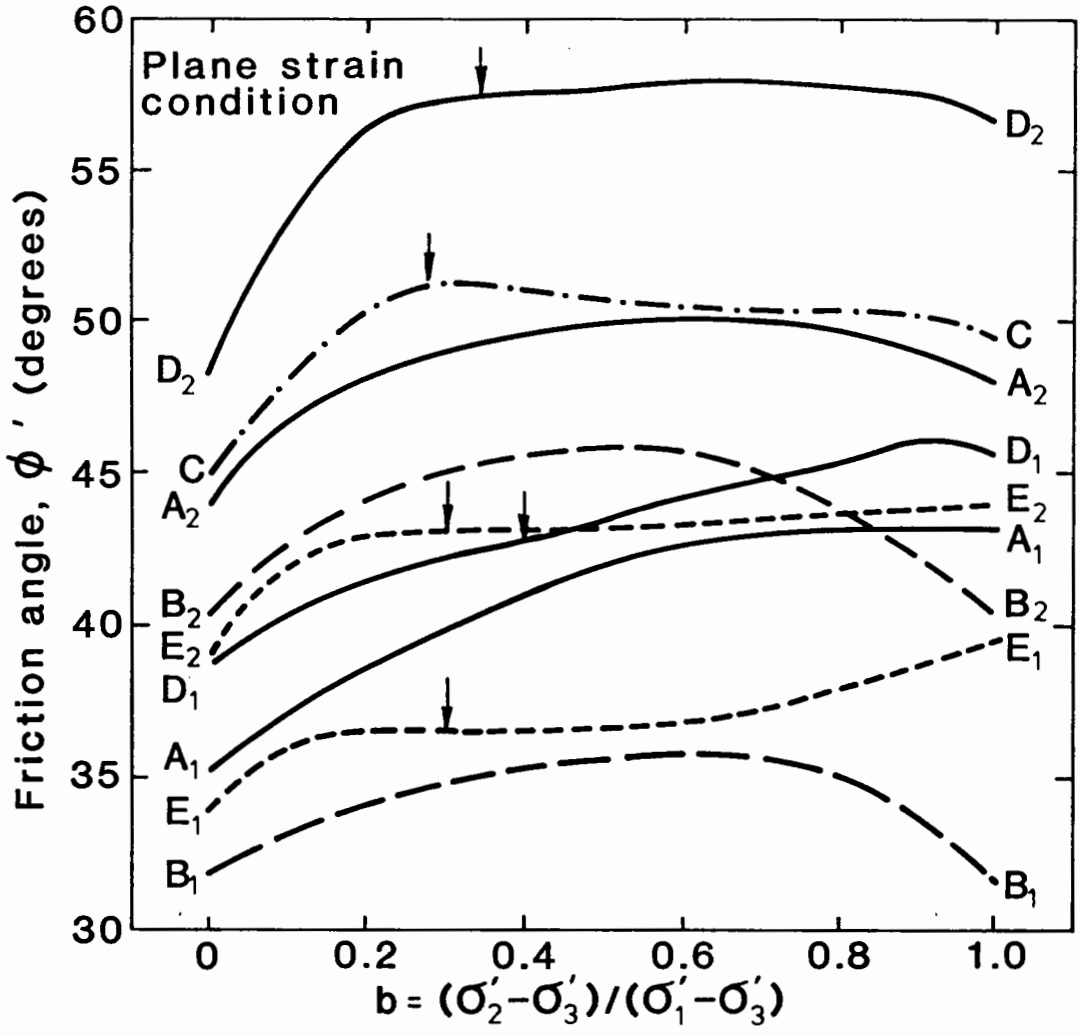

LINE	SAND	D_r (%)	REFERENCE
A_1	Ottawa	med.loose	Ko and Scott (1968)
A_2		med.dense	
B_1	Med Fine Loch Aline	30	Sutherland and Mesdary (1969)
B_2		80	
C	River Welland	dense	Proctor and Barden (1969)
D_1	Monterey No. 0	27	Lade and Duncan (1973)
D_2		98	
E_1	Ham River	loose	Reades and Green (1974)
E_2		dense	

Fig. 4.8 EFFECT OF INTERMEDIATE PRINCIPAL STRESS ON THE DRAINED FRICTION ANGLE OF SEVERAL SANDS.

appear to be some confusion, however, about the behaviour of Φ as b approaches 1. Some reports indicate that the value of Φ increases, some that it decreases. This discrepancy is usually considered to be due to experimental problems e.g. the rigidity of the σ_2 platens when testing close to b = 1 may cause restraint which will increase sample strength.

It is most important at this stage to note the difference between the various parameters used to describe mobilized strengths and yield. Reades and Green (1976) and Lade and Duncan (1973) have shown that as b increases so does Φ. If, however, the stress ratio (η) is used to describe mobilized strength, a very different pattern appears and a plot of η_f vs. b will show the reverse effect: as the value of b increases, the strength decreases. The use of Φ_f as a strength parameter in most studies to date may possibly have been the result of Bishop's 1966 Rankine Lecture. In this he introduced data (from Cornforth) which tended to indicate that the Mohr-Coulomb yield criterion was appropriate, and that the Tresca and Von Mises criteria overestimated the strength which would be mobilized in a granular material. Subsequent work at Imperial and elsewhere has shown that b is an important parameter. As can be seen from Fig. 4.8 above, the Mohr-Coulomb criterion derived from triaxial compression tests underestimates the shear strength Φ which can be mobilized, whereas the Von Mises criterion derived from similar tests overestimates the strength η_f which may be mobilized. This is shown in Fig. 4.9 using test results abstracted from Lade and Duncan 1973. The reduction in value of η_f is given as a proportion of η_f at b = 0 (compression triaxial). Superimposed are the results obtained by Shaw (1980) and Pappin (1979). Shaw used single-size and Pappin used graded crushed limestone and both noted the loss in η_f during extension space monotonic testing. Lade and Duncan (1975) propose the use of the criterion f, where:

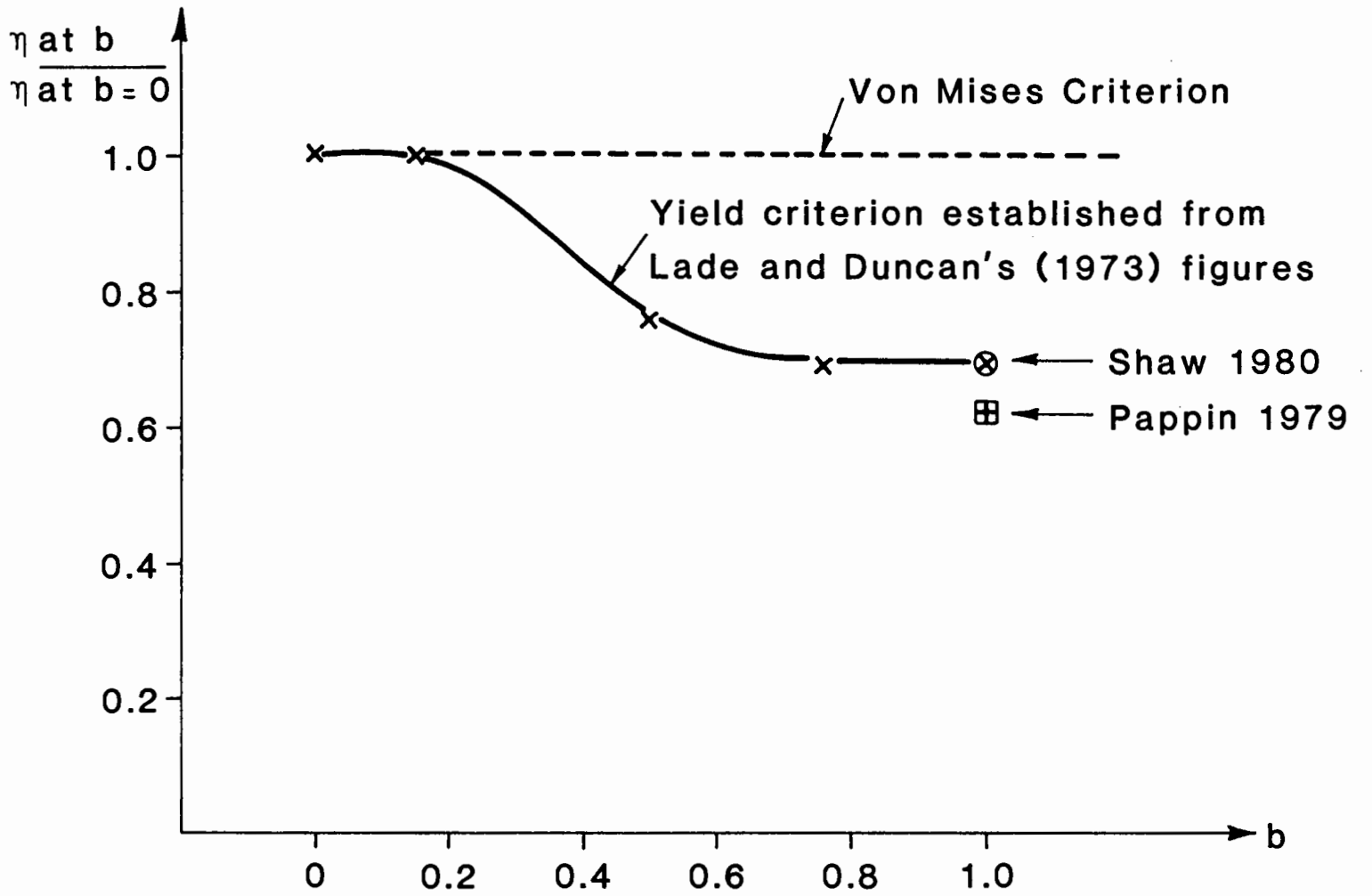

Fig. 4.9 THE EFFECT OF THE INTERMEDIATE PRINCIPAL STRESS PARAMETER (b) ON THE YIELD STRENGTH

$$f = I_1^3/I_3$$

$$I_1 = \sigma_1 + \sigma_2 + \sigma_3 \qquad \text{(Eqn. 4.10)}$$

$$I_3 = \sigma_1\,\sigma_2\,\sigma_3$$

Fig. 4.10 shows the results of failure tests carried out by four independent researchers. As can be seen, the Lade and Duncan model agrees fairly accurately with their results although it invariably overestimates strengths at intermediate values of b.

(b) Strains at Failure

Fig. 4.11(a) shows the axial strain at the peak strength of the material from the tests carried out by Reades and Green. This is greatest at b = 0 (20% for a loose sample) and least at b = 1 (4% for a loose sand). The volumetric strains at failure are shown in Fig. 4.12. As can be seen, the most dilatant strains occur in the vicinities of b = 0 and b = 1 and the most compressive strains occur in the region $0.4 < b < 0.5$.

Lade and Duncan (1973) also found that the axial strains at failure were greatest at b = 0. Unlike Reades and Green, however, their results showed that the value of axial strains at failure always decreased with increasing value of b. But in tests on loose sand, they found that the reduction in the axial strain at failure is very small as b increases from about b = 0.6 to b = 1.0. This tendency (as shown in Fig. 4.13) might lead to the conclusion that if the voids ratio of the sand was further increased, a minimum value of axial strain at failure would occur at a value of $b < 1$. This could then agree with the results of Reades and Green.

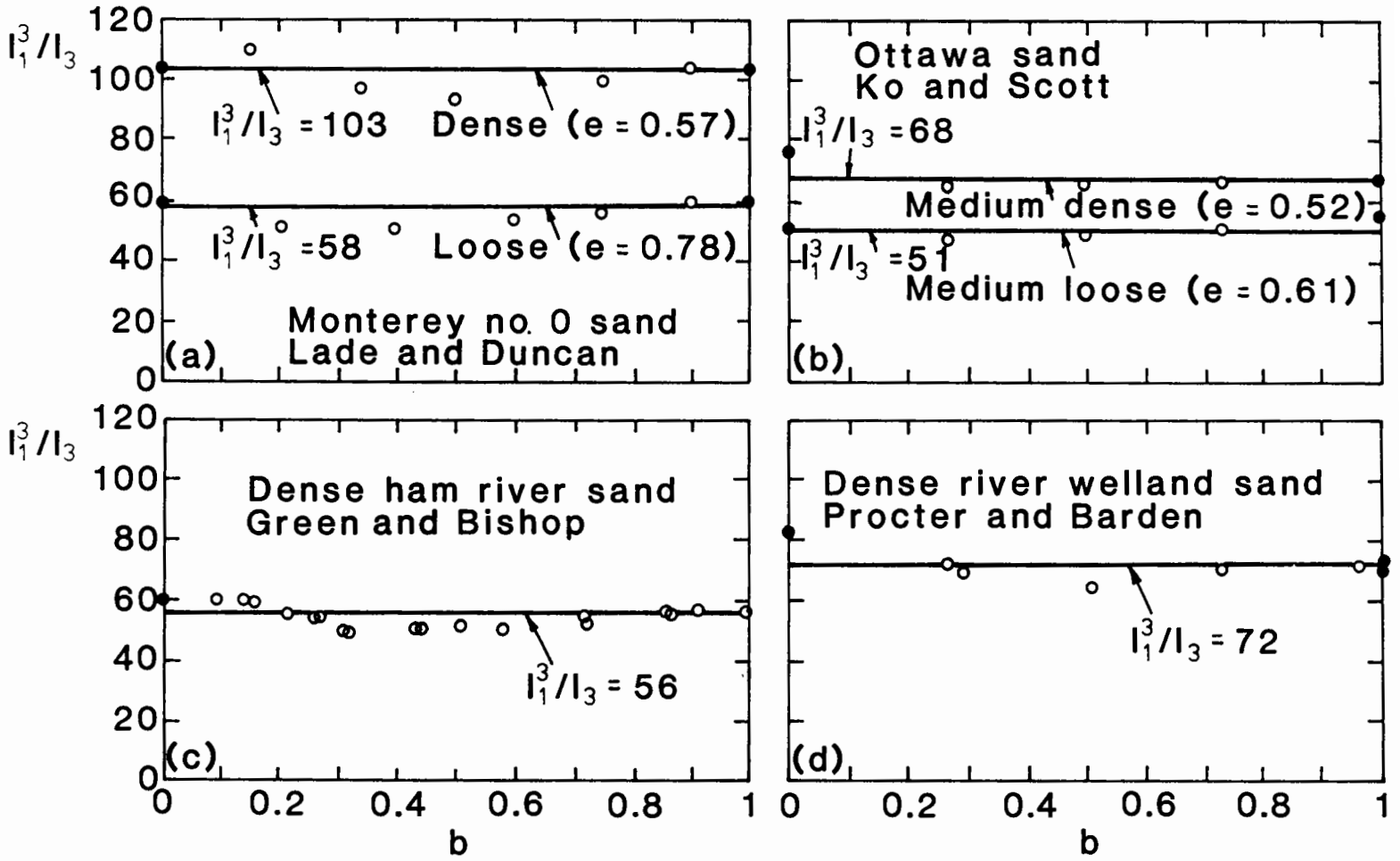

Fig. 4.10 THE COMPARISON OF LADE AND DUNCAN (1975) FAILURE CRITERION WITH DATA FROM FOUR INDEPENDENT SOURCES

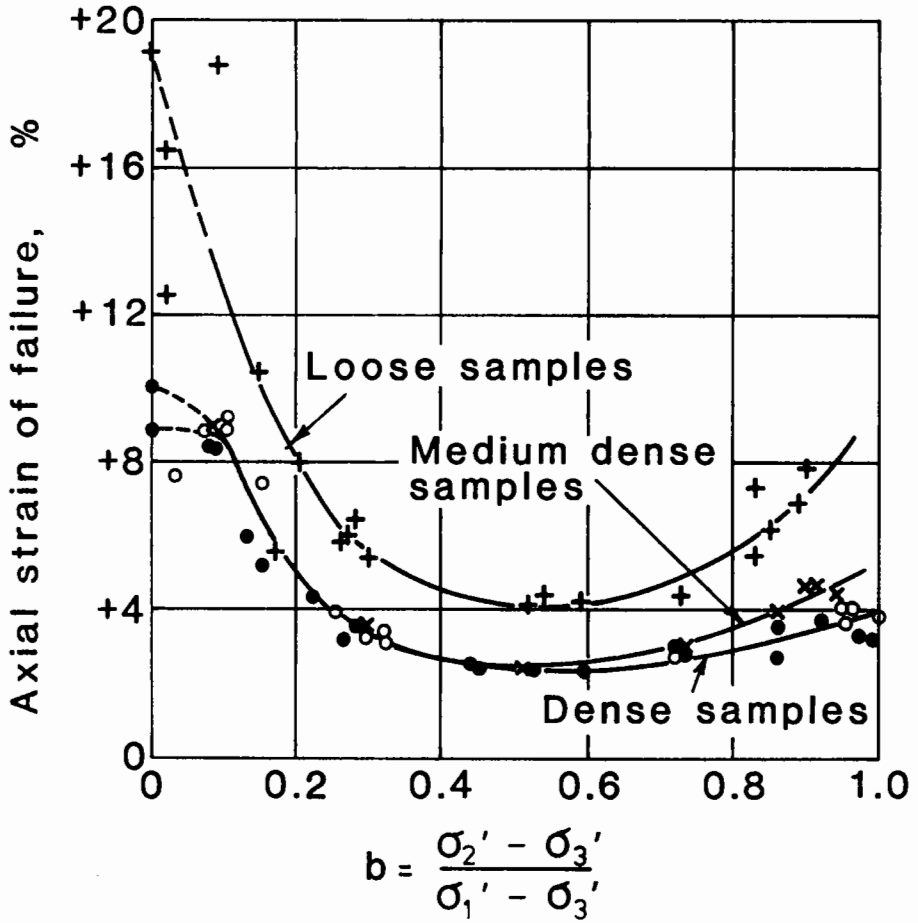

Fig. 4.11 AXIAL STRAINS AT FAILURE

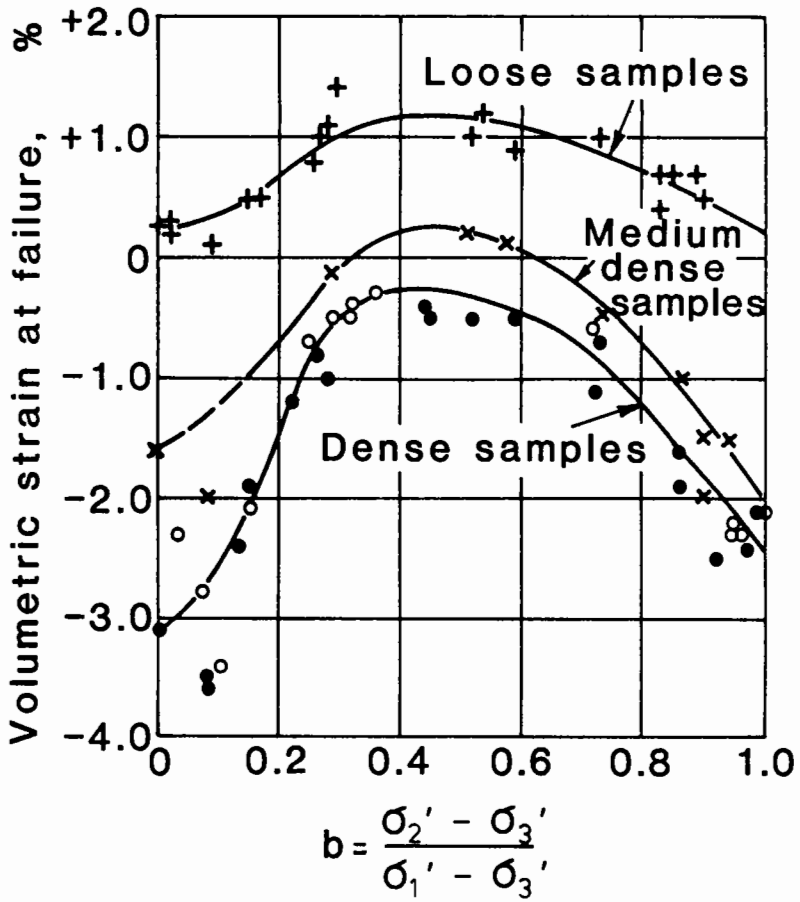

Fig. 4.12 VOLUMETRIC STRAINS AT FAILURE

THE INFLUENCE OF THE INTERMEDIATE PRINCIPAL STRESS ON STRAINS AT FAILURE (READES AND GREEN 1976)

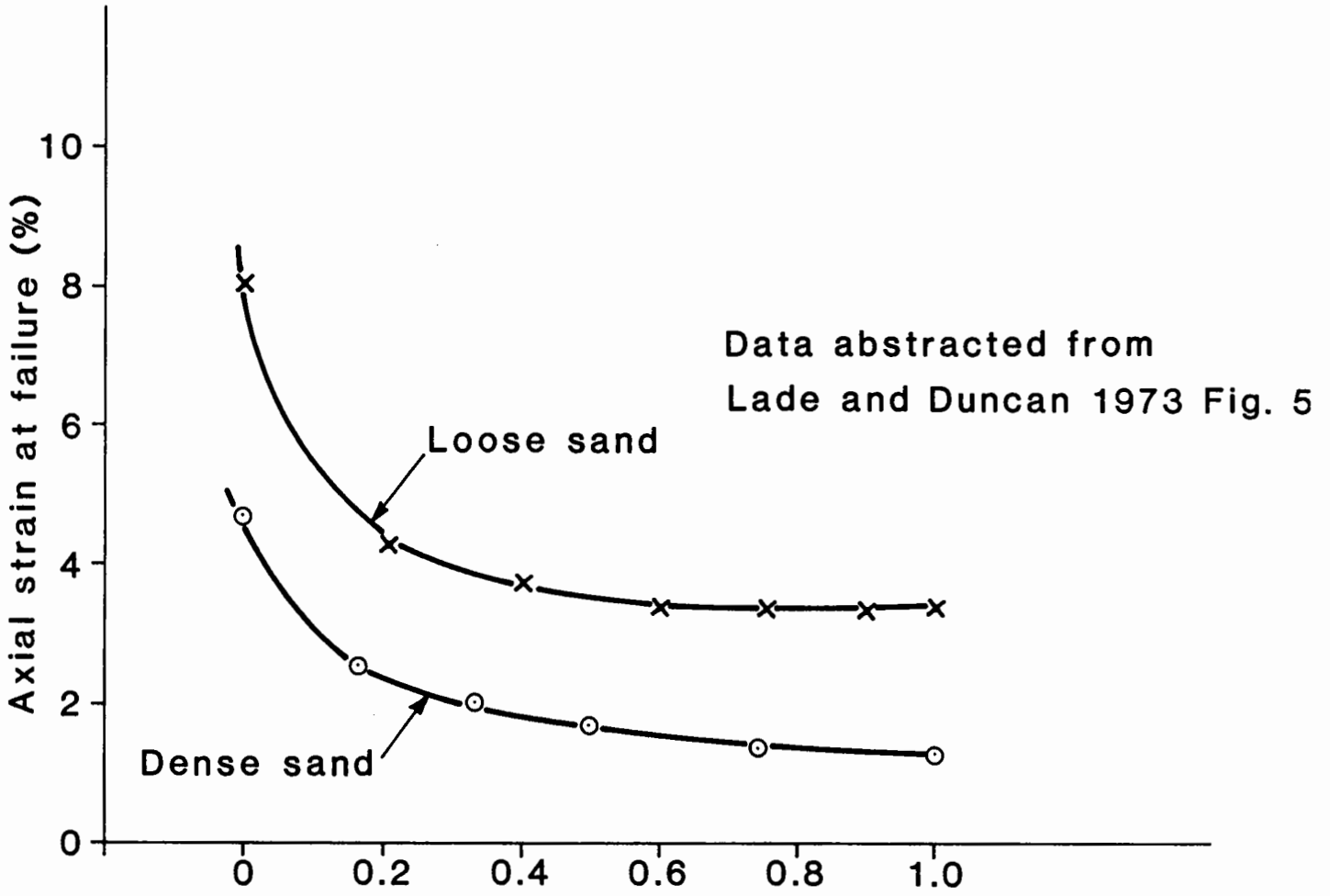

Fig. 4.13 THE INFLUENCE OF THE INTERMEDIATE PRINCIPAL STRESS ON AXIAL STRAIN AT FAILTURE (AFTER LADE AND DUNCAN 1973)

4.3.4.3 Influence of b on Stress-Strain Behaviour

(a) Pre-failure Strains in Monotonic Tests

Lade and Duncan (1973) present the results of monotonic tests on both dense and loose Monterey Sand using a range of different values of b and keeping σ_3 constant. Fig. 4.14 shows their results using the dense samples: both axial and volumetric strains are given. The maximum principal stress difference at failure is an indication of the material's strength relative to the Mohr-Coulomb failure criterion. The results in Fig. 4.14 have been abstracted from Lade and Duncan's paper and are shown again in Fig. 4.15 in terms of (η), the shear to normal stress ratio. It appears that the material increases in stiffness with rising value of b when shown against the Mohr-Coulomb parameter, but decreases in stiffness with increasing value of b when shown against (η), the Von Mises parameter.

(b) The Effect of b on Resilient Behaviour

Work at Nottingham has involved triaxial testing in both compression space (b = 0) and extension space (b = 1). Pappin (1979) realised that behaviour was likely to differ according to whether compression or extension space was being used, and he made a correction to allow for this. Having surveyed the literature, he decided that the Mohr-Coulomb criterion was "conservative but still much better than the other two criteria (Extended Von Mises and Extended Tresca)." His correction involved extending the Mohr-Coulomb criterion for use in sub-failure stress conditions in order to transform the stresses in triaxial extension to an equivalent triaxial compression stress state. He noted that this correction produced better predictions for shear strains, although not for volumetric strains.

Pappin's work showed that it was possible to achieve sensible results by extending the yield criterion into the elastic region and by using the

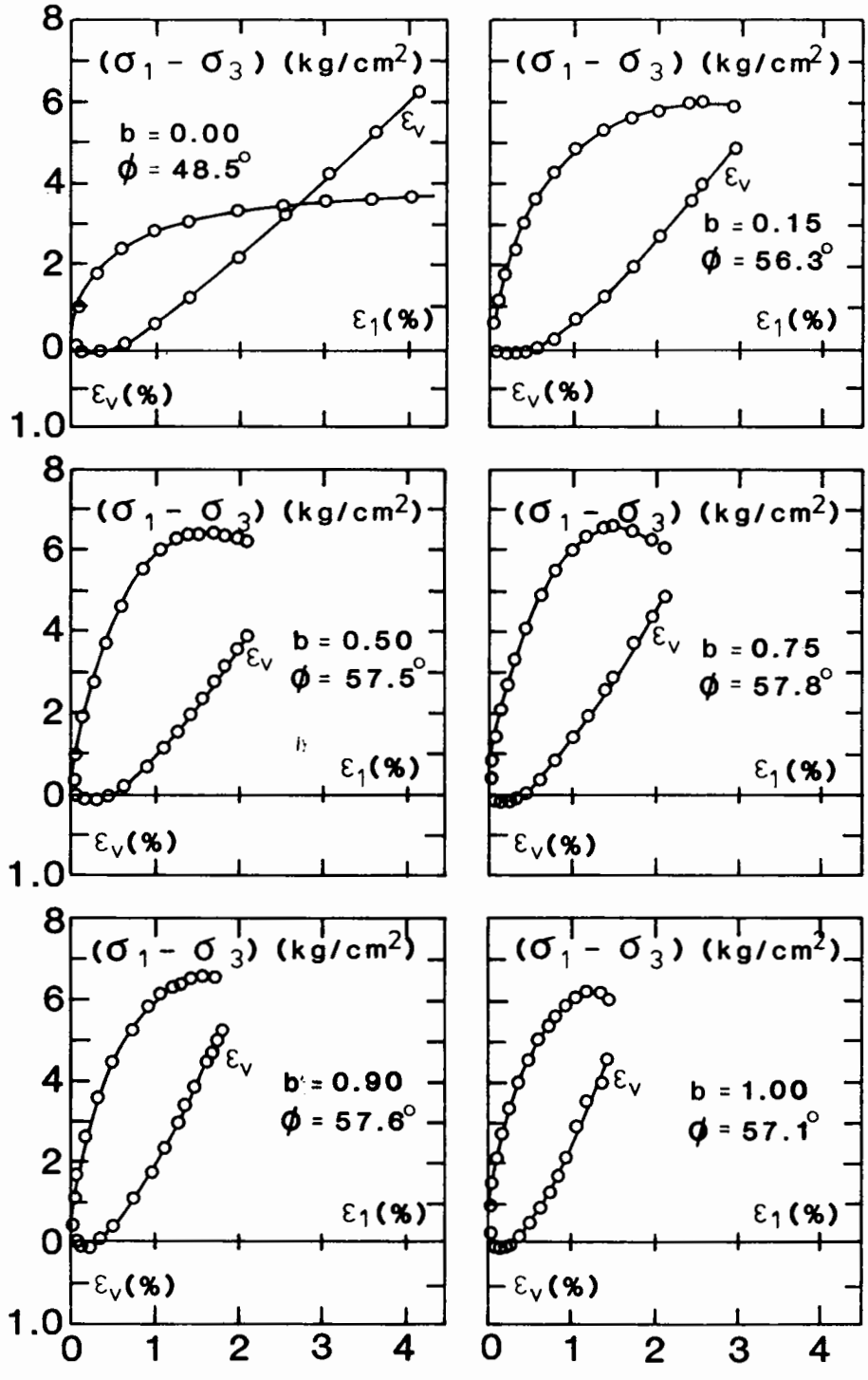

Fig. 4.14 STRESS - STRAIN RESULTS FROM A SERIES OF TESTS CONDUCTED WITH A RANGE OF b VALUES (LADE AND DUNCAN 1973)

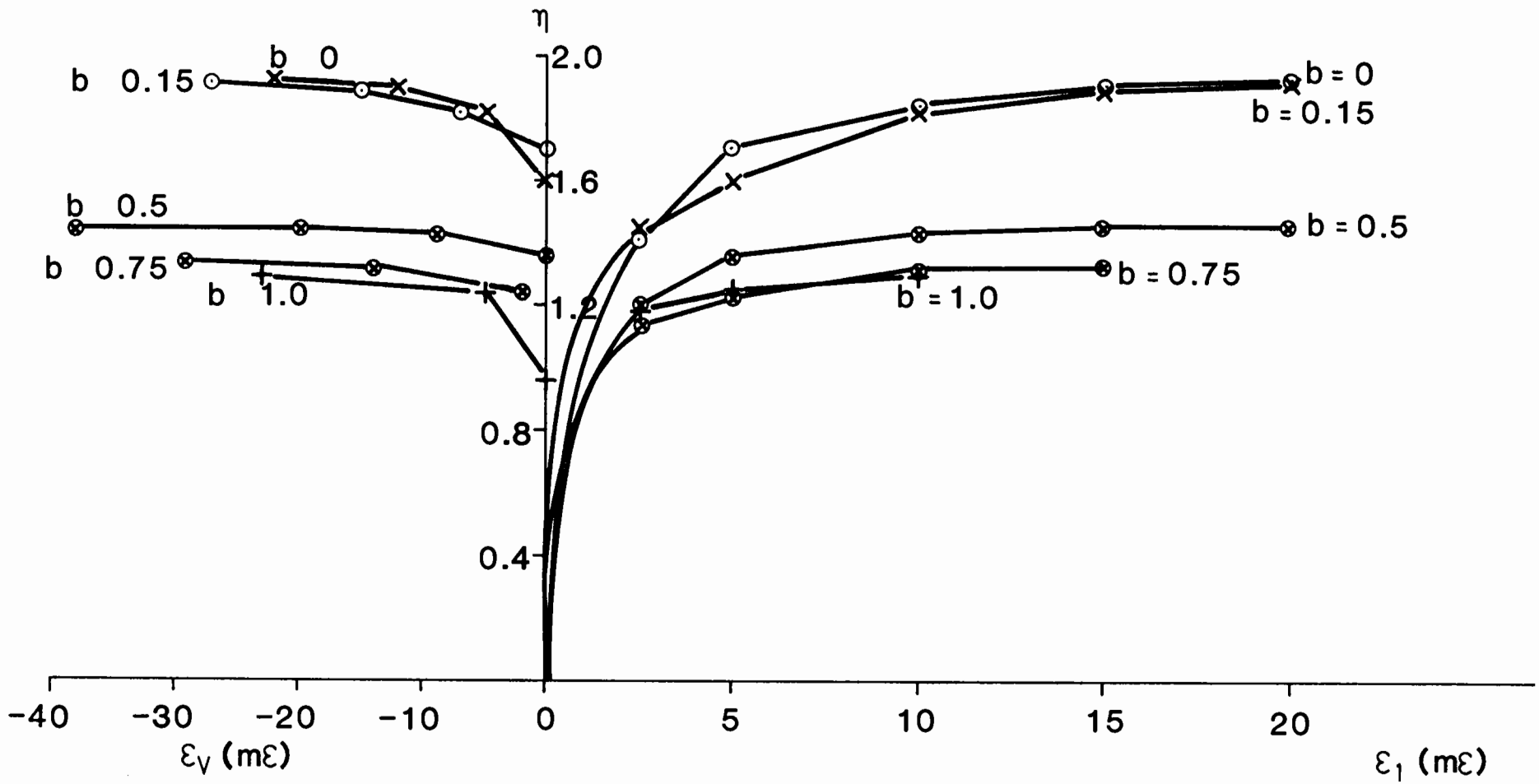

Fig. 4.15 LADE AND DUNCANS (1973) RESULTS SHOWN AGAINST THE VON MISES RATIO (η)

yield formulation as the basis for the strain contours in a generalised stress space. Since he chose to work with the Mohr-Coulomb criterion, however, the model might be expected to overpredict the strains (since the criterion is conservative for failure). The use of the extended Lade and Duncan yield surface as the basis for a generalised strain model may possibly be a useful extension of Pappin's work in this field.

Shaw (1980) used a "biaxial shear box" to apply a three dimensional stress state to a cubical sample. Stresses could be independently controlled in two directions and in the third, plane strain conditions were maintained, the stresses being measured. This provided more variety in the stress states which could be applied. Unfortunately, details of the stresses measured are not given in Shaw's thesis; however, a common conclusion from plane strain tests is that the b value remains fairly constant throughout with a value of around 0.3 (the plane strain direction being the direction of the intermediate principal stress). It appears likely, therefore, that a fairly small range of b values was used.

Wong and Arthur (1985) using the Directional shear cell, found that in plane strain:

$$\sigma_2 = (\sigma_1 + \sigma_3) \times \text{constant} \qquad \text{(Eqn. 4.11)}$$

If this is correct, then the value of b is not constant during plane strain, but varies with the mobilised strength. If b is to remain constant independently of the ratio σ_1/σ_3, the following equation must be satisfied

$$\sigma_2 = (1 - b)\sigma_3 + b\,\sigma_1 \qquad \text{(Eqn. 4.12)}$$

Unless b = 0.5, this cannot be done. Wong and Arthur found that the value of b lay in the region $0.27 < b < 0.33$, and it may consequently be

assumed that the value of b was not a constant during cyclic load testing.

Shaw produced data which showed that satisfactory predictions could be made using the existing compression space (b= 0) model modified by the Mohr-Coulomb transformation. The accuracy of the model in predicting strains is in some ways remarkable considering the experimental difficulties inherent in obtaining reliable results from such a piece of apparatus (eg. shear stresses across non-flexible boundaries and the errors likely to arise from the use of external instrumentation).

No work appears to have been done to consider behaviour when b is a variable while other factors are held constant. In compression testing, extension testing and plane strain testing, the value of b is at least approximately constant throughout. Compression-extension does of course cause a jump in the value of b from 0 to 1. Behaviour when b is continuously changed, however, is not reported, although the HCA arrangement makes this possible. It is likely that as more HCA testing is performed this area will be investigated.

4.3.5 Tests involving Principal Stress Rotation

In many soil structures, principal stress rotation occurs. In order to simulate this feature of the stress history, three major pieces of apparatus have been developed; the well-known simple shear apparatus (Roscoe, 1953), the hollow cylinder apparatus (e.g. Hight, 1983), shown in Fig. 4.16, and the directional shear apparatus shown in Fig. 4.24.

Simple Shear Apparatus: Wroth (1958) tested rotund particle assemblies in the Cambridge Simple Shear Apparatus (CSSA) (Roscoe, 1953). Two materials were used.

(a) Small spherical glass beads with a range of diameters between 0.75 and 0.80mm.

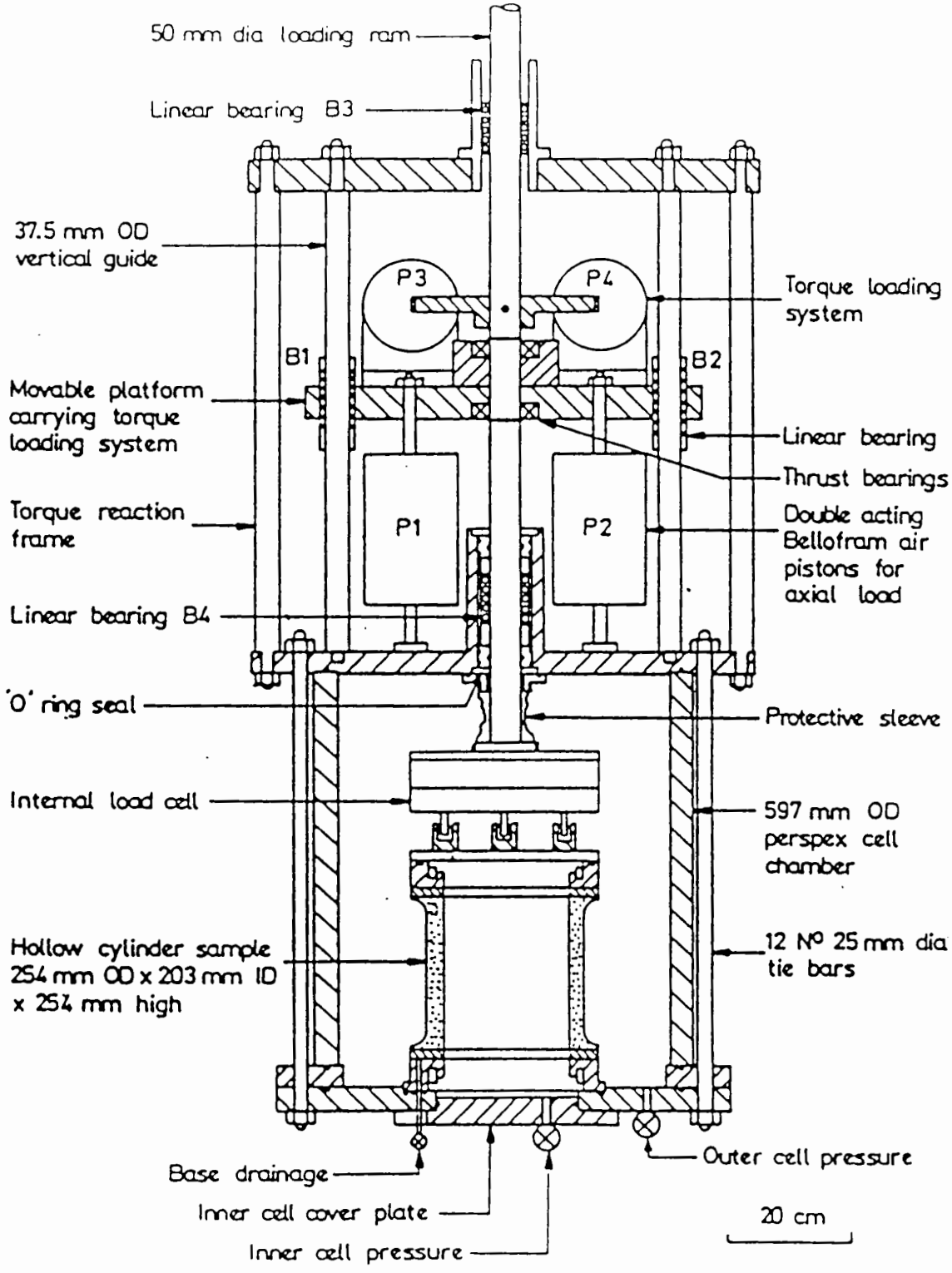

Fig 4.16 Imperial College Hollow Cylinder Apparatus

(Hight 1983)

(b) Industrial reject ball bearings of 1mm diameter tested in both the polished and rusted condition.

These materials were randomly packed in the CSSA and subjected to shear reversals. The shear strain was of a magnitude capable of producing critical state conditions (i.e. constant voids ratio during shearing). Fig. 4.17(a) shows the shear stress during each deformation and Fig. 4.17(b) the voids ratio varying with increasing number of reversals. It is noticed that the voids ratio decreases by a substantial amount as the number of reversals increase. Fig. 4.18 shows how the shear stress changes with the number of shear reversals. As can be seen, the applied shear stress is greatly reduced in the case of the steel balls, but only slightly in the case of the glass beads. By setting the test samples in gelatine at the conclusion of testing, Wroth demonstrated that the particles had become regularly arranged, completely in the case of the steel balls, but not so markedly in the case of the glass beads. He attributed the non-formation of regular arrays by the glass beads to the fact that a range of particle sizes existed.

Youd (1972) performed cyclic shear tests on Ottawa sand in a NGI simple shear apparatus. During each test the shear strain amplitude was held approximately constant. He noticed that all samples experienced considerable compaction. The rate of compaction was dependent on shear strain amplitude as shown in Fig. 4.19 and was observed to be independent of vertical stress or rate of loading (between 0.2 and 2 Hz).

Ansell (1977) developed a simple shear apparatus at Nottingham and performed tests on a single-size crushed limestone, in an attempt to simulate the behaviour of railway ballast in the track. The applied stress paths in q,p' space have the form shown in Fig. 4.20(a) and tests were performed at a number of stress ratios below the static failure ratio. Fig. 4.20(b) shows the permanent shear strain contour chart which Ansell

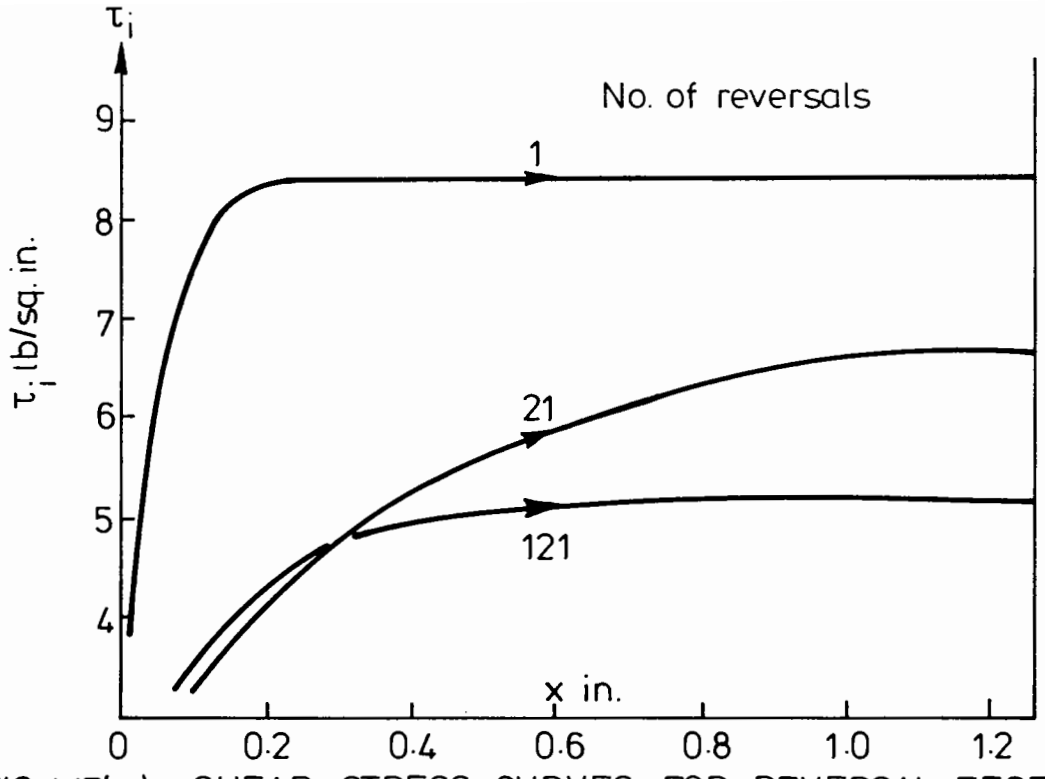

FIG.4.17(a) SHEAR STRESS CURVES FOR REVERSAL TESTS ON STEEL BALLS

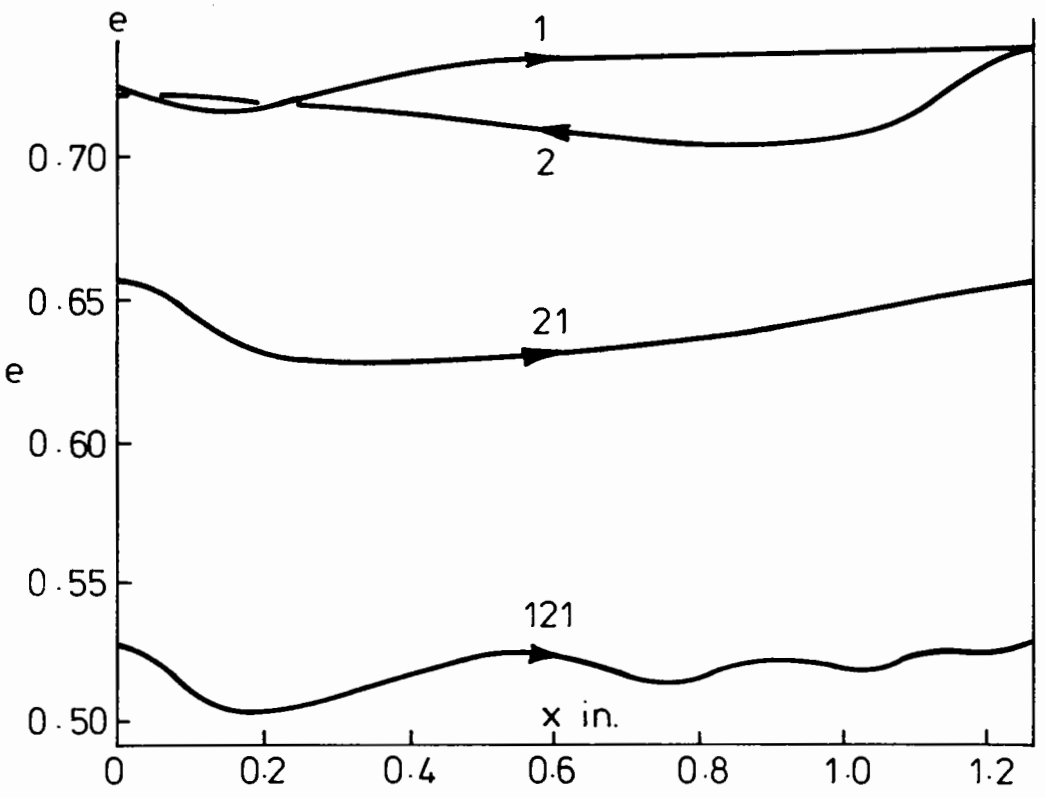

FIG.4.17 (b) VOIDS RATIO CURVES FOR REVERSAL TESTS ON STEEL BALLS (after Wroth (1958)

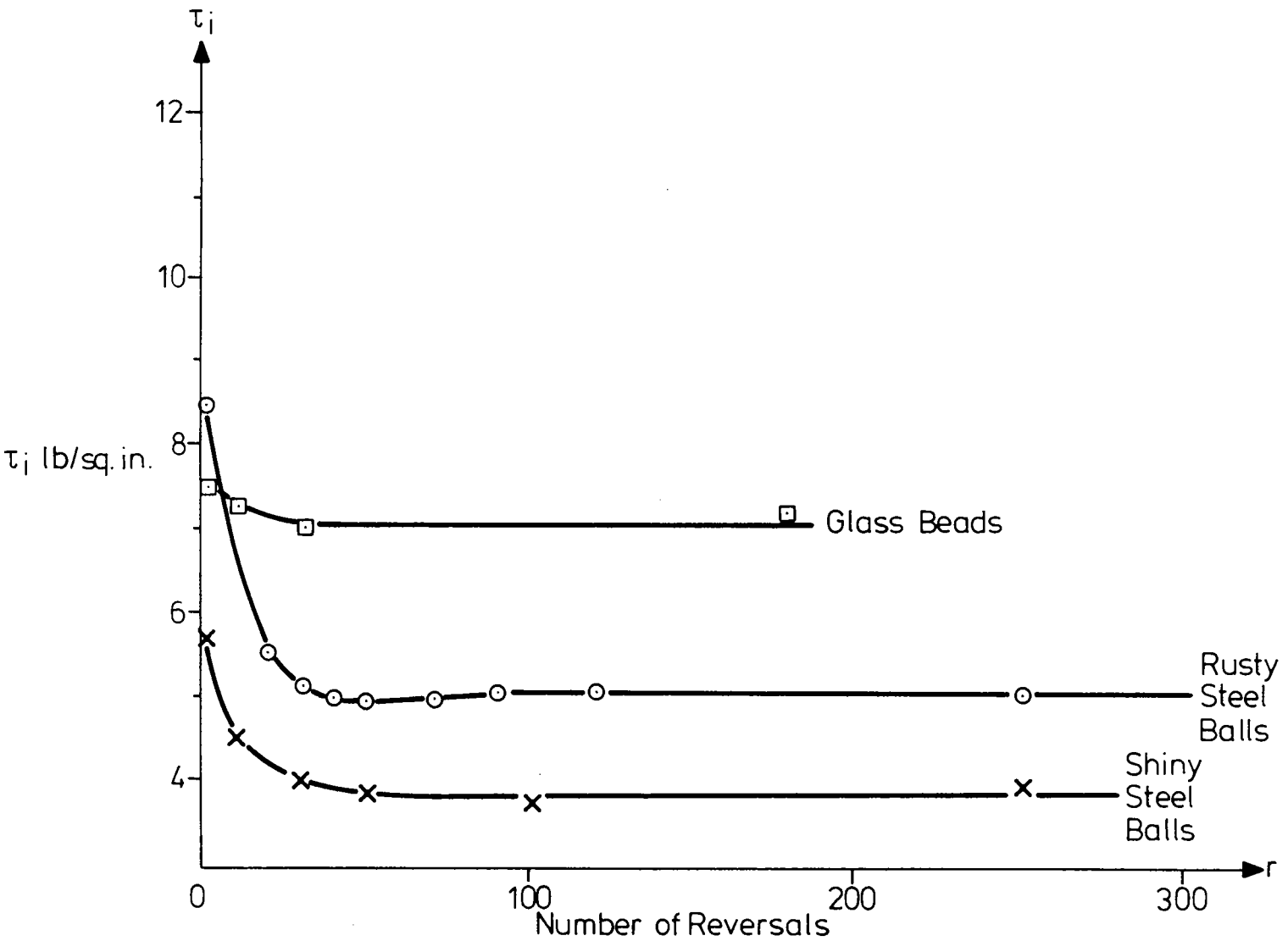

FIG. 4.18 SHEAR STRESS CURVES FOR REVERSAL TESTS ON SEVERAL MEDIA (after Wroth 1958)

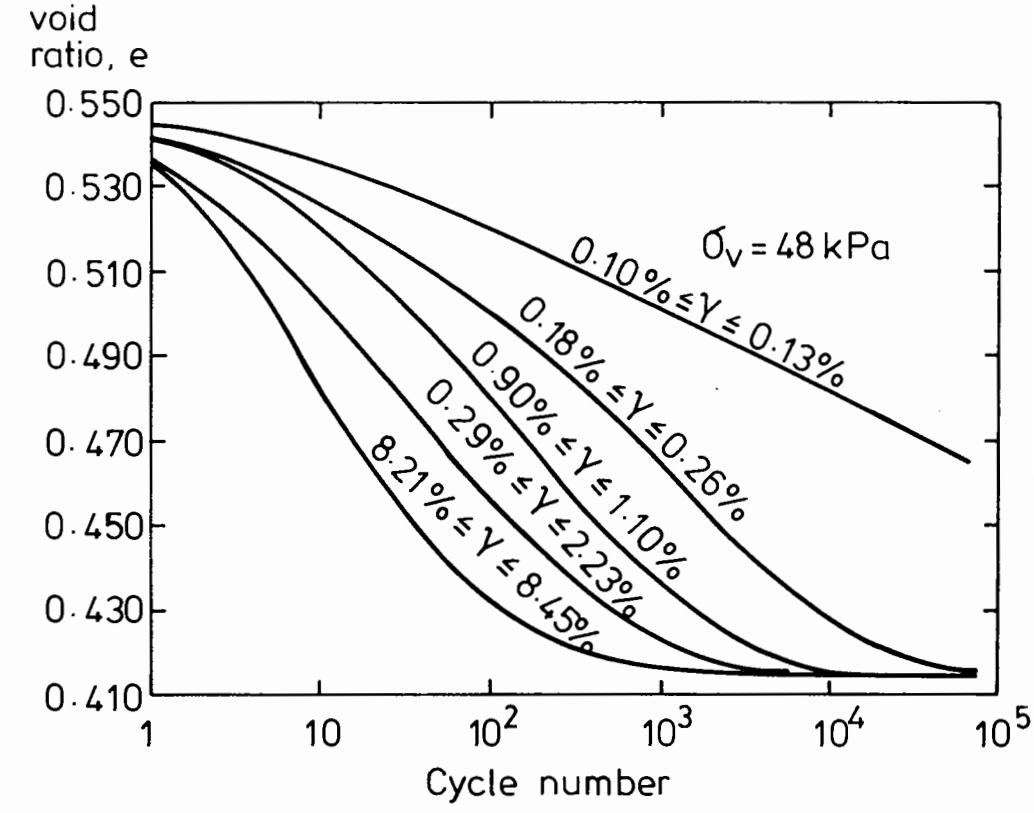

(a) Effect of Shear - Strain Amplitude on Compaction

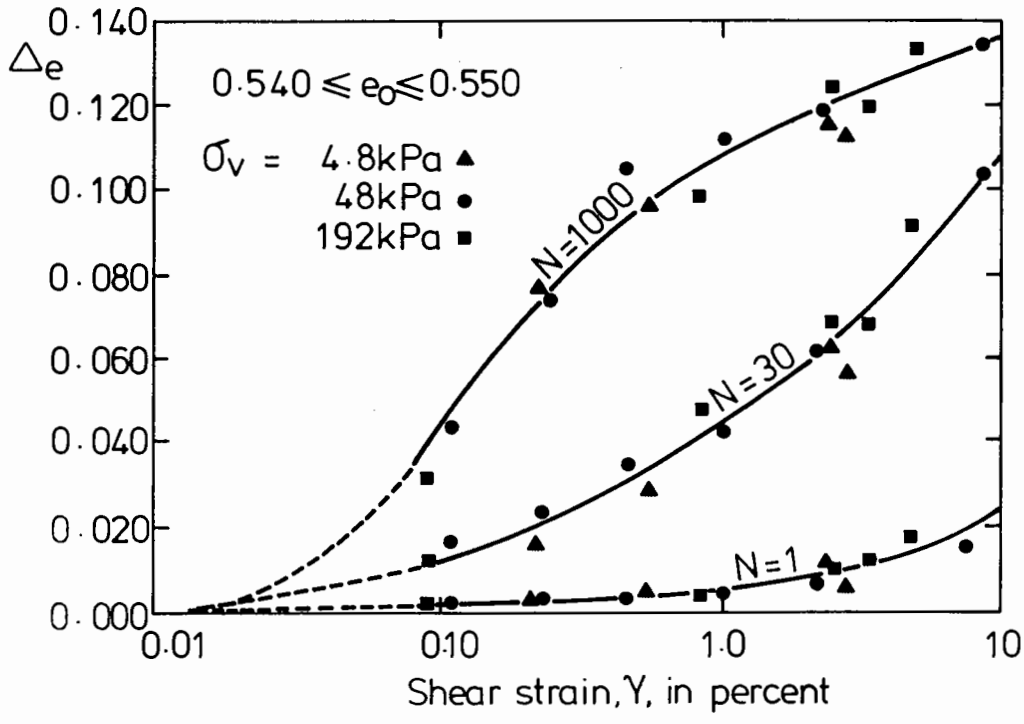

(b) Void Ratio changed as a Function of Shear-Strain and Number of Cycles (N)

Fig. 4·19 Simple Shear Tests on Ottawa Sand (from Youd 1972)

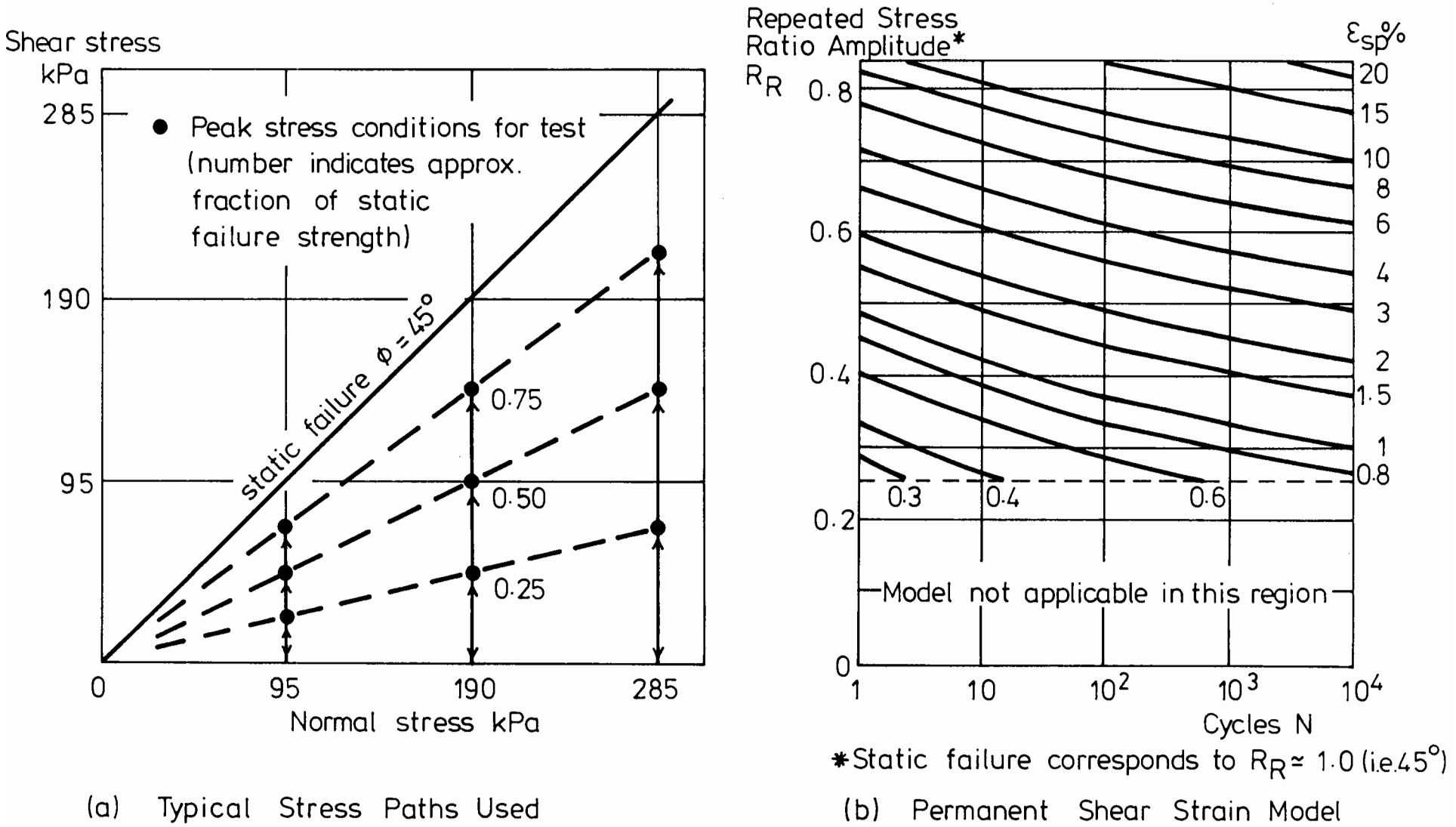

Fig. 4.20 Permanent Shear Strain Behaviour of Single-Size Crushed Limestone (from Ansell 1977)

derived. The same material was subsequently tested by Shaw (1980) in the triaxial apparatus, and Fig. 4.21 shows how permanent shear strains developed in that apparatus, for several stress paths. If, for example, path PA in Fig. 4.21(a) is considered, it can be seen that at 10^4 cycles in the triaxial apparatus a permanent shear strain of slightly over 1% was recorded (see Fig. 4.21(b)). Now consider the contour model derived by Ansell. Path PA (Fig. 4.21(a)) corresponds to a value of R_R somewhat greater than 0.8. Thus, at 10^4 cycles, Ansell's model predicts a permanent shear strain of approximately 20%. As can be clearly seen, a large disparity exists and this must be explained. If the stress paths which Ansell assumed were approximately equal to the actual applied stress paths then either:

(a) strains calculated for deformation measurements made at the boundaries were substantial overestimates of the actual strains occurring within the interior of the granular sample, or

(b) the continuous rotation of the principal stress direction has a profound effect on the material behaviour.

Shaw (1980) modified Ansell's apparatus and improved the facilities for measuring stresses at the boundaries. However, when compared with stress values predicted by Wood, Drescher & Budhu(1979), Shaw noted a considerable difference between the stress state which the load cells indicated and predicted values. He attributed this to the shortcomings of his own instrumentation and adopted Wood et al's predicted values calculated from:

$$\sigma_1 = 1 + \frac{R^2}{k} \quad \sigma_y \qquad \text{(Eqn. 4.13)}$$

$$\sigma_3 = (1 - k)\ \sigma_y$$

where σ_y = the normal stress applied to the top of the sample

R = applied shear stress/σ_y

K = a material constant

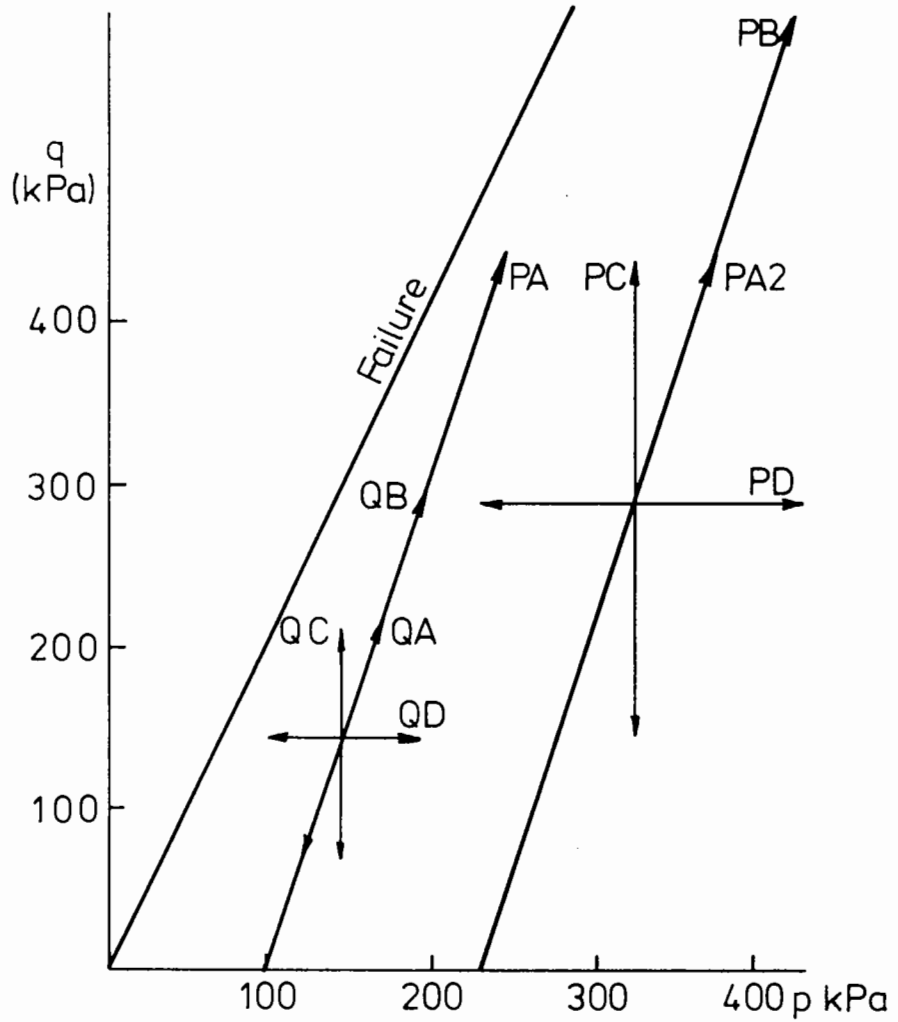

(a) Stress Paths Used During Permanent Strain Tests

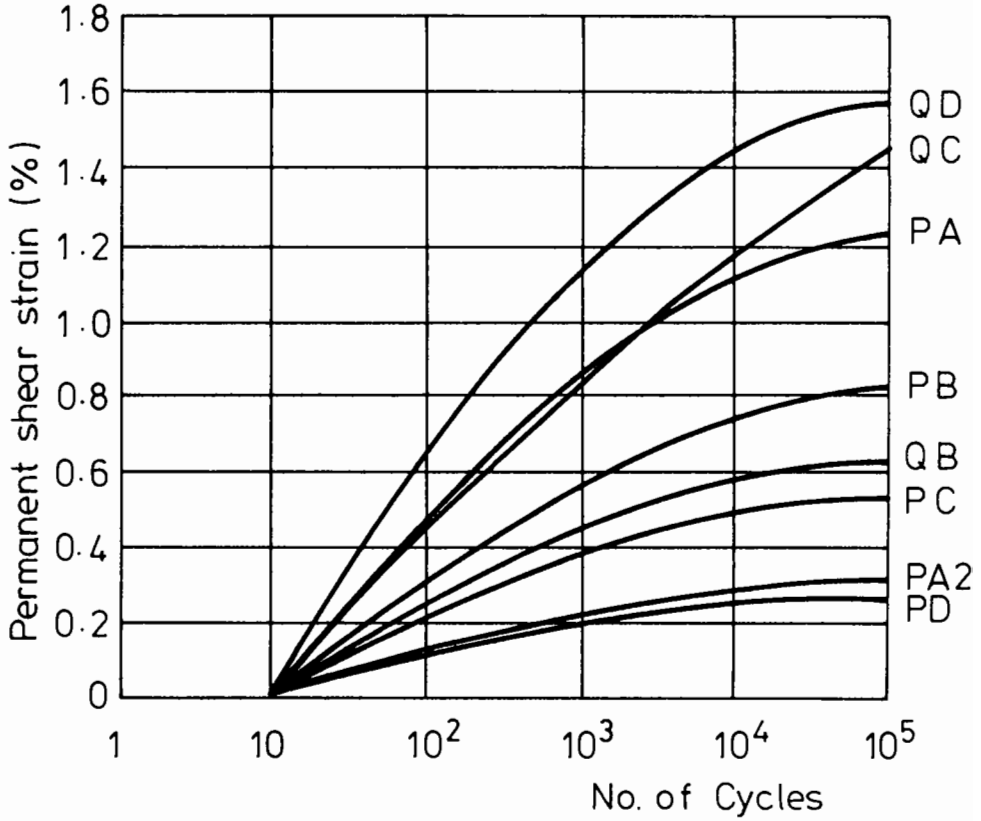

(b) Permanent Shear Strain Development

Fig. 4·21 Permanent Shear Strain Development During Repeated Loading (from Shaw 1980)

In Fig. 4.22(a), the stress ratio for plane strain (t/s) is plotted against R for various values of k where, $t = (\sigma_1 - \sigma_3)$, $s = (\sigma_1 + \sigma_3)$. As will be noted, the stress ratio is not greatly affected by change in R especially as $k > 0.8$. Thus, it follows that the application of a shearing force to a sample with a high k value will cause the principal stress magnitudes and directions to change but will leave the stress ratio substantially unaltered, so that the stress path followed during a simple shear test will be similar to that shown in Fig. 4.22(b). Shaw adopted a value for k of 0.949, and after back-analysis, concluded that both his tests and those performed by Ansell were so close to the failure condition that comparison with, for example, results from triaxial apparatus was invalid. It is submitted, however, that the value of k (0.949) adopted by Shaw was extremely high, especially when Wood et al state:

$$k \simeq \sin\Phi_{cv} \qquad \text{(Eqn. 4.14)}$$

thus giving a value for Φ_{cv} of 72°, where 40°-50° is more probable. Moreover, the assumptions made by Wood et al appear to show that reliance upon their method is a last resort. What is clear, however, is that the stress state which exists within a sample in the simple shear apparatus is not fully understood. Consequently, the results obtained from such apparatus should be treated with extreme caution, particularly when dealing with small strains where stress changes are of great importance.

Hollow Cylinder Apparatus: In 1936 Cooling and Smith subjected unconfined hollow cylinders of soil to torsion in order to investigate anisotropy. Since then a number of researchers have used this sample arrangement in order to investigate behaviour, e.g. Kirkpatrick (1957) who investigated the influence of the intermediate principal stress σ_2. Drnevich and

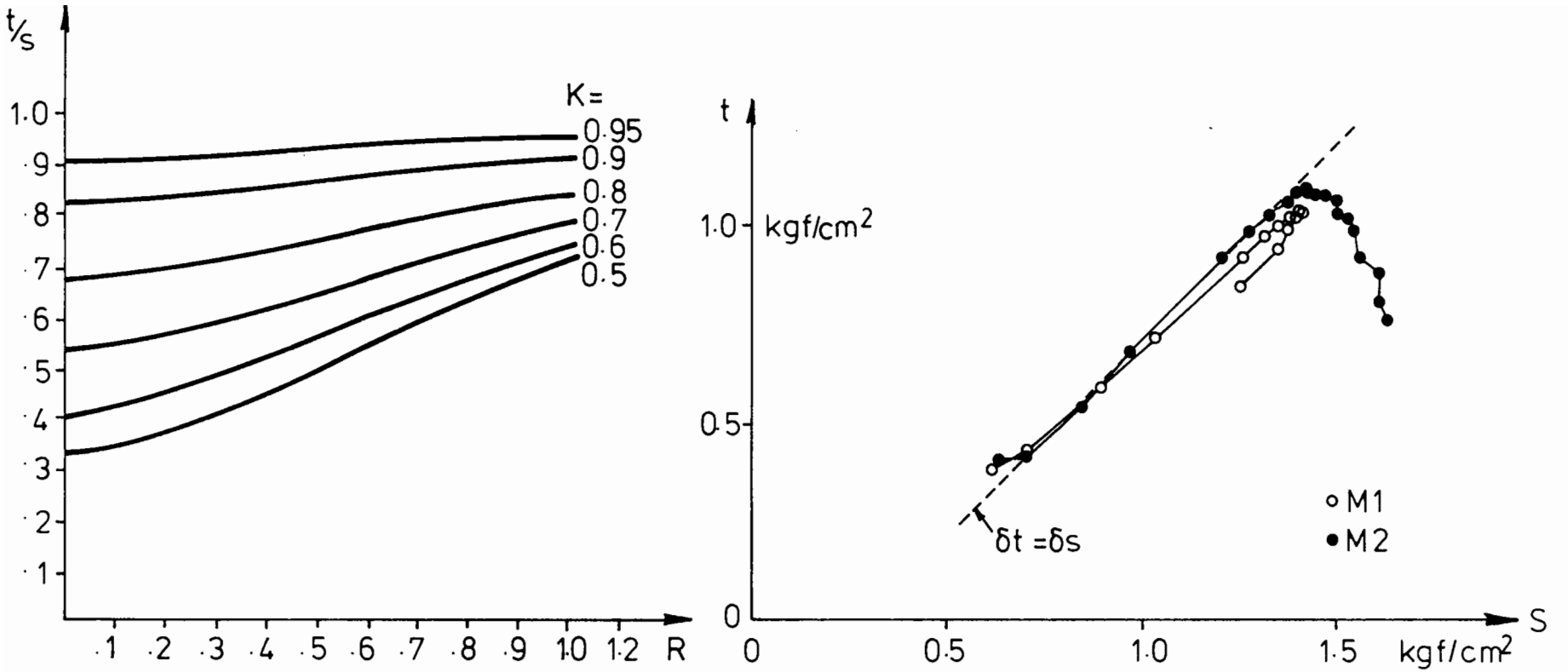

(a) Shear Stress Ratio as a Function of Applied Stress

(b) Predicted Stress States During Simple Shear Test (from Wood et al 1979)

Fig. 4·22 Calculations of Stress States in the Simple Shear Apparatus

Richart (1970) describe repeated load tests on uniform Ottawa sand using a small hollow cylinder apparatus. The internal diameter of the samples was 40mm, with wall thickness of 5 and 10mm. A maximum shear strain of 0.06% was applied. At this amplitude only small permanent strains (less than 1%) were measured at 10^6 cycles.

Hight, Gens and Symes (1983) describe the hollow cylinder apparatus (HCA) at Imperial College, London, used to test sand. In this apparatus the ratio of internal to external diameter of the cylinder is 0.8 and finite element analyses indicated that this will result in a high degree of stress uniformity. In addition to this, deformations are measured using internally mounted instruments and it is, consequently, to be expected that the results obtained are likely to be of high quality.

Detailed results are published in Symes (1983). Very little testing involving repeated stress paths was performed but one test in particular (M1) is worthy of note. Fig. 4.23(a) shows the repeated stress path in q,α space where, in this case:

$$q = (\sigma_1 - \sigma_3)/2$$
$$\alpha = \text{angle of } \sigma_1 \text{ from vertical} \qquad \text{(Eqn. 4.15)}$$

Fig. 4.23(b) and (c) show the resulting shear and volumetric strain behaviour. The sample is loaded monotonically to point A and then α is cycled 4 times between 0 and 45° until the strains at point B were recorded; the sample was taken to failure at point C. As can be seen, large permanent shear and volumetric (contractant) strains develop although the stress state in terms of principal stress magnitudes has remained constant. Symes notes that: "during the cycles of principal stress rotation, the octahedral shear strain continued to increase. The magnitude of the increase reduced with each cycle, although the increase still had a

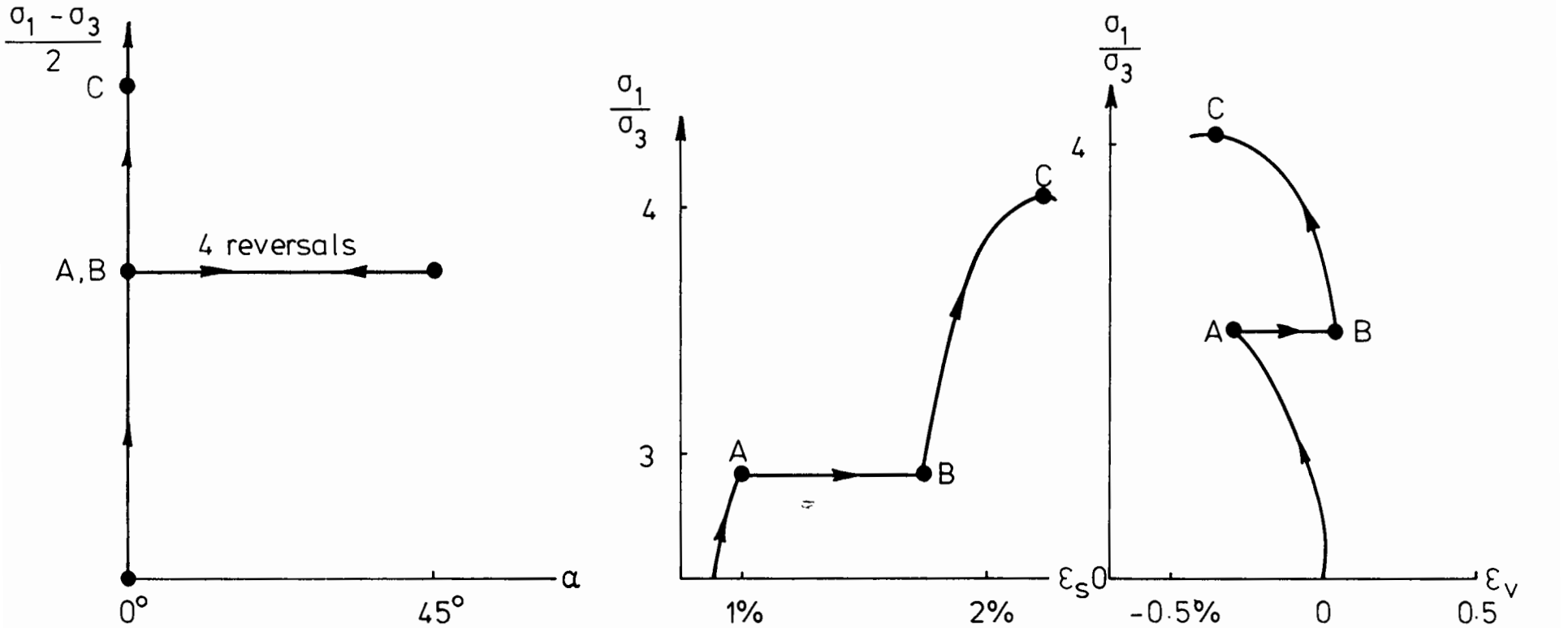

(a) Stress Path Followed (b) Shear Strain Behaviour (c) Volumetric Strain Behaviour

Fig. 4.23 H.C.A. Test on Sand (Symes 1983)

significant magnitude on the fourth cycle ..." The number of cycles that could be applied was limited by the operator's patience, since stress control was largely a manual process. It seems likely, however, that an equilibrium situation would have resulted where the permanent strains developed during any cycle were very small (in the same way as resilient behaviour is known to develop under uniaxial triaxial conditions).

The results obtained by Symes suggest that the occurrence of principal stress rotations may have an effect on the general behaviour of granular materials. Thus the constitutive models obtained from uniaxial triaxial testing may be inadequate for predicting behaviour where stress rotation is a feature.

The Directional Shear Apparatus: This piece of apparatus is described in detail in Arthur, Chua and Dunstan (1977). A cubic sample of 100mm edge dimension is subject to both normal stresses applied to the faces of the cube, but also to shear stresses tangential to the four vertical planes. These shear stresses are applied by "pulling sheets" - see Fig. 4.24. This then allows stress directions to be rotated, since stress increments can be applied which are not co-axial with the total stress state. Strains are measured using a technique in which lead shot (set into the sample during preparation) are radiographed after each load increment. Strains are then determined using a comparator.

Although strain measurements are "on sample" and can be expected to be reliable, the sensitivity of the system precludes the recording of the very small strains which can be measured in the standard triaxial or hollow cylinder apparatus using electrical transducers.

Due to the nature of the D.S.C. test arrangement, there may be problems in achieving stress uniformity; it may be significantly affected by friction and non-uniform stress distribution along the "pulling sheets".

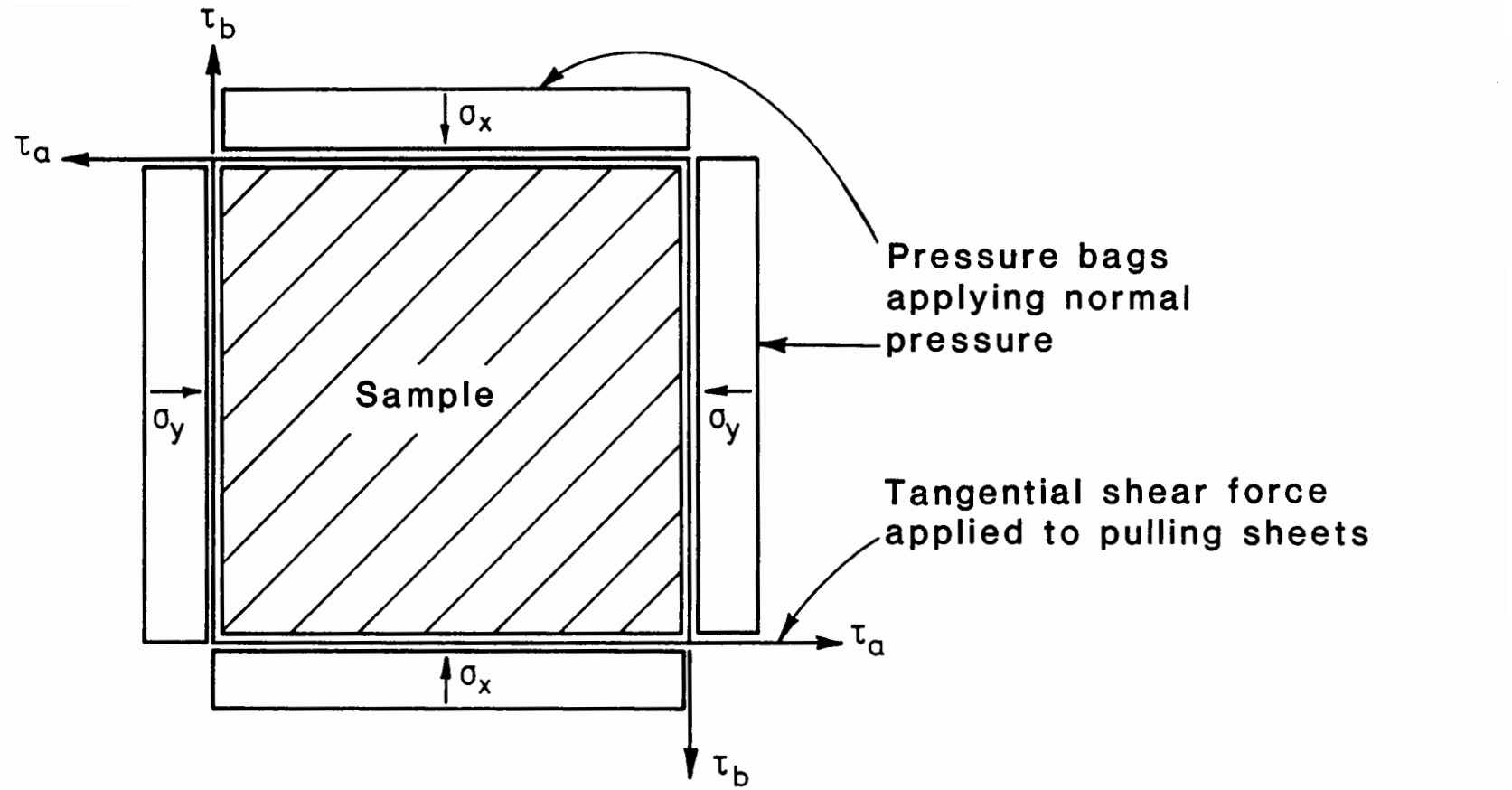

Fig. 4.24 SCHEMATIC ARRANGEMENT OF SAMPLE LOADING SYSTEMS IN THE DIRECTIONAL SHEAR CELL

Wong and Arthur (1985) carried out two series of tests in the D.S.C. In the first series, the applied stresses were varied in magnitude alone by applying cycled loads to the faces of the cubic sample. In the second series of tests, the same cycled stress levels were applied but the direction of stresses during cycling was rotated by applying constant shear stresses to the sample faces. Fig. 4.25 shows the difference in shear strains observed. As can be seen, stress rotation causes much greater shear straining. Wong and Arthur found that during some tests the shear strain kept accumulating, whereas in others, it reached a steady value. Analysis showed that this appeared to depend upon (a) the mobilised value of shear strength and (b) the amplitude of stress rotation. Fig. 4.26 shows this relationship in graphical form. The stress ratio mobilised during any test is normalised against the maximum possible shear stress ratio (i.e. material strength in a monotonic test). Stress paths which include points above this line exhibit continued accumulation of shear strain, whereas those that remain below reach a steady value of shear strain.

4.3.5.1 Volume Changes and Principal Stress Rotation

It has generally been observed that principal stress rotation causes an increase in permanent shear strains. A range of ideas have been advanced as the basis for models of this. Youd (1972), for example, related shear strain accumulation to the shear strain magnitude and Wong and Arthur (1985) related (Fig. 4.26 above) shear strain accumulation to both mobilised stress ratio and stress rotation amplitude.

The experimental evidence relating to volumetric strains during stress rotation appears to be less consistent. The work of Wroth (1958) and Ansell (1977), for example, suggests that stress rotation caused contractant volumetric strains even at high stress ratios. The work at

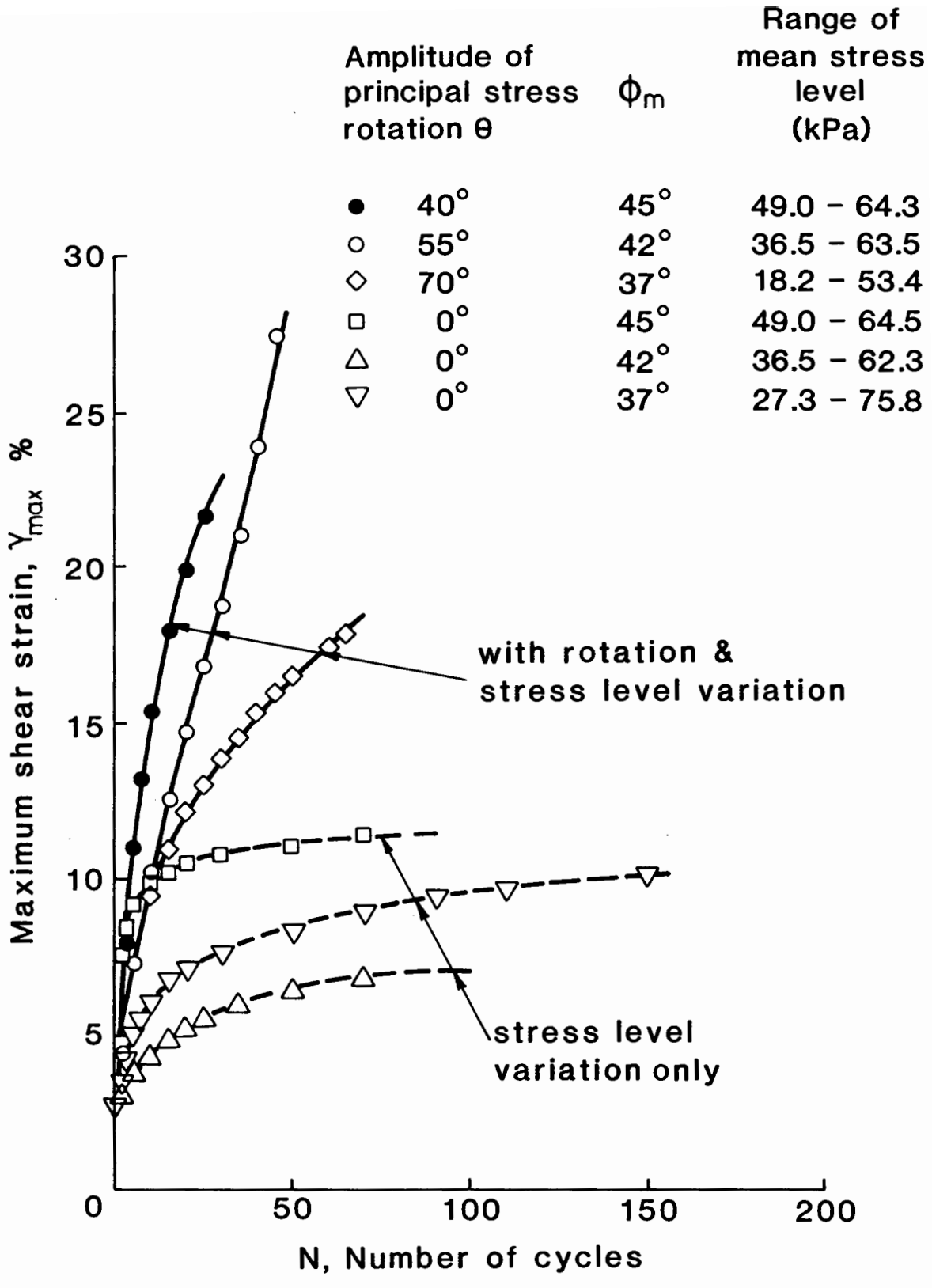

Fig. 4.25 THE INFLUENCE OF PRINCIPAL STRESS ROTATION ON SHEAR STRAINS DEVELOPED DURING CYCLIC LOAD TESTS (FROM WONG AND ARTHUR 1985)

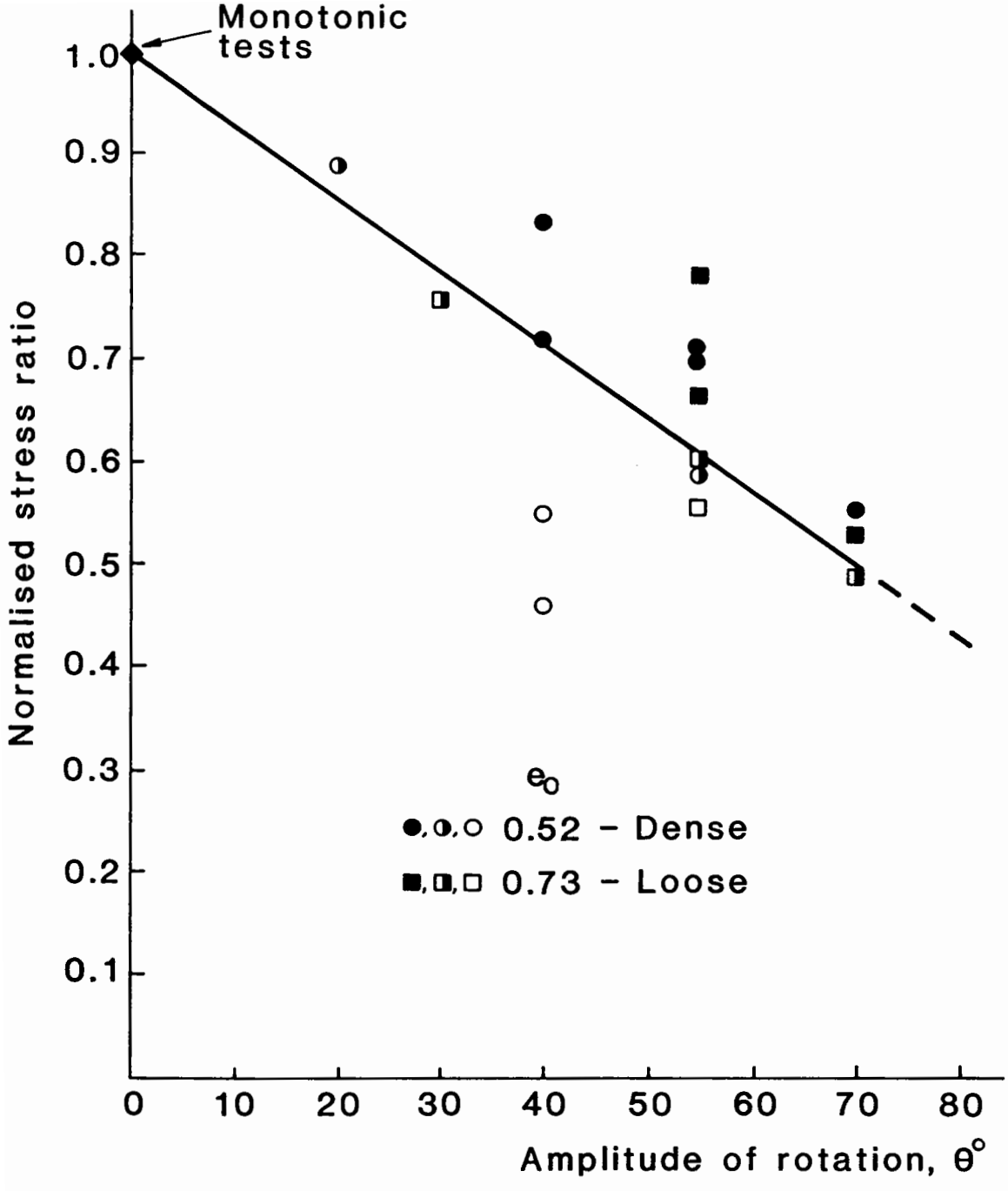

Fig. 4.26 THE MAXIMUM NORMALISED STRESS RATIO vs AMPLITUDE OF PRINCIPAL STRESS ROTATION AT WHICH PERMANENT SHEAR STRAINS TEND TO A STEADY VALUE (FROM WONG AND ARTHUR 1985)

University College (Wong and Arthur 1985), however, shows that large dilatant volumetric strains could occur at high stress ratios.

One significant feature of Wong and Arthur's work is that it was performed at very low stresses ($7 < \sigma_3 < 20$ kPa). The mean stress level has, of course, a great bearing on volumetric strain behaviour. It could be that if higher stresses were imposed (as in Wroth and Ansell's work), contractant strains would be observed at all stress ratios. The volumetric strain behaviour during these tests is, of course, of primary importance. If generally dilatant in a closed structure such as a TES, stress levels will build up and stress ratios decrease eventually producing an equilibrium. If, on the other hand, behaviour is generally contractant, it is possible that large settlements will take place in the TES.

Work at Imperial College (Symes, Gens and Hight 1984) on undrained sand has resulted in the construction of a Stress Boundary Surface model. This is normally represented in q, p, α space (although the researchers involved point out that this 3-D space is only a b = constant slice from the 4-D q, p, α, b space). During undrained loading the volumetric strain is zero, but volume change "propensities" manifest themselves as pore pressure changes. Since the Imperial College model can predict this behaviour it is likely that using similar ideas, the model might be extended to volumetric strain "actualities" as well as "propensities".

Indeed, it may well be that in connection with the work at Imperial College on offshore foundations, the case of undrained loading may be too conservative. It may be desired to extend the generality of their models to a range of drainage conditions through from undrained to completely drained.

4.3.5.2 The Relationship between Stress and Strain Increment Directions

In traditional material science theories the general assumption is

that during elastic behaviour, the strain and stress increment directions coincide, but that when yield is reached, the strain increment is normal to the yield locus in stress space and is independent of the instantaneous stress increment.

It has become clear, however, that granular materials exhibit extremely complex behaviour. In order to model a structure with a granular component under changing load, it is of vital interest to know the directions of strain changes. In structures in which stress rotation is a feature, this is particularly important since the direction of stress increment may be changing rapidly compared with the direction of the total stress. Unfortunately, the evidence in this area is confusing. Tests in the early 1970's using the Cambridge Simple Shear Apparatus tended to indicate that strain increment direction coincides with stress increment (eg. Stroud 1971). Work at Imperial College, however, (Hight et al 1983) tends to show that at low stress ratios the strain increment direction appeared to be consistently between the stress and the stress increment directions. At higher stress levels the stress and strain increments appeared to converge and finally to coincide at failure. Wong and Arthur 1985 suggest that their results using the D.S.C. tend to suport the Stroud (1971) position. It is submitted from inspection of their results (see Fig. 4.27), however, that although there is dependence upon the stress increment direction, that the role of the total stress tensor is significant. Indeed, if anything, the results from University College appear to support the Hight et al position.

This aspect of granular material behaviour appears to be receiving an increased amount of attention, and it is hoped that within a short time, a complete study will reveal the true behaviour and its implications for granular material models.

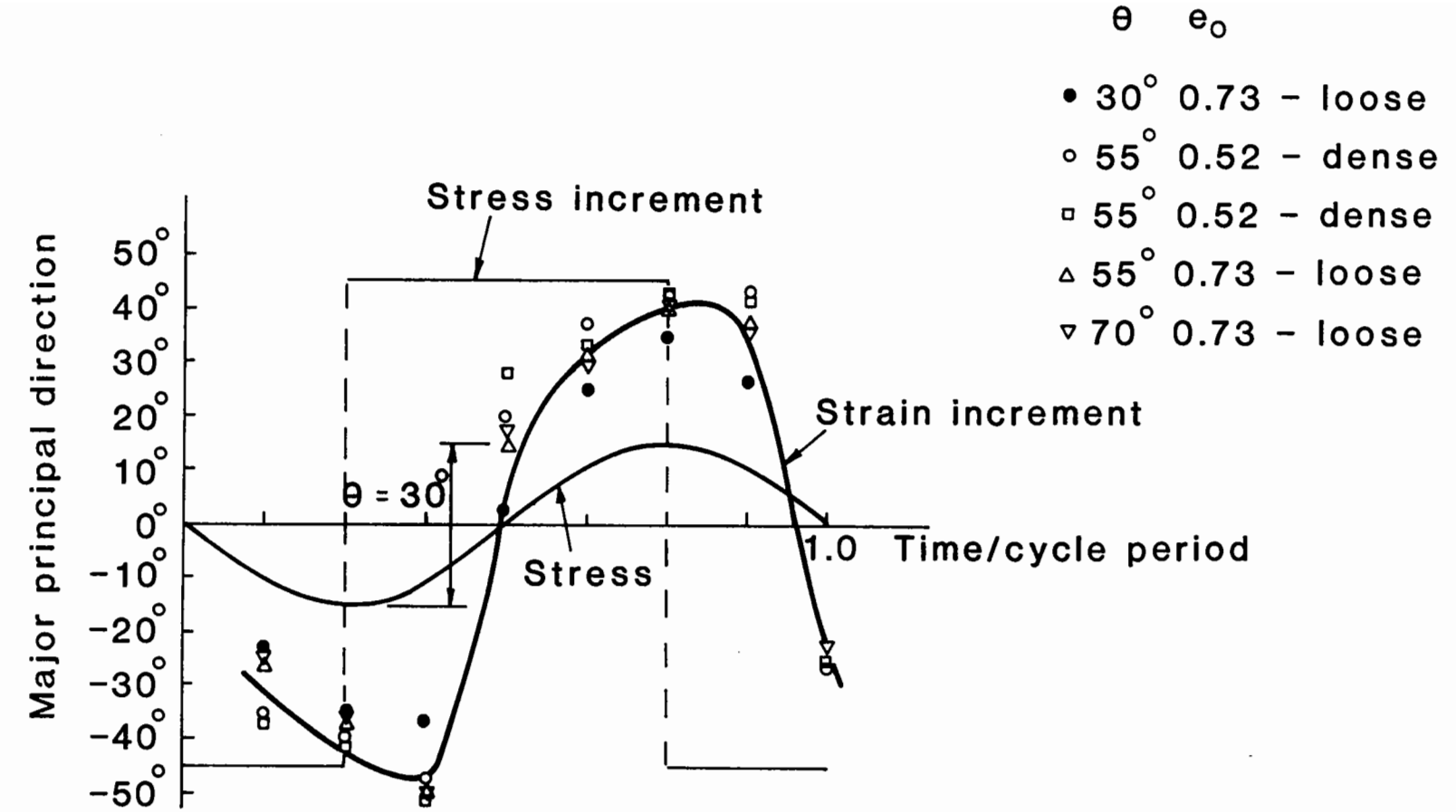

Fig. 4.27 THE RELATIONSHIP BETWEEN STRESS, STRESS INCREMENT AND STRAIN INCREMENT DIRECTION DURING A SINGLE LOAD CYCLE (FROM WONG AND ARTHUR 1985)

4.3.6 The Effect of Mean Normal Stress on Granular Material Properties

It is a well-known phenomenon that (in general) an increase in mean normal stress leads to a decrease in the maximum value of Φ at failure. In view of the fact that a TES is likely to experience high stresses, it is important to know to what extent this is likely to influence material behaviour in these structures.

In normal construction the problem arises mainly in connection with compacted rockfill which is built up in embankments to heights of 50m or more. In these structures which may form part of a dam, slope stability is of prime importance. Consequently, the type of material most commonly investigated is compacted rockfill. Charles and Watts (1980) present data for four common rockfill materials (Fig. 4.28). As can be seen, the stress ratio which can be mobilised decreases rapidly as the cell pressure is increased. As the stress increases beyond about 300 kPa, the rate of strength loss appears to decrease. In fact, data presented by Bishop (1966) from Skinner's work (Fig. 4.29) shows that there comes a point at which strength (in terms of Φ) is recovered by increasing the cell pressure. Bishop explained that this phenomenon was associated with particle breakdown. In tests in which higher stresses were used, the requirement for the particle to slide over each other and dilate was overcome by particle breakage, as shown in Fig. 4.30(a). This means that less dilation will occur at higher mean normal stresses. Bishop presents data from Tomb's work (Fig. 4.29(b)) which illustrates this. Data from Skinner (presented in the same lecture) (Fig. 4.30(b)) shows the grading changes which occur as a result of Ham River Sand (a) being sheared to failure at cell pressures of 1000 and 4000 psi and (b) the grading change between being consolidated to 4000 psi, and then subsequently being sheared to failure at the same cell pressure.

It will be noticed that the materials discussed above are all angular

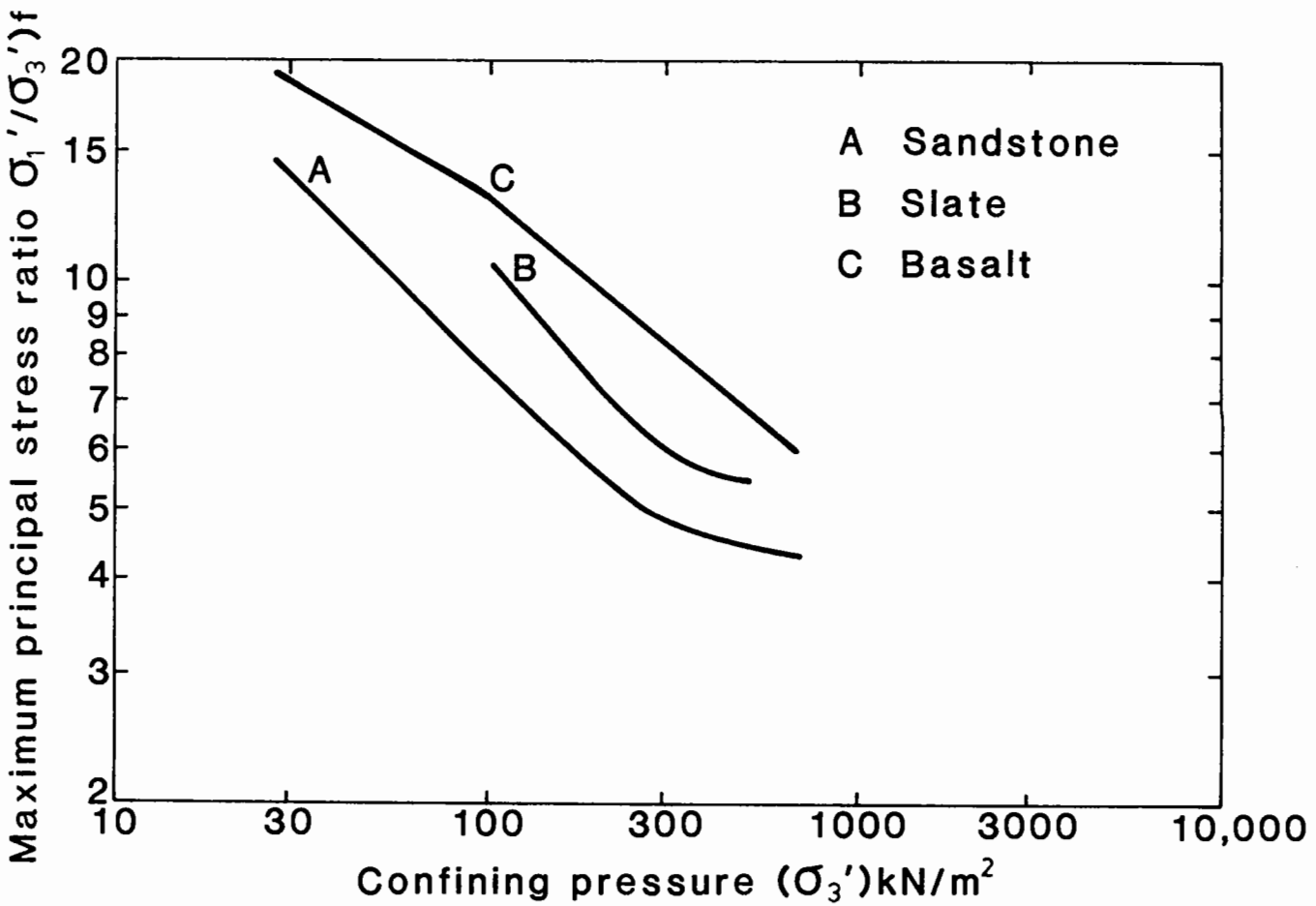

Fig. 4.28 INFLUENCE OF CONFINING PRESSURE (σ_3') ON MAXIMUM PRINCIPAL STRESS RATIO (σ_1'/σ_3')f. FROM CHARLES AND WATTS (1980)

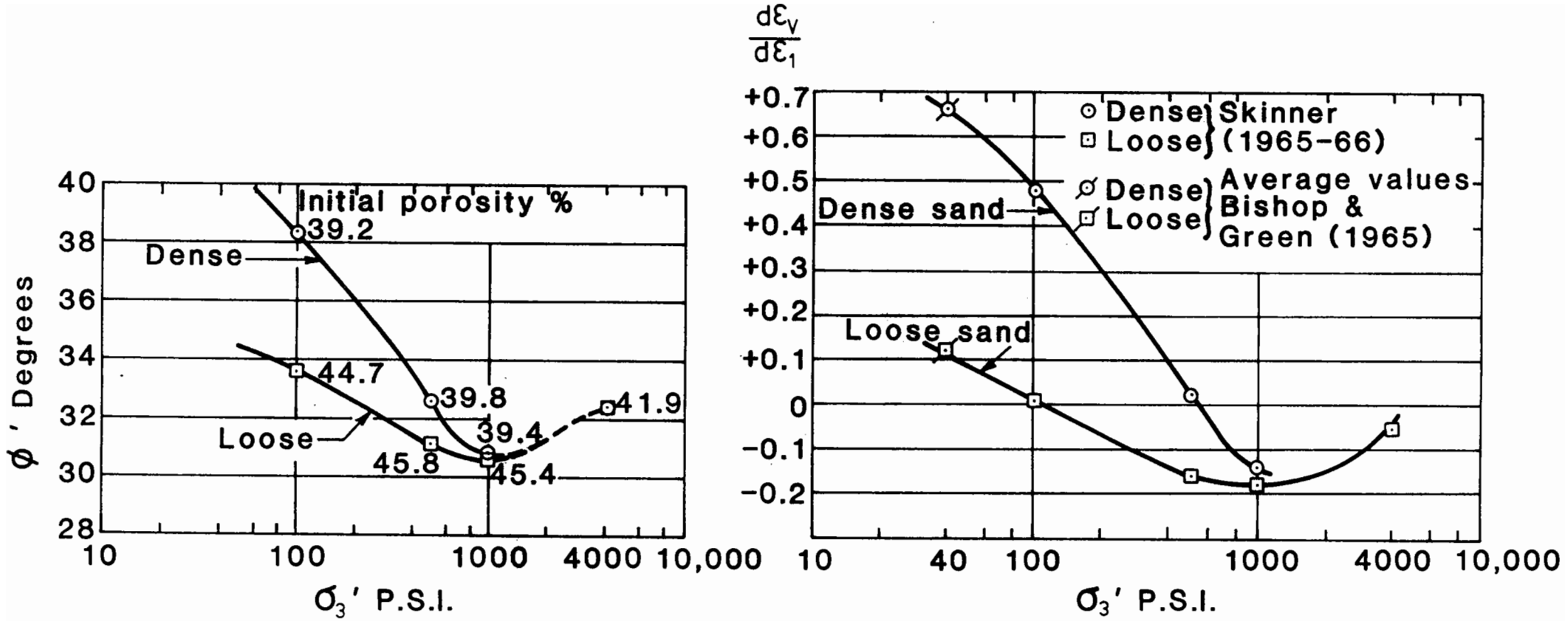

(a) Variation of Strength

(b) Variation of Rate of Dilatancy of Failure

Fig. 4.29 VARIATION OF STRENGTH AND RATE OF DILATANCY AT FAILURE WITH σ_3

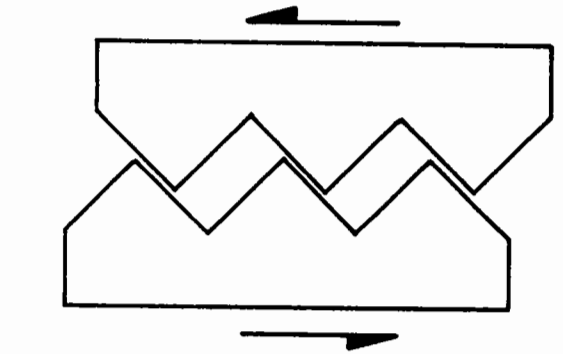

(ii) Low mean normal stress

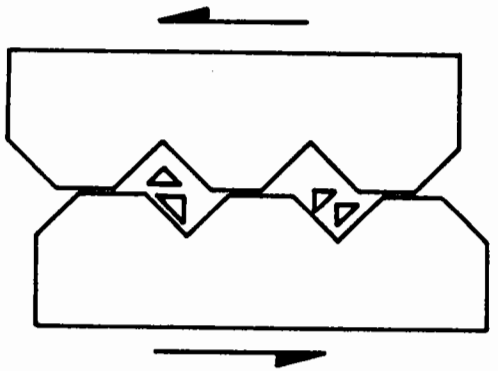

(i) High mean normal stress

(a) Mechanism of Shear and Dilation

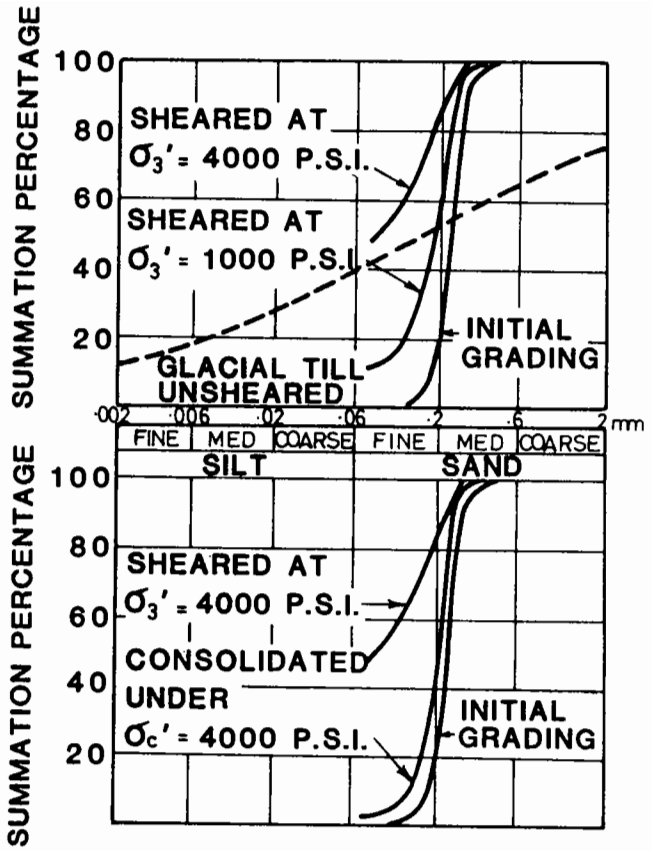

(b) Grading Changes for Different Stress Histories (Data from Skinner 1966)

Fig. 4.30 PARTICLE DEGRADATION DURING SHEAR OF GRANULAR MATERIALS

minerals. A consideration of the materials involved in this project requires a knowledge of the ways in which their special material properties will affect the influence of increased normal stress. The following observations may be made:

1. The Denstone materials have very high crushing strengths (see Chapter 3): at what stress on an assembly crushing will occur is difficult to say. The findings of researchers such as Konishi (1972) and Oda (1974) suggest that stress is transmitted not over the whole granular material but through heavily loaded contigunous chains. It would, therefore, be necessary to multiply an "average normal contact load" many times to find the highest contact force. However, the tests by Skinner on sand (Fig. 4.30(b) show that, even for angular particles, degradation does not occur to a great degree during consolidation even to 4000 psi, but that shearing stress is its main cause.
2. It appears that since in the majority of particle degradation occurs during shearing, an increase in a material's resistance to breakage as a result of tangential forces will arrest degradation. Denstone and modified Denstone have spherical particles which are likely to be very resistant to this type of loading, unlike the crushed rock materials which, having numerous asperities and imperfections, are likely to be very susceptible to degradation.

In conclusion, it appears that the loss of shear strength which accompanies the increase in mean normal stress is likely to be less of a problem for an assembly in which strong spherical particles are used. It is necessary to point out that if loss of strength were to occur, this would lean to more favourable conditions in a closed system such as TES.

4.4 STATIC LOADS IN VERTICAL WALLED CONTAINERS

When a container which is shallow compared to its width is filled, the influence of side wall friction is small. Consequently as the container is filled, the horizontal stress approximates to:

$$\sigma_v = K_o . \sigma_z \qquad \text{(Eqn. 4.16)}$$

This is confirmed by Blight (1983) using maize, and Blight and Midgley (1981) using coal for fill depths up to the container diameter. When a deeper bin is used, the influence of side-wall friction becomes considerable.

4.4.1 Basic Ideas

In 1884 Roberts discovered that although the pressure at the bottom of a vertical walled bin increased during the initial stages it reached an asymptotic maximum when the height of fill (wheat) was equal to twice the diameter of the circle inscribed by the bin cross-section. He found that the horizontal pressure was approximately independent of bin diameter, and the expressions which he proposed for calculations of wheat-filled silos may be written:

$$\sigma_{v\ (max)} = k.D.Y \qquad \text{(Eqn. 4.17)}$$

$$\sigma_{h\ (max)} = C \qquad \text{(Eqn. 4.18)}$$

where k and C are constants, Y is the material bulk density and D is the bin diameter

He correctly attributed this general effect to the friction which exists between the container walls and the granular medium within.

In 1895 Janssen reported an analysis based on the equilibrium of a

static horizontal slice of granular material. He assumed that there was a constant ratio K_o between horizontal and vertical stresses. He performed experiments in small wooden bins and determined a value K_o for wheat, and incorporated a value μ for the friction coefficient. His analysis yields an expression for the normal stress on the bin wall (σ_N) as follows:

$$\sigma_N = -\frac{pgA}{\mu L} - \left[Pk_o - \frac{pgA}{\mu L} \right] . e - \left[\frac{\mu L k_o z}{A} \right] \qquad \text{(Eqn. 4.19)}$$

L = perimeter length

A = X sect. area

P = surcharge at z = 0

Jenike et al (1973) appear to be the first writers to notice that Janssen's formula is in fact a lower bound as he assumes that the friction is fully mobilised. Cowin (1977) performed a more sophisticated re-analysis of Janssen's problem using the inequality:

$$\tau_z \leqslant \mu\sigma_N \qquad \text{(Eqn. 4.20)}$$

He was able to derive Janssen's result (as a lower bound solution) and upper bound given by:

$$\sigma_N = pgk_o z + Pk_o \qquad \text{(Eqn. 4.21)}$$

The upper bound result is that predicted by standard earth pressure theory, i.e. $\sigma_n = k_o\sigma_v$. Cowin (1979) considers the effect of material compressibility on the stresses upon the wall. He uses constants m and n such that

$$k \leqslant k_o (1 + mV) \qquad \text{(Eqn. 4.22)}$$

$\geq k_o (1 - nV)$

where V is the overconsolidation pressure

Calculations for cereals show considerable deviation from the Janssen formula when compressibility is taken into account. Results from tests on coal show that it is relatively incompressible. However, at high pressures, a substantial change in pressure ratio is possible; values of n and m for coal were 0.51 $(MPa)^{-1}$ and 0.8 $(MPa)^{-1}$ respectively. Thus if V is 400 kPa (0.4 MPa)

$$k \leq k_o (1 + 0.4 \times 0.8) \qquad \text{(Eqn. 4.23)}$$
$$\leq 1.32\ k_o.$$

4.4.2 Stressing in Bins due to Temperature Changes

Blight (1983) instrumented a 20m diameter steel maize silo with pressure and temperature sensors. Continuous readings were taken over a week-end (so that pressures would not be affected by loading or discharging). The coefficient of thermal expansion of the maize was lower than that of the steel container. As the temperature rose, horizontal stresses decreased, and as temperatures fell, horizontal stresses increased. This is expected from standard earth pressure theory so that increasing temperature corresponds to a tendancy towards active pressure, whereas falling temperature corresponds to a tendency towards passive pressure conditions. The range of temperature was approximately 20°C. This resulted in the value of k changing by factors of up to 2.8. One point of particular interest was observed:

"there is a tendency for the pressure to rise progressively as each diurnal cycle of temperature takes place. This is presumably because the grain settles against the sides of the bin as the bin walls move outwards. Subsequent decreasing temperatures therefore result in higher pressures than in the previous temperature cycle."

This observation is evidence of the possibility of racheting occurring within granular material containers when temperature fluctuations occur.

4.4.3 Full Scale Granular Material Heat Store

Bartel and Skvarna (1984) describe a 10-MWe Solar Energy generating station which is in operation in California. The system ("Solar One"), includes a Thermal Energy Store (TES) which acts as a buffer between the solar receiver and the generators. The storage facility selected for this was a bed of rock and sand within a steel container 63 feet in diameter and 44 feet high (19.2m x 13.4m). The bed is immersed in a thermal oil. Temperature is transmitted to and from the granular material by the oil. The temperature range within the TES is approximately 425°F to 575°F (218°C to 302°C).

In the published literature on this project no mention is made of the problem of differential thermal expansion, and attempts to contact the designers have not been successful. There are three major reasons why in the Solar One project this problem may not have been given a great deal of consideration.

1. the height to width ratio of the store is only 0.7, which constitutes, in silo engineering terminology, a "shallow bin".
2. the self-weight of the granular fill is reduced by approximately one-third due to its immersion in oil.
3. the temperature range is only 84°C.

Although these figures show that the Solar One TES differs greatly from one which may be incorporated in a Compressed Air Storage System, any information concerning its structural performance would have been useful. In a paper published shortly after the commission of the Solar One TES (Friefeld, Moore and Morgan 1982), it was mentioned in the "conclusions" that the TES was "undergoing shakedown tests" although these were not described. A paper published two years later describing the operation of the TES (Morgan, Cannon and Coleman 1984), did not mention the result of these tests and one must presume that no structural problems were encountered.

CHAPTER FIVE

EXPERIMENTAL APPARATUS

Two major pieces of apparatus were used in order to obtain experimental data concerning the mechanical properties of the candidate materials. Both of these were of the uniaxial triaxial type: in order to distinguish between them, they are called by their main characteristic feature. The first, the "Large triaxial apparatus" is described in section 5.1. The second, the "Repeated load triaxial apparatus" is described in section 5.2.

5.1 LARGE TRIAXIAL APPARATUS

A large soils triaxial testing facility has been modified for this project. Test specimens 230mm in diameter and 500mm long were tested under axial strain control and at constant cell pressure. Measurements of cell pressure, deviator stress, axial deformation and either volumetric or radial deformation were made.

5.1.1 Sample preparation: previous arrangement

The existing arrangement had end-platens of the same diameter as the sample. The three-piece split mould was lined with a rubber membrane sealed to the lower platen, as shown in Fig. 5.1(a). The test material was then placed in the mould and the top platen positioned when filling was complete.

5.1.2 Development of Sample Preparation Technique

Dimpled Mould Liner: It was noted during the packing density tests that single size material tends to form a close-packed layer at any boundary.

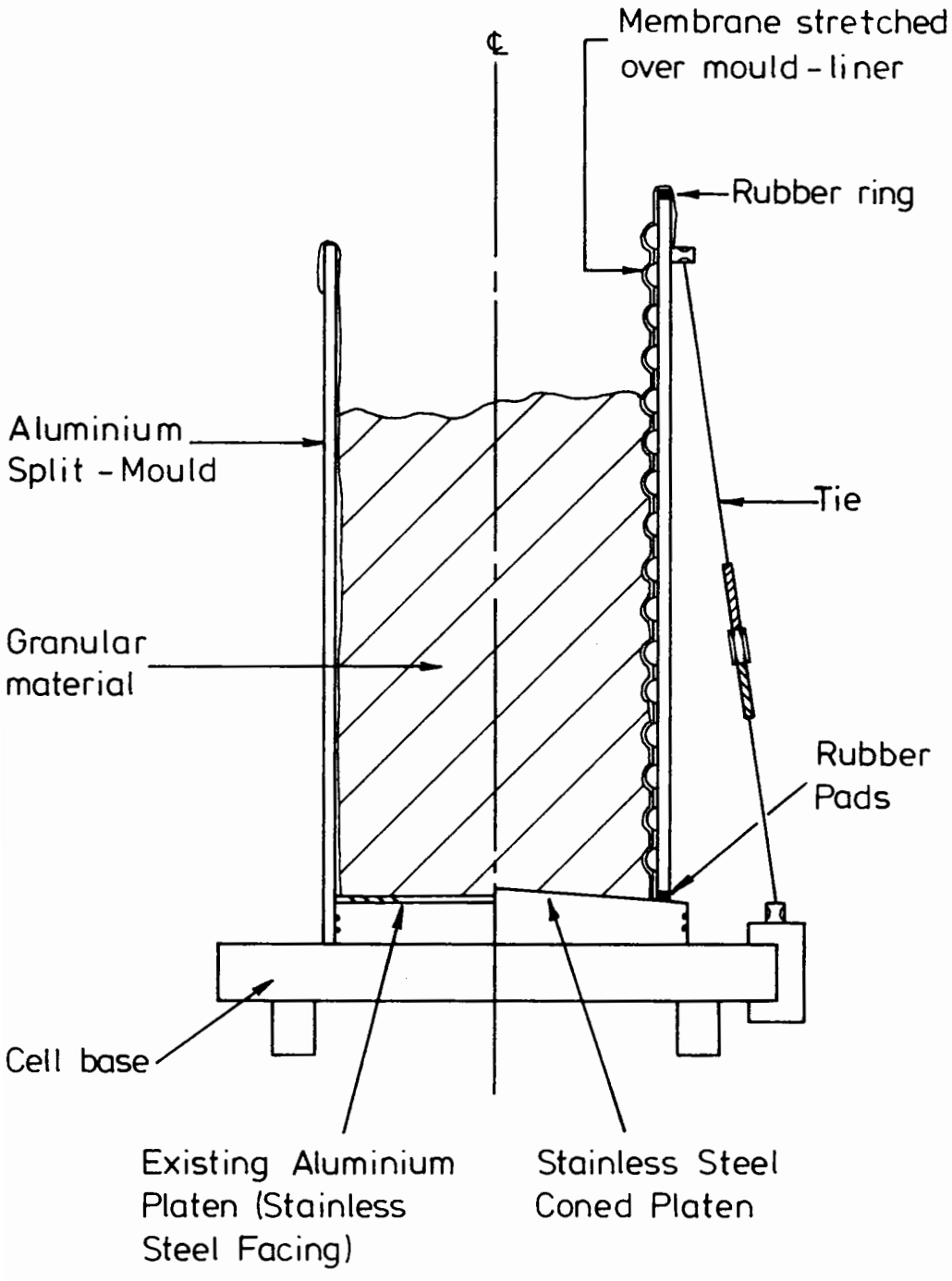

FIG. 5.1 SAMPLE PREPARATION

This regular arrangement increased as the ratio of container diameter to particle diameter increased. It was considered that this would lead to two undesirable effects.

(a) A particle structure unlikely to be encountered in the prototype, and,

(b) A strong closely-packed annular ring of particles around the whole sample which would resist the horizontal pressures more efficiently than would a random arrangement. This would lead to high circumferential stressing in the outer layer with lower stresses in the interior region.

In order to combat these effects, it was decided to devise a method for breaking-up the surface arrangement. Several methods were attempted including silicone rubber nodules (placed manually) close to the membrane inside the sample but, after due consideration, a dimpled mould-liner placed between the sample membrane and the mould was considered the most effective method.

The liner was made in five parts, each the height of the sample and one fifth of the circumference. Steel of 0.5mm thickness was used since this was the strongest material that could be readily indented with dimples.

The dimples were approximately 20mm diameter and 5-8mm deep indented in a generally hexagonal array, although they were sufficiently random to prevent any major regular arrangements from forming. The mould-liner was used throughout the test programme but it is difficult to assess its efficacy. It would be inadequate simply to carry out a complete test programme of samples prepared both with and without mould-liners. The results of such a programme would merely be a comparative exercise and would not decide the real question, which is whether samples prepared using the mould-liners are more representative of a random element within the material than those prepared without.

In view of this, another method of assessing the value of using mould-

liners was adopted which involved examining the density of the samples produced. In Chapter 3, an empirical relationship was derived for the packing density of Denstone. By extrapolation it was possible to arrive at an estimate for the density of an infinite volume of material. The density of a representative element within such an infinite volume will be equal to that of the whole mass. The volume of the sample produced using the mould-liner was measured by pouring water into a membrane in the mould. The volume of particles used to form the sample was measured by weighing them (the particle density being known).

The measurements confirmed that the density when using the liner was higher than that which would be expected by using a flat-walled mould. Indeed, in many cases, the density achieved reached the predicted maximum value. The mould-liner would, therefore, appear to be effective.

End Platen Friction: The traditional method of reducing the friction at loading platens in the triaxial test has been to provide a high vacuum silicone grease and rubber membrane sandwich (Rowe and Barden, 1964), and many investigations have taken place in order to improve the friction reducing properties of various materials, (e.g. Brown, 1975). The testing of large uniform particles caused a special problem, that of very high point contacts which make the situation different from the case of a fine-grained soil. Tests were carried out on latex membranes and single and double layers of polythene.

The friction testing device shown in Fig. 3.3 was modified as shown in Fig. 3.4(b) in order to test these materials. Horizontal and verticle loads were applied as before. The results are presented in Fig. 5.2. The general trend is that as the normal load increases the friction of the latex membrane increases, whereas that of the polythene membranes decrease. It was decided that in the interests of eliminating as many experimental

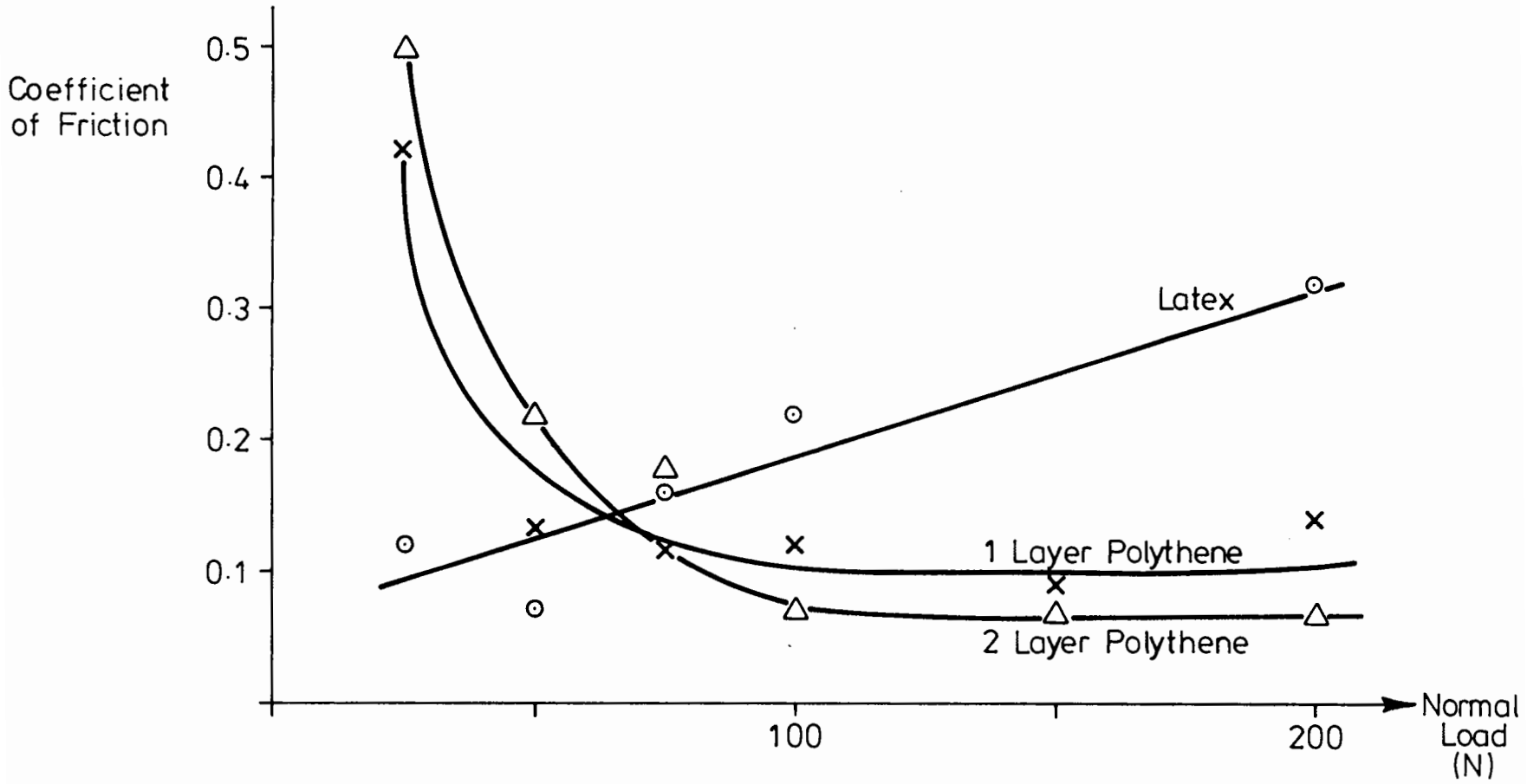

FIG. 5.2 THE EFFECT OF NORMAL LOAD ON THE FRICTION PROPERTIES OF VARIOUS LUBRICATING MEMBRANES

variables as possible, the friction-reducing membrane material used for this series of tests should be standardised. Therefore, considering both the friction results and the requirement for as thin a membrane as possible, the single-layer polythene sandwich was thought to be the appropriate choice.

Two preliminary triaxial tests were performed using the polythene membrane but the sheared samples showed considerable barrelling despite this. The presence of the end restraint is significant for two reasons:

(a) A major assumption of the triaxial arrangement is that there is a principal plane in the horizontal direction. A principal plane is defined as being one across which no shearing stress is present. But the presence of platen end-restraint clearly imposes shearing stress and invalidates this assumption.

(b) When a barrelled shape occurs, errors arise in the measurement of radial strain and these could affect the whole understanding of the material properties.

In view of these problems, it was decided to attempt the further reduction of end-platen friction by a different method. It was considered that a real possibility existed for cancelling out end friction by means of coned platens. In this arrangement, a horizontal stress is applied to the sample in the direction opposite to the one applied by end friction by virtue of the slope. Fig. 5.2 shows that the coefficient of friction at the platen is dependent on the normal load. It was decided that, due to the speculative nature of the task, a value of 0.07 should be used for this parameter since it was the lowest measured. This would, at least, ensure that over-compensation did not occur and, in view of the fact that during machining it was found that the angle of the cone could be altered without major problems, it was considered that such an attitude was reasonable. Therefore, an angle of 4° (being the friction angle corresponding to μ =

0.07) was selected. The platen material was a hardened stainless steel and it was machined as a single unit rather than using (as previously) a stainless steel facing plate. This was done for ease of manufacture and also for structural considerations. It did, however, involve a considerable amount of workshop time. The base platen is shown in Fig. 5.3.

The new platens were used for all tests performed except the two preliminary tests.

All of these tests have been limited to investigation of behaviour at axial strains upto 1 or 2%. Consequently, it has proved to be impossible to check visually that the coned platens have been effective, since very little visible barrelling would take place even if considerable friction existed at the platens. Testing the effectiveness of the coned platens could have been done by instrumenting the sample across many diameters to determine radial strain distributions along the sample length. In this way, the strain non-uniformity could have been measured, and an indication of stress non-uniformity given. However, it was considered too costly - both in time and money - to install the large number of highly sensitive instruments which would have been needed. Determination of the detailed stress non-uniformity was not thought to justify the inconvenience it would cause.

From simple mechanical theory it can be shown that the use of coned platens will increase sample stress uniformity. This has been demonstrated by material engineers who use coned platens for testing metals and plastics (e.g. Siebel and Pomp, 1927). Even for the small strain tests, accurate analysis requires stress uniformity. Since coned platens improve stress uniformity, it is submitted that their use must be an improvement over the existing flat-platen system.

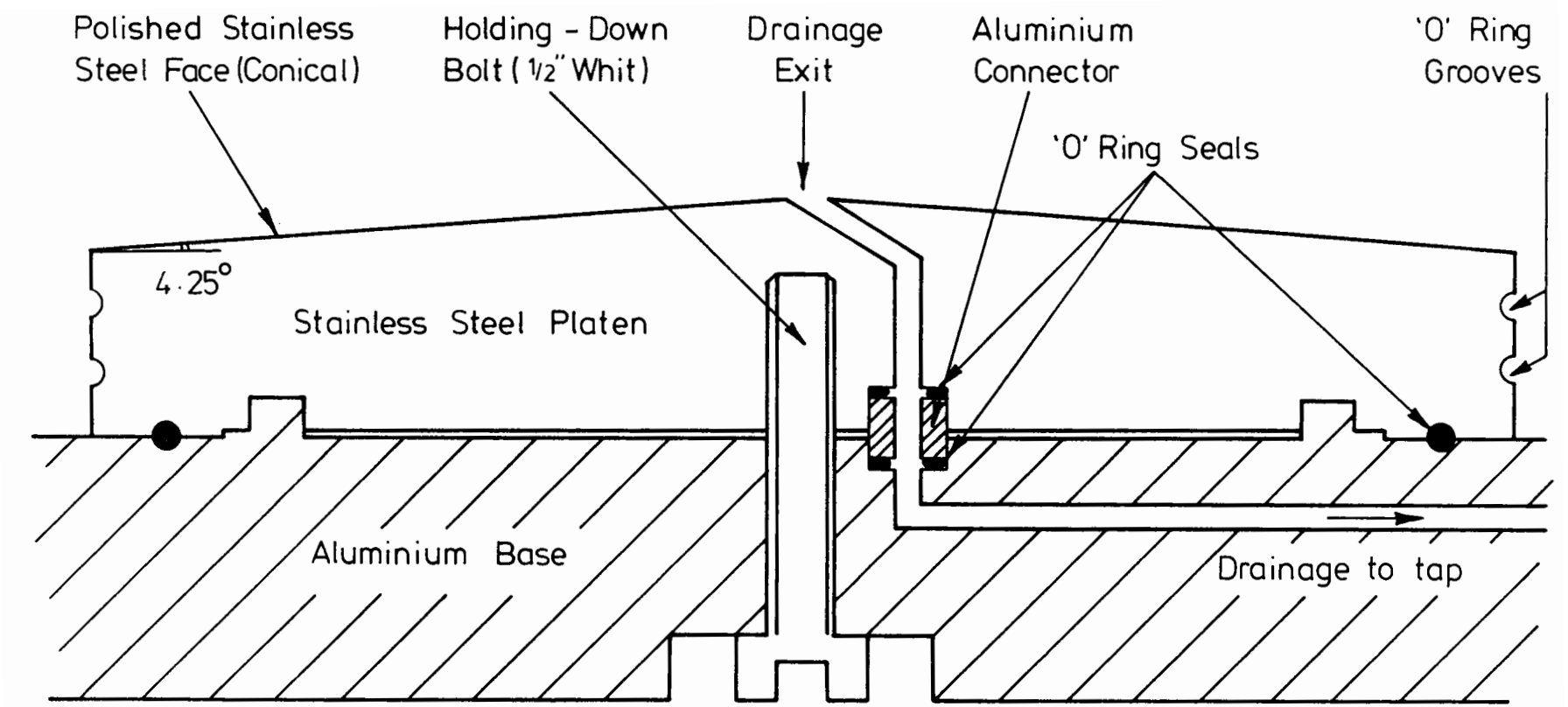

FIG. 5.3 DETAILS OF CONED BASE PLATEN CONSTRUCTION AND INSTALLATION

5.1.3 Sample Preparation: New procedure

It is good practice to provide over-sized platens to allow for increasing sample diameter in compression. Hence, when the existng platens were replaced by coned ones, these were made over-sized and a new method of fixing the sample mould was developed, as illustrated in Fig. 5.1(b). The mould was now simply placed on the platen with a rubber ring to protect the sample membrane. It was centralised by eye and locked into position by ties. The sample mould is filled as previously and, on reaching the top, a further rubber ring was placed on the mould and the top platen was accurately positioned and attached to the sample membrane.

5.1.4 Development of Volume Measuring Techniques

The need to measure strains in both the axial and radial direction was considered important to gain an understanding of the material properties. Axial deformations could be measured using a simple dial gauge (initially it was intended that this piece of apparatus only be used for large strain tests) but radial deformations posed a major problem. It was decided to measure total volume change together with axial deformations, from which the required strain parameters could be calculated. Fig. 5.4 shows the arrangement of the volume measurement system in schematic form. The untested dry sample was placed in position in the testing rig supported by an internal vacuum applied via the sealed burette. Taps 1, 2 and 3, as shown in Fig. 5.4, were an integral part of this system and, at this stage of the preparation, tap 1 was open while taps 2 and 3 were closed.

The sample was saturated with de-aired water from the resevoir, shown in Fig. 5.4. Tap 2 was opened, allowing the water to enter the sample via the drainage system, which is shown in detail in Fig. 5.3. The tubing in use was approximately 3mm bore and this ensured that the flow rate was sufficiently low to allow a good vacuum to be maintained in the sample.

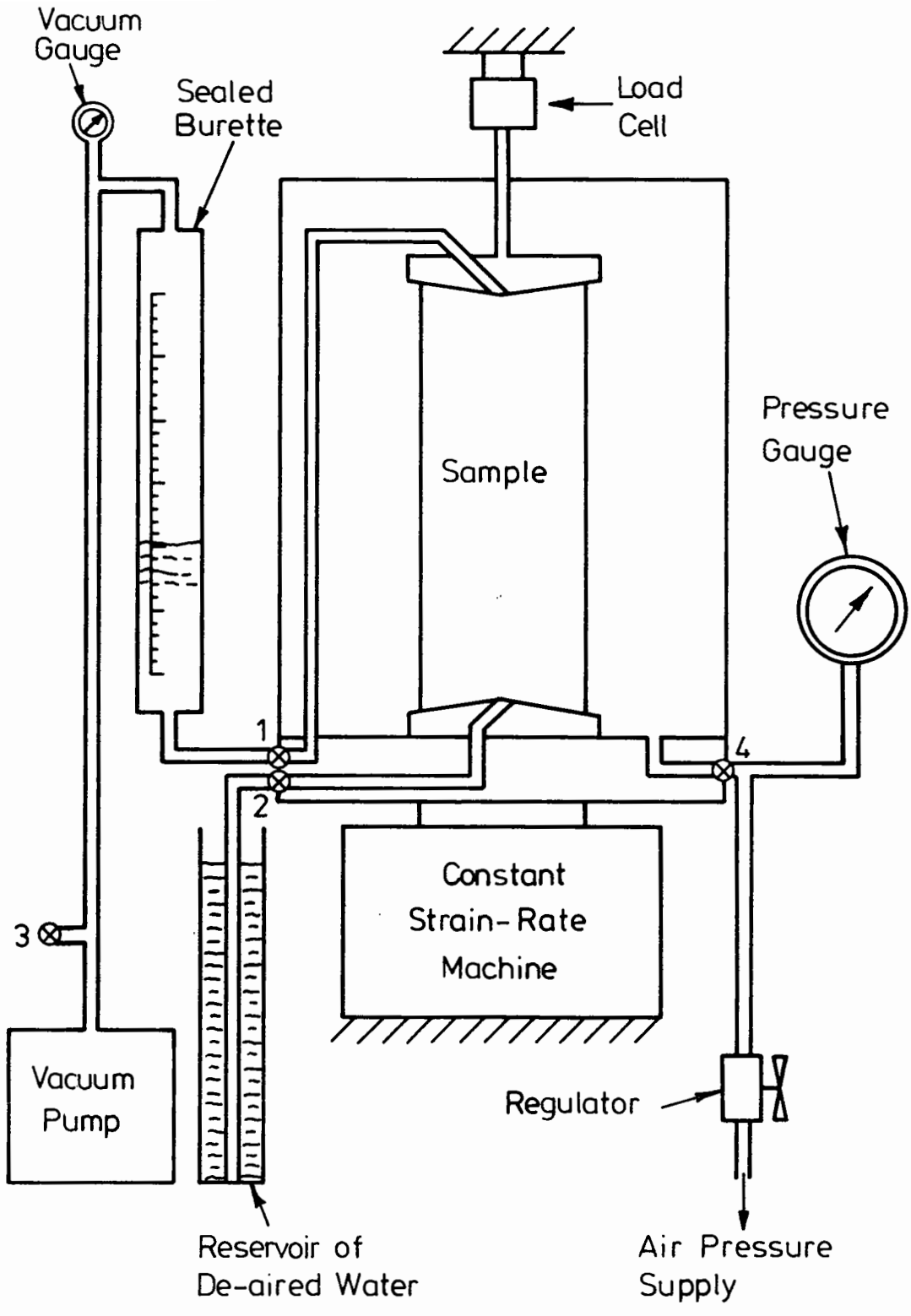

FIG. 5.4 ARRANGEMENT OF MONOTONIC TRIAXIAL RIG

When the sample was completely saturated, water flowed through tap 1 and into the burette. When the water reached a fixed mark on the burette, tap 2 was closed to prevent further flow. The cell pressure was then applied by the regulated compressed air system. This supported the sample externally, thereby allowing the internal vacuum to be released.

During the testing, the volume changes were measured simply by reading the volume of water in the calibrated burette.

5.1.5 Development of Radial Strain Measuring Technique

Using the volume measurement system described above, the calculation of radial strains was performed by subtracting axial strain. In the two preliminary tests, it was noticed that the resolution of the volumetric strain measuring system was such that very small strains could not be measured. When the importance of behaviour at small strains became apparent, it was considered necessary to design a more sensitive system. The use of strain gauged araldite hoops (similar to those used for the repeated load triaxial apparatus, see section 5.2) was considered, but was rejected as being too expensive and time consuming. The hoop moulds would have required a considerable amount of machining and the hoop, once cast, would have had to undergo a lengthy curing process to reduce brittleness and creep susceptibility.

The system eventually chosen was an inductive coil arrangement. It was easily available, being already used at Nottingham for instrumenting road foundations, and was sensitive enough for this new application. It is based on the principle that when an alternative current flows in a coil, then nearby coils will have a current induced in them. If two coils are placed in proximity so that they are facing each other, the current induced in the passive coil will be a function of their separation distance. Knowing the induced current, therefore, allows their separation to be

calculated.

In the final design, four coils were used as in Fig. 5.5. Two small coils of 25mm diameter (a and b) are attached to the sample across a diameter. Two 100mm diameter coils (A and B) were fixed to the triaxial cell structure itself. The alternating currents flowing in A and B induced currents in coils a and b respectively. The sample diametral deformation was equal to the sum of the changes in separation from A to a and B to b.

The large (100mm) coils (A and B) were each set into a non-conducting plate made of Tufnel. This plate was then attached to a frame so that the coil may move up or down in order that it may be positioned co-axially with its partner coil (a or b) on the sample. There are two major advantages of using a large coil as the active coil.

(a) The current induced in the smaller coil is very insensitive to large movements (up to several millimetres) parallel to the large coil. Thus when the sample deforms vertically the relative movement of the coils in the vertical direction does not contribute greatly (less than 5%) to the change in output.

(b) Its large diameter enables currents to be induced in coils at a considerable distance and allows it to be placed outside the cell. This provides many advantages; access to the coil for alignment purposes, for example.

The main advantages of using small coils on the sample were that they weigh less and are easier to fix. A rubber solution adhesive was used to attach the coils to the sample membrane.

Calibration of the system was carried out in the cell as all nearby conducting material (for example the cell ties) would affect the recorded outputs. During normal operation the typical resolution of the system was approximately 50$\mu\epsilon$. This is considerably more sensitive than the original burrette system.

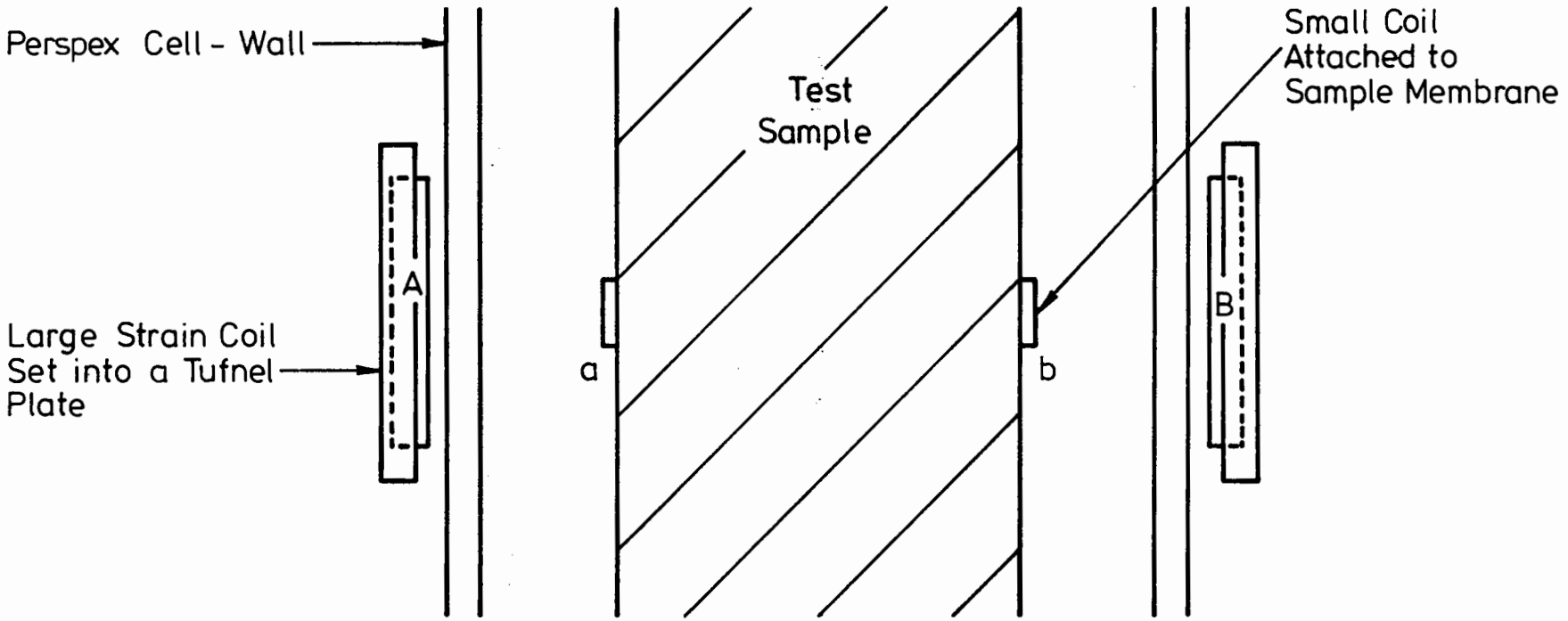

Fig. 5.5 Radial Deformation Measuring System

5.1.6 Measurement of Axial Strain

The original axial measurement system consisted of using a dial gauge to measure the movement of the deviator loading rod. An attempt was made to compare the material stiffnesses obtained using this arrangement with those measured in the repeated load triaxial apparatus using the "on-sample" instrumentation system. It was observed that stiffnesses calculated from the external measurement system were much lower than those obtained by the "on-sample" system. It was concluded that the external instrumentation system was measuring not only the sample deformation but also equipment movements and deformations. In addition to this, at the interface between platen and sample, large deformations occurred as a result, not only of deformation of the friction-reducing membrane, but also because of particle rearrangement in this zone. Recent work at Imperial College (e.g. Symes and Burland, 1984) also points to this conclusion.

As a consequence of these large deformations, the stiffness calculated using the original system was considerably (orders of magnitude) below the real value. As behaviour at small strains was important, it was necessary to provide a more accurate arrangement. It was decided to use a system similar to that used for the repeated load triaxial apparatus (see Section 5.2). At first, axial deformations were measured using potentiometers, but these were eventually replaced by LVDT's (Linear Variable Differential Transformers) for the following reasons:

(a) The potentiometers contained return springs. This meant that the rods to which the instruments were connected were being loaded. Errors in axial measurement would be caused if the rods were to move as a result of this load. By using a non-contacting system such as LVDT's, this problem was avoided.

(b) It became apparent during the tests using potentiometers that the material under investigation was capable of carrying high stresses at

very low values of strain. The LVDT's were able accurately to measure much lower strains than the potentiometers.

Fig. 5.6(a) shows the arrangement using potentiometers. Fig. 5.6(b) shows how the LVDT's were connected. It was decided to use a "pendulum" system to suspend the LVDT cores. This ruled out the possibility of friction which may have developed between the core and LVDT body in a rigid system (it is not feasible to do this in the repeated load apparatus since at higher frequencies dynamic effects would cause errors in measurement).

The locating studs were those normally used in the repeated load apparatus. They were stabilised in the same way with silicone rubber (see Section 5.2 below).

5.1.7 Measurement of Axial Load

During all tests, loads were measured external to the triaxial cell. The friction between the loading ram and the seal at the top of the cell was ignored. The use of an internal load cell was considered but rejected due to the lack of space at the top of the sample in the cell. However, great care was taken to eliminate as much friction as possible. The sealing bush and loading rod were polished and greased before each test. Considerable effort was also made to align the sample so that the ball-bearing through which load was transferred to it was directly below the loading rod. This avoided the possibility of horizontal loads.

5.2 REPEATED LOAD TRIAXIAL APPARATUS

A servo-hydraulic repeated load triaxial apparatus for granular materials, has been developed at the University of Nottingham over a number of years, Boyce (1976) and Pappin (1979).

Fig. 5.7 shows the main components of the servo-hydraulic system.

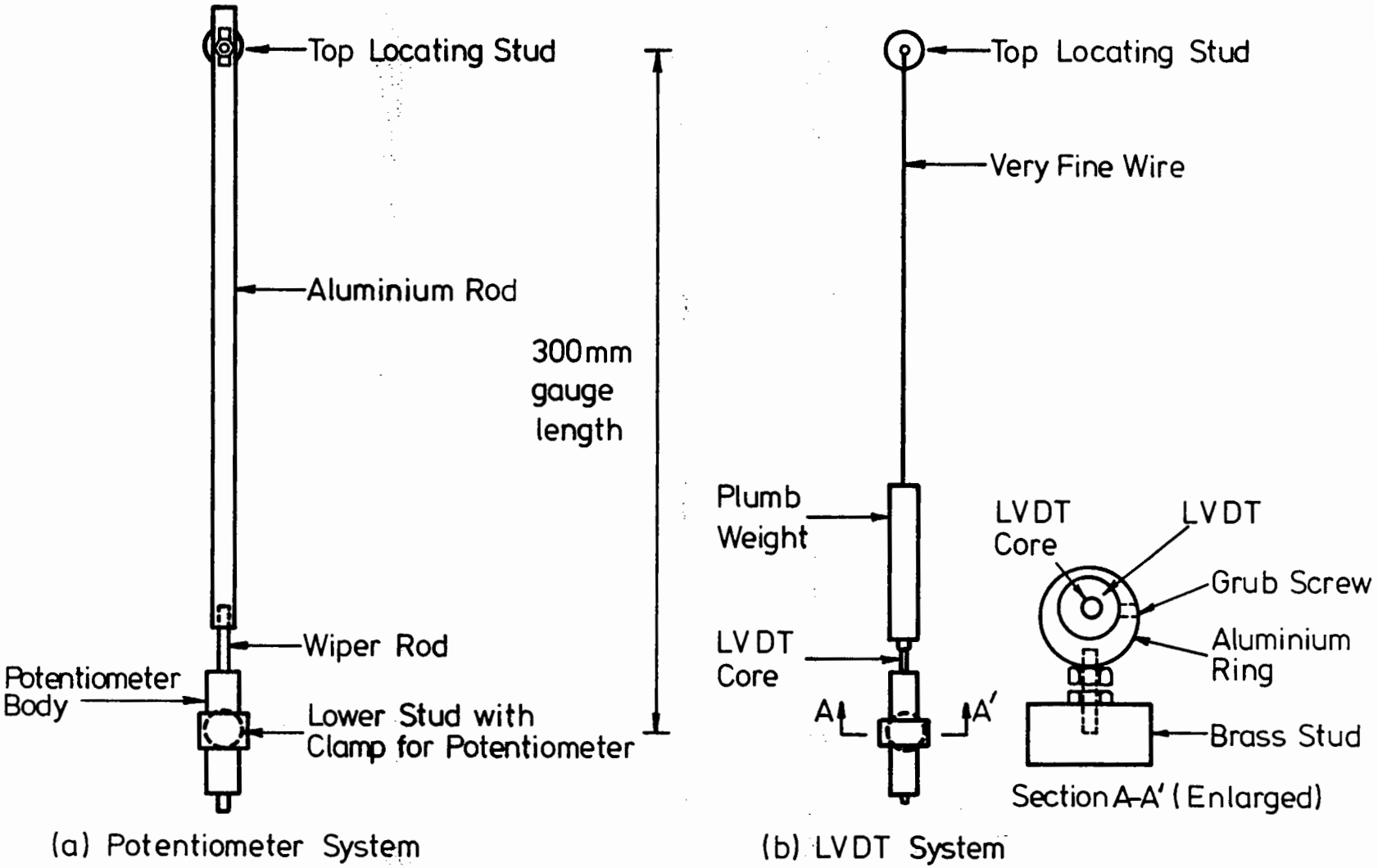

Fig. 5.6 Axial Deformation Measuring Systems

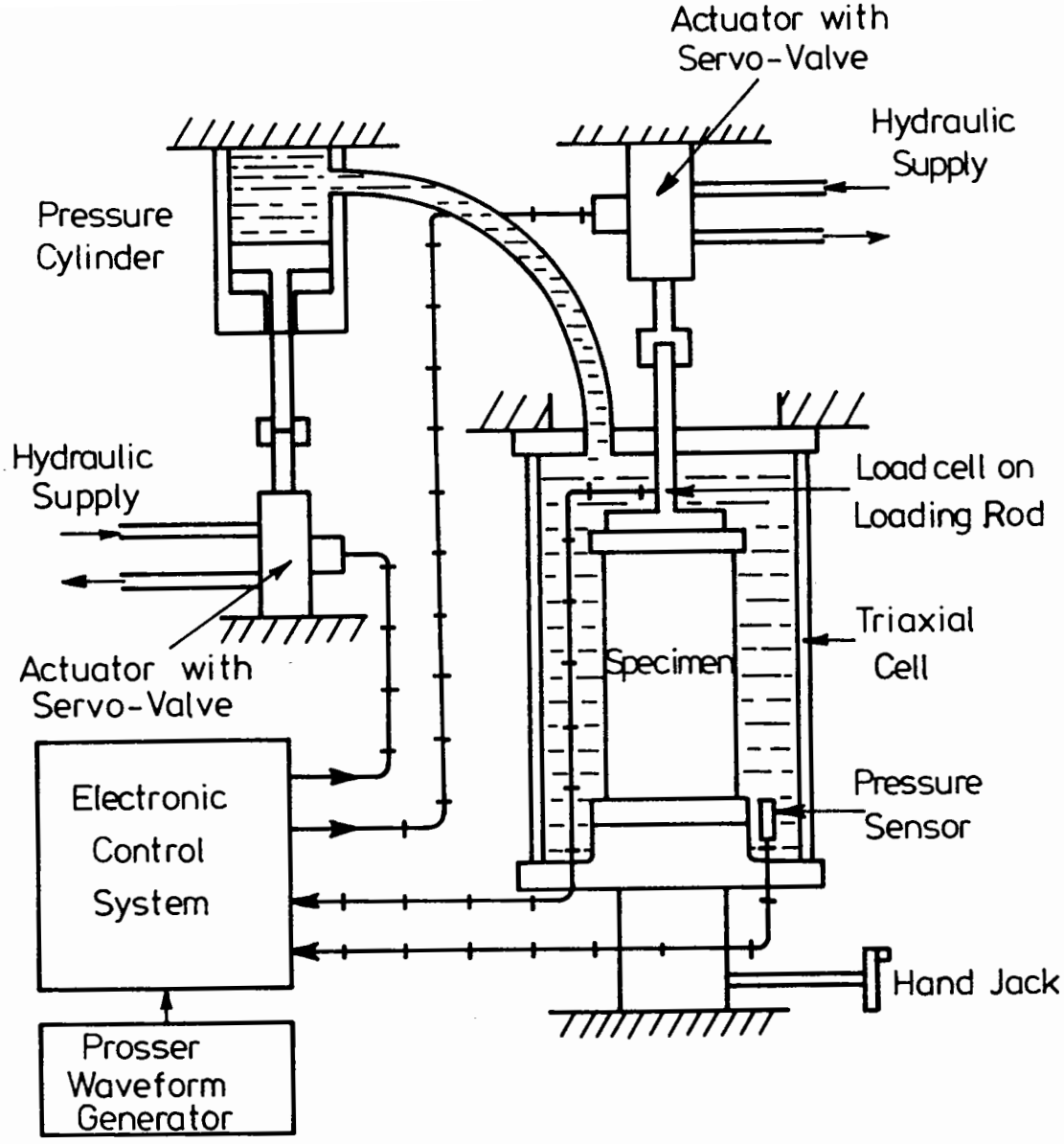

FIG. 5·7 DIAGRAM OF LOADING EQUIPMENT

Axial load is applied by an actuator and monitored by a load cell which forms an integral part of the axial loading arrangement. This is illustrated in greater detail in Fig. 5.8. Cell pressure is applied through the silicone fluid surrounding the test specimen. The pressure is controlled by another hydraulic actuator which loads a piston in a pressure cylinder. It is monitored by a sensor in the triaxial cell. During repeated loading, the feedback signals from the axial load and cell pressure sensors are compared with the command signals from the electronic control system. An error signal is then applied to the servo-value on the hydraulic actuators which modifies the applied load.

5.2.1 Equipment Capability

The axial loading system has a load capability of approximately ±20 kN. This allows deviator stresses in the range ±1200 kPa to be applied. The ability to apply a negative deviator stress is effected by the sealed and evacuated cavities which connect the load ram to the top platen and the bottom platen to the cell base. This arrangement is illustrated in Fig. 5.8. The cell pressure is limited by the area of the piston in the pressure cylinder and the maximum hydraulic actuator load that may be applied to the piston. The present arrangement enables cell pressures in the range 0 to 400 kPa to be applied, although this may be increased by changing either the area of the piston or the capacity of the actuator. A further limitation is the safe working pressure of the triaxial cell (approximately 600 kPa).

The equipment may apply testing rates in the range 0.001 Hz to 20 Hz. Preliminary tests using denstone showed that in the range 0.01 Hz to 2 Hz, no discernable difference in measured strains was observed using the same stress path on the same sample.

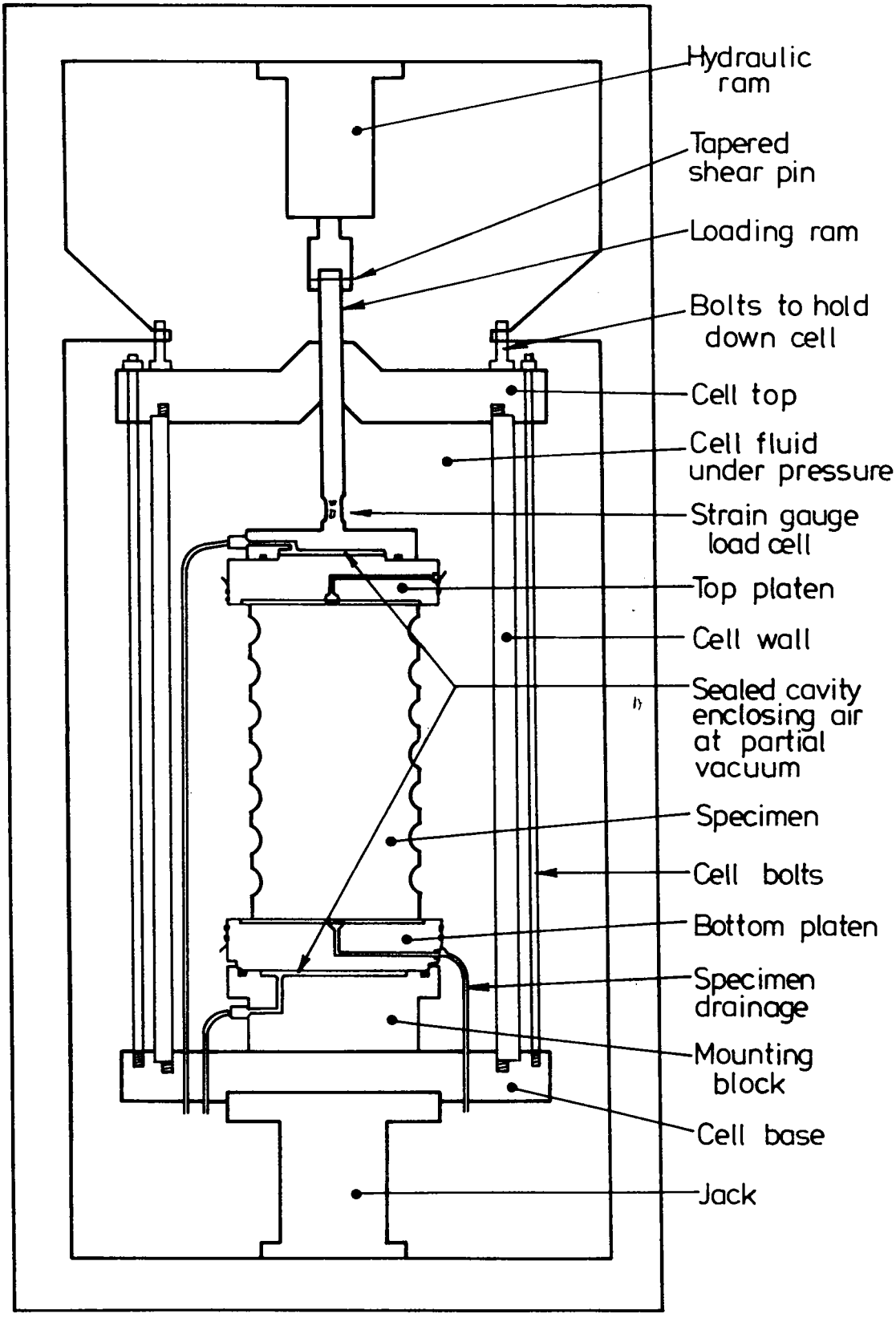

FIG. 5.8 AXIAL LOADING ARRANGEMENT

5.2.2 Sample Preparation

Each sample was approximately cylindrical, being formed in a four-piece split-mould fitted with a dimpled liner (the function of which was discussed in section 5.1 above). The sample was enclosed by two membranes; the inner one of 0.3mm latex was stretched over one of the platens and held tight against the mould-liner by a vacuum which was applied to the cavity between it and the four-piece mould. Fig. 5.9 shows the preparation in progress. The stud locaters were fitted to the inner latex membrane and to the mould liner at the outset of preparation. The material was placed in ten layers of approximately 30mm, each layer being compacted by hand tamping. This method of compaction was more likely to yield densities which may be expected in the prototype and it avoided the possibility of areas of regularly arrayed material forming, which may have changed the sample properties (eg. see Wroth, 1958).

5.2.3 Deformation Measurement

Strains were determined from deformation measurements taken from points on the sample by means of location studs, as illustrated in Fig. 5.10. These studs were developed by Boyce (1976) for use with graded materials. They were also used successfully for the samll single-size crushed rock material tested by Shaw (1980). In the Denstone particles, however, the studs had a tendency to be unstable and rotate with applied load. This effect was greatly accentuated with increase in particle diameter to stud diameter ratio. The probable explanation for this behaviour is that as this ratio increased the number of contacts between particle and stud decreased, leading to a greater probability that the loading on the stud will be eccentric. After the sample had been formed and was free-standing supported by internal vacuum, the instrumentation, as shown in Fig. 5.10, was attached by screwing a rod into the stud and then

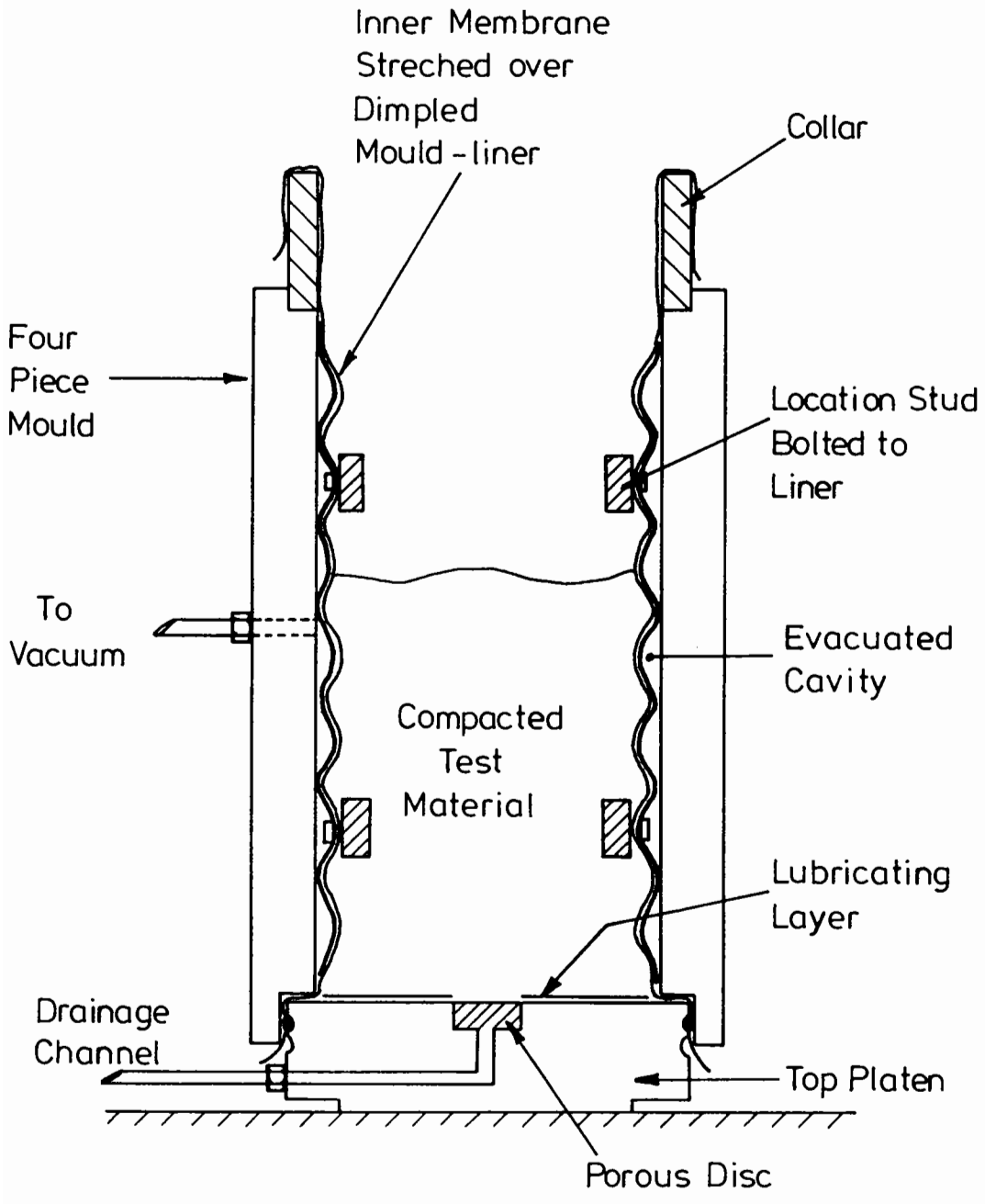

FIG. 5.9 SAMPLE PREPARATION FOR REPEATED LOADING

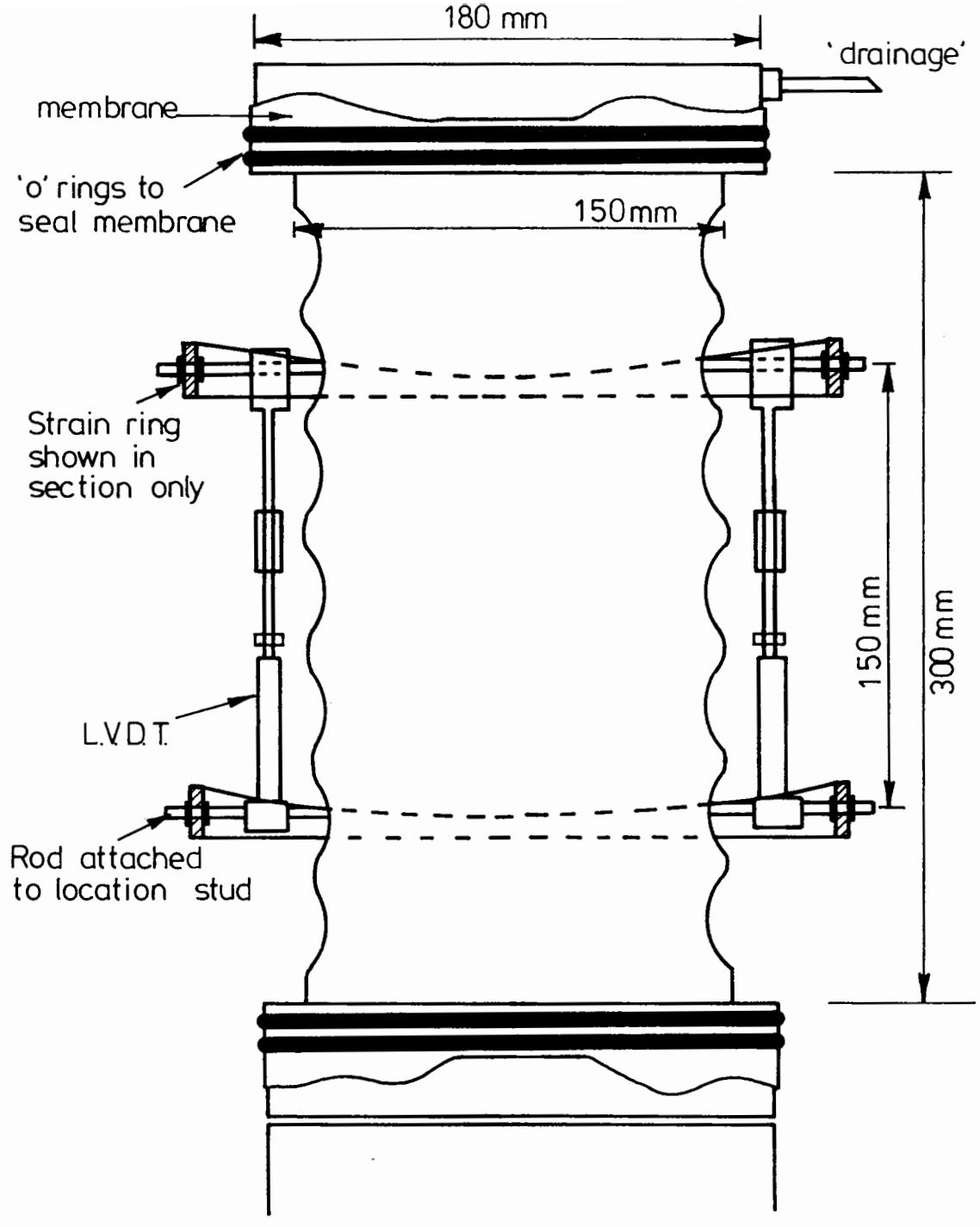

FIG 5.10 POSITION OF STRAIN TRANSDUCERS ON SAMPLE

connecting the strain transducers to this rod. During this procedure a certain amount of 'manhandling' was inevitable and this tends to loosen the studs even further, making them more unstable than before.

Stud Stabilisation: To overcome this, silicone rubber was injected into the sample before the attachment of any instrumentation. This provided a certain strength in the region of the stud and ensured that any contacts between the particles and the stud are maintained during the fixing of instruments. Details of the location studs are shown in Fig. 5.11. A sample was made from 6mm denstone and this method of stud stabilisation was used. The studs were shown not to rotate by placing two LVDTs (Linear Variable Differential Transformers) on the rod, one close to the sample and the other at a distance of approximately 40mm. The deformation measured between these points and a horizontal fixed rod on an independent scaffold were the same during cyclic loading and this indicated that no rotation was taking place. This test was performed satisfactorily with all four stabilised studs at strains of up to 500$\mu\epsilon$.

Radial Strain Hoops: Radial strains were measured using araldite strain hoops, the details of which are shown in Fig. 5.12. Each hoop was cast and subsequently heat-treated and strain cycled in order to remove any creep behaviour. The hoops were strain gauged, as shown in Fig. 5.12, in a simple bridge arrangement, and output was linear with strain over a large range of deformations (greater than 5mm). The hoops were susceptible to air currents but once immersed in cell fluid they became very stable. The hoops were attached to the sample, as shown in Fig. 5.10.

5.2.4 Data Recording

The outputs from the electronic control system drove an oscillograph

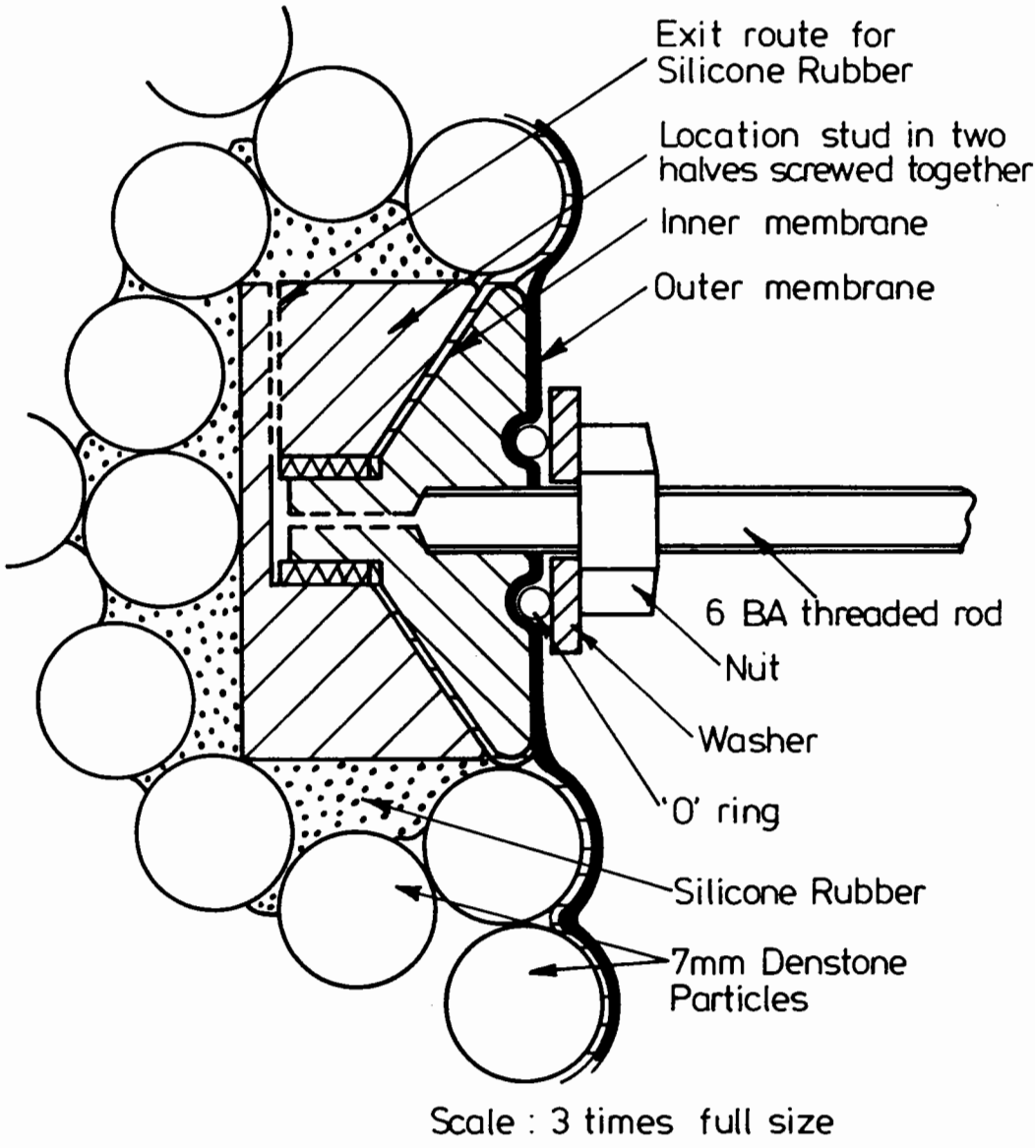

FIG. 5.11 LOCATION STUD FOR STRAIN TRANSDUCERS SHOWING SILICONE RUBBER STABILISATION

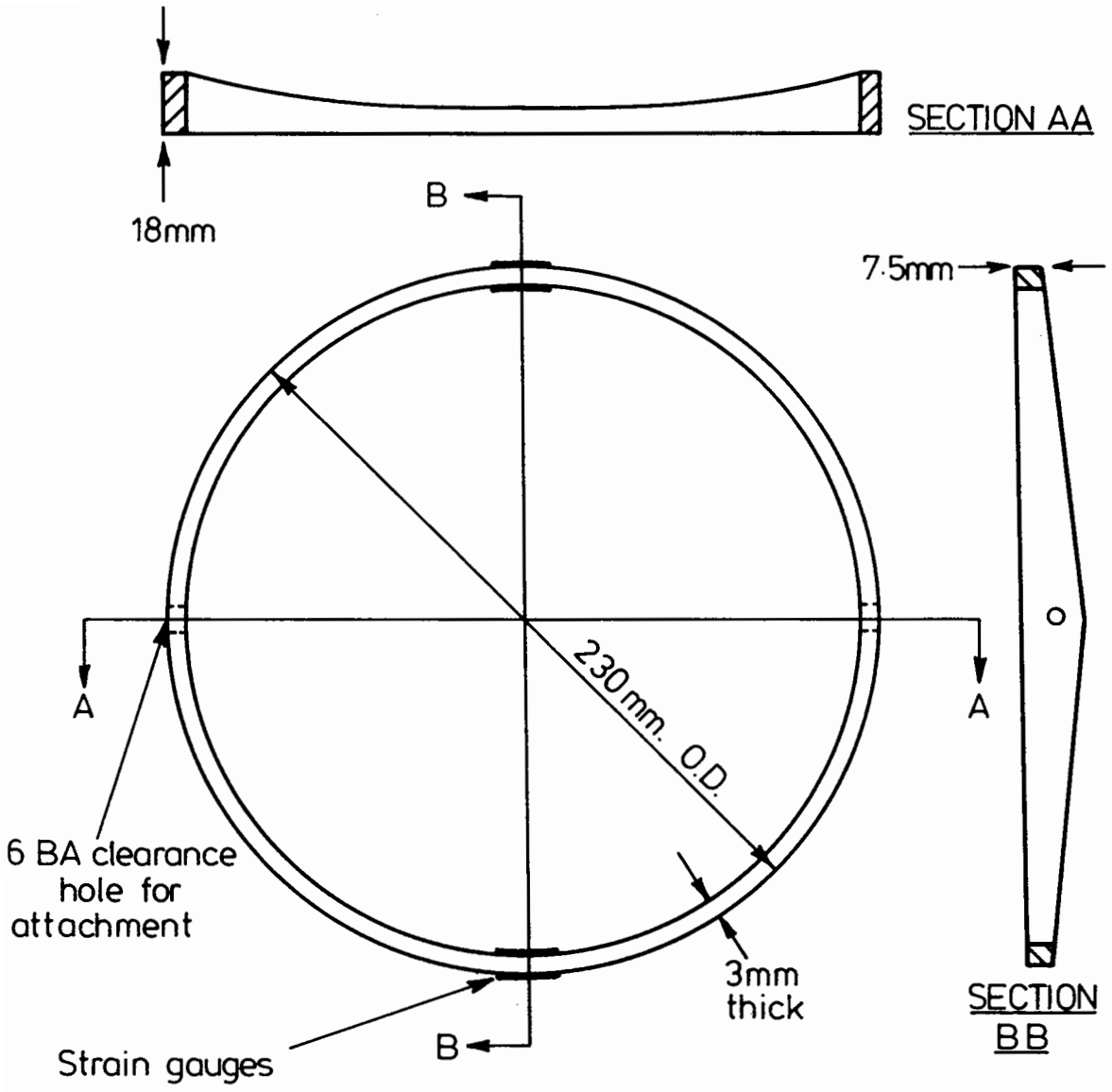

FIG. 5.12 ARALDITE STRAIN RING

U.V. recorder. Six channels were used:

1. Axial load
2. Cell pressure
3. Axial deformation
4. Radial deformation
5. Elastic axial deformation
6. Elastic radial deformation

Channels 5 and 6 presented the same data as channels 3 and 4 but were amplified and offset. The galvanometers which display the data on the screen were therefore always within range, despite large permanent deformation. Various ranges of amplification were available and strain resolution down to 5 $\mu\epsilon$ was possible at maximum gain. The benefit of this system was that the oscillograph produced a continuous and permanent record of a large number of variables. The outputs also drove an X-Y plotter via a signal combination box which combined various inputs. It produced a range of useful variables for plotting, including the critical state soil mechanics stress and strain invariants. The benefit of using an X-Y plotter was that important information concerning hysteresis effects was immediately apparent.

CHAPTER SIX

EXPERIMENTAL RESULTS

6.1 INTRODUCTION

The results from experimental research are presented in this single chapter in order to facilitate cross-referencing of results. The layout requires some explanation.

The chapter is divided into three main sections:

A. Initial loading (monotonic) behaviour

B. "Intermediate" behaviour

C. Resilient behaviour

In this classification, "intermediate" refers to behaviour before the resilient equilibrium is reached. It includes the effects of increasing numbers of cycles on stiffness, permanent strain, hysteresis and dilatancy.

The results from each test are presented in that section of the chapter to which they specifically apply. If they are relevant to more than one section, they are presented in the earliest section to which they relate, and the reader is later referred back. The results from the large triaxial apparatus, for example, are presented in full in Section A, although many of these tests are also relevant to Section B.

SECTION A - MONOTONIC BEHAVIOUR

6A.1 TEST PROGRAMME

Table 6.1 gives a list of the tests which have been performed using the large triaxial apparatus. The code identifies the test conditions and a guide to the code is given beneath Table 6.1. The initial letter of the code (A, B or C) identifies the test series.

TABLE 6.1 TESTS PERFORMED IN LARGE TRIAXIAL APPARATUS

Test No.	Date Tested	Remarks
A9-352-1	Nov 1982	Coned Platens Not Used. Large Strains
A19-210-1	Dec 1982	" "
B9-100-1	Sept 1983	
B6-100-1	Sept 1983	Repeated Loading
BIO-100-1	Oct 1983	Repeated Loading
C6-133-1	Jan 1984	Repeated Loading
C6-400-1	Feb 1984	
C9-133-1	Jan 1984	
C19-133-1	Jan 1984	Studs Rotated
C19-133-2	Jan 1984	Axial Strain Measurements Only
C19-266-1	Feb 1984	Studs Rotated
CM-133-1	Feb 1984	Mixed Material 19mm, 9mm, 6mm Denstone

NOTES

1. Explanation of Test Code Numbers

eg. B 9 - 100 - 1

Test Series	Particle Size (mm)	Cell Pressure (kPa)	Identification Number

The type of material in the test code is indicated as follows:

Denstone - the particle diameter is given. "M" indicates that equal proportions (by weight) of sizes 6mm, 9mm and 19mm have been used.

Iron Oxide - IO.

All tests were performed at constant cell pressure with positive deviator stress, so that the only component of stress which was varied during the test was the magnitude of σ_1. The direction of all three principal stresses remained constant throughout.

The majority of the tests involved simple monotonic loading. Three tests (B6-100-1; B10-100-1, C6-133-1) involved several cycles of increasing and decreasing load.

All samples in series B and C were compacted by prolonged tamping. Specific volumes of approximately 1.5 were achieved for all samples (except CM-133-1 which was a partially graded specimen).

6A.1.1 Test Series A

Two tests were performed in this series and the results are presented in Section 6A.3. As well as providing preliminary data on which to found a test programme, the main purpose of these tests was to investigate behaviour at high strains. Using a water-burette system, dilatant volumetric strains of up to about 5% were recorded.

6A.1.2 Series B

Three tests were performed in this series. During these tests, axial strains were measured using a single potentiometer mounted on the sample in order to avoid the gross errors discussed in Chapter 5. Radial strains were measured using the strain coil arrangement also described in Chapter 5.

6A.1.3 Series C

After several tests in Series B, it was decided to replace the potentiometer with a pair of LVDT's in order to increase accuracy and resolution. The tests performed using this new instrument arrangement have

been denoted "Series C."

Seven tests were carried out in this series. Four were completely successful. During two tests the studs rotated (see Section 6A.2.2 below) and, in one test the radial deformation measurement system failed.

6A.2 INSTRUMENT PROBLEMS

6A.2.1 Insensitivity of Instruments used during Series A

It has already been observed (Chapter 5) that the dial gauge system of measuring axial strains and the burrette system of measuring radial strains were found to be inadequate except for determining behaviour at high strains. These systems were replaced by the more sensitive instrumentation systems described in Chapter 5.

6A.2.2 Stud Rotation

In two tests (C19-133-1 and C19-266-1), the studs to which the LVDT's were attached appeared to rotate. Fig. 6.1 shows the axial strains recorded during test C19-133-1. The particles being tested during C19-133-1 and C19-266-1 were of comparable size to the brass stud. It seems likely that the small number of initial particle-stud contacts, as well as the tendency for particles to rotate during shear, caused the stud itself to rotate. In test C19-133-2, this problem was overcome by placing a mixture of particle sizes in the immediate vicinity of the locating stud.

6A.2.3 Radial Strain Offsets

During most tests in Series B and C, the recorded radial strains appeared to change rapidly during the first moments of loading, so that when the results are approximated to a smooth curve they show an initial

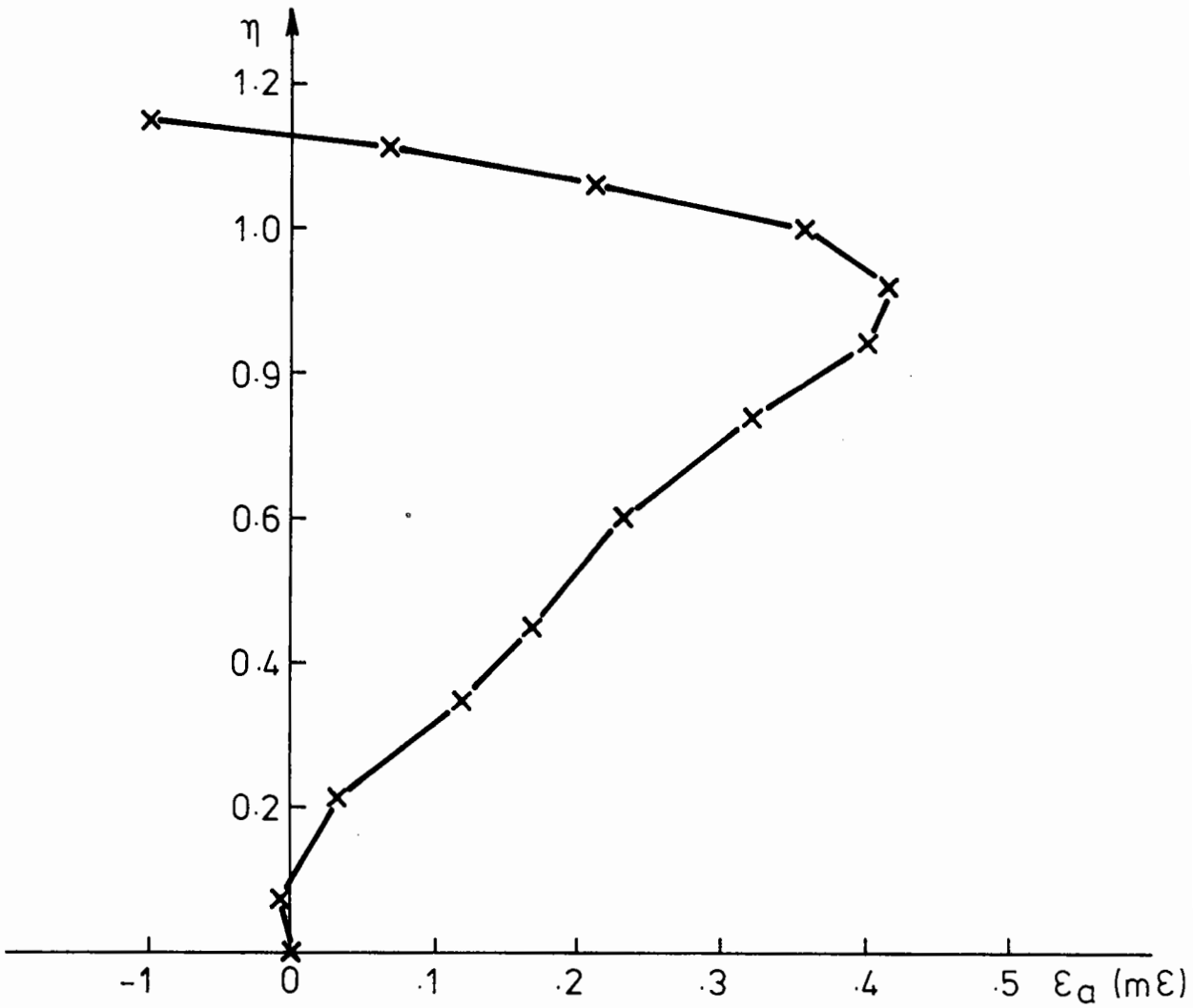

Fig. 6.1 Axial Strains Recorded During Test C19-133-1

offset. Examples are given in Fig. 6.14(a), where the radial strain behaviour during tests C9-133-1, CM-133-1, C6-400-1 and C6-133-1 are shown - when a smooth curve is fitted to the recorded data points, a non-zero initial strain is recorded. As can be seen, its value is not constant, but appears to be random about the zero point.

The explanation for this phenomenon is not known. The apparent offsets have been compensated for by merely subtracting them from the recorded values of strain. Table 6.2 gives a list of offset values recorded for the various tests. The subjectivity of the process of deciding upon an offset value has not been overlooked, but no viable alternative has been found.

6A.3 SERIES A - TESTS

In order to gain some indication of the way in which the material might be expected to behave, two preliminary tests were performed with the original flat platens, at an axial deformation rate of 1mm per minute. Sample A9-352-1 was formed from 9mm nominal size Denstone densely packed. Sample A19-210-1 was formed from 19mm Denstone loosely packed (no vibration or tamping was used). The results of the monotonic tests carried out are shown in Figs. 6.2 (deviator stress vs axial strain) and 6.3 (volumetric strain vs axial strain). In Fig. 6.4, the paths followed in (q, p, v) space are shown. As can be seen, a peak strength of $\eta = 1.5$ was observed for both samples despite (a) the differences in specific volume at failure, and (b) the differences in dilation rate at failure.

6A.4 SERIES B AND C - PRESENTATION OF RESULTS

Following the practice of Critical State Soil Mechanics, stresses and

TABLE 6.2 OFFSET RADIAL STRAIN VALUES

Test No.	Radial Strain Offset (με)
B9-100-1	-1100
B6-100-1	0
BIO-100-1	0
C6-100-1	-150
C6-400-1	+60
C9-133-1	+150
CM-133-1	+180

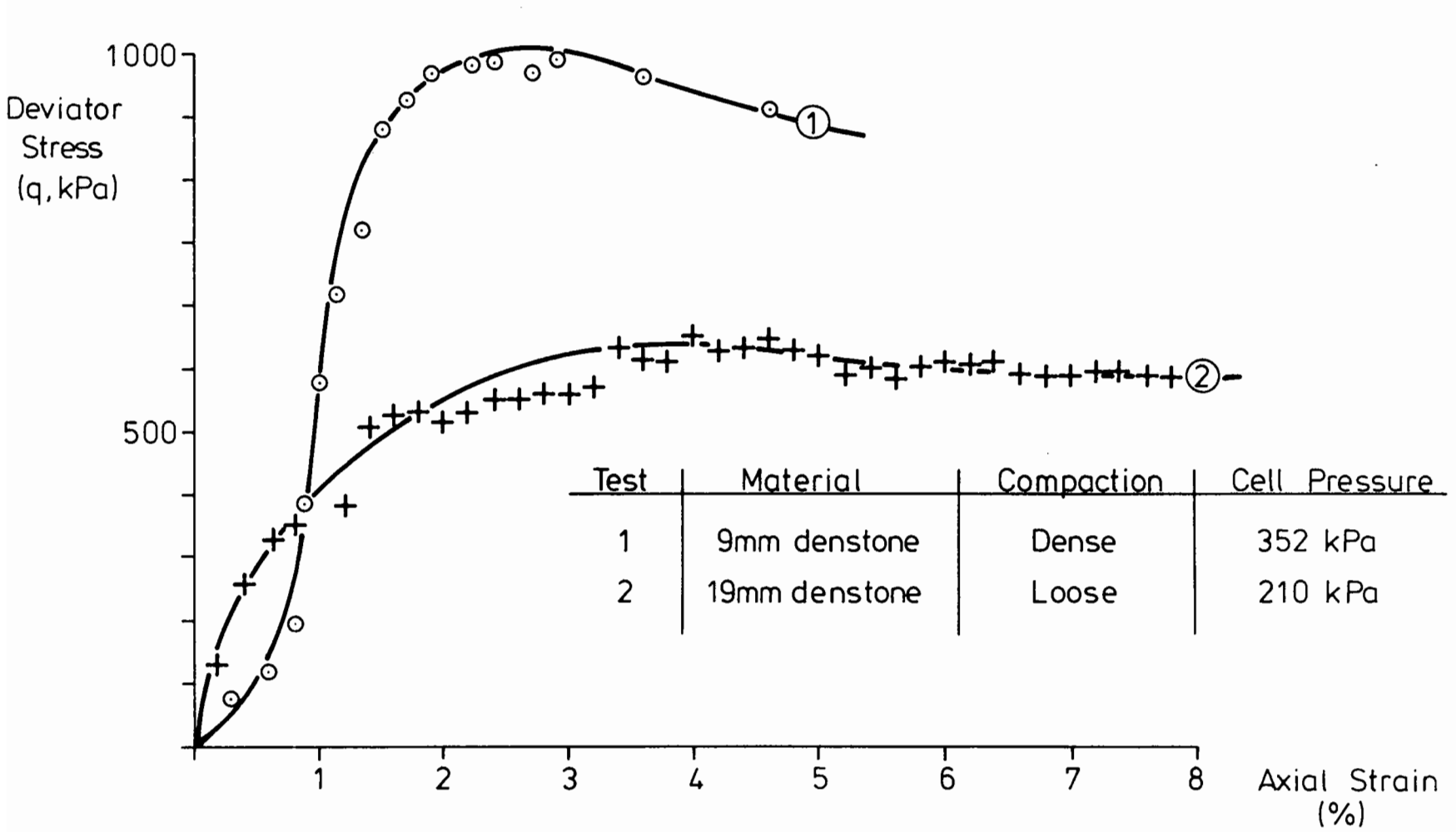

FIG. 6.2 RESULTS OF PRELIMINARY MONOTONIC TRIAXIAL TESTS

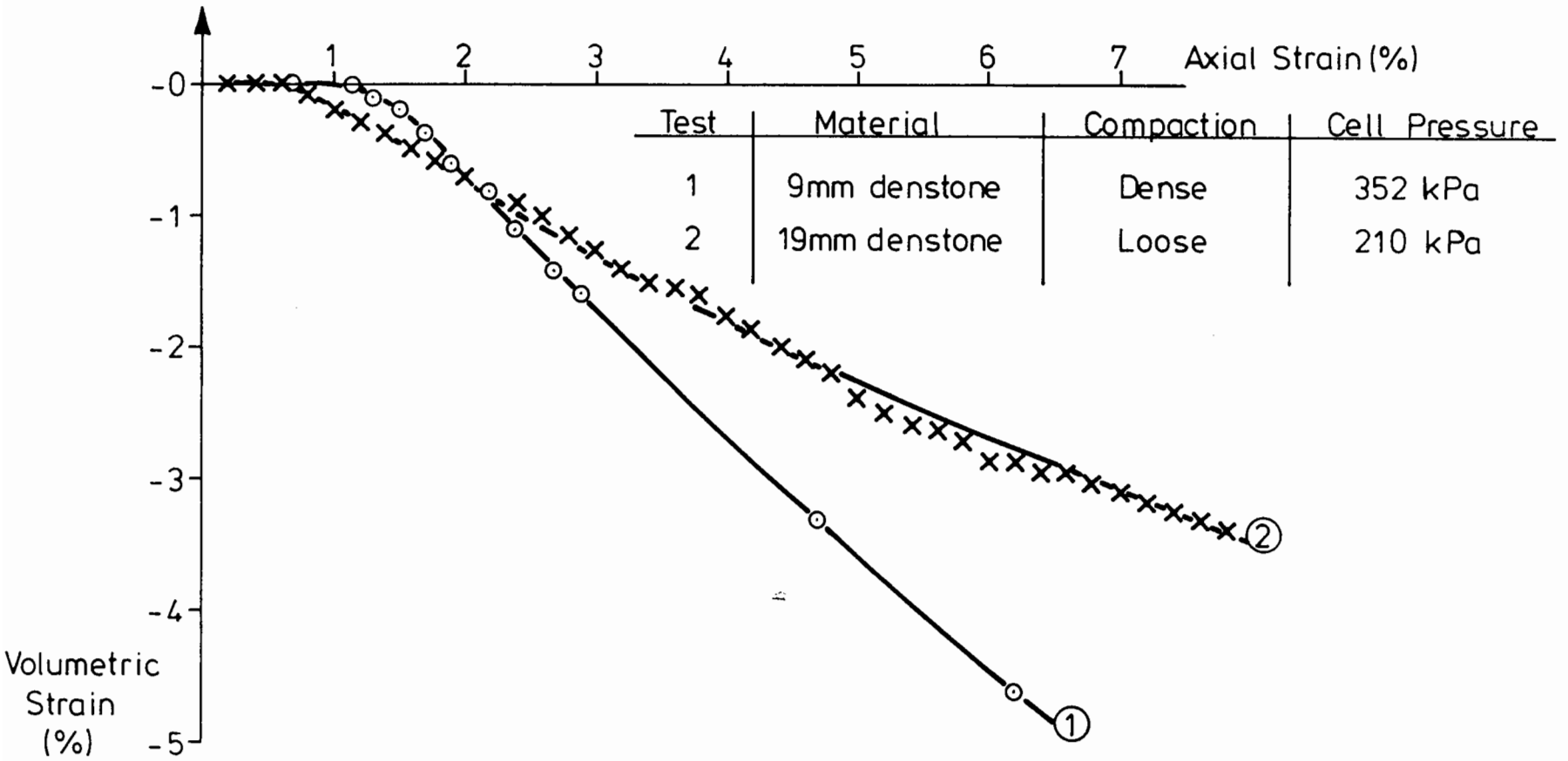

FIG. 6.3 RESULTS OF PRELIMINARY MONOTONIC TRIAXIAL TESTS

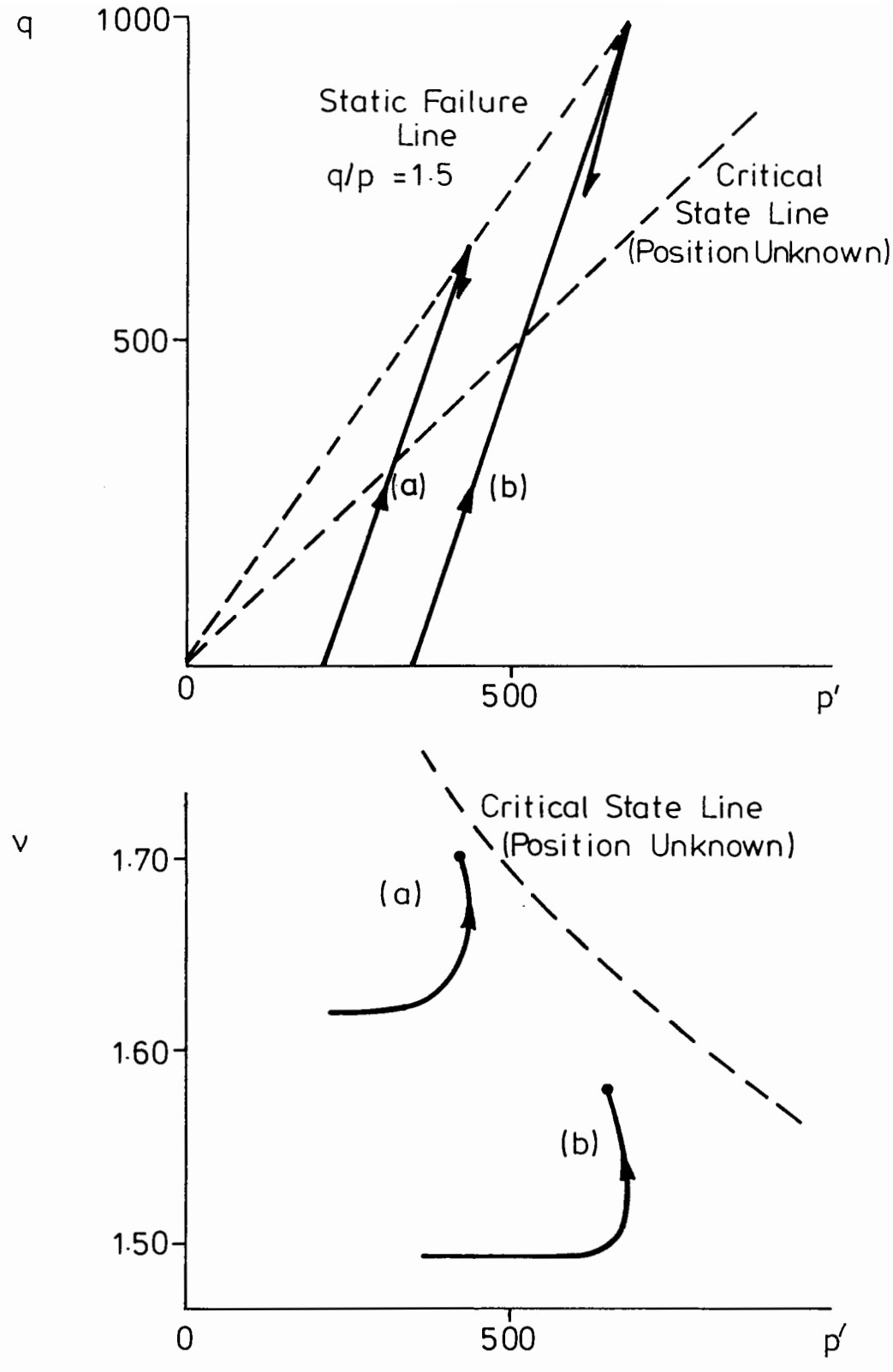

FIG. 6.4 STRESS-STRAIN PATHS IN q, p', v SPACE

(a) Cell Pressure = 210 kPa (b) Cell Pressure = 352 kPa

strains will be divided into the deviatoric (shear) and spherical (volumetric) components whenever possible.

As an unbound granular material is frictional, its shear behaviour will be greatly influenced by the mean normal stress. Therefore, when comparing the results from tests performed at different initial mean normal stresses, the shear stress to mean normal stress ratio η (= q/p') has been used.

The axial and radial deformation measuring systems were completely independent and the shear and volumetric strains were calculated from the values given by these two systems. It appears from the plots of axial and radial strains observed during Series C, that the axial measurements were not subject to the same random distortions as the radial measurements (compare 6.13 and 6.14(a)). Consequently, when discussing behaviour at very small strains (less than about 500$\mu\epsilon$ or 0.5% ϵ), where such distortions will account for a large proportion of the recorded strain, it is often useful to refer to axial strains.

In addition to graphs of shear and volumetric strains, typical plots of axial and radial strain are presented. Table 6.3 gives a list of graphs of results. These results are tabulated in Appendix A.

All samples were preconsolidated to a pressure of 200 kPa before the application of any deviator stresses.

6A.5 MATERIAL STRENGTH

6A.5.1 Denstone

The two Series A tests showed that the material failed (i.e. was unable to sustain a greater stress) at η = 1.5. Most researchers indicate that axial strains of several percent are required in order for the

TABLE 6.3 TABLE OF GRAPHS

Fig. Numbers	Description
6.5	Typical Recorded Axial Strains
6.6	Comparison between Axial Strain Results
6.7	Typical Recorded Radial Strains
6.8	Comparison between Radial Strain Results (Corrected)
6.9 (a) - (d)	Shear and Volumetric Strains
6.10 (a) and (b)	Strains from Test B6-100-1
6.11 (a) and (b)	Strains from Test BIO-100-1
6.12	Shear and Volumetric Strain Test C6-133-1
6.13	Behaviour of Denstone at Small Axial Strain
6.14 (a)	Recorded behaviour of Denstone at Small Radial Strains
6.14 (b)	Corrected Radial Strains
6.15 (a) - (d)	Small Strain (Shear and Volumetric) behaviour of Denstone
6.19	Axial Strains from Modified Denstone Test

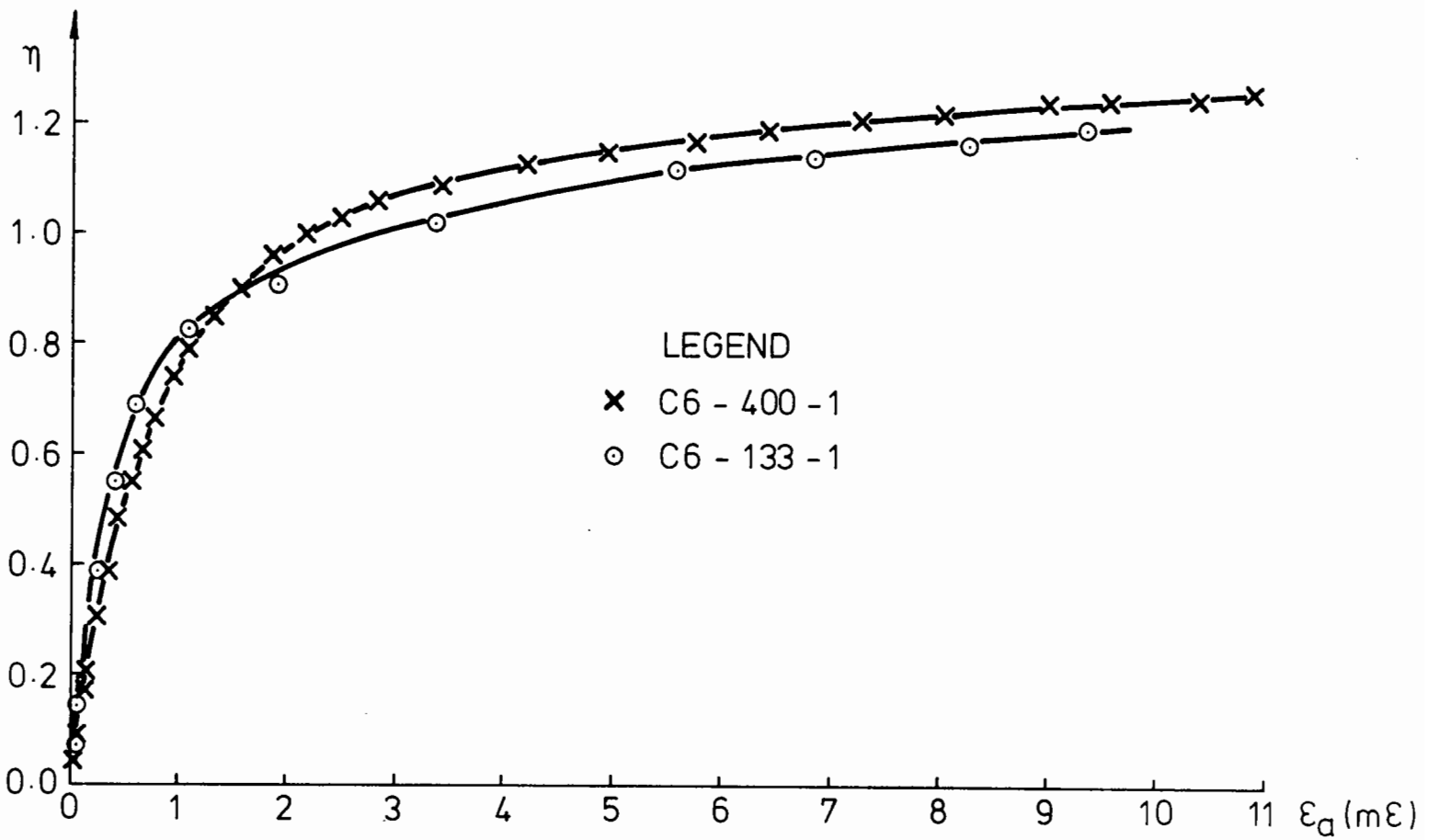

Fig. 6.5 Typical Recorded Axial Strains

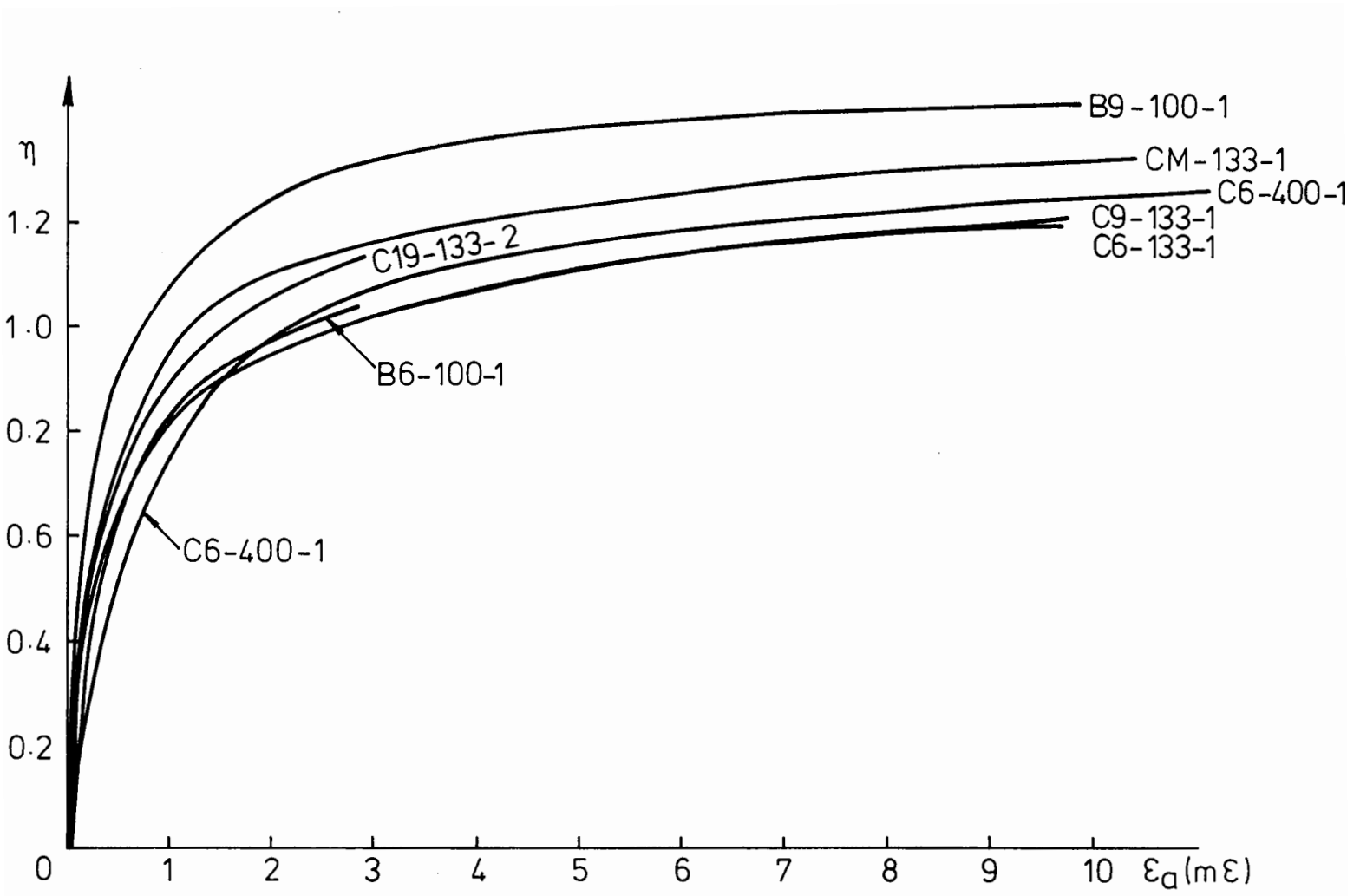

Fig. 6.6 Recorded Axial Strains

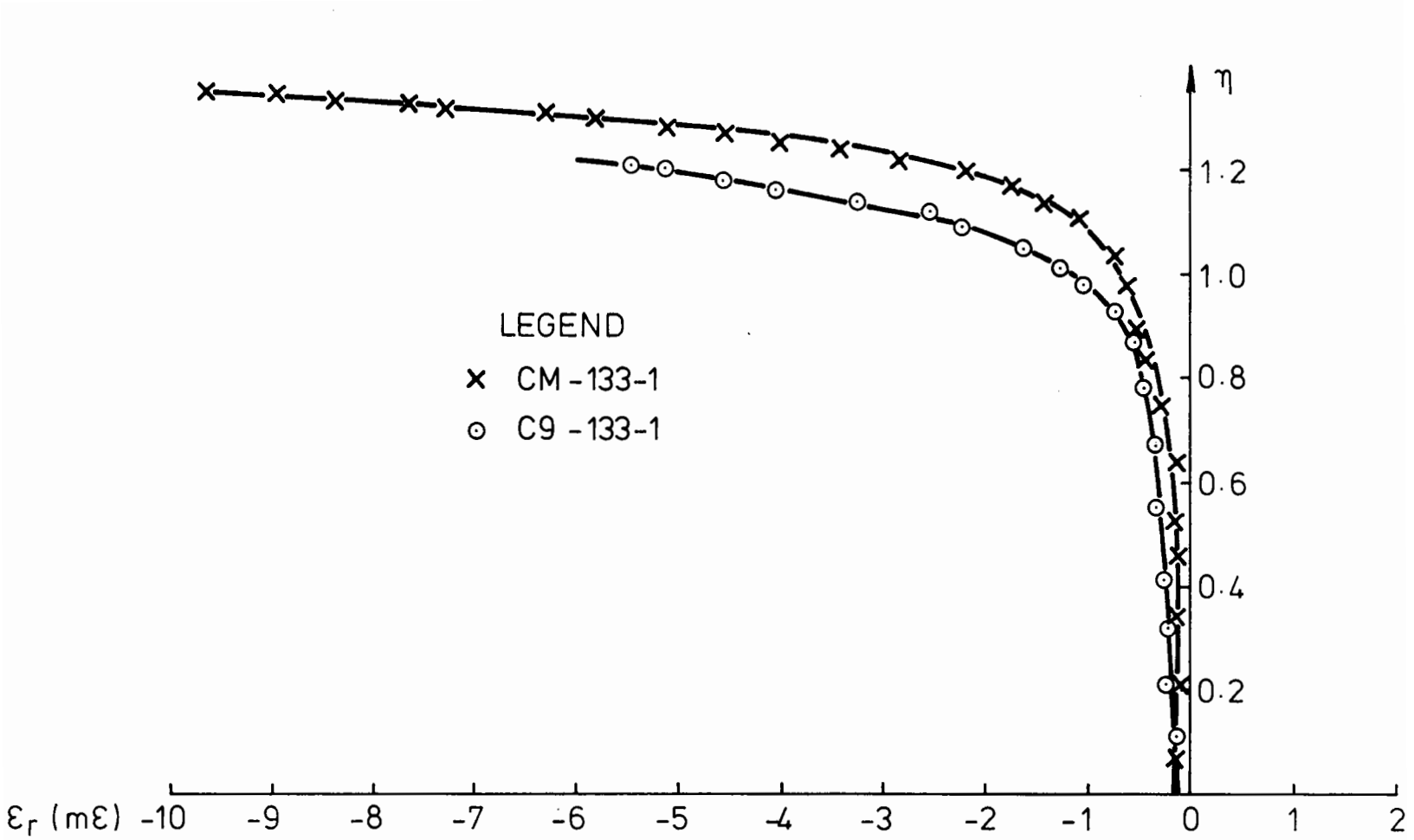

Fig. 6.7 Typical Recorded Strains

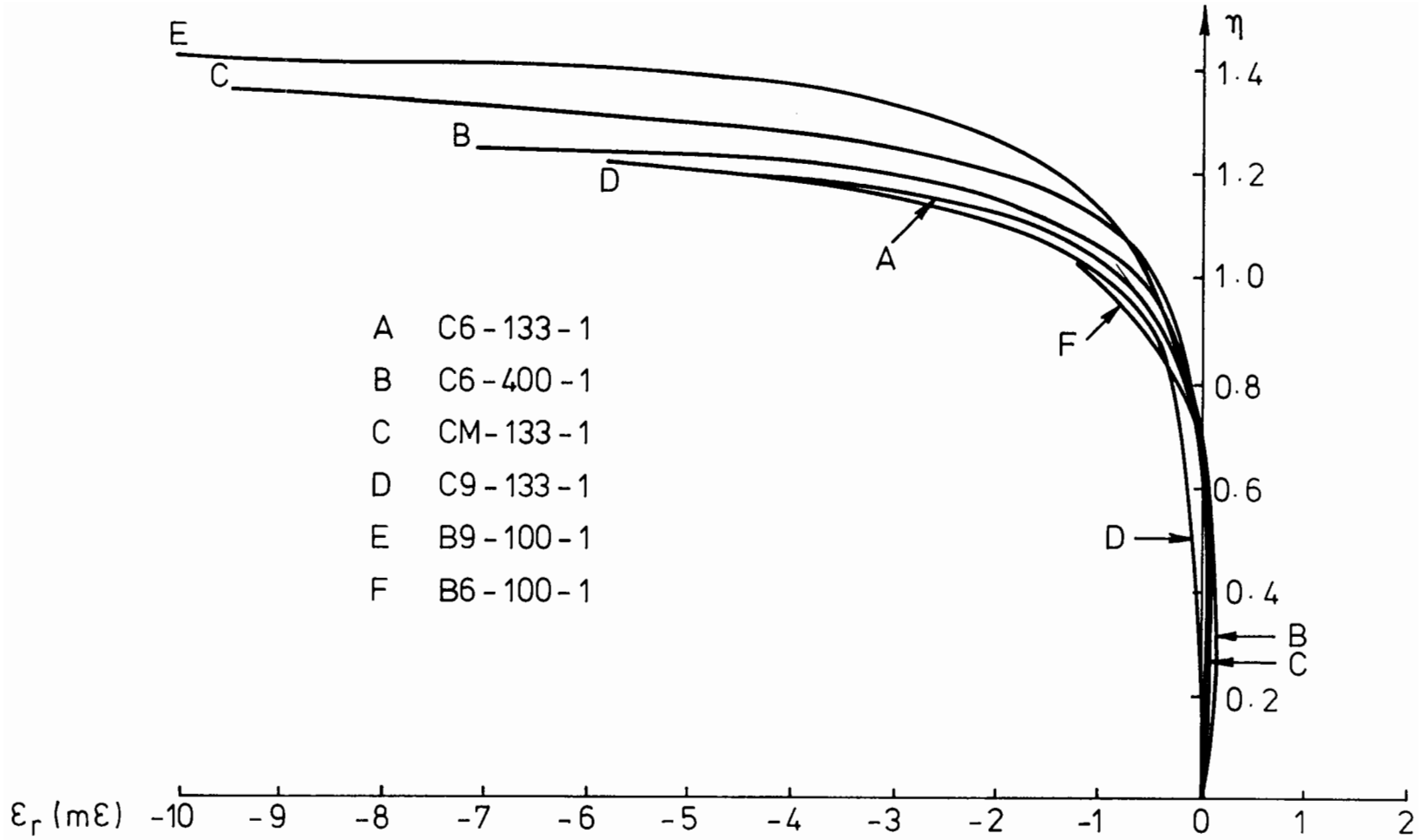

Fig. 6.8 Corrected Radial Strains During Monotonic Loading

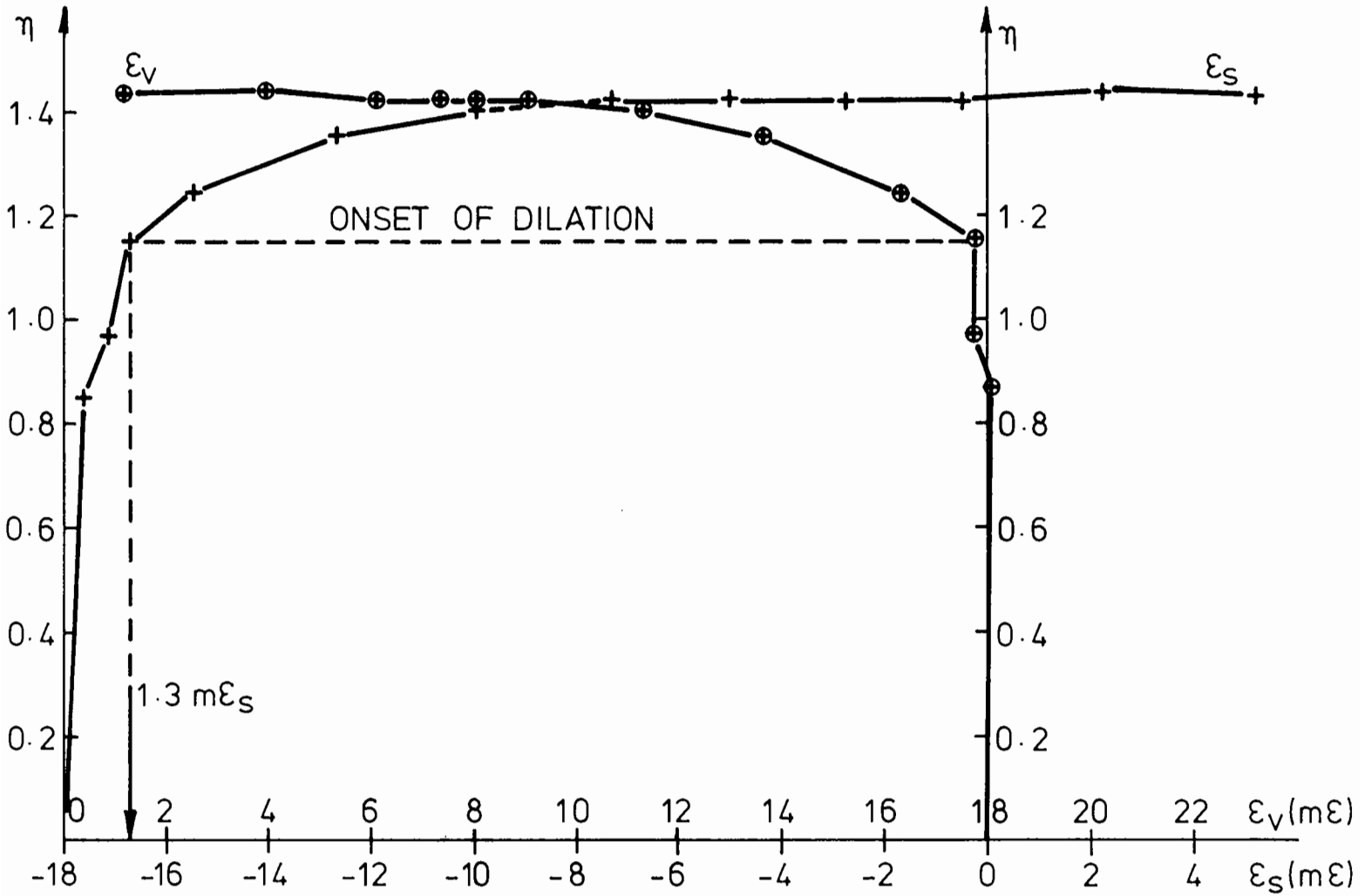

Fig. 6.9 (a) Shear and Volumetric Strains - Test B9 - 100 - 1

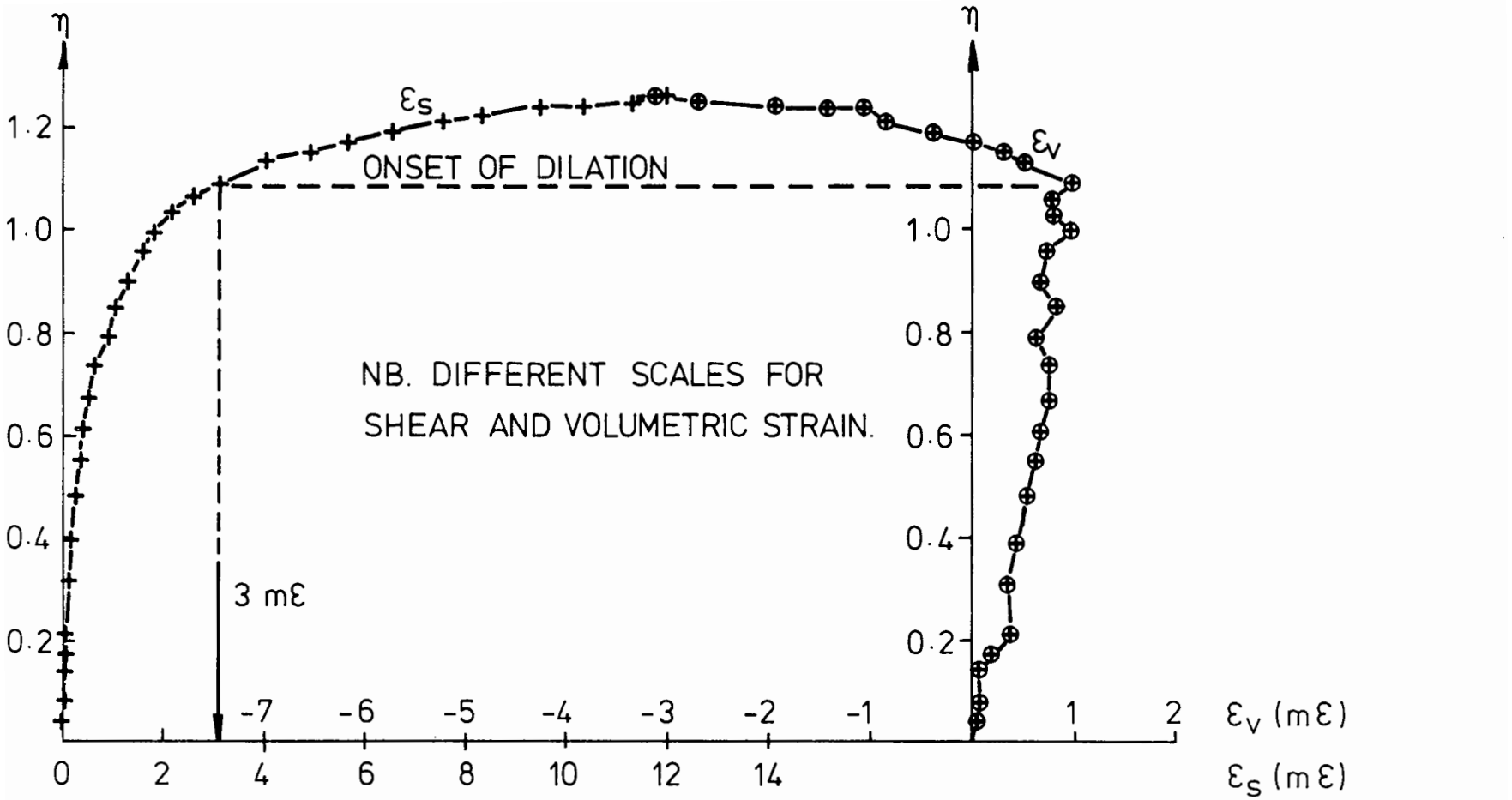

Fig. 6.9 (b) Shear and Volumetric Strains : Test C6-400-1

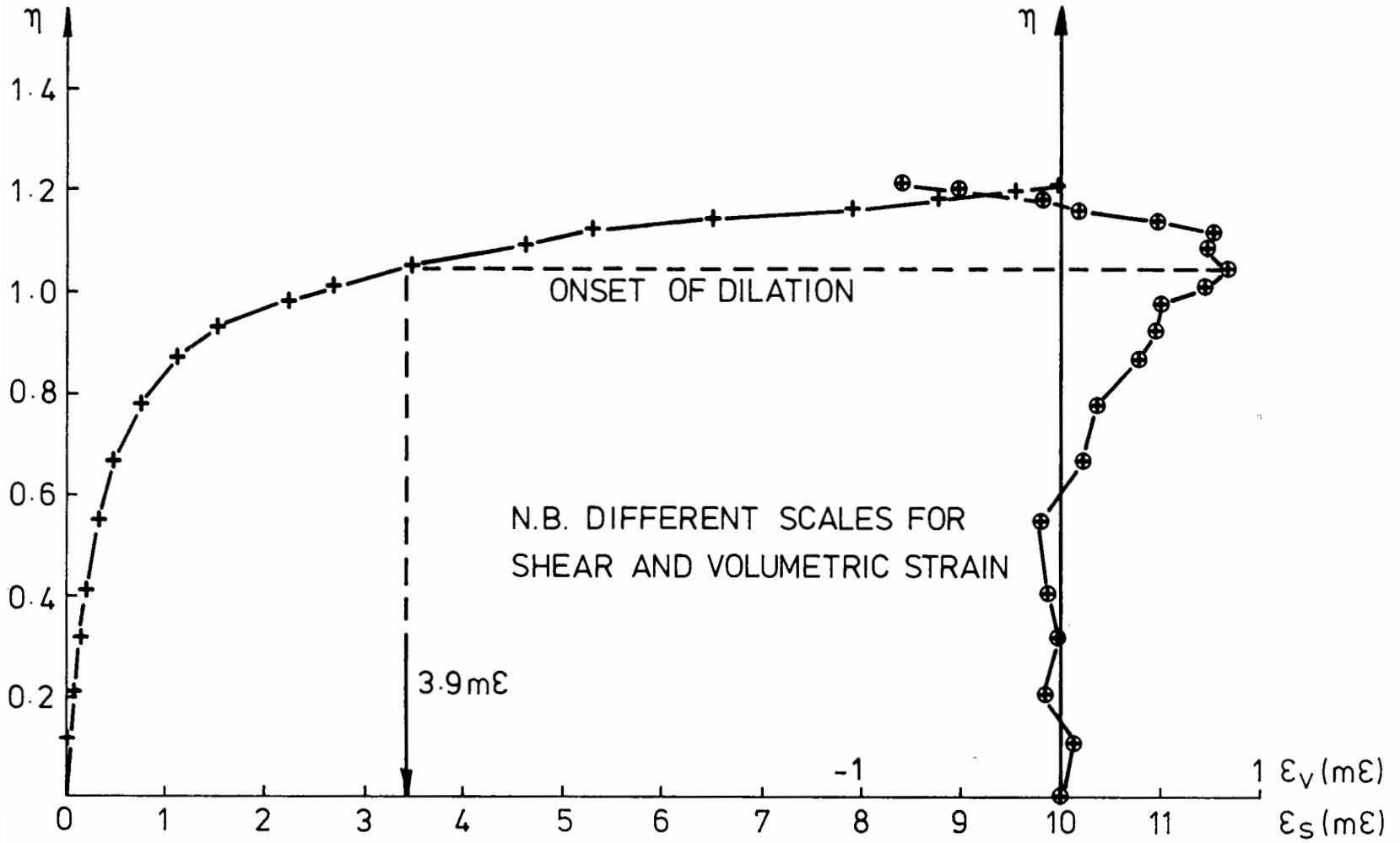

Fig. 6.9 (c) Shear and Volumetric Strain : Test C9 - 133 - 1

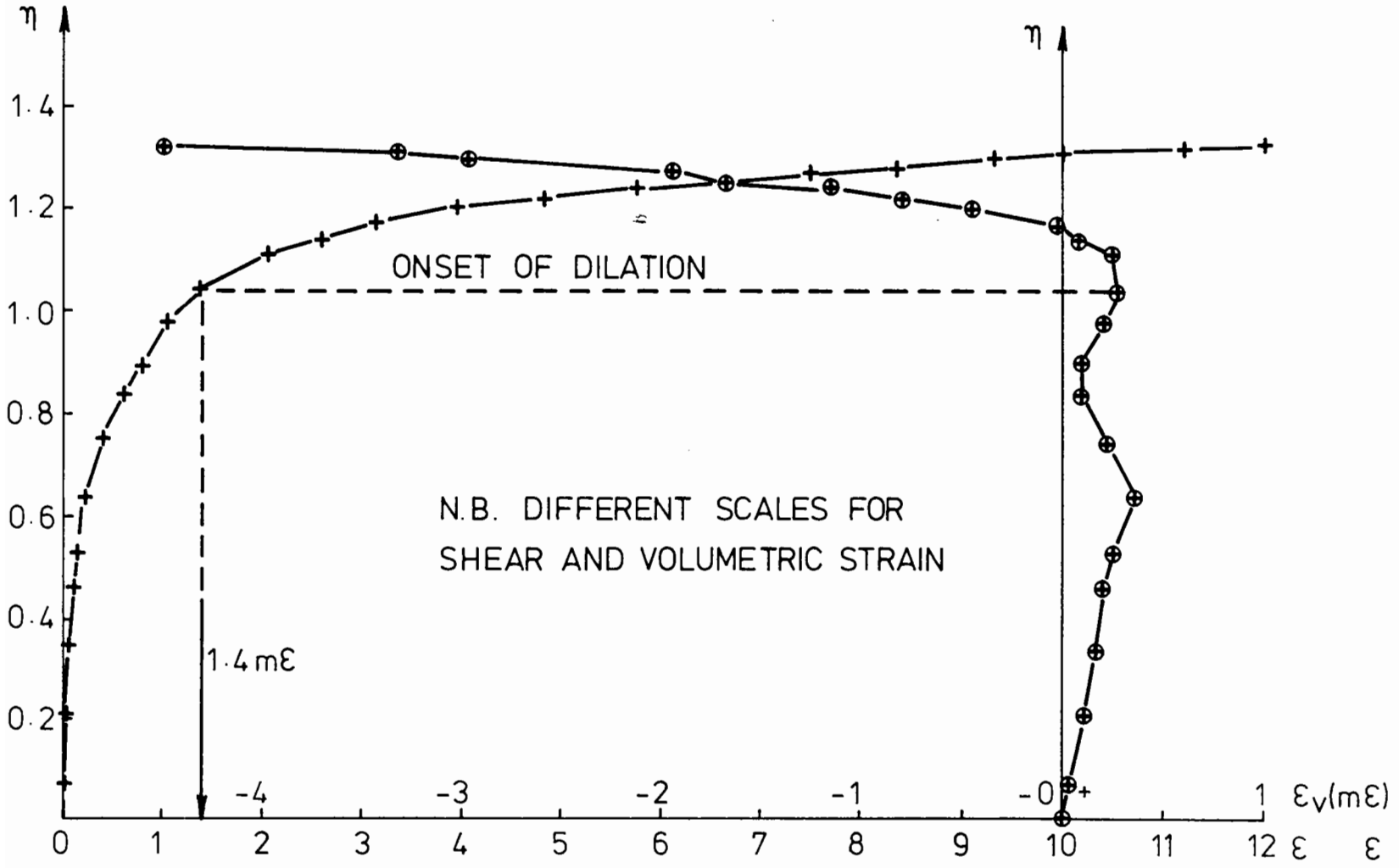

Fig. 6·9 (d) Shear and Volumetric Strains : Test CM-133-1

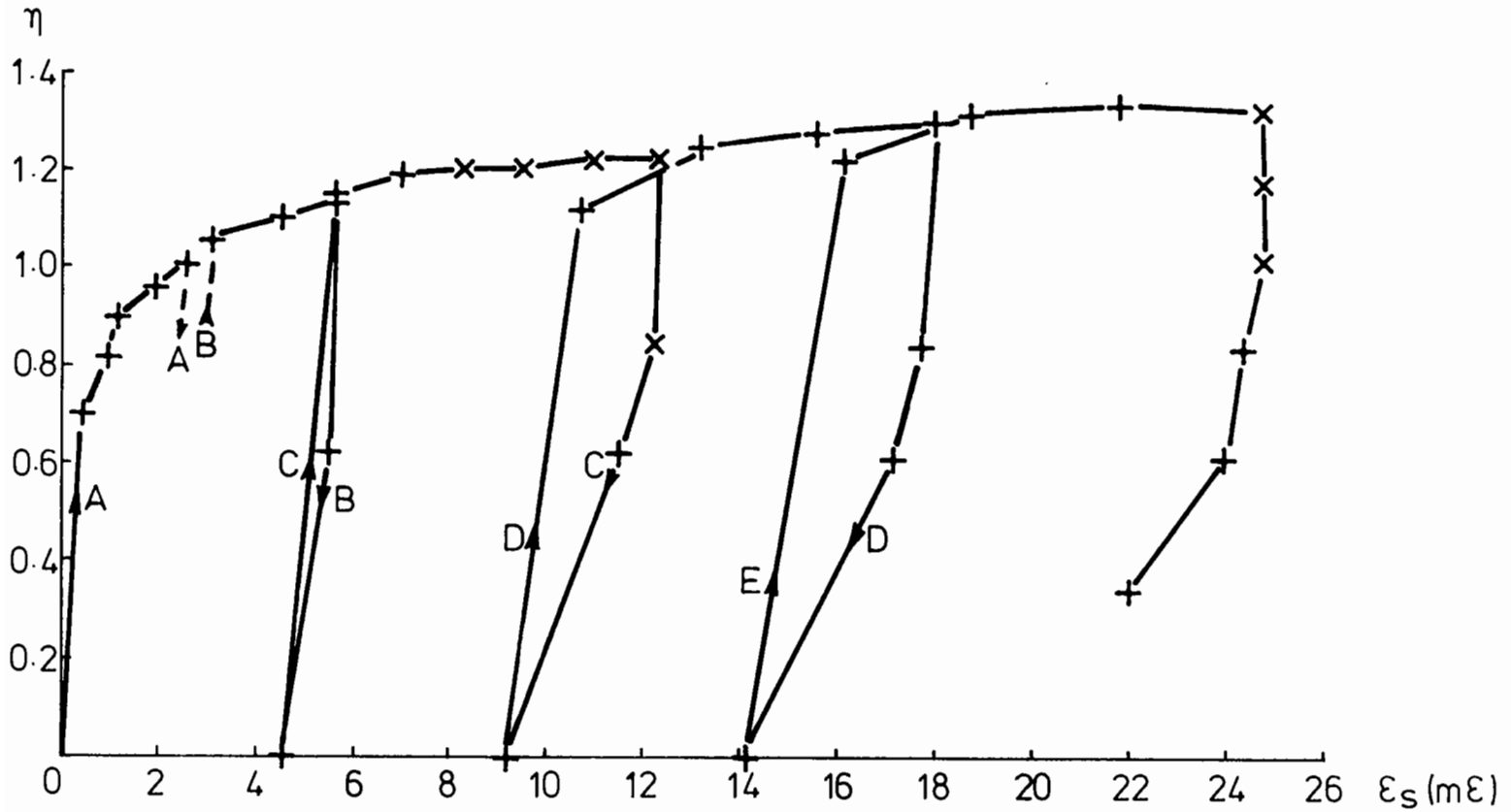

Fig. 6.10(a) Shear Strains Recorded During Test B6-100-1

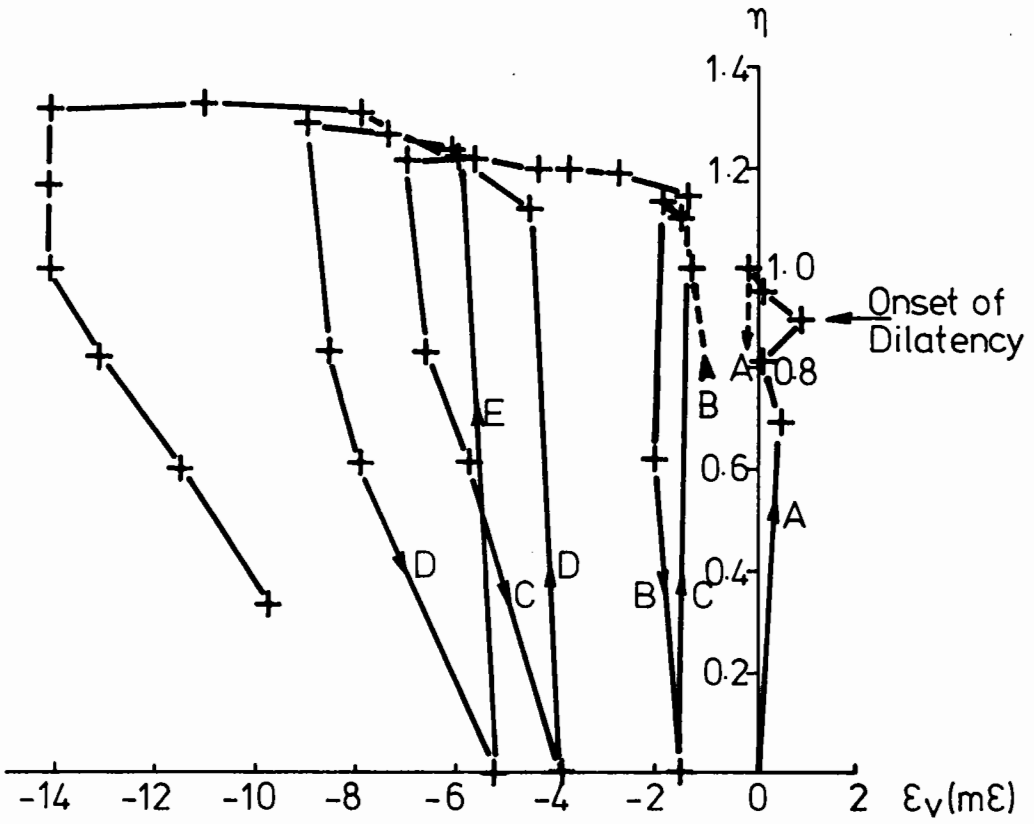

Fig. 6.10 (b) Volumetric Strain Recorded During Test B6-100-1

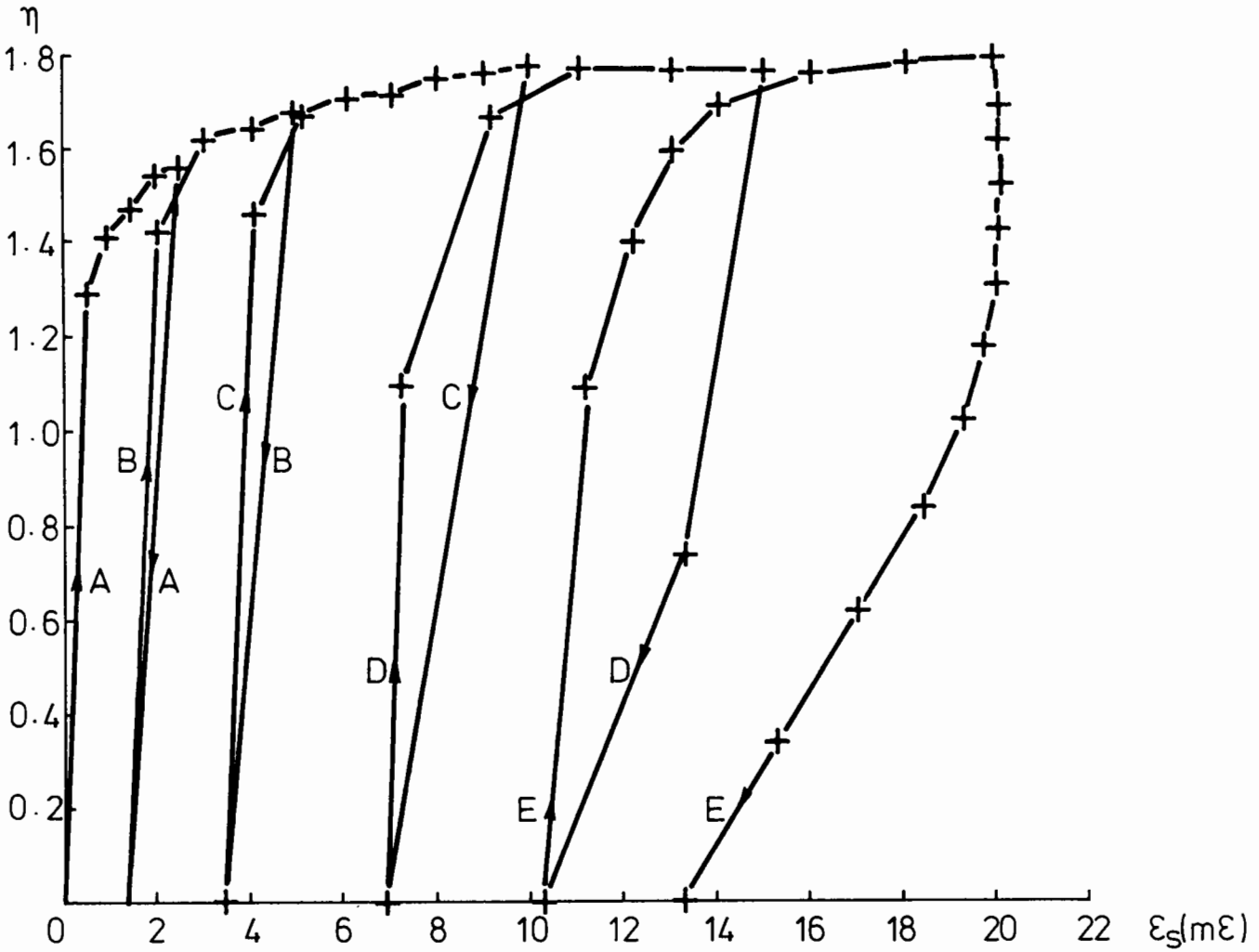

Fig. 6·11 (a) Shear Strains Recorded During Test BI0 - 100 - 1

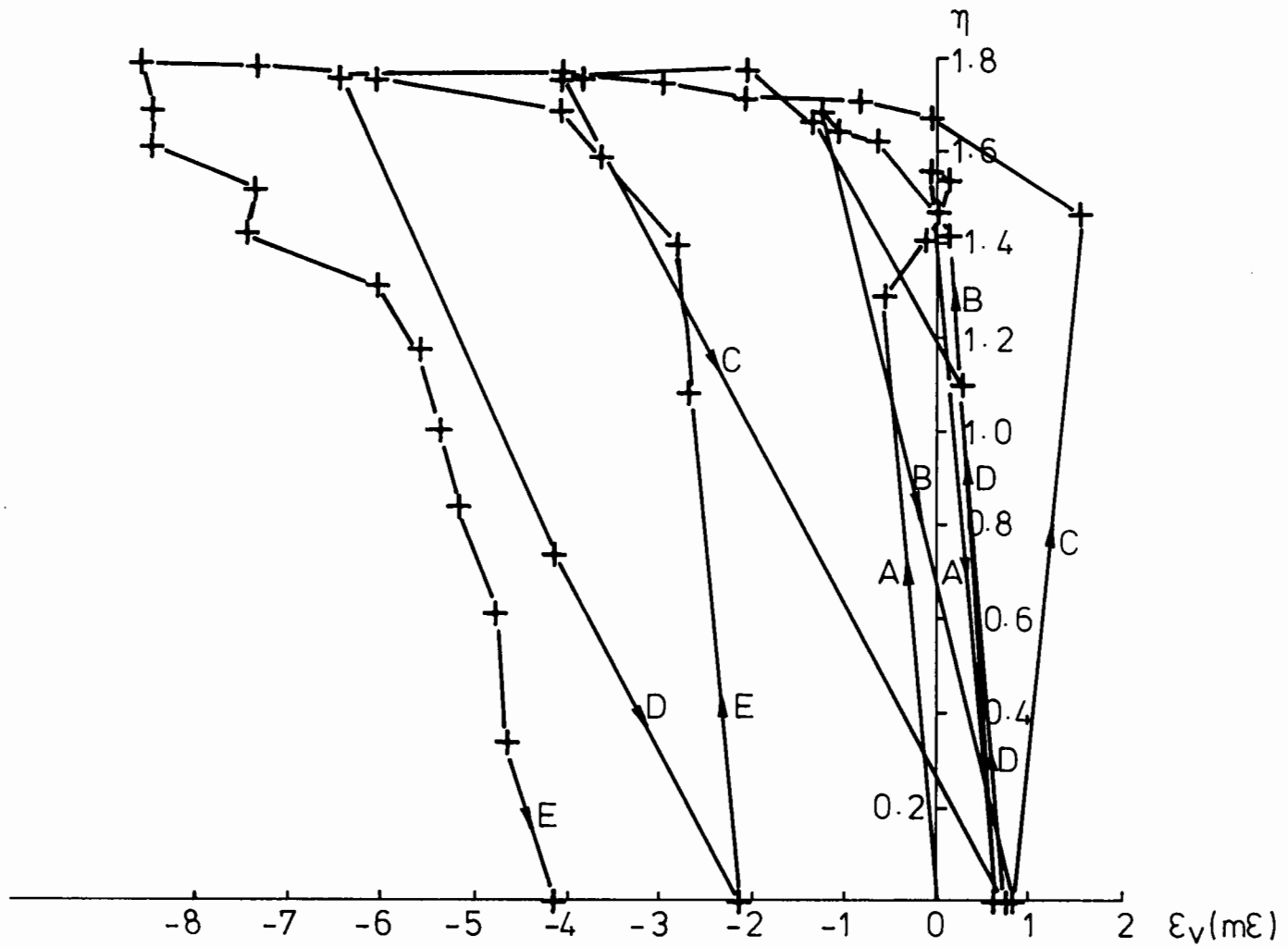

Fig. 6.11 (b) Volumetric Strains Recorded During Test BIO-100-1

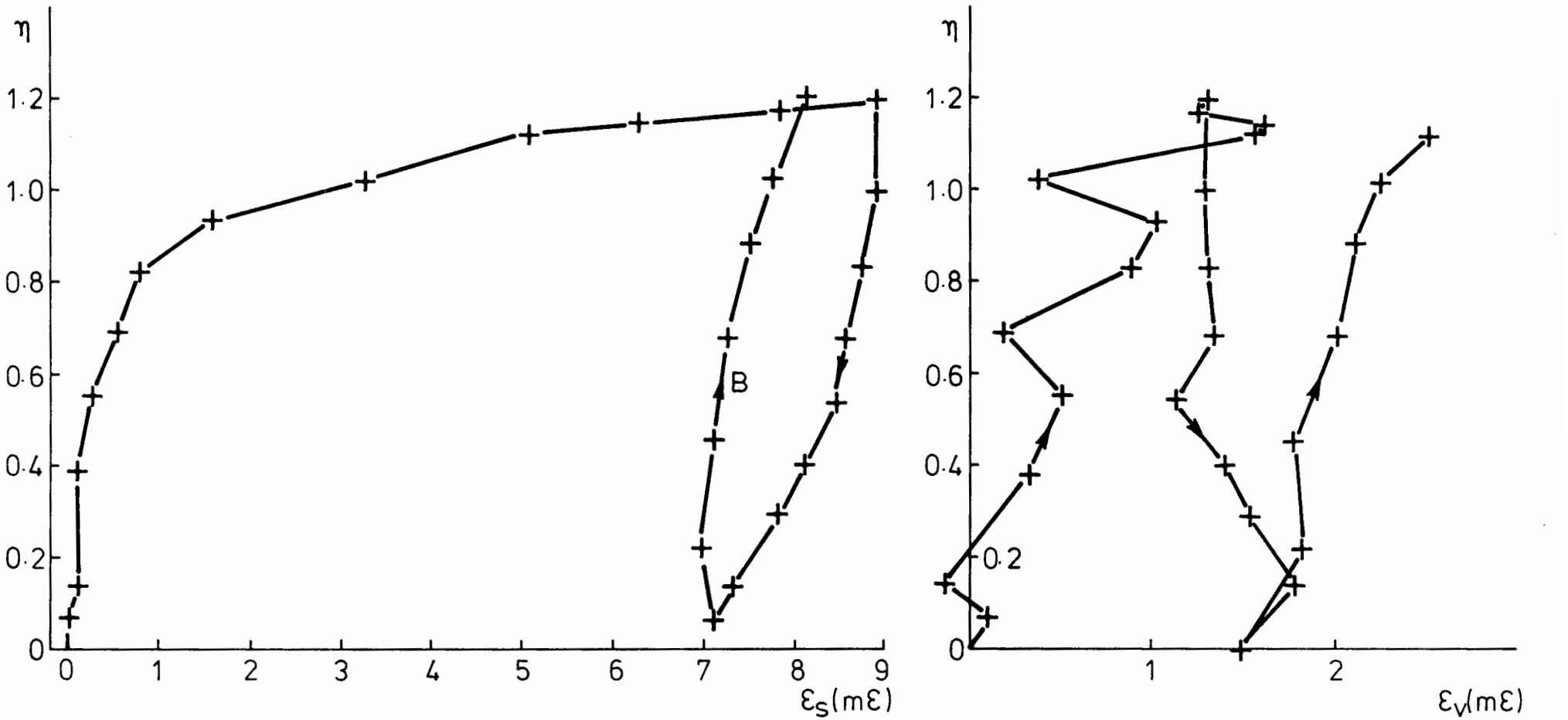

Fig. 6.12 Shear and Volumetric Strains Recorded During Test C6-133-1

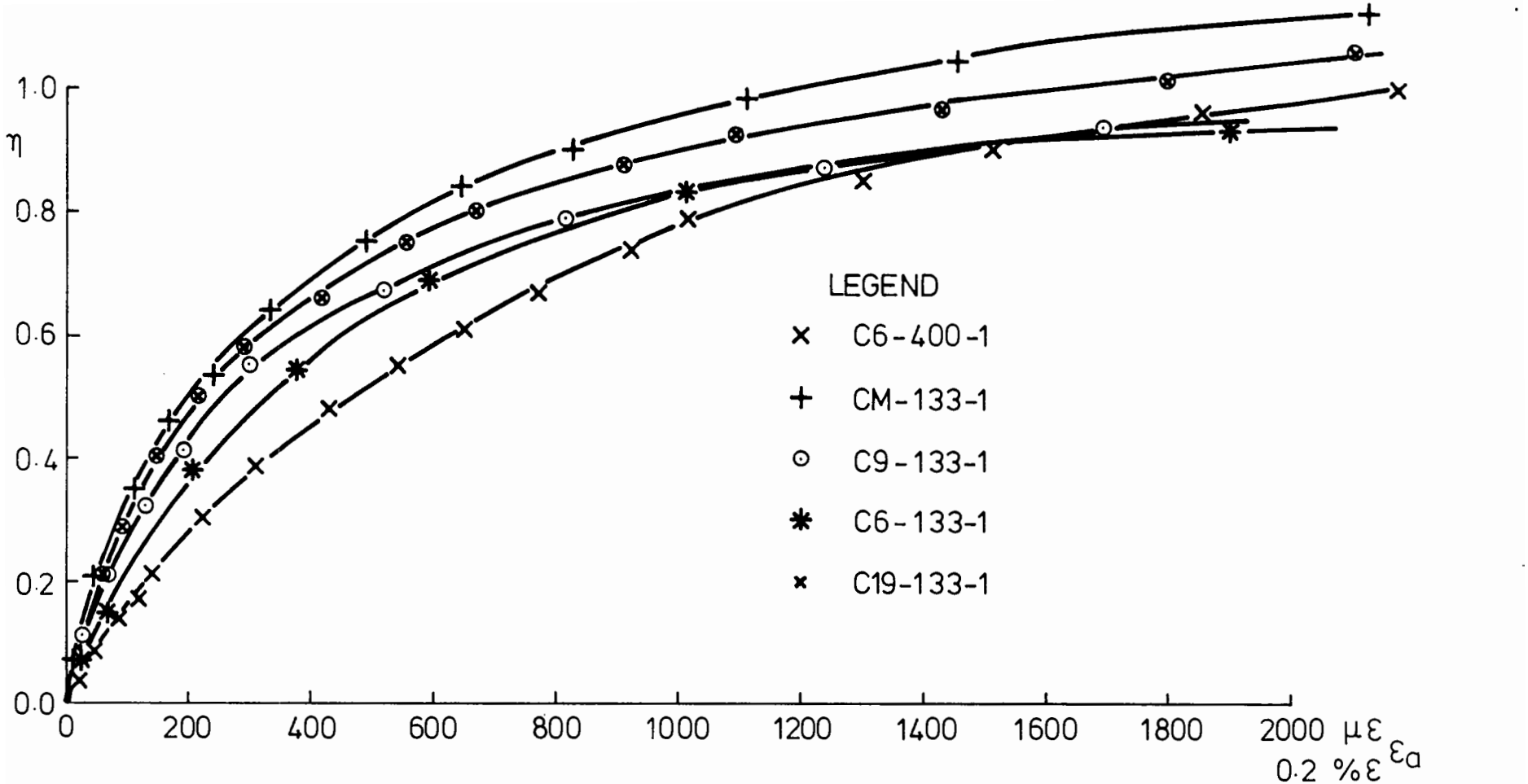

Fig 6.13 Axial Strain Behaviour of Denstone at Low Strains

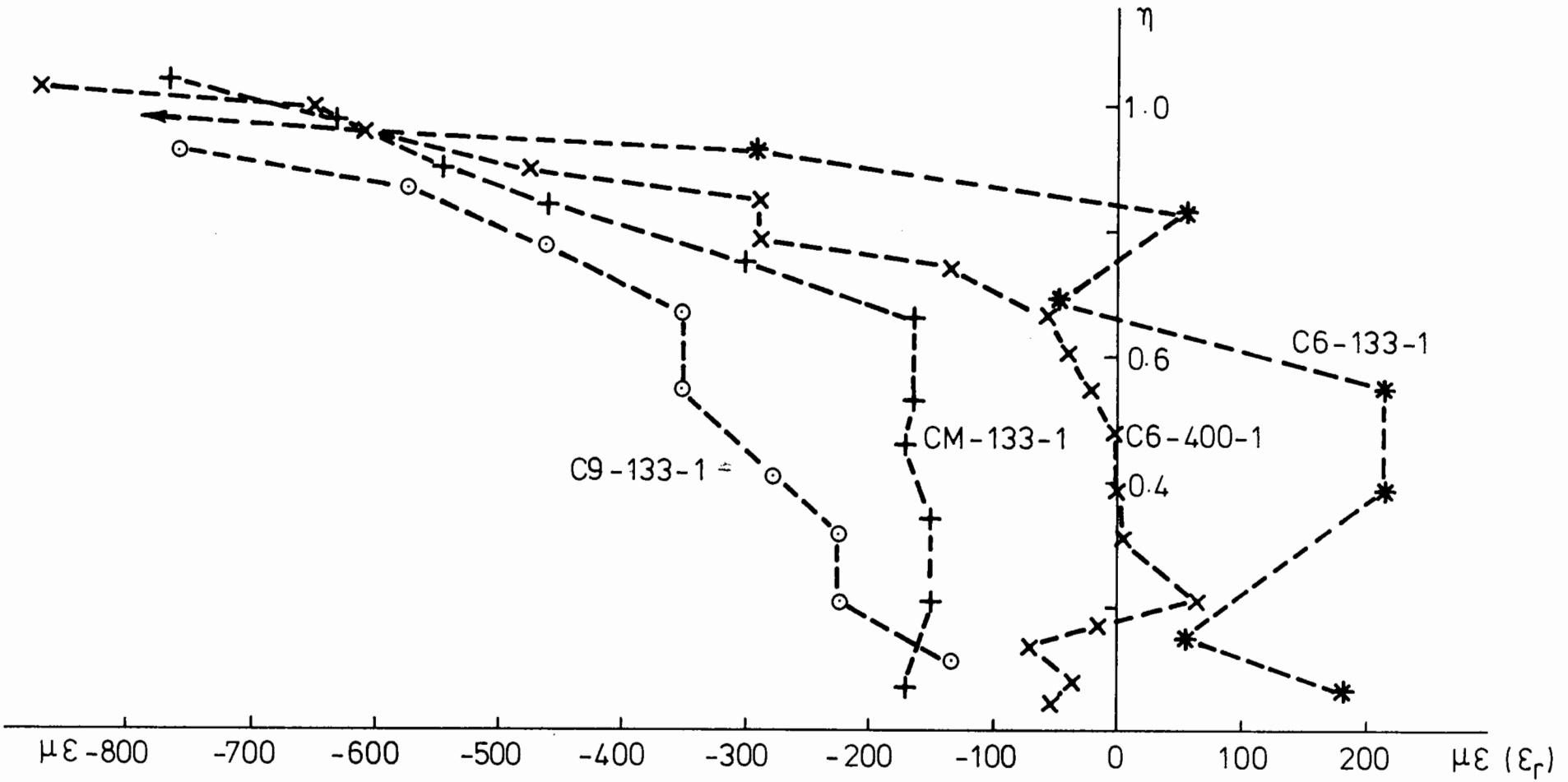

Fig. 6·14 (a) Recorded Radial Strains during Monotonic Loading

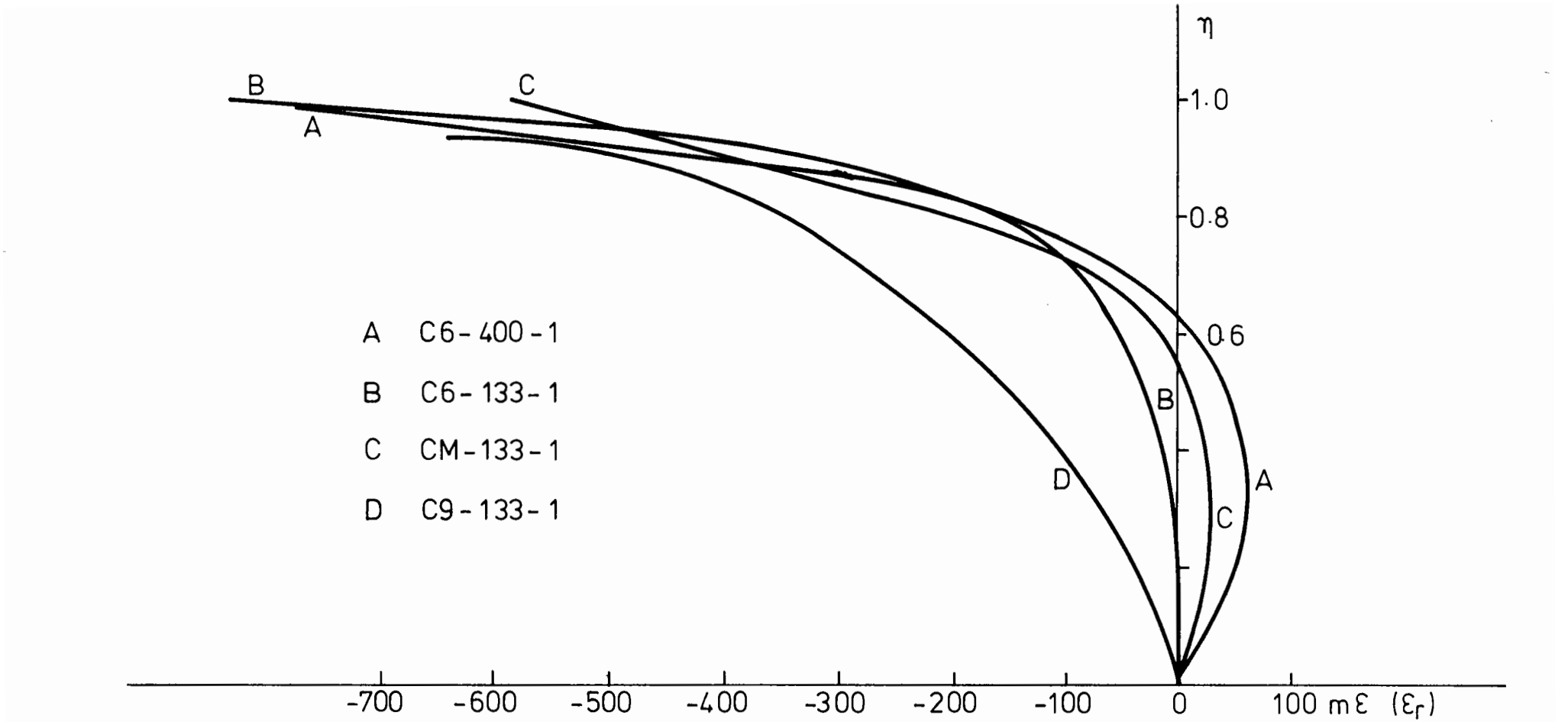

Fig. 6·14 (b) Corrected Radial Strain Curves during Monotonic Loading

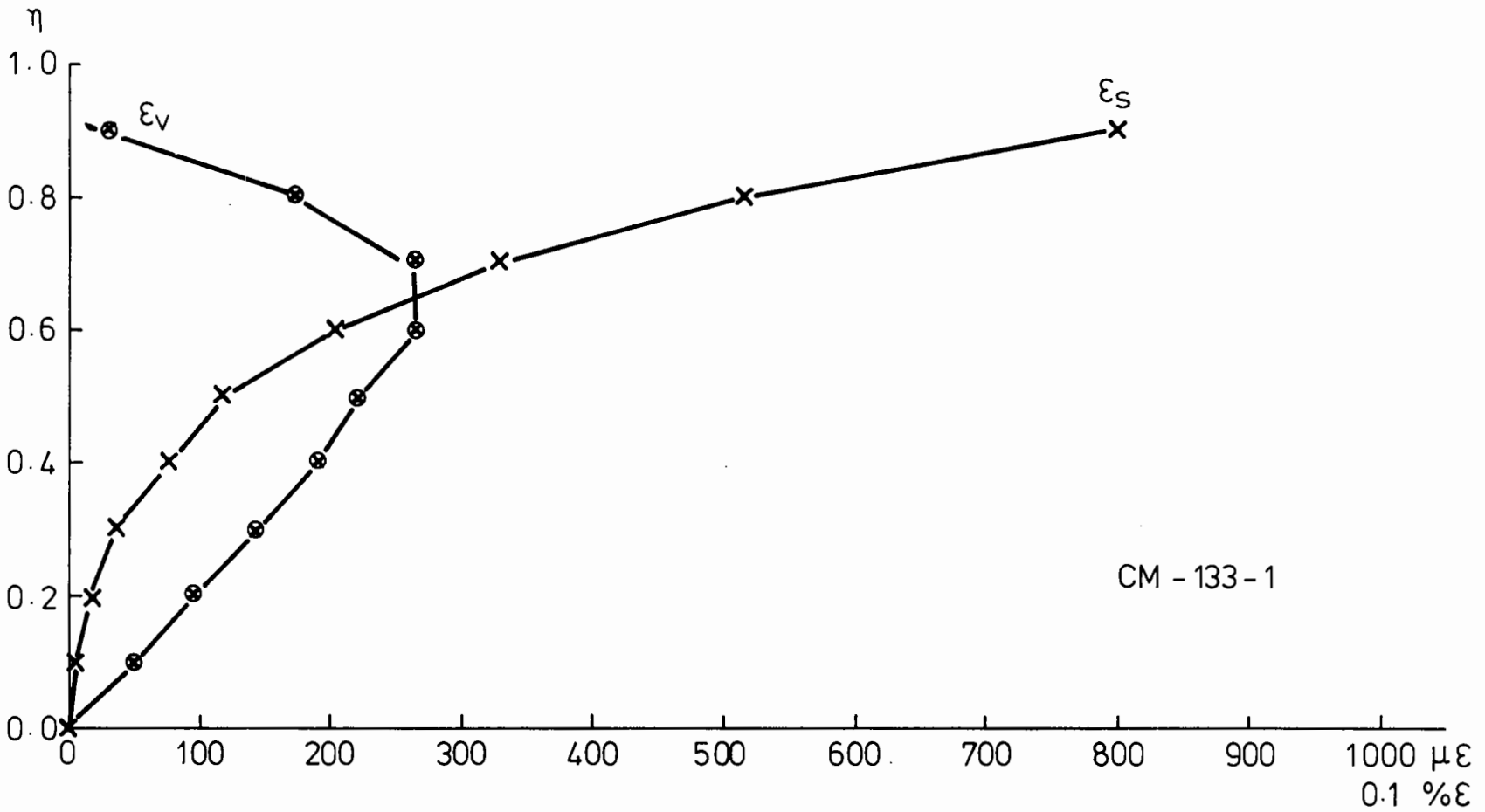

Fig. 6.15 (a) Shear and Volumetric Strains - Test CM-133-1

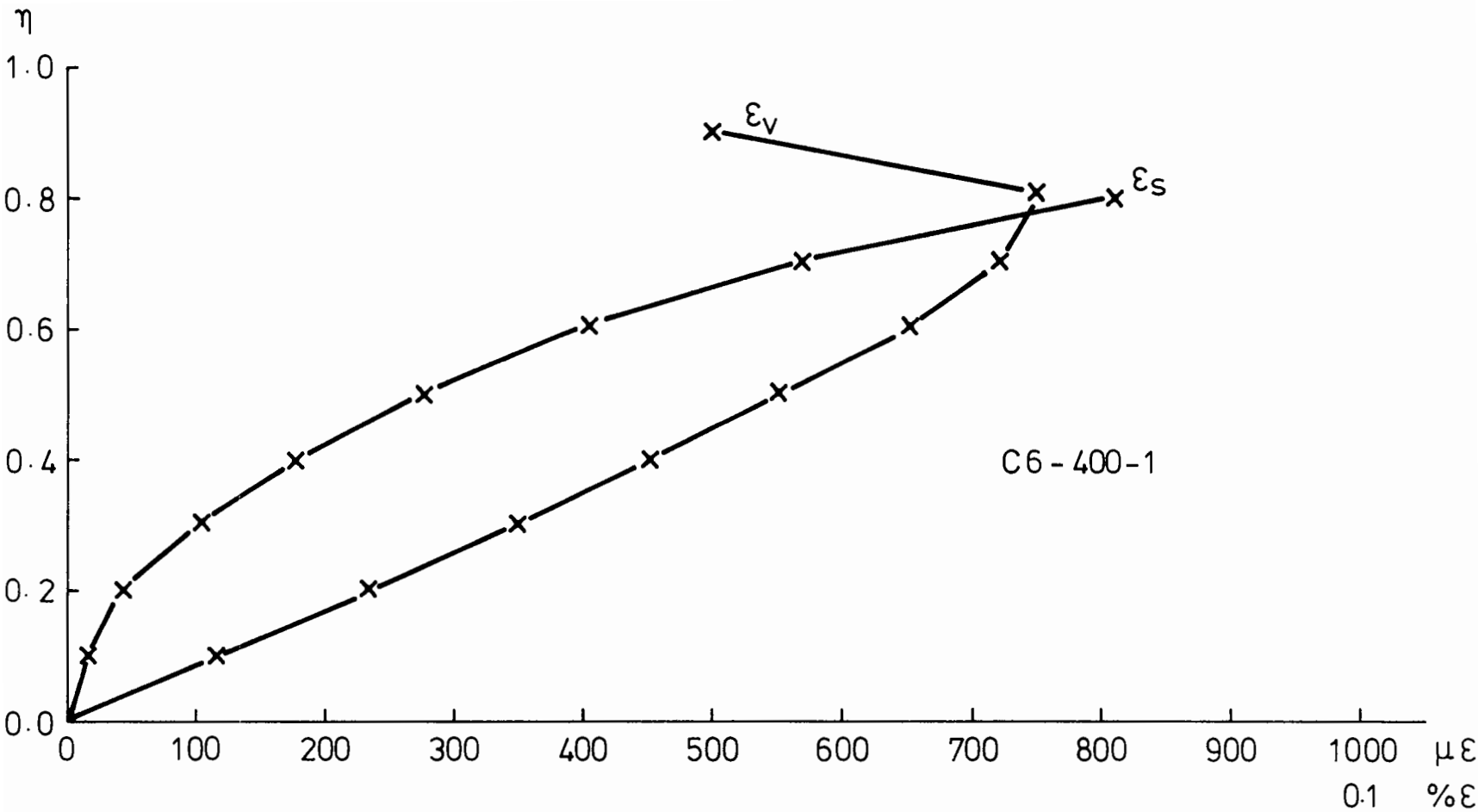

Fig. 6.15 (b) Shear and Volumetric Strains - Test C6 - 400 - 1

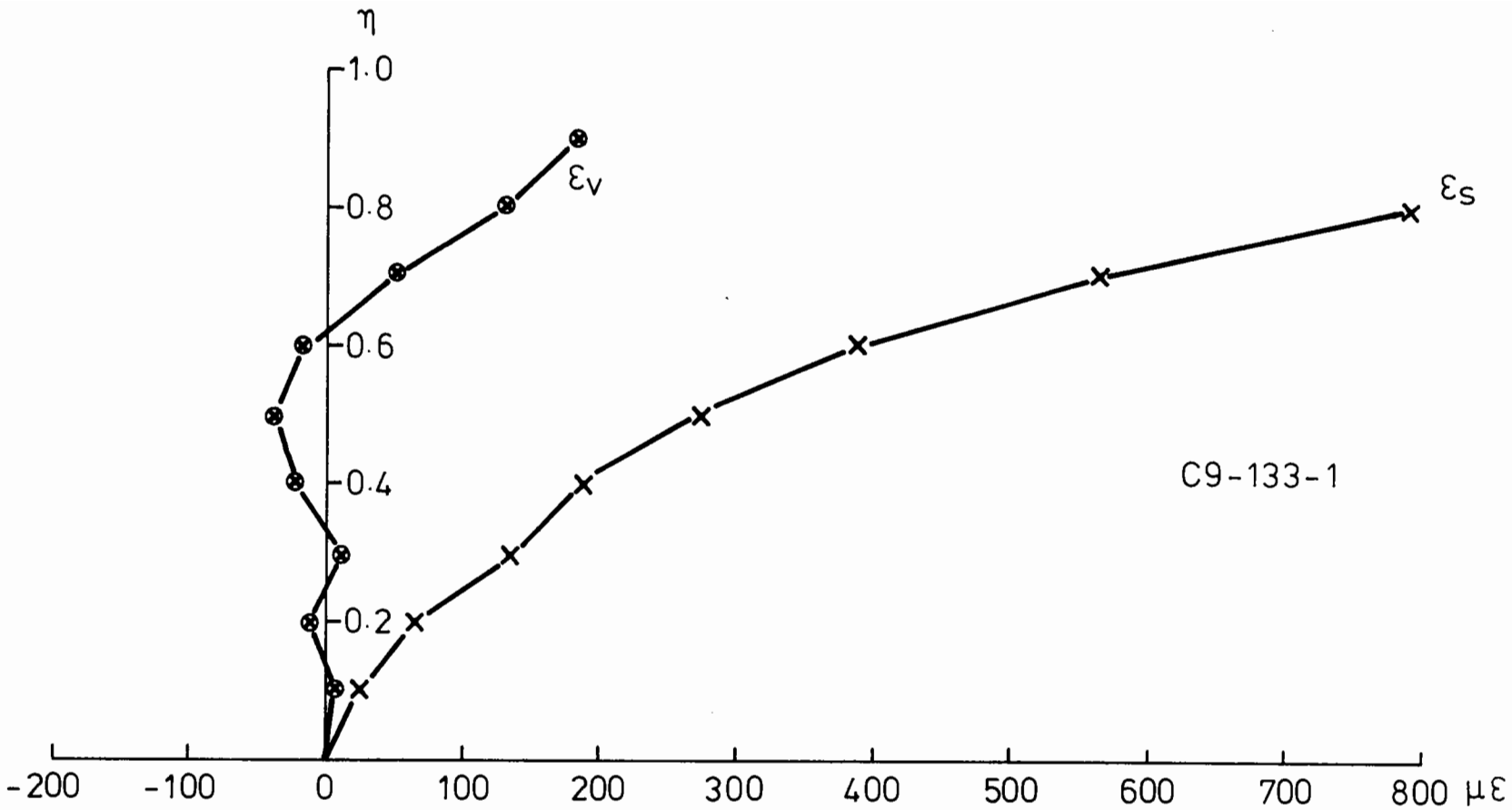

Fig. 6.15 (c) Shear and Volumetric Strains : Test C9-133-1

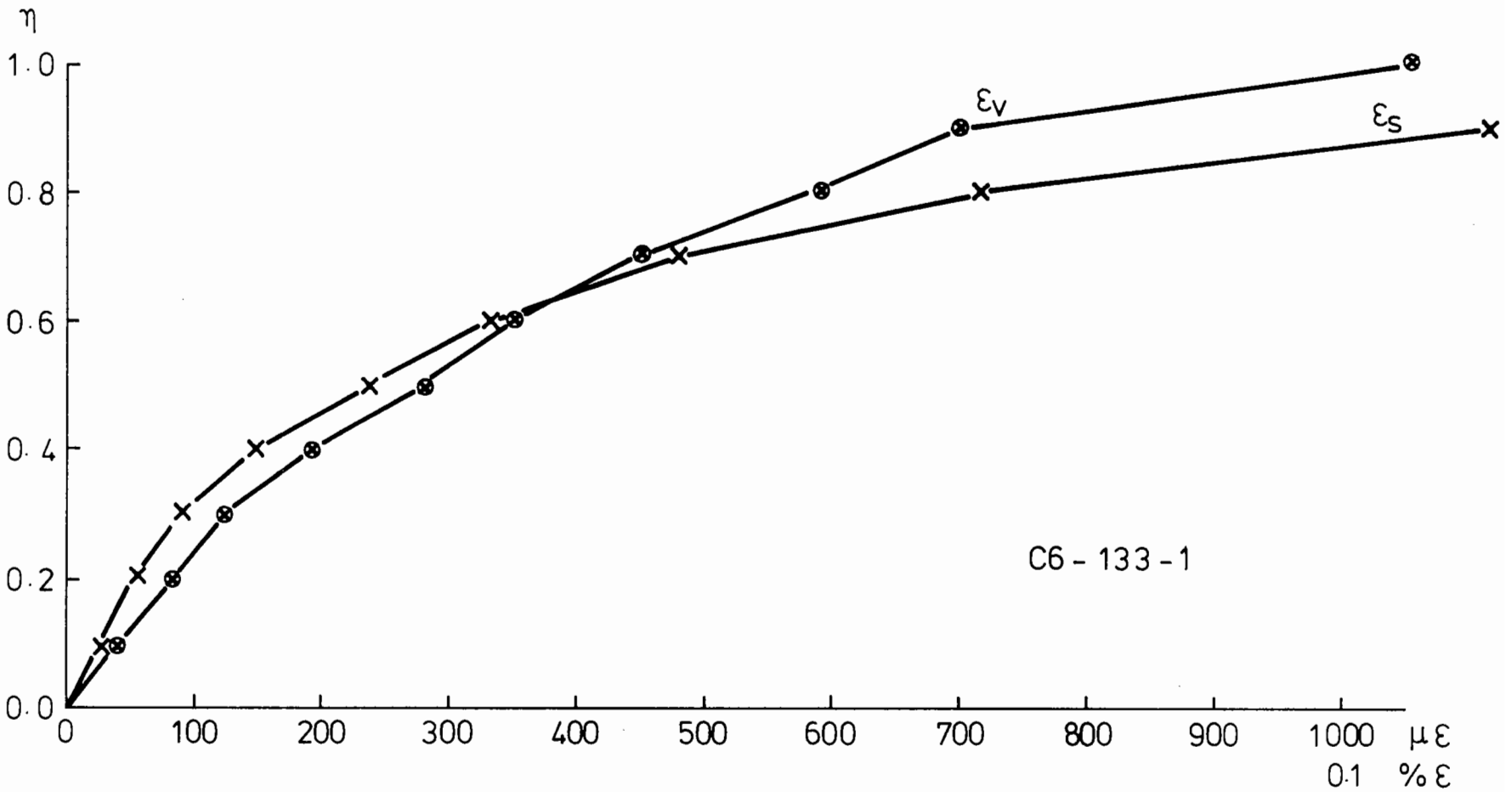

Fig. 6.15 (d) Shear and Volumetric Strains : Test C6 - 133 - 1

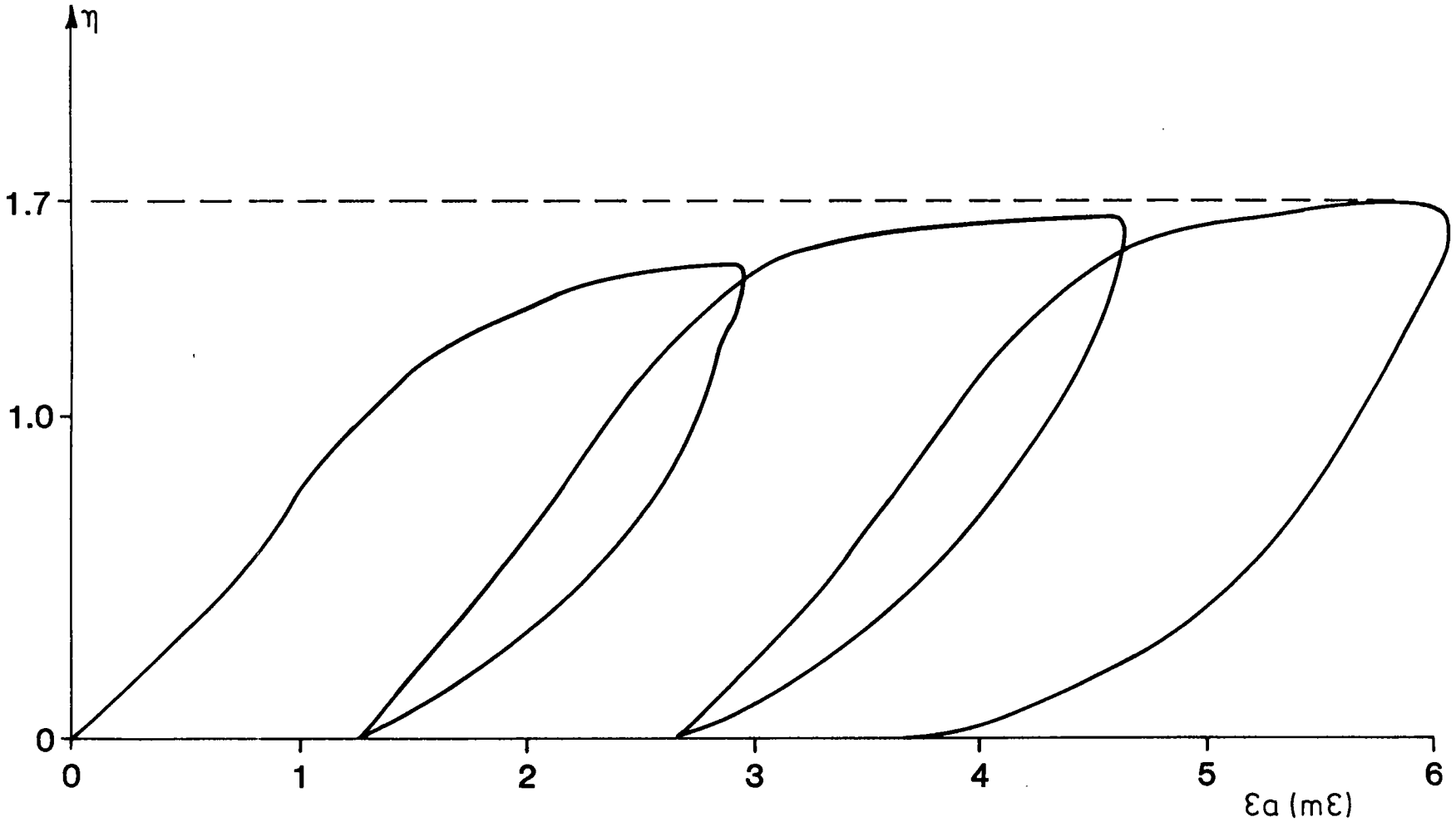

Fig. 6.19 **STRENGTH TEST ON MODIFIED DENSTONE MATERIAL**

material to reach its maximum strength. Clearly, the large strain tests in Series A enabled the material to achieve this strength and the characteristic post-failure reduction in strength also indicates that this is the case. The tests performed in Series B and C were usually discontinued at just over 1% axial strain and so could not be expected to exhibit a peak strength.

Table 6.4 shows the material strength at 1% axial strain. The average value for the single size materials (i.e. not including CM-133-1) is η = 1.27, which is 85% of the expected maximum value of 1.5.

Effect of Grading: In test CM-133-1, (in which equal proportions of 6, 9 and 19mm Denstone were mixed together), the recorded strength at 1% axial strain is η = 1.32 (Fig. 6.6). This is only slightly more than the average value for single size Denstone, (1.27), and so it appears that increasing the grading range does not have a great effect on the material strength.

Effect of Particle Size: Table 6.5 shows the average recorded strengths at 1% axial strain for the three Denstone materials. Although too few tests were carried out to draw any firm conclusions about the effect of particle size on material strength, an inspection of Table 6.5 suggests that there is a trend for materials composed of larger particle sizes to exhibit higher strengths.

Two possible explanations may be advanced to account for this phenomenon:

(a) As the particles increase in size their shape or surface properties may change slightly. In Chapter 3, the maximum and minimum dimensions of random samples of each material were measured. Although the survey showed that for Denstone all three sizes 6mm, 9mm and 19mm could be described as approximately ellipsoidal with maximum to minimum axes

TABLE 6.4 MATERIAL STRENGTHS AT 1% AXIAL STRAIN

Test	η at 1% Axial Strain
B9-100-1	1.44
B6-100-1	1.22
C6-133-1	1.2
C6-400-1	1.25
C9-133-1	1.205
C19-133-2	1.32*
CM-133-1	1.32

TABLE 6.5 AVERAGE STRENGTHS MEASURED FOR VARIOUS MATERIALS AT 1% AXIAL STRAIN

Particle Size	Average η at 1% Axial Strain
6	1.22
9	1.32
19	1.32*

*** Calculated at 0.85% axial strain**

ratios of 1.14, it was not detailed enough to distinguish more subtle differences which might be important.

(b) During compaction the intention was to produce not only a dense configuration but also an isotropic fabric. This, it was hoped, would be achieved by forming the sample in 50mm layers and by rodding to a depth of approximately 75mm so that the orientation of the long axes of the ellipsoidal particles would be random. It was noted during the compaction process that the smaller the particle size, the easier it was to rod the material. Indeed, the 19mm particle material was very difficult to rod.

As the material was tipped into the mould the tendency was for the long axes of the particles to lie horizontally. With smaller particles this tendency could easily be disrupted by rodding. With larger particles the preferred orientation would remain in the horizontal plane, since difficult rodding means less effective disruption.

Thus, a sample made of the larger material would exhibit an anisotropic fabric, the stiffer and stronger direction being vertical.

6A.5.2 Iron Oxide

The strength of the iron oxide material (Test BIO-100-1) at 1% axial strain was $\eta = 1.76$. This is clearly much greater than the strength for any of the Denstone materials. Since it has been shown that neither surface friction nor grading (insofar as it was studied) contribute significantly to the material strength, the disparity must be accounted for by the much lower sphericity of the iron oxide pebbles.

6A.5.3 Modified Denstone

During the time that testing was in progress using the large triaxial apparatus, the Modified Denstone material was not available. When a supply

became available it was decided not to recommission the large triaxial apparatus because of the time involved recalibrating instruments etc., but simply to use the smaller repeated load apparatus. A similar stress regime was applied as in tests B6-100-1 and B10-100-1. The radial strain hoops were removed during this test to avoid being damaged if a rapid and uncontrolled failure occurred. As a consequence, only axial strains were recorded. The results are shown in Fig. 6.19. The peak failure stress ratio was 1.7. This lies between the values of 1.78 for the iron oxide material and 1.5 recorded for the standard Denstone material.

6A.6 DILATANCY

Any granular material at a greater density than that corresponding to the critical state will, on loading, firstly compress when subjected to a monotonically increasing shear stress. Further increase in shear stress, however, will result in dilation as the granular structure is disrupted (Reynolds, 1885).

6A.6.1 The Onset of Dilatancy

The onset of dilatancy may be described (see Fig. 6.16(a) as the point at which

$$\frac{d\epsilon_v}{d\epsilon_s} = 0$$

The results recorded during the test programme show many local effects and it is difficult to determine the exact point at which the overall trend changes from compressive to dilatant behaviour. It is consequently necessary to make a partially subjective decision about when dilatancy begins. Table 6.6 lists these estimated points for a range of tests - see

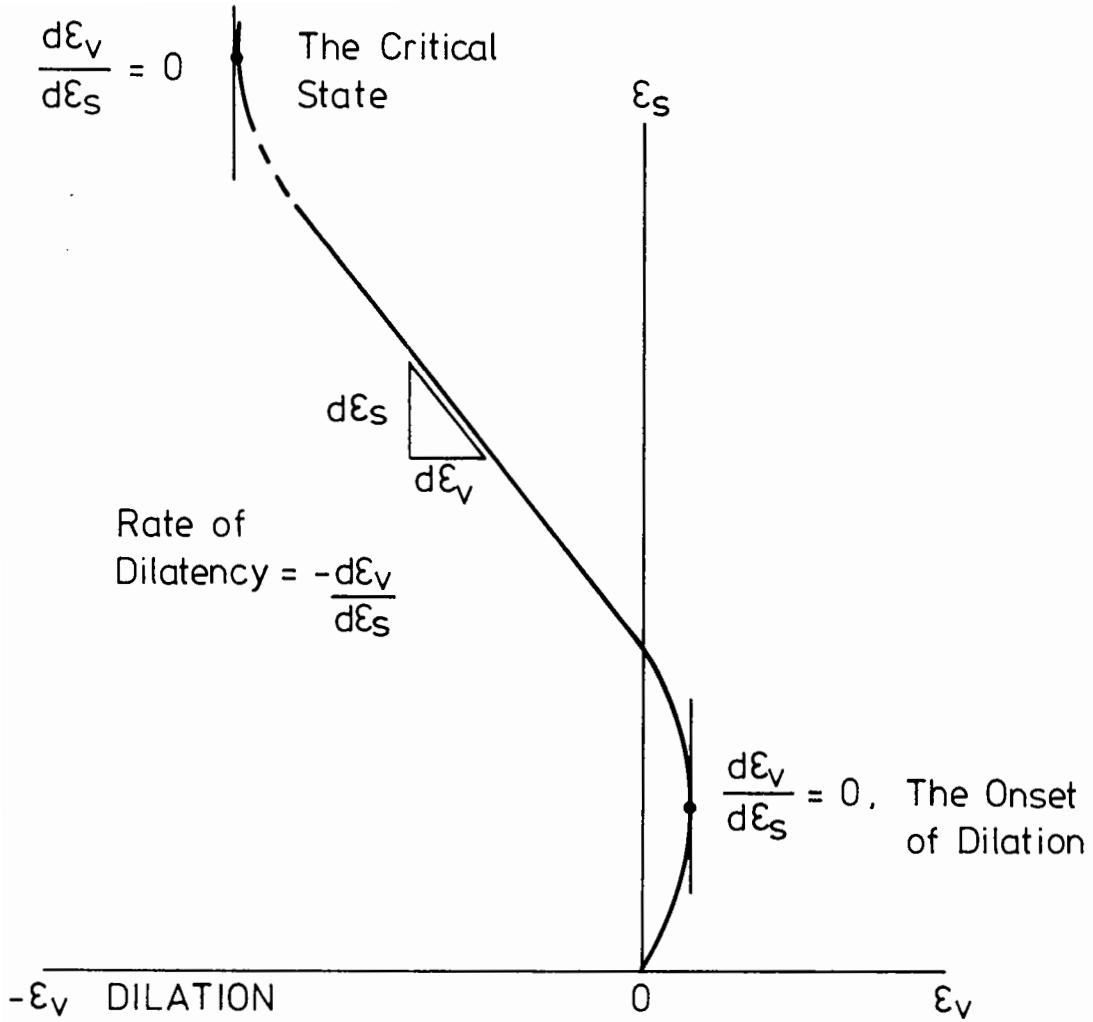

Fig. 6.16(a) Dilatency Nomenclature

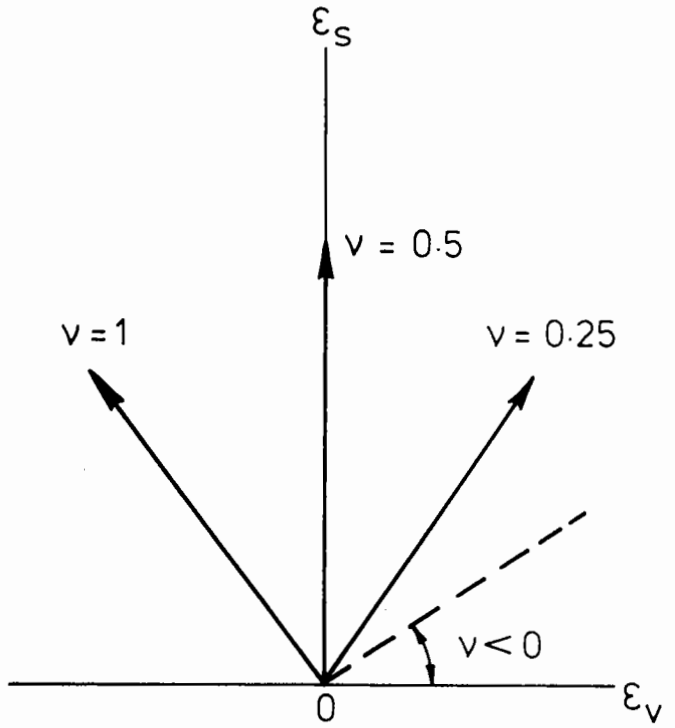

Fig. 6.16(b) Behaviour of Materials with Constant Poissons Ratio in $\varepsilon_s - \varepsilon_v$ space

TABLE 6.6 THE ONSET OF DILATANCY

Test	η_D	ε_{SD} (mε)
B9-100-1	1.15	1.3
C6-400-1	1.08	3.1
C9-133-1	1.05	3.9
CM-133-1	1.04	1.4
B6-100-1	0.90	1.2
BIO-100-1	1.6	2.6

TABLE 6.7 MEASURED RATES OF DILATION

Test	Range of ε_S (mε)	D
A19-210-1	22 - 69	0.45
A9-352-1	21.3 - 77.3	0.71
B9-100-1	2.5 - 23.2	0.73
C6-400-1	5.7 - 11.9	0.51
C9-133-1	6.5 - 10.0	0.37
CM-133-1	4.9 - 11.2	0.45
B6-100-1	Cycle C	0.84
	D	0.79
	E	0.84
BIO-100-1	Cycle C	0.81
	D	0.59
	E	0.55

also Figs. 6.9, 6.10, 6.11. The onset of dilatency is given as both a stress ratio (η_D) and a shear strain (ϵ_{SD}).

The average values for Denstone are $\eta_D = 1.04$ or $\epsilon_{SD} = 2.2m\epsilon$.

For the iron oxide material, only one result was recorded $\eta_D = 1.6$; $\epsilon_{SD} = 2.6\ m\epsilon$. Despite the lack of corroboration, it appears clear that the onset of dilatancy for iron oxide occurs at a similar value of shear strain as for the Denstone material.

6A.6.2 The Rate of Dilation

The rate of dilation may be described by:

$$D = -\frac{d\epsilon_v}{d\epsilon_s} \quad \text{, see Fig. 6.16(a)}$$

[Note that this is not the same as $D = (1 - (dV/d\epsilon_1))$ used by Rowe (1962). Since shear strains, not major principal strains, cause dilatancy, it is felt more appropriate to use the former in the definition of dilatancy.]

The value of D appeared to remain fairly constant during any particular test once dilation had begun. The tests in Series A, despite volumetric strains of 4–5%, showed no tendency towards a reduced dilatancy rate. This indicates that to reach the critical state, much greater values of shear strain were required than actually occurred. Wroth (1958), using ball-bearings as a particulate material, showed that strains of the order of 20% were required before the critical state could be attained.

Table 6.7 shows the recorded rates of dilation for the various tests. The second column "range of ϵ_s" gives the range of shear strains over which the rate of dilation was averaged. The values given for the tests B6-100-1 and BIO-100-1 (which are repeated loading tests) are the slopes obtained from the graphs of the various cycles as shown in Figs. 6.21 and 6.22.

The recorded values shown in Table 6.7 exhibit a wide variation ranging from D = 0.37 in C9-133-1 (equivalent to a poisson's ratio, ν = 0.72) to D = 0.84 in B6-100-1 (equivalent to ν = 1.08). No coherent pattern appears to exist. The average value of D for the seven tests on Denstone is 0.58 (equivalent to ν = 0.86). The single test on the iron oxide material gives an average value of D = 0.65 (equivalent to ν = 0.91).

6A.7 MATERIAL STIFFNESS

6A.7.1 Presentation of Results

As was explained in 6A.4, the fundamental approach of dividing behaviour into spherical and deviatoric components will be used whenever possible. Following this, the shear and volumetric moduli (G and K) will be used in preference to the more traditional approach of using Young's modulus and Poisson's ratio. At very low strains, however, the radial strain instrumentation exhibited some random distortion and consequently it was necessary to use axial stiffness to compare materials in this range.

Fig. 6.17 shows the various moduli which may be used to describe non-linear behaviour. The tangent modulus is associated with a particular stress state and is the instantaneous stiffness of the material at that stress. The chord modulus is the stiffness between any two given stress states. The secant modulus is the stiffness from a given "zero" stress state (zero deviator stress, for example) to any other given stress state.

Fig. 6.18 shows the way in which the secant and tangent shear and volumetric moduli are related to various phenomena observed during granular material testing. The main points to note are:

(a) That the volumetric modulus becomes infinitely positive at some stress ratio $\eta-$ and infinitely negative at stress ratio $\eta+$. The position of

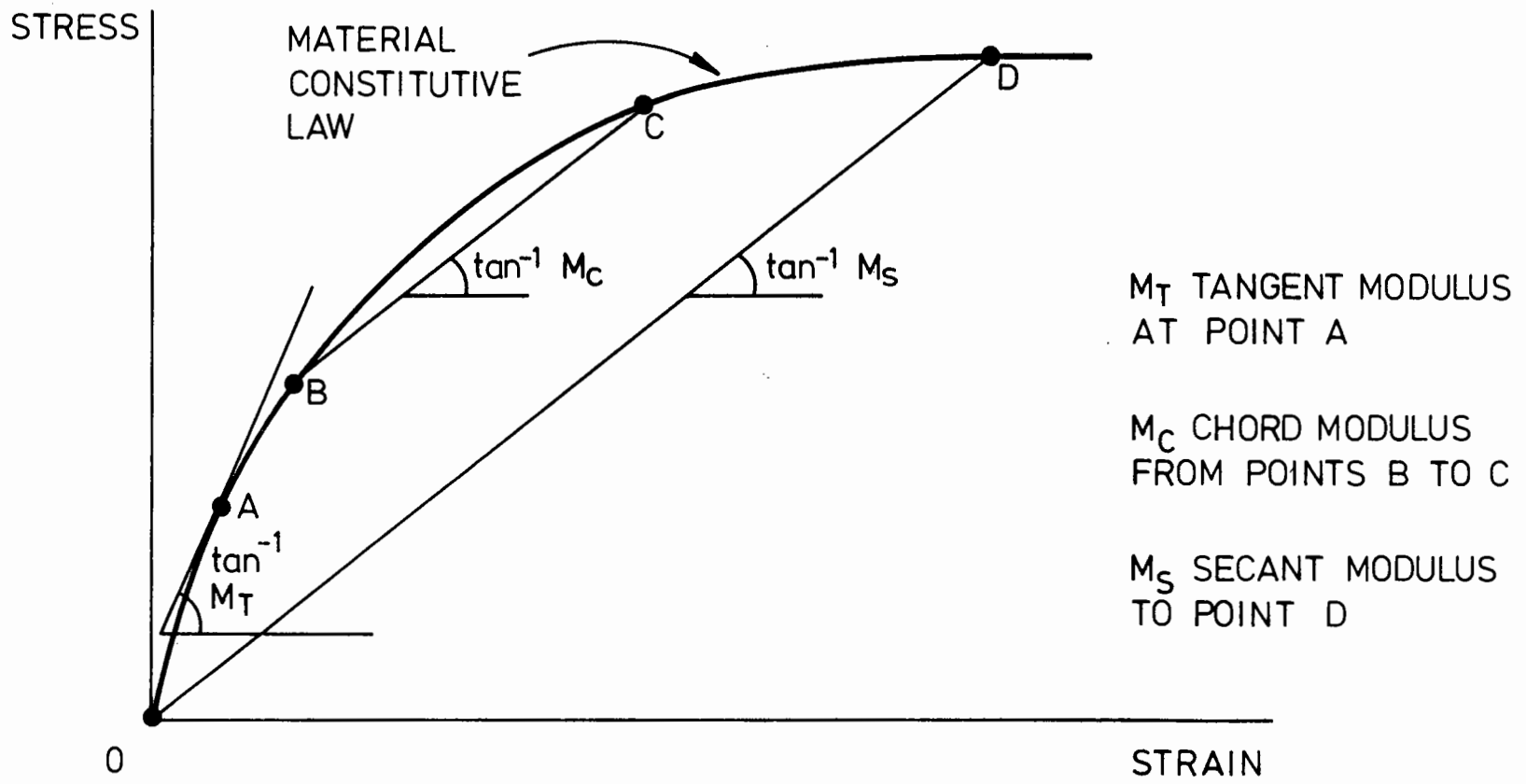

Fig. 6·17 Definition of Non-Linear Material Stiffness

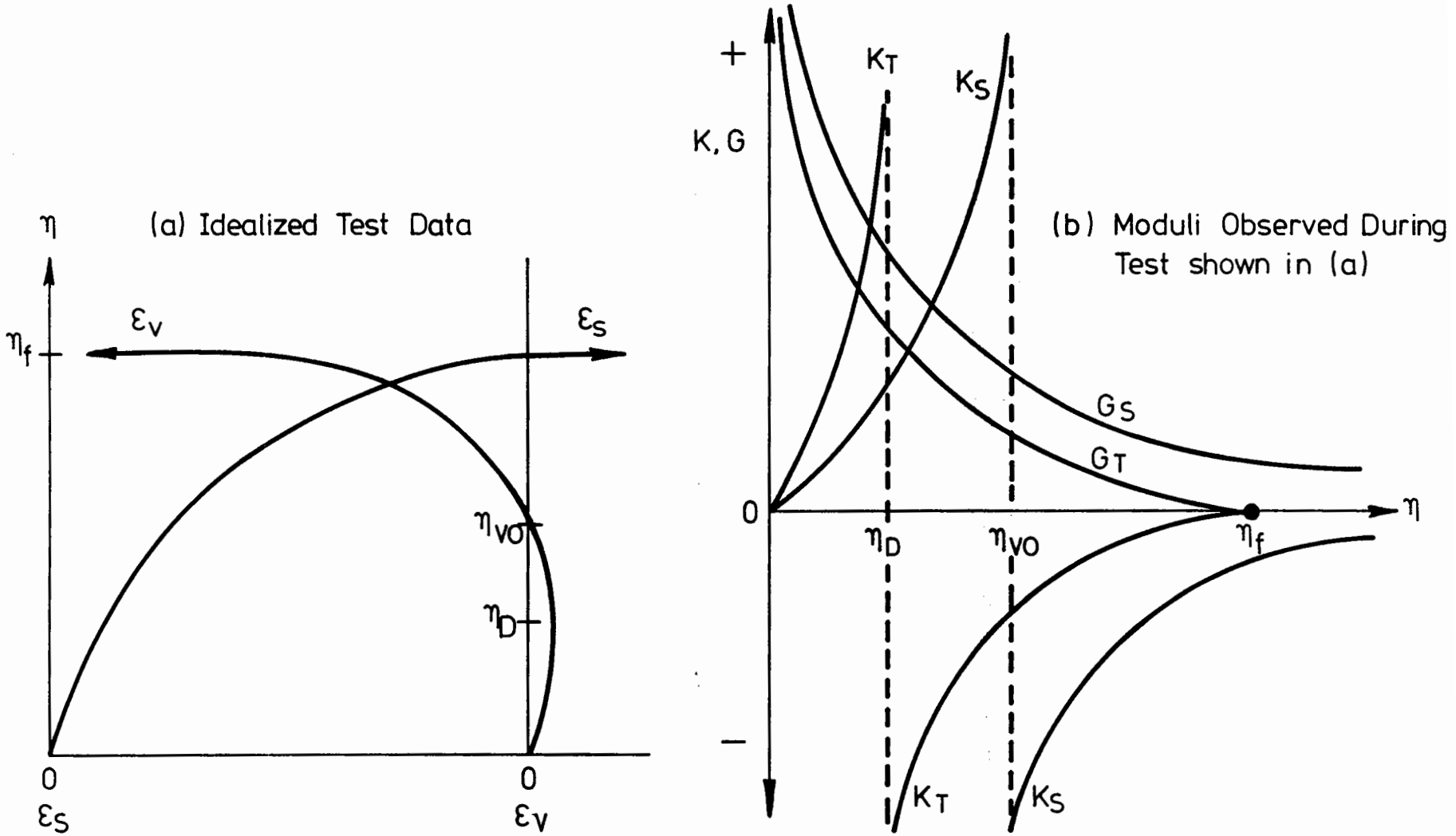

Fig. 6.18 The Relationship Between Secant and Tangent Moduli During Monotonic Shearing of Granular Material

this asymptote depends on the type of modulus under consideration. The tangent modulus asymptote occurs at η_D (the stress ratio at the onset of dilation), whereas that of the secant modulus occurs at η_{vo} (the stress ratio at which $\epsilon_v = 0$).

(b) Tangent moduli become 0 at η_f (the stress ratio at failure), whereas secant moduli indicate that the material still retains substantial stiffness.

(c) The chord modulus shown would have a value lying between the tangent and secant moduli.

6A.7.2 Denstone, Secant and Tangent Moduli

Four successful monotonic tests were carried out in Series B and C (that is a full range of axial and radial data were collected). The results from these tests (B9-100-1, C6-400-1, C9-133-1 and CM-133-1) are shown in Fig. 6.9(a)-(d).

Moduli are generally given in terms of stress. In Table 6.8, however, the measured values from Fig. 6.9 are given in terms of stress ratio $\eta = q/p$ and are calculated from:

$$S = \frac{\eta}{\epsilon_s}$$

$$V = \frac{\eta}{\epsilon_v}$$

The following features should be noted:

(a) There appears to be a great disparity between some of the tangent moduli and secant moduli particularly when the material approaches the failure stress ratio. This will obviously be the case for any non-linear material for which the rate of change of slope of the stress

TABLE 6.8 SHEAR AND VOLUMETRIC MODULI IN TERMS OF STRESS RATIO

Test	S_S ($m\varepsilon^{-1}$)	S_T ($m\varepsilon^{-1}$)	V_S ($m\varepsilon^{-1}$)	V_T ($m\varepsilon^{-1}$)	η
B9-100-1	Insufficient Data				0.5
	1.05	0.31	-6.7	-0.8	1.0
	0.6	0.09	-1.0	-0.06	1.2
C6-400-1	1.67	0.9	0.83	0.83	0.5
	0.56	0.13	1.18	3.6	1.0
	0.17	0.03	-2.0	-0.06	1.2
C9-133-1	1.67	1.05	-5	-5	0.5
	0.38	0.05	1.5	-0.45	1.0
	0.13	0.02	-2.4	-0.05	1.2
CM-133-1	3.33	2.75	1.11	1.11	0.5
	0.9	0.2	2.0	-4.8	1.0
	0.3	0.03	-2.4	-0.06	1.2

NOTES

1. Subscript "T" refers to tangent moduli; subscript "S" refers to secant moduli

ratio-strain graph is great ($d^2\eta/d\epsilon^2 >> 0$).

(b) The volumetric moduli (V) appear to show an inconsistent pattern. There are two main reasons for this. Firstly, the radial strain instruments exhibited random deviations which caused errors in the measured radial strains, which have a large effect on volumetric strains. Secondly, as the material behaviour in the region being investigated is characterised by a change from compressive to dilatant behaviour and, therefore, by high rates of change of volumetric modulus, it is unlikely that highly self-consistent results would emerge from so few tests.

The shear and volumetric behaviour at small strains recorded during four tests (C6-133-1, C6-400-1, C9-133-1 and CM-133-1) are presented in Fig. 6.15(a)-(d). The secant and tangent moduli measured from these graphs are given in Table 6.9. As in Table 6.8 there is a disparity between the secant and tangent shear moduli and also a large scatter of volumetric moduli is observed. An additional feature to be noted is the relatively high initial stiffness observed during test CM-133-1. This may be ascribed to the large number of particle contacts with this graded material. At low stress ratios the compression at particle contacts is a major source of the overall strain and so a material with a larger number of contacts will be able to distribute stresses more evenly thereby straining less. At high stress ratios, slips and rotations become the dominant deformation mechanisms. The modular ratio between a graded and single size material will consequently tend to be reduced. This predicted reduction in the stiffness of the graded material used in CM-133-1 relative to the stiffness of the single size material may be clearly seen from Tables 6.8 and 6.9.

The axial strains recorded during the initial stages of monotonic loading in five tests (C6-400-1, CM-133-1, C9-133-1, C6-133-1, C19-133-2) are presented in Fig. 6.13. Table 6.10 gives a list of secant axial moduli

TABLE 6.9 RECORDED MODULI AT LOW STRAINS

Test	S_S ($m\epsilon^{-1}$)	S_T ($m\epsilon^{-1}$)	V_S ($m\epsilon^{-1}$)	V_T ($m\epsilon^{-1}$)	η (kPa/kPa)
C6-133-1	3.63	3.16	2.5	2.5	0.2
	2.67	1.38	2.1	1.25	0.4
	1.77	0.77	1.7	1.1	0.6
C6-400-1	4.44	2.4	0.9	0.9	0.2
	2.2	1.14	0.89	1.0	0.4
	1.5	0.71	0.92	1.1	0.6
C9-133-1	3.08	1.82			0.2
	2.2	1.5	V. large		0.4
	1.54	0.7			0.6
CM-133-1	10.0	6.2	2	2	0.2
	5.0	3.5	2.1	2.9	0.4
	2.9	0.98	3	4.3	0.6

TABLE 6.10 SECANT AXIAL MODULI FOR A RANGE OF MATERIALS

Test	Material Size	$E_{0.25}$	$E_{0.5}$
C6-133-1) C6-400-1)	6mm	2.45	1.52
C9-133-1	9mm	3.13	1.92
C19-133-2	19mm	3.57	2.33
CM-133-1	Mixed	4.03	2.63

Notes

1. The subscript of "E" indicates the stress ratio at which the modulus was calculated

(E) which were extracted from Fig. 6.13 at stress ratios of η = 0.25 and η = 0.5 where:

$$E = \frac{\eta}{\epsilon_a}$$

As was mentioned above, the graded material (test CM-133-1) exhibited the highest initial stiffness. There appears to be a trend amongst the single size materials which indicates that those with large particles are stiffer. The reasons for this may be similar to those given to explain why materials with larger particles exhibited greater strength. The possibility of bad compaction producing an anisotropic fabric with a relatively large number of particle contacts in the vertical direction, would be particularly likely to produce a sample with a greater axial stiffness, especially during the initial stages of loading.

6A.7.3 Iron Oxide

Only one test was carried out on this material and, unfortunately, no measurements were made at very small strains. The iron oxide material, however, appeared to exhibit greater stiffness than the Denstone materials. In addition, the iron oxide seemed to develop a higher proportion of its ultimate strength (η_f) at a given value of shear strain than the Denstone would have done - see Fig. 6.11.

SECTION B - INTERMEDIATE BEHAVIOUR

6B.1 INTRODUCTION

Three types of test were carried out in this category:

(a) repeated loading in which large permanent strains were forced to develop during each cycle. These tests were carried out in the large triaxial apparatus and are intended as a rough (and exaggerated) simulation of the granular component of a structure during a shakedown failure.

(b) repeated loading in which either the stress or strain level was controlled. These tests aim to simulate an element in a TES in which conditions are stabilising.

(c) stress-history test: in this test a sample was subjected to a series of stress paths in both compression and extension space. This was done in order to gain an insight into the mechanisms operating during general granular material behaviour.

In past projects involving repeated loading, there has been a tendency for researchers to carry out "permanent strain tests" which involve subjecting a granular sample to many load cycles - Fig. 4.21, for example, shows the results of tests carried out by Shaw (1980) on a single-sized crushed limestone. Subsequent research (eg. Symes, 1983, Wong and Arthur, 1985) has shown that principal stress rotation has a profound effect on the accrual of permanent strain. In view of this, it was decided that little was to be gained from carrying out a similar series of tests on the present materials.

6B.2 FORCED PERMANENT STRAIN TESTS

Two tests were carried out using the large triaxial apparatus which

involved the application of forced permanent strain cycles. The results of these tests are presented in Figs. 6.10 and 6.11.

In addition, a forced permanent strain test was carried out on a sample of modified Denstone in the repeated load apparatus. Only axial strains were recorded - see Fig. 6.19.

6B.2.1 Relationship between Monotonic and Load-Unload Behaviour

An inspection of Figs. 6.10, 6.11 and 6.19 shows that the following observations may be made:

1. the general shape of the "stress-strain envelope" is very similar to those obtained from monotonic tests;
2. during repeated loading (as opposed to unloading - see 6B.2.2 below), the material increases in stiffness;
3. on reloading to the previously attained maximum stress the stiffness is lost once more as the monotonic stress-strain envelope is re-joined.

These observations (which are true for both shear and volumetric strain behaviour) correspond exactly to the type of behaviour recorded in the literature.

6B.2.2 Unload-Reload Stiffness

The unload-reload loops in Figs. 6.10 and 6.11 show that there is a significant loss of stiffness as the magnitude of the forced strain is increased. Fig. 6.20 shows the value of the unload stiffness in terms of S ($= \eta/\epsilon_s$) plotted against the value of shear strain at the beginning of unloading. Both iron oxide and Denstone materials show the same characteristic graph shape. Another feature that can be observed in Figs. 6.10 and 6.11 is that the area of the hysteresis loop increases greatly

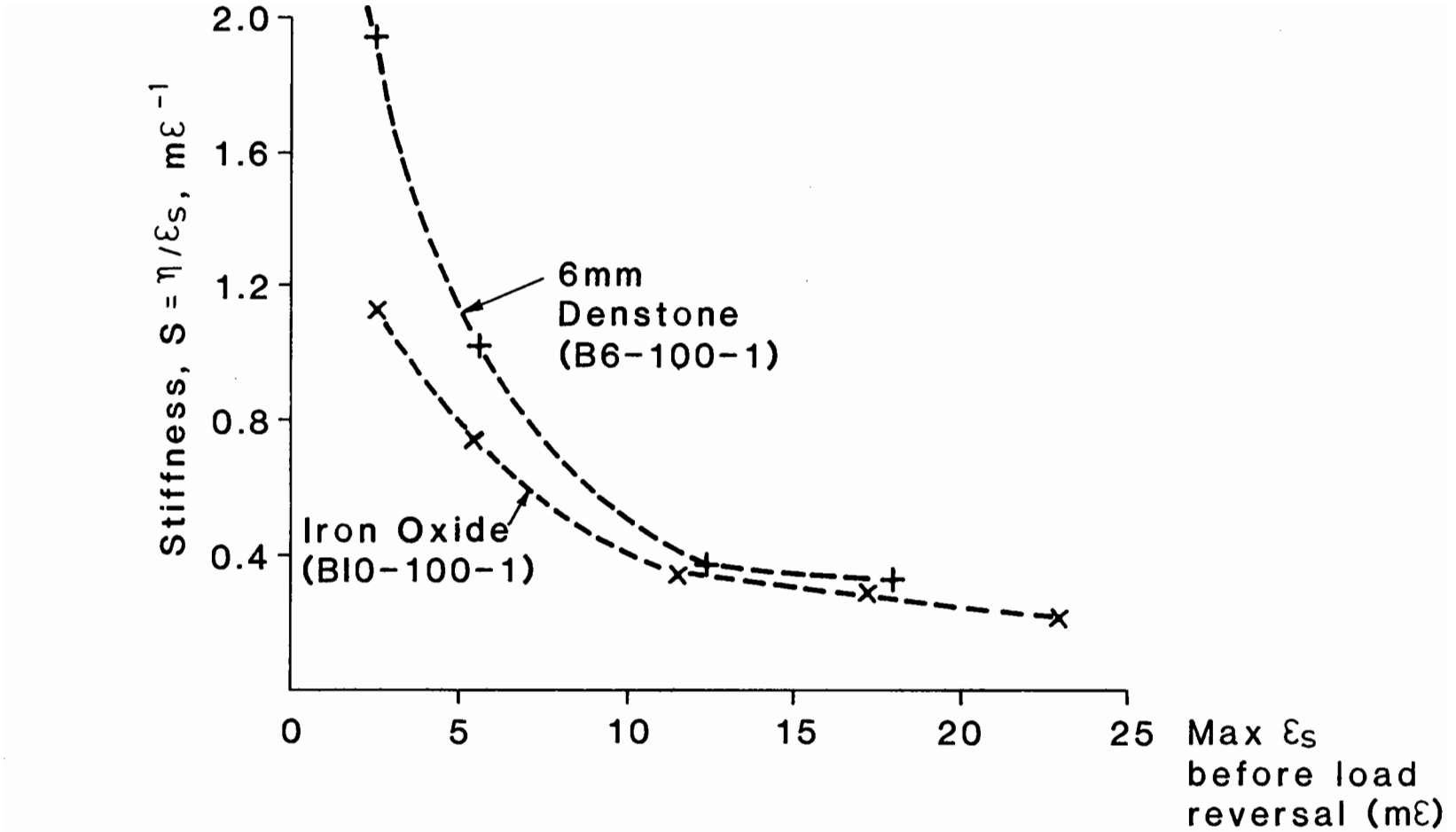

Fig. 6.20 THE LOSS OF STIFFNESS DURING FORCED STRAIN TESTS

with the number of forced cycles. Unfortunately, insufficient data points were recorded to provide an accurate quantification of this effect.

6B.2.3 Dilation during Forced Permanent Strain Tests

Figs. 6.21 and 6.22 show the $\epsilon_s - \epsilon_v$ plots for tests B6-100-1 and BIO-100-1 respectively. Two points are particularly worthy of note:

(a) As the number of cycles increases, the duration of the compression phase ($d\epsilon_v/d\epsilon_s > 0$) diminishes. For example, in test B6-100-1 (see Fig. 6.21), the material undergoes substantial compression (about 1000$\mu\epsilon$) during the initial stages of the first cycle. During the initial stages of cycles B and C, a slight compression phase is also recorded. By cycles D and E, however, the material appears to dilate almost as soon as the shear strain is observed, i.e. very little compression appears to occur.

(b) During unloading, the material does not retrace the loading line but follows a path such that:

$$\left(\frac{d\epsilon_v}{d\epsilon_s}\right)_{\text{(unloading)}} > \left(\frac{d\epsilon_v}{d\epsilon_s}\right)_{\text{(loading)}}$$

This means that the ratio of permanent (plastic) volumetric strains to permanent shear strains observed at the end of any loading cycle is lower than the ratio D. That is:

$$\frac{\epsilon_{vp}}{\epsilon_{sp} - \epsilon_{sD}} < D$$

where the suffix p denotes permanent strain.

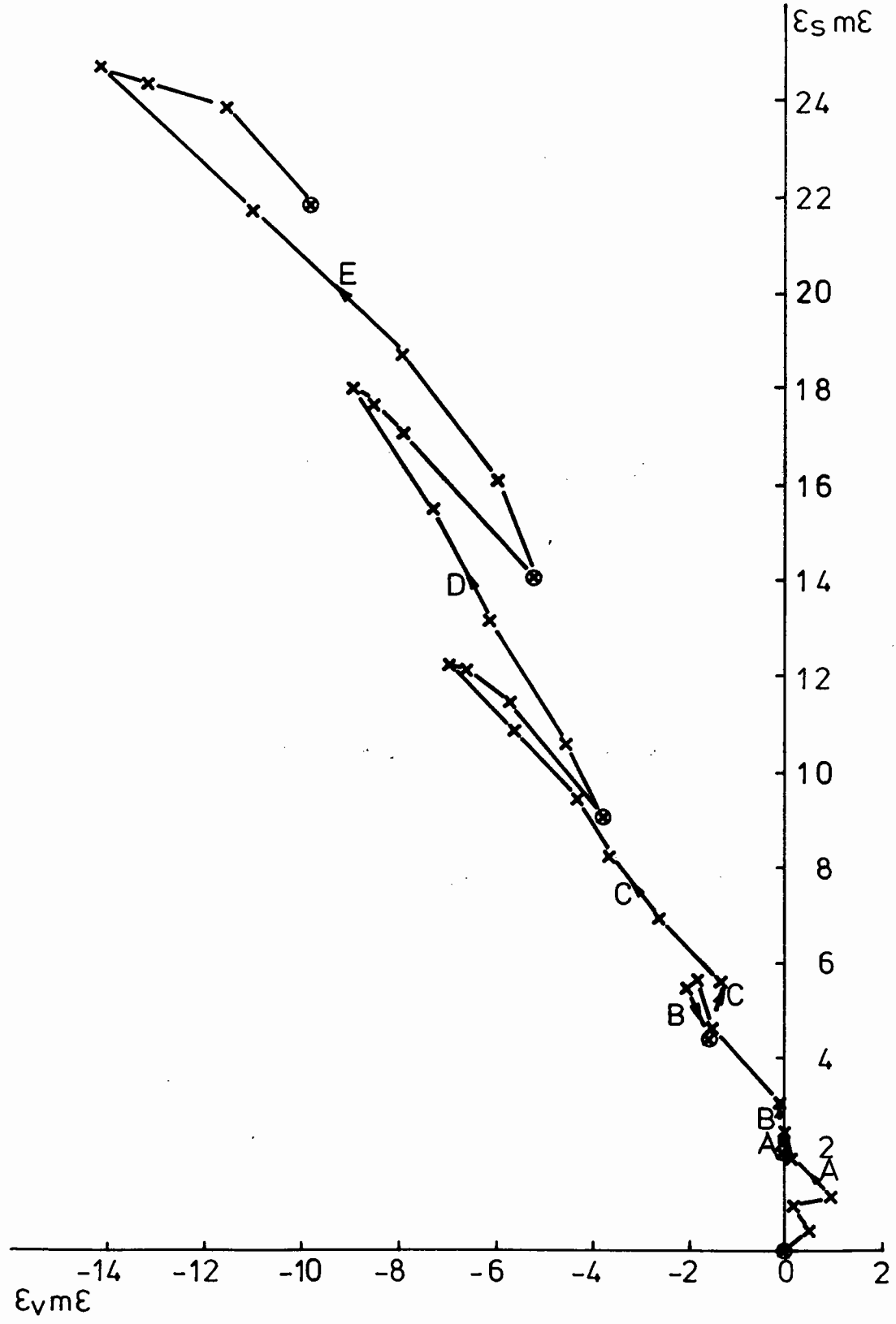

Fig. 6.21 The Relationship Between Shear and Volumetric Strain During Repeated Loading of Sample B6-100-1

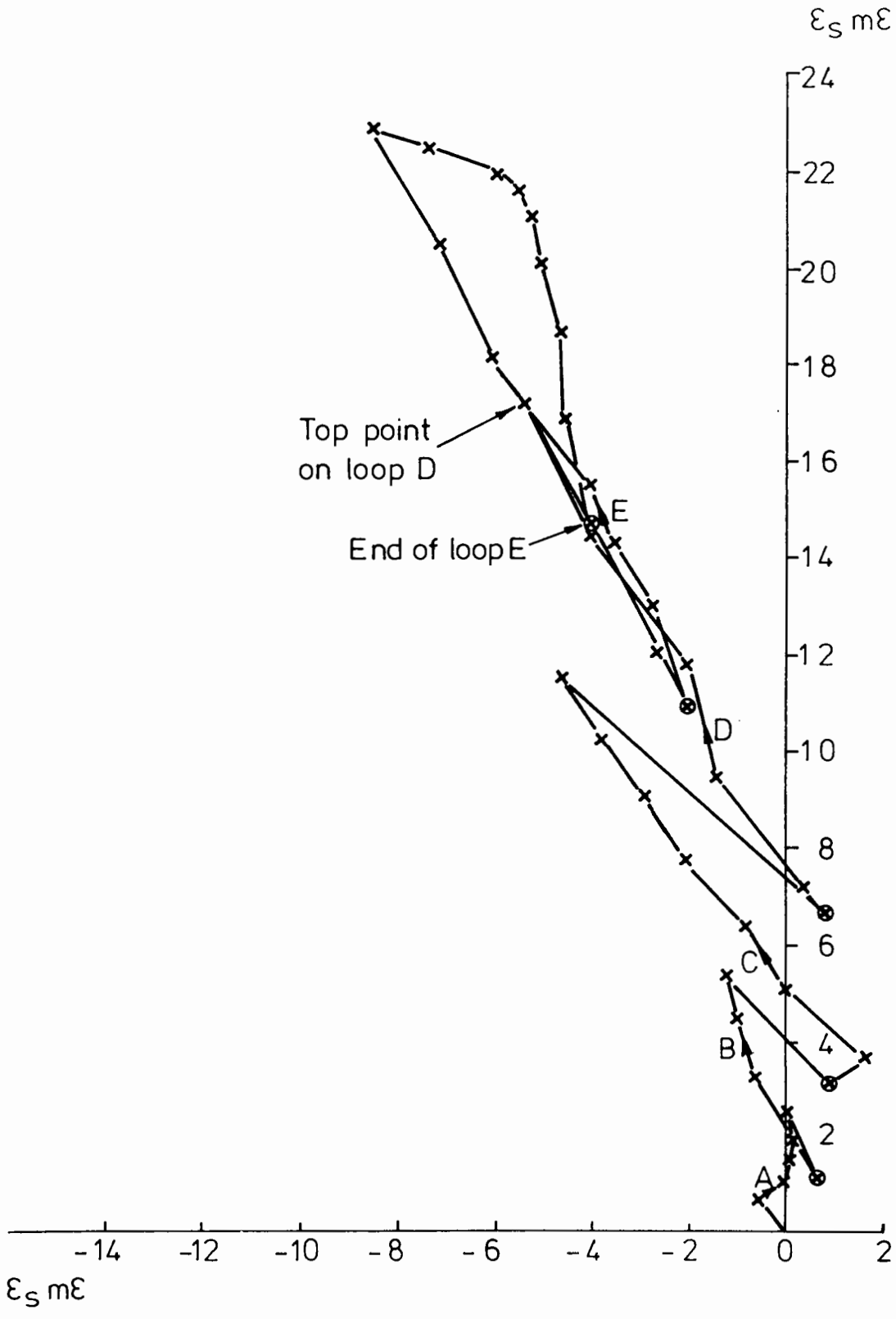

Fig. 6.22 The Relationship Between Shear and Volumetric Strain During Repeated Loading Sample BI0-100-1

6B.3 STRESS AND STRAIN CONTROLLED INTERMEDIATE TESTS

All the tests in this category were carried out using the repeated load apparatus. Six samples were tested, although not all were used for controlled intermediate testing. The samples are listed in Table 6.11. The initial letter(s) of the code indicates the test material: "D" for 6mm Denstone and "MD" for modified Denstone.

All samples were compacted by prolonged tamping. Specific volumes of approximately 1.5 were achieved in all cases.

6B.3.1 Stress Controlled Tests

The results of tests in which a triaxial sample is subjected to a constantly repeated deviator stress between 0 and some defined value are well-known. Fig. 4.2 shows the results of such a test carried out by Lau (1975) on a sand.

It was decided to carry out a rather different type of test in which the deviator stress was cycled between large positive and negative stress ratios.

Fig. 6.23 shows the q-ϵa plot from a test involving sample D-3. A constant cell pressure of 200 kPa was maintained while the deviator stress was cycled between -100 kPa (η = -0.6) and +400 kPa (η = 1.2). The axial strain amplitude recorded during cycle no. 1 was approximately 0.5% (5000$\mu\epsilon$). The value of this strain decreased with increasing numbers of cycles and by cycle 500 was approximately 1500$\mu\epsilon$. Thus, the axial stiffness of the material increased by a factor of about 3. One interesting feature of the test was that no large shift in mean axial deformation was observed.

6B.3.2 Strain Controlled Tests

Sample D-4 was subjected to a series of strain controlled tests at a

TABLE 6.11 SAMPLES TESTED IN REPEATED LOAD TRIAXIAL APPARATUS

Test Code	Date Tested
D1	April 1983
D2	May 1983
D4	February 1984
D5	May 1984
MD 1	October 1984
MD 2	December 1984

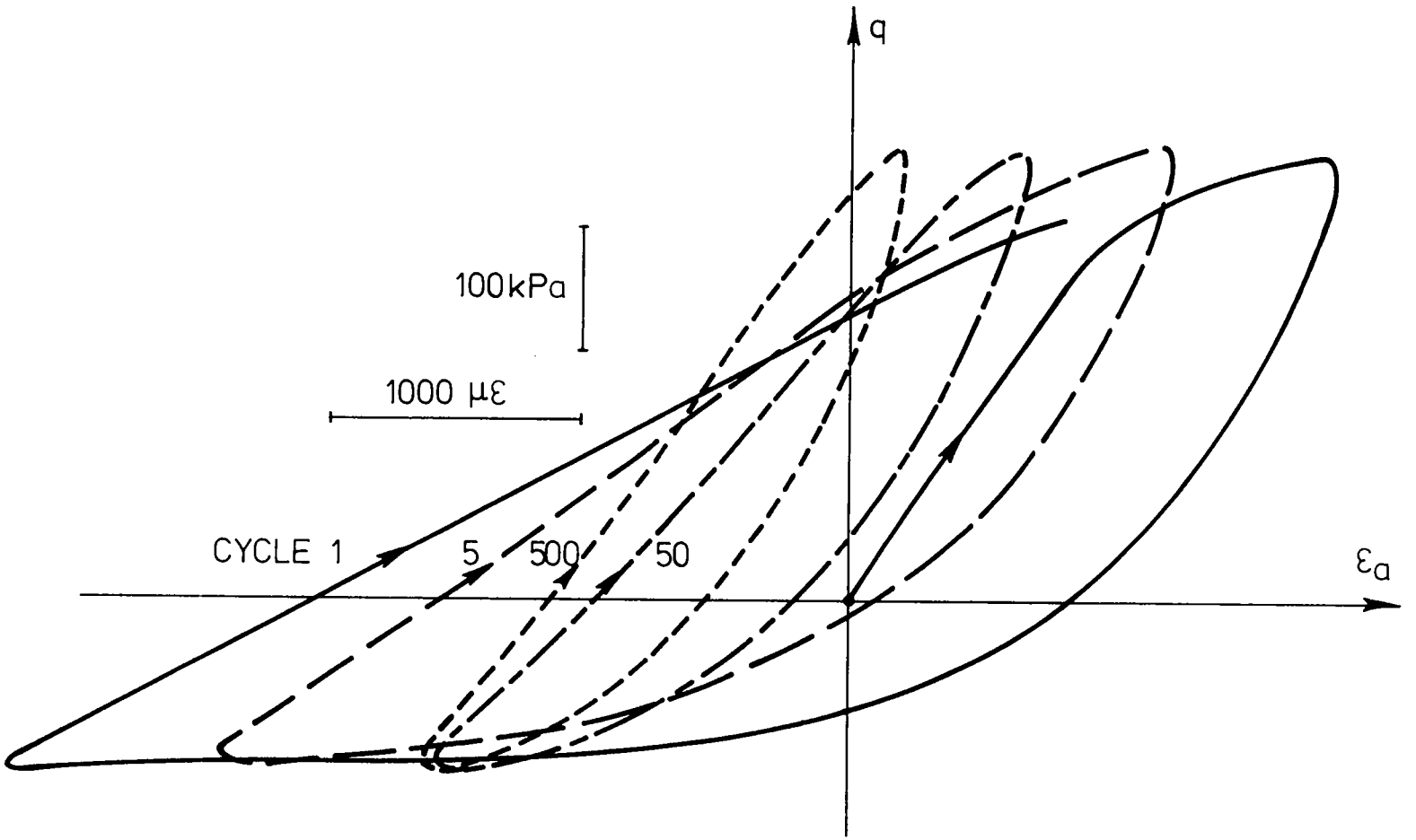

Fig. 6.23 Stress - Strain Behaviour During Test on Sample D-3

constant cell pressure of 200 kPa. A total of four compression-extension tests (A-E) were carried out. The general form of these tests is shown in Fig. 6.24 with the strain regime and the resulting stresses being given as a function of time. The strain amplitudes of each test are listed in the table on Fig. 6.24. Test C was performed in order to investigate how two "identical" strain path tests (A and C) would be affected by an intervening test in which much higher stresses and strains were imposed.

The stress-strain behaviour of tests A to D is presented in Fig. 6.25. The material behaviour is presented only for selected cycles so that the general pattern is more clearly shown.

The following points may be noted:

(a) An increase in axial stiffness is observed to occur during each cycle of strain.

(b) The largest increase in stiffness occurs during the first cycle. When the applied strain amplitude is small (eg. Test A), the behaviour appears to reach an equilibrium within a very small number of cycles - when a larger strain amplitude is imposed the material appears to increase in stiffness by a considerable amount even during later cycles.

(c) The behaviour during Tests A and C appears to be quite similar despite the intervening Test B.

Tests were carried out on samples MD-1 and MD-2 in which the axial strain was the controlling factor. The tests were performed at constant cell pressure and the values of deviator stress and radial strain were observed. The results of a test on sample MD-1 are shown in Fig. 6.26: the axial strain was cycled between $-1925\mu\epsilon_a$ and $+1100\mu\epsilon$. Fig. 6.27 shows the results of a test on sample MD-2 in which the axial strain was cycled between 0 and $+885\mu\epsilon$.

In both tests it was noted that the radial strain had a distinctly

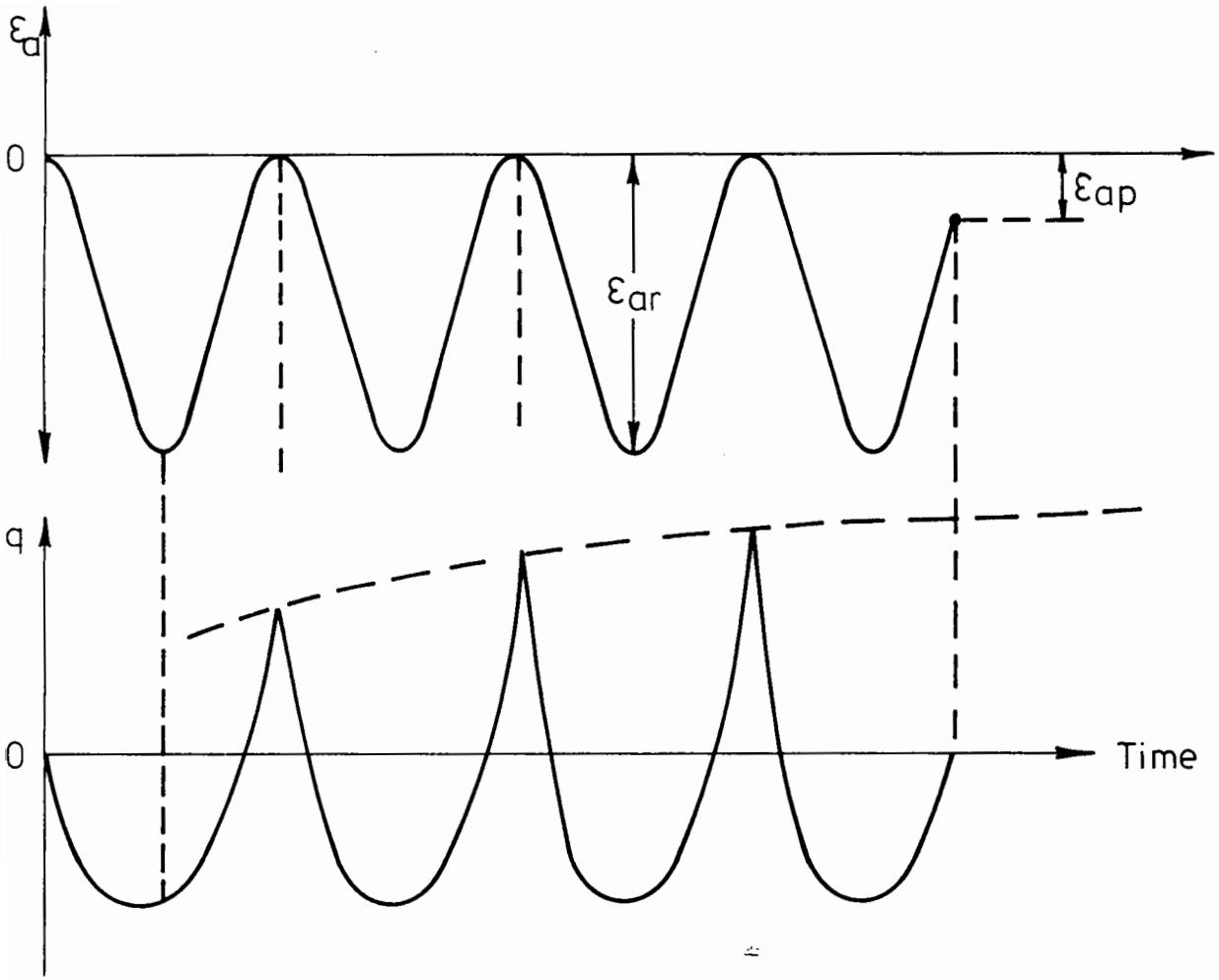

Test	ε_{ar} ($\mu\varepsilon$)
A	150
B	450
C	150
D	900

Fig. 6.24 Variation of Applied Strain and Resultant Stresses with Time for Tests A to D (Sample D-4)

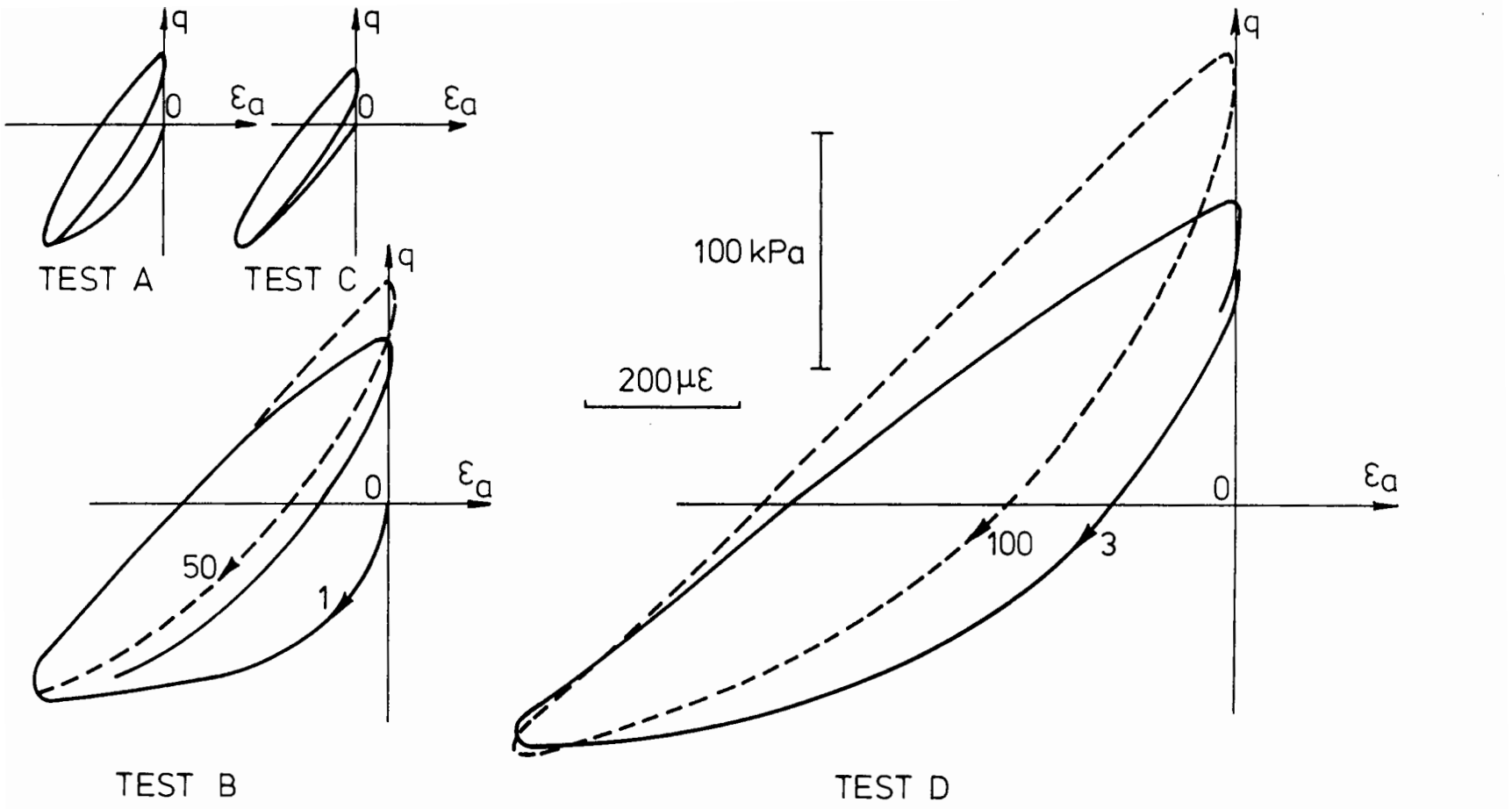

Fig. 6.25 Stress - Strain Plots from a Series of Tests on Sample D-4

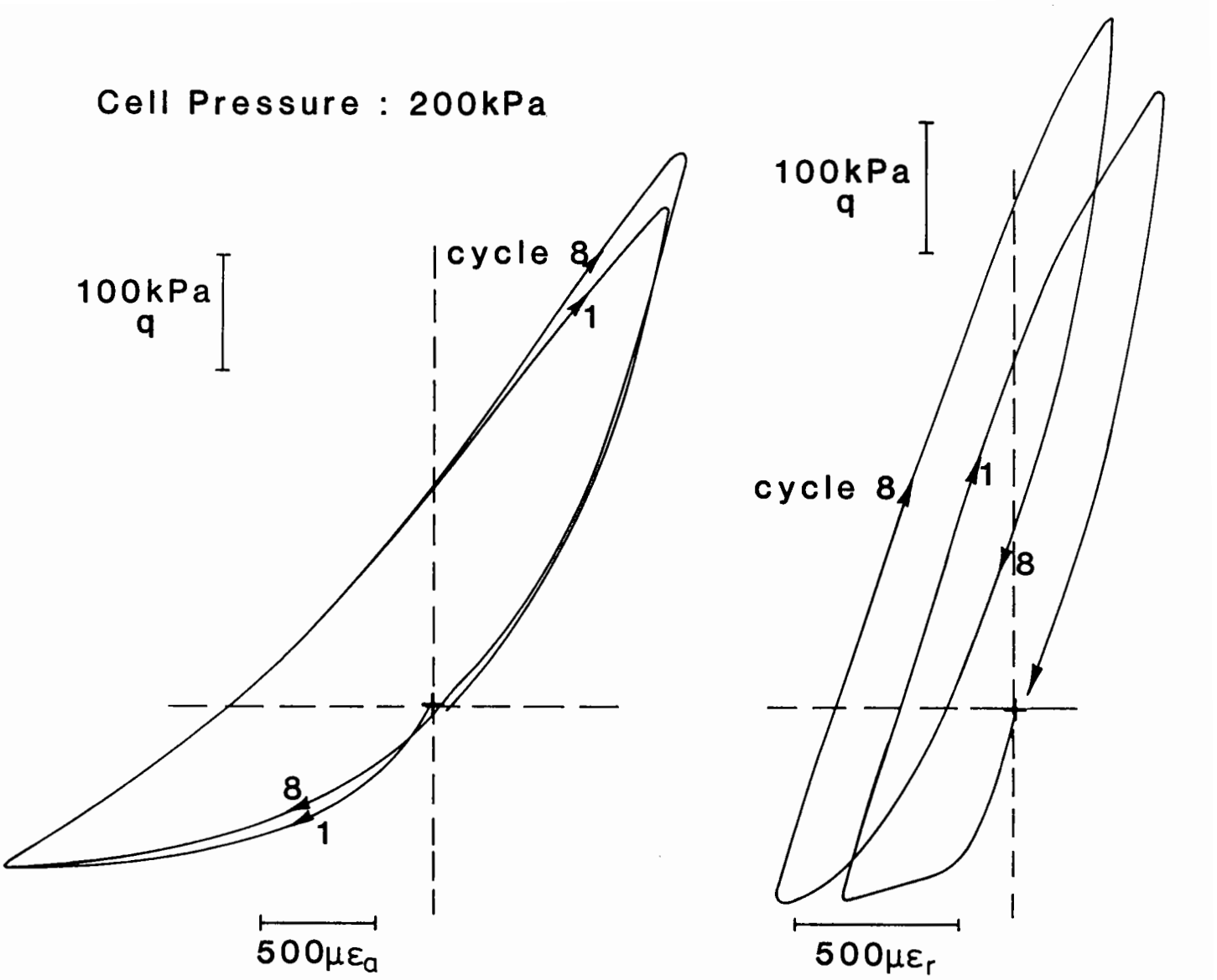

Fig. 6.26 AXIAL STRAIN CONTROLLED TEST - SAMPLE MD-1

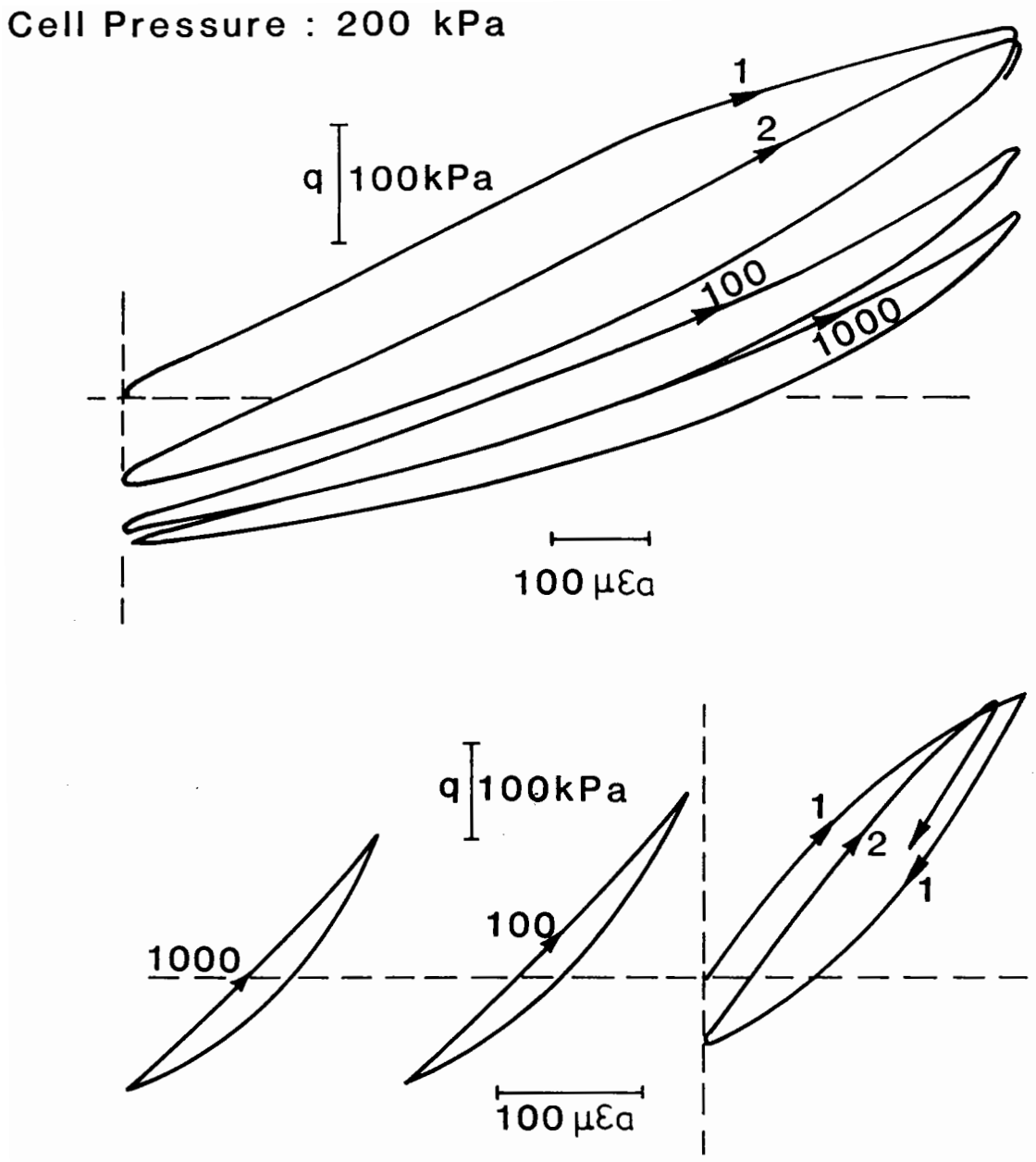

Fig. 6.27 AXIAL STRAIN CONTROLLED TEST - SAMPLE MD-2

positive trend although the axial strain remained constant throughout. The test shown in Fig. 6.26 was not continued long enough to determine whether this radial "contraction" would continue. In the test shown in Fig. 6.27, it was demonstrated that this was in fact the case. The results from Fig. 6.27 (given in terms of axial and radial strain) were used to calculate the shear and volumetric strain behaviours shown in Figs. 6.28 and 6.29 respectively. In Fig. 6.28, the patterns of shear behaviour during cycle 1 and cycle 1000 are shown. The maximum and minimum points of cycles 10 and 100 are also shown (these are not included in full as this would have confused the diagram). As the number of cycles increases, the mean deviator stress falls (approximately logarithmically). The mean shear strain also diminishes, and it does so in a manner almost linear with respect to the mean deviator stress. With each successive cycle, the area of the hysteresis loop also diminishes.

Fig. 6.29 shows the volumetric strain behaviour during cycles 1, 10, 100 and 1000. As the number of cycles increases so does the mean volumetric strain, in an approximately logarithmic manner. The area of the hysteresis loop diminishes dramatically, and in cycle 1000 is almost non-existent. The shape of the stress-strain loop in cycle 1000 is quite unusual.

6B.3.3 Discussion of Stress and Strain Controlled Test Results

Insufficient data have been collected as yet to attempt development of any general model.

The main feature emerging from the testing is the tendency towards greater stiffness which occurs during constant amplitude stress and strain controlled testing. Initial attempts at providing an expression for this rate of increase in stiffness indicate that it may, for example, be approximately proportional to the logarithm of the cycle number for both

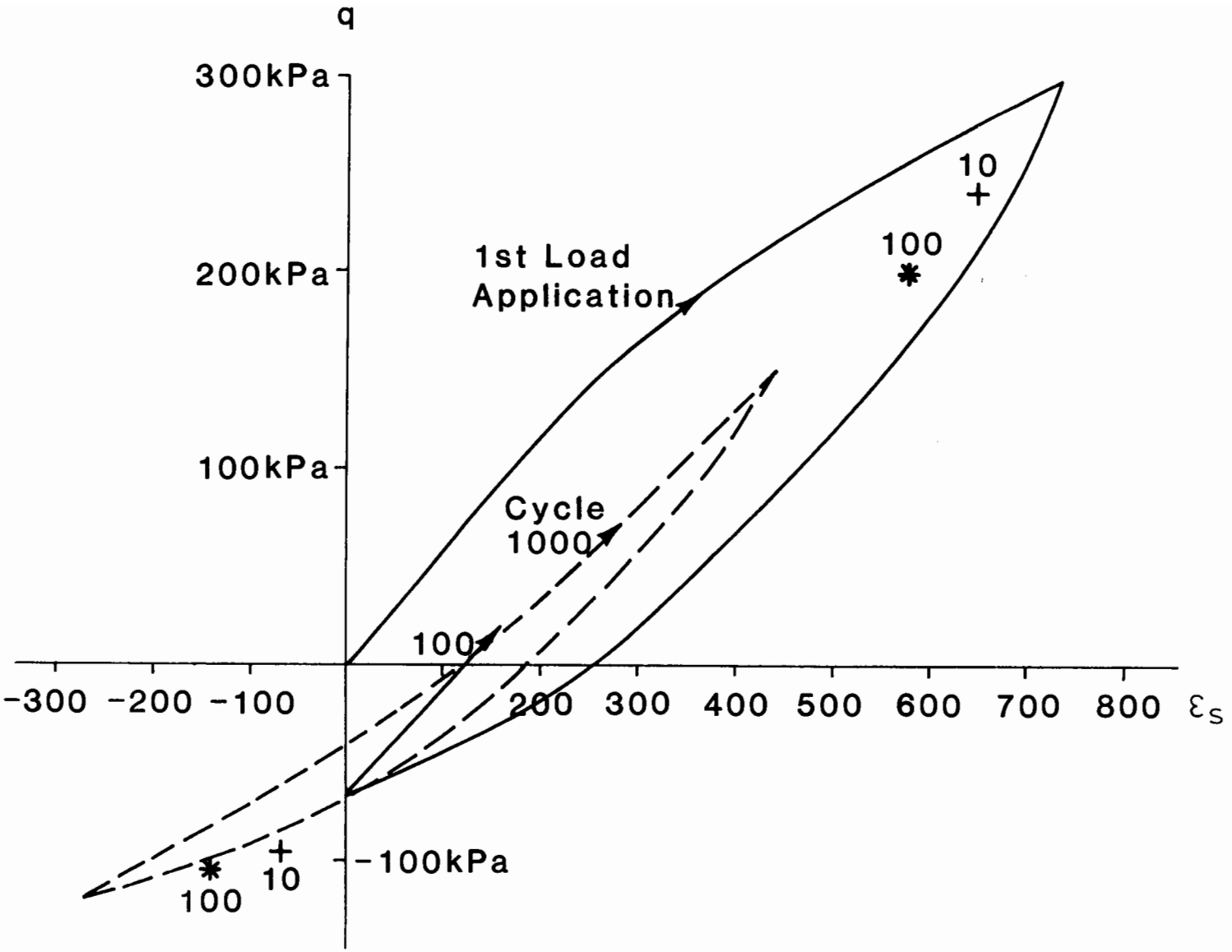

Fig. 6.28 SHEAR STRAIN BEHAVIOUR FOR AXIAL STRAIN CONTROLLED TEST SHOWN IN Fig. 6.27

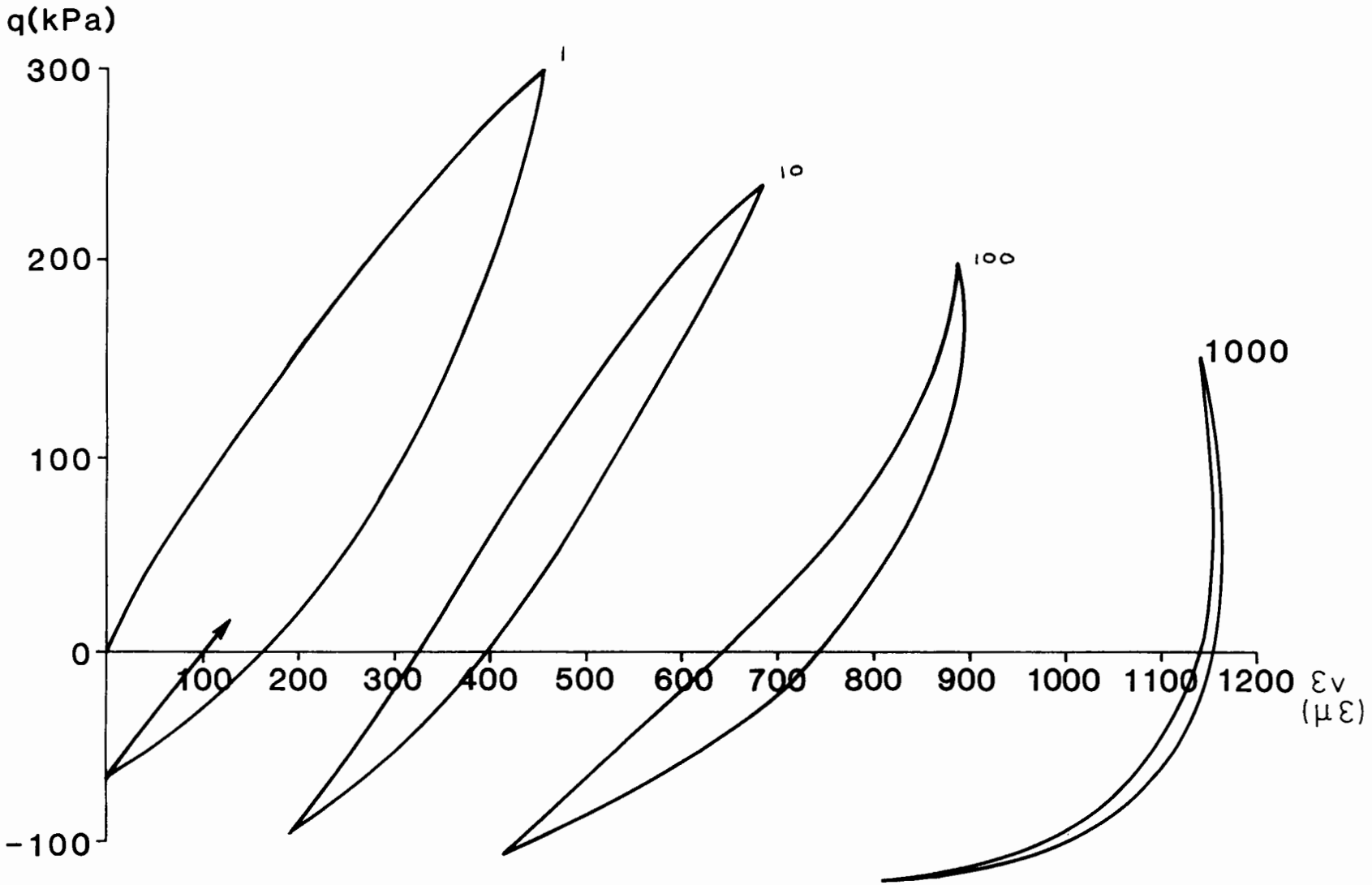

Fig. 6.29 VOLUMETRIC STRAIN BEHAVIOUR FOR AXIAL STRAIN CONTROLLED TEST SHOWN IN FIG. 6.27

stress and strain controlled tests.

Both sets of tests described above involved deviator stresses which cross the p' axis (i.e. they were compression-extension tests). This is necessary for constant strain tests since the material exhibits plastic behaviour during cycle no. 1. For stress controlled tests, however, loading may be entirely within compression or extension space. The jump in principal stress directions is a factor which must not be overlooked when considering the results from these tests.

6B.4 KNOWN STRESS HISTORY TEST

Sample MD-1 was subjected to the stress history shown in Fig. 6.30. No measurements of strain were taken before point 3 (when the cell pressure was increased to 200 kPa). After this point, both axial and radial strains were recorded. Axial strains are shown in Fig. 6.31 and radial strains in Fig. 6.32. The dashed lines in these figures indicate only that the recording pen was moved to avoid confusion. The radial strains have been presented with positive (i.e. compressive) strains going from left to right in order to show similarities between the axial and radial strain behaviour. These results provide evidence for two propositions about granular material behaviour:

1. for any stress path the plastic strain accrued during cycle 1 is much greater than that for any other individual cycle.

   This proposition appears to hold true for both axial and radial (and, hence, shear) strain.

2. when the material is cycled along path (p_1, q_1) to (p_2, q_2) in compressive stress space until it reaches resilient equilibrium, and then cycled along a stress path in extension stress space before being resubjected to stress path (p_1, q_1) to (p_2, q_2), the material undergoes

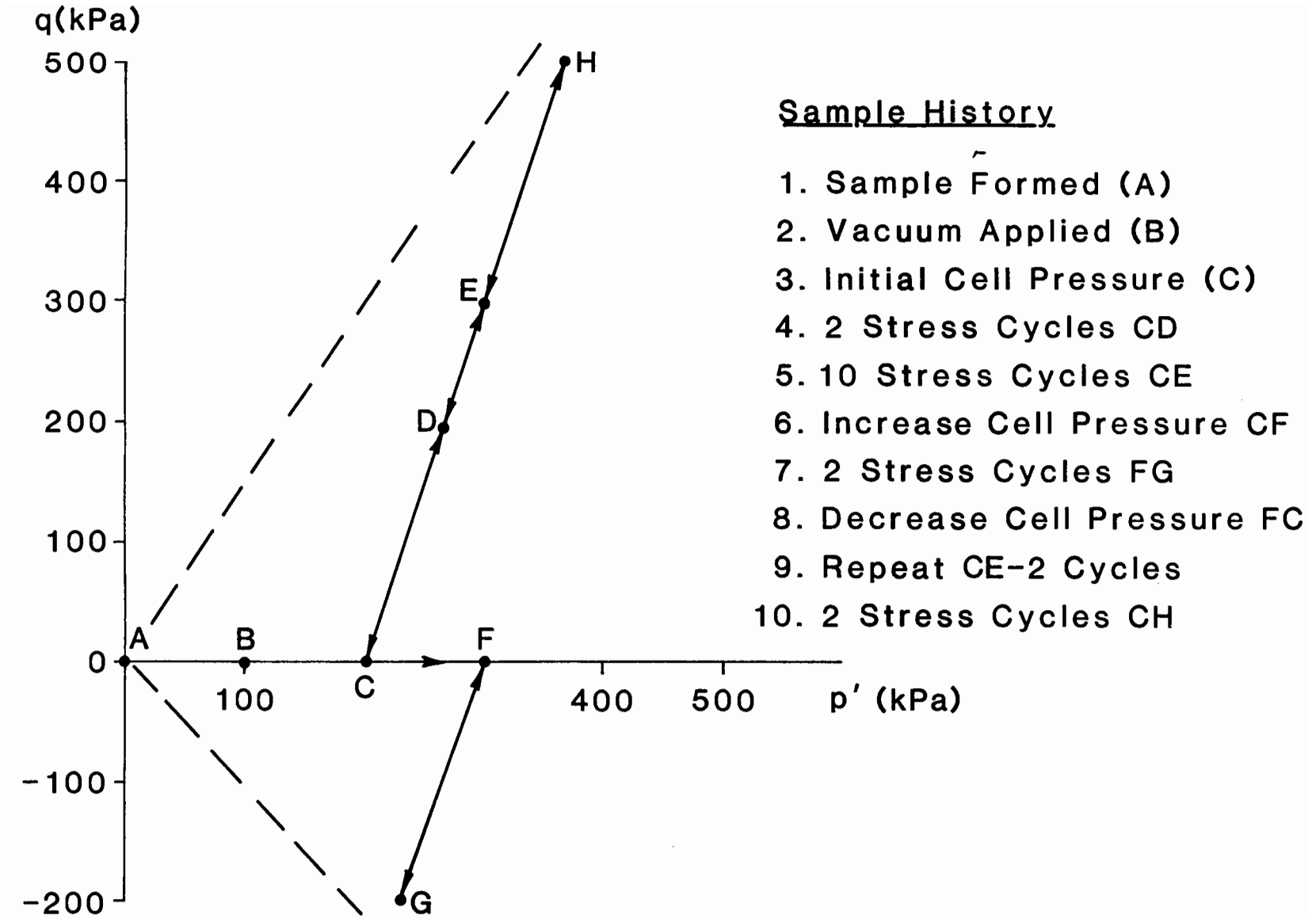

Fig. 6.30 STRESS HISTORY OF SAMPLE MD-1

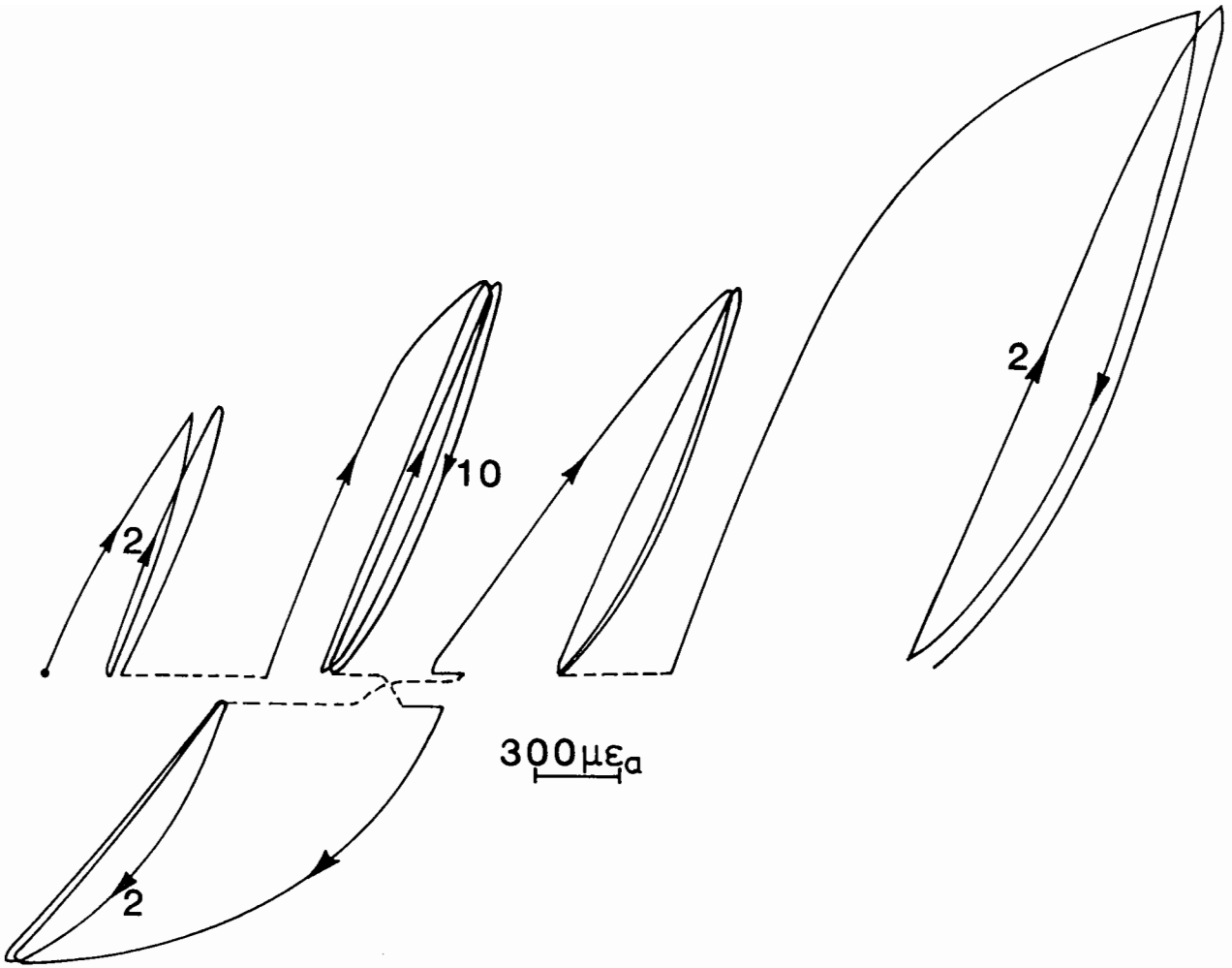

Fig. 6.31 AXIAL STRAINS RESULTING FROM STRESS HISTORY SHOWN IN FIG. 6.30

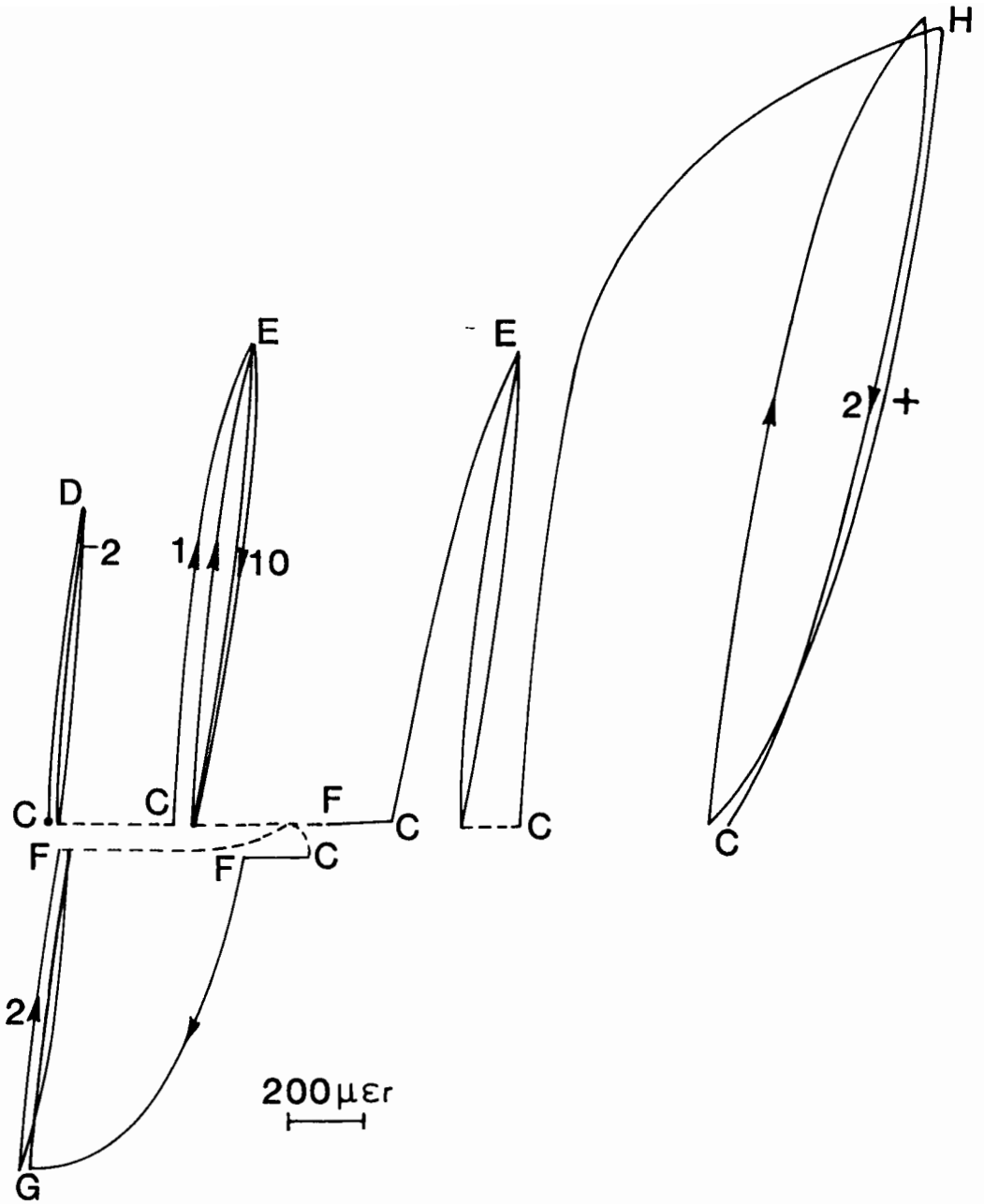

Fig. 6.32 RADIAL STRAINS RESULTING FROM STRESS HISTORY SHOWN IN FIG 6.30

large permanent strains during the first cycle of the revisited stress path despite the fact that it had previously reached equilibrium along that very same path. Furthermore, the material stiffness during the first revisited cycle is less than that of the material during the very first cycle.

These effects can be simulated by the simple sliding-block model as shown in Fig. 6.33 (Zytynski et al 1978), which would appear to indicate that normal yield locus models based on metal (i.e. non-frictional material) behaviour must be modified to account for the observed behaviour of granular materials. The modification must be such that when stresses enter extension space the compression space yield locus alters its position in stress space.

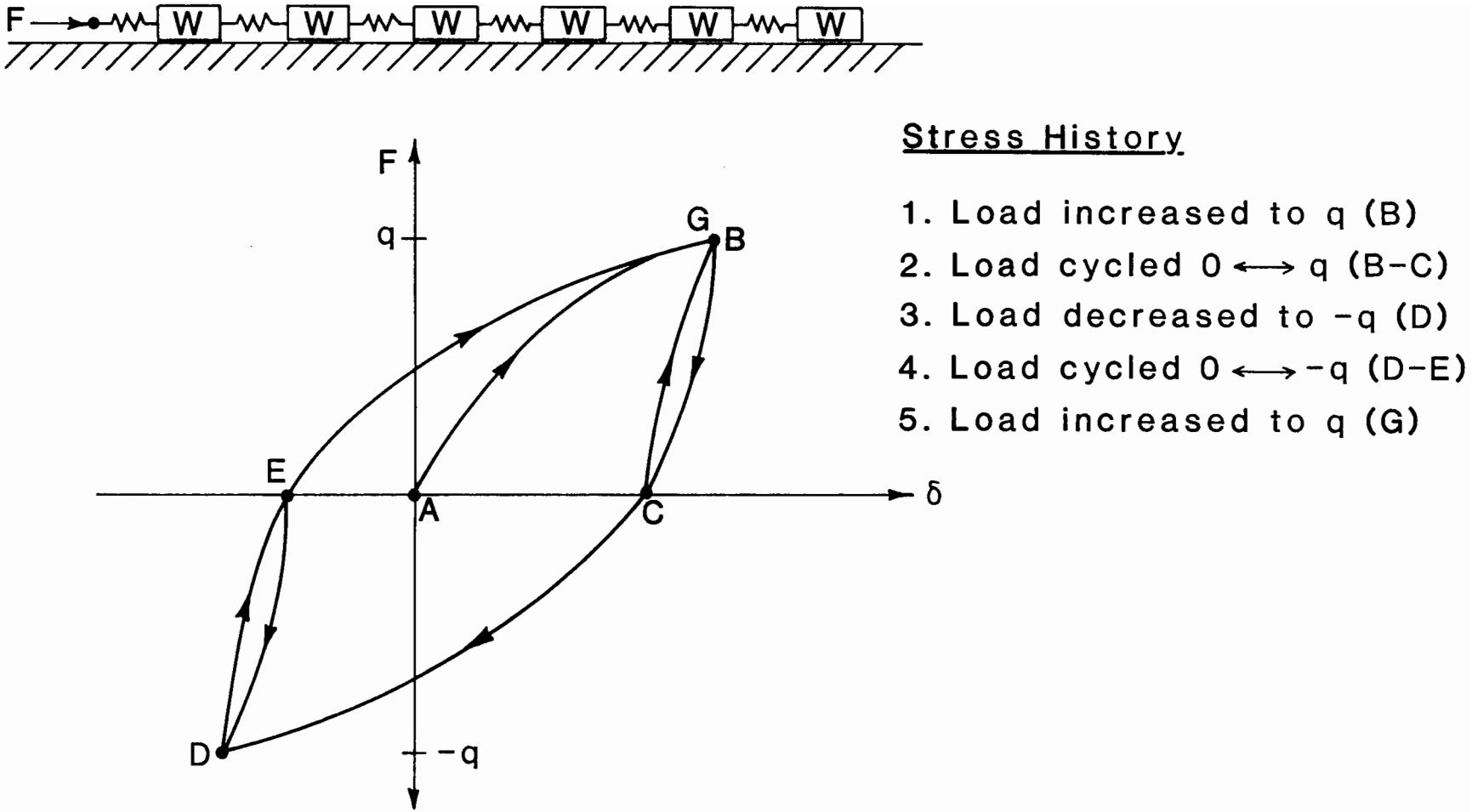

Fig. 6.33 BEHAVIOUR OF SPRING AND BLOCK MODEL UNDER REPEATED LOAD AND LOAD REVERSALS

SECTION C - RESILIENT BEHAVIOUR

6C.1 INTRODUCTION

When a granular material is subjected to a repeating load, and when the plastic strains incurred during each cycle of loading are very small compared to the recoverable strain, then that material is said to behave resiliently. Resilient behaviour has been the subject of much investigation, particularly with reference to highway and railway engineering.

In this section, a variety of behavioural aspects which have been observed during resilient loading are discussed, including hysteresis, dilation and closed loop testing. Finally, the possibility of developing a new form of model for resilient behaviour is discussed - it is hoped that this will enable behaviour at all stages throughout the resilient cycle to be predicted.

6C.2 RESILIENT STRAIN MODELS

The resilient models presented below are given in a form similar to that used by Pappin (1979). In a later section (6C.8), possible improvements on this type of model are discussed, and a new formulation is tentatively proposed. This new method attempts to predict behaviour over a much wider range of conditions by considering the interaction between the different mechanisms which are considered to be at work within the material. Although the basic ideas are simple enough, it has proved difficult to derive accurate material constants from the sparse information gathered so far; this task has not been completed.

6C.3.1 Test Programme

In order to determine the resilient properties of the materials presently under investigation, a network of stress paths in (q,p') space was used. These paths are shown in Fig. 6.34. The stress-strain behaviour was recorded using an X-Y plotter which initially recorded the output from the servo-control unit. During the testing of samples D-4, MD-1 and MD-2, however, an analogue computer was used. This combines axial and radial stress and strain outputs to produce the critical state soil mechanics invariant parameters.

A stress path is identified using four parameters; p'_m, p'_r, q'_m, q'_r (see inset on Fig. 6.34), which refer to the mean and repeated components of mean normal and shear stress respectively. A list of stress paths and the resultant resilient strains is given in Appendix B.

6C.3.2 Resilient Strain Models for Denstone

Resilient Shear Strain: The model which has been derived to predict resilient shear strains occuring as a result of repeated loading along stress path (p_1, q_1) to (p_2, q_2) is:

$$\epsilon_{sr} = 440\,(\eta_2 - \eta_1) \cdot \left[\frac{\ell_r}{p_m}\right]^{0.2} \cdot \left[\frac{|q_2 - q_1| + 2}{100}\right]^{0.2}$$

where, $\eta_1 = q_1/p_1$, $\eta_2 = q_2/p_2$

and $\ell_r = ((q_2 - q_1)^2 + (p_2 - p_1)^2)^{\frac{1}{2}}$

The core of the model is the expression:

$$\epsilon_{sr} = 440\,(\eta_2 - \eta_1) = 440.\Delta\eta.$$

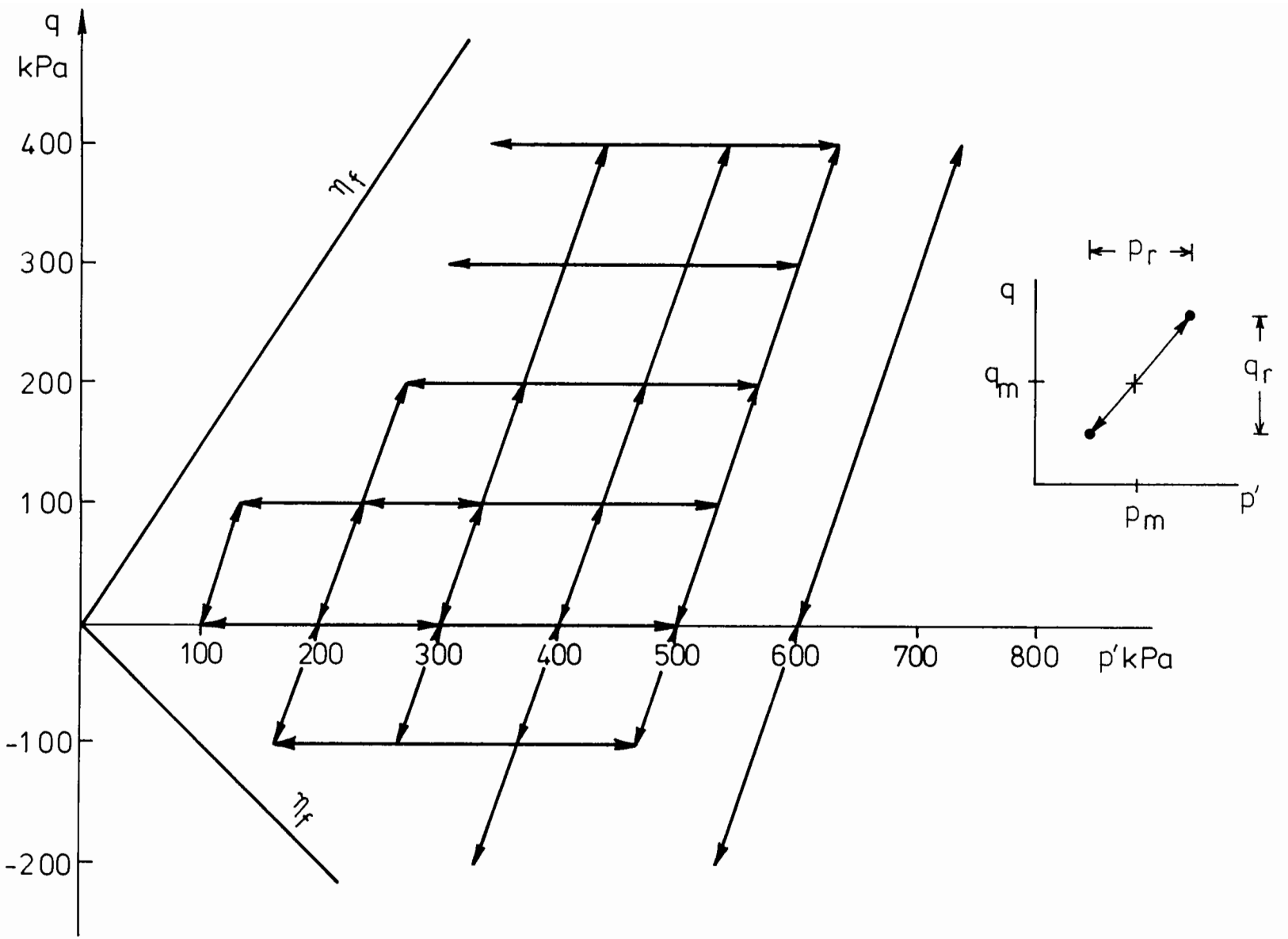

Fig. 6·34 Stress Paths used in Resilient Strain Testing

The factors which follow this main expression modify the strains to allow for effects due to the length of the stress path (i.e. reduction in stiffness when the stress path length is increased). The first, $(\ell_r/p_m)^{0.2}$, accounts for relative stress path length dependency. Pappin (1979) noted that shear strain behaviour was dependent not only upon the change in stress ratio, but also upon the length of the stress path, and he included a similar factor to account for this. When processed, however, the results appeared to be dependent not only upon the relative stress path length, but also upon the absolute change in shear stress. The second factor, $(|q_2 - q_1| + 2/100)^{0.2}$ accounts for this.

The correspondence between the predicted and observed shear strains is shown in Fig. 6.35(b) for the tests carried out on samples D-1 and D-2 and in Fig. 6.35(a) for tests carried out on samples D-3 and D-4.

As can be seen, the model accurately predicts the observed strains.

Resilient Volumetric Strains: The model which has been derived to predict resilient volumetric strains is given by:

$$\epsilon_v = 124 \left[p_2^{0.48} (1 - 0.12(\eta_2)^3) - p_1^{0.48} (1 - 0.12(\eta_1)^3) \right]$$

The core of this model is the expression:

$$\epsilon_v = 124.\Delta (p^{0.48})$$

This is the isotropic stress path-resilient volumetric strain relation. It is obtained by subjecting the sample to repeated isotropic (i.e. no shear stress) loading and matching a curve to the recorded volumetric strains.

The factors $(1 - 0.12\eta^3)$ in the model are introduced to take into account the effect of shear stress on the volumetric strains. Pappin

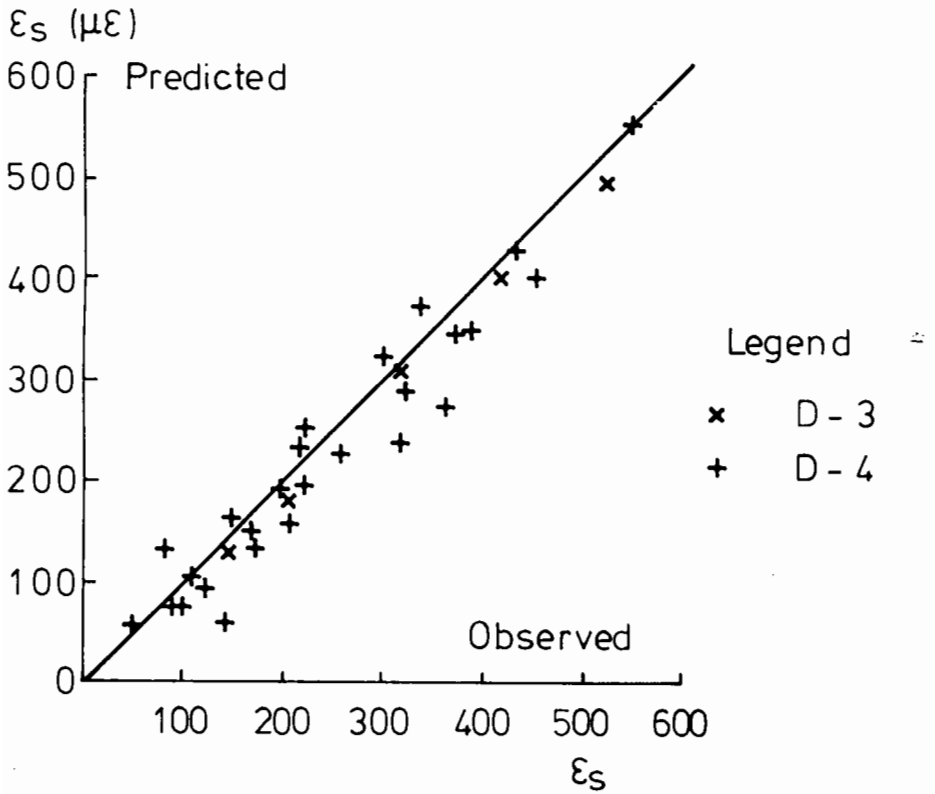

Fig. 6.35 (a)

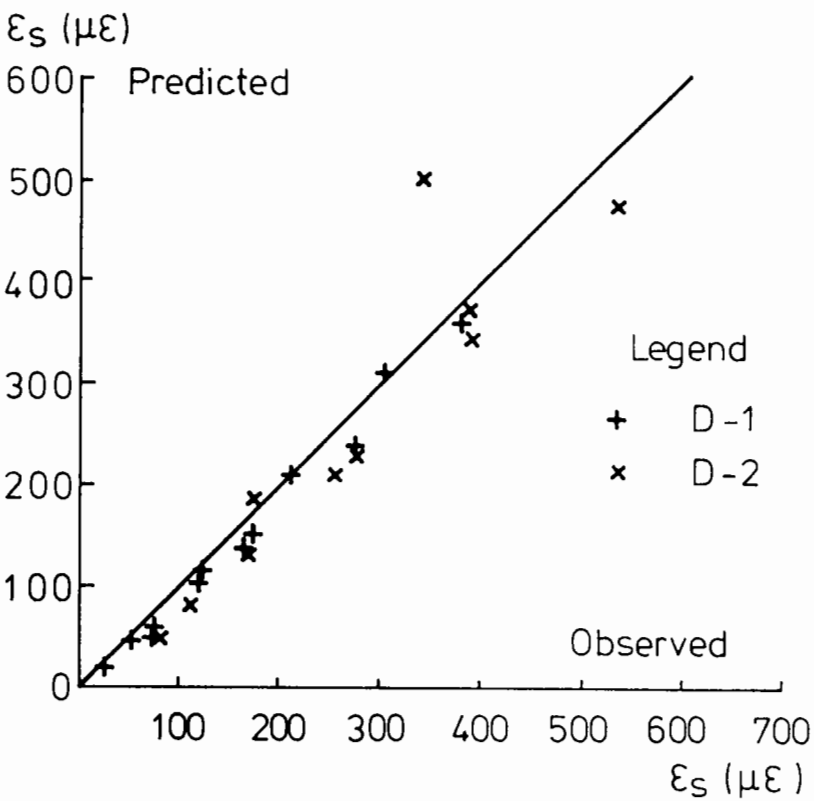

Fig 6.35(b)

Fig. 6.35 Comparison of Predicted and Observed Resilient Shear Strains

(1979) observed that the shear stress affected volumetric strain (e.g. if a sample is loaded at constant p', volumetric strains will still occur). He accounted for this in his model by the introduction of a factor of the above type.

The correspondence between predicted and observed resilient volumetric strains is shown in Fig. 6.36(b) for tests carried out on samples D-1 and D-2, and in Fig. 6.36(a) for tests carried out on samples D-3 and D-4.

As can be seen, the model predicts strains with some success, although the correlation between predicted and observed values is much weaker than that for the shear strain model.

6C.3.3 Resilient Strain Models for Modified Denstone

The results obtained from samples MD-1 and MD-2 have been compared in Figs. 6.37. Fig. 6.37(a)(i) shows the comparison of resilient shear strain and Fig. 6.37(a)(ii) shows the comparison of resilient volumetric strains recorded for the same stress paths.

An interesting feature of these comparisons is that the lines shown on the graphs which correspond to "best-fit" are not lines of equality. They correspond to the following relationships:

$$\epsilon_{s\ (MD-1)} = \epsilon_{s\ (MD-2)} \times 1.2$$

$$\epsilon_{v\ (MD-1)} = \epsilon_{v\ (MD-2)} \times 1.1$$

A partial explanation for this may be found by considering the shape of the plots of deviator stress vs. axial strain. Fig. 6.37(b) shows the outputs from the two axial deformation transducers used to measure strains on sample MD-2. As can be seen, transducer 1 records no change in deformation immediately after a change in the direction of increase in deviator stress. This is probably due to there being some friction between

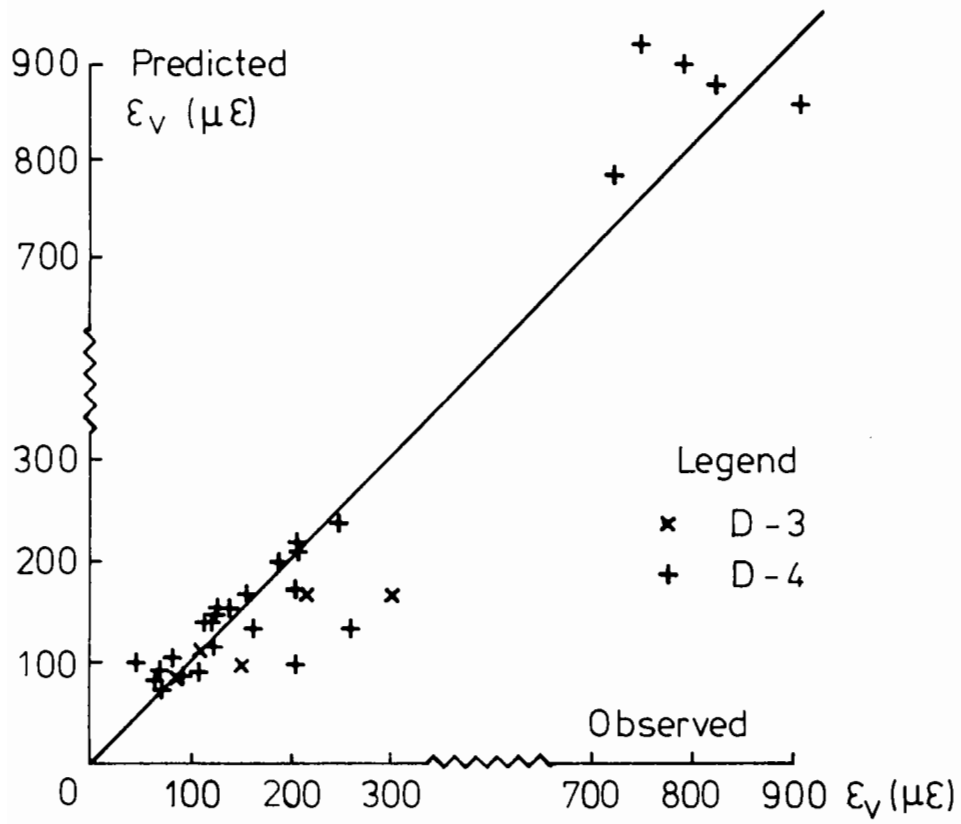

Fig.6.36(a)

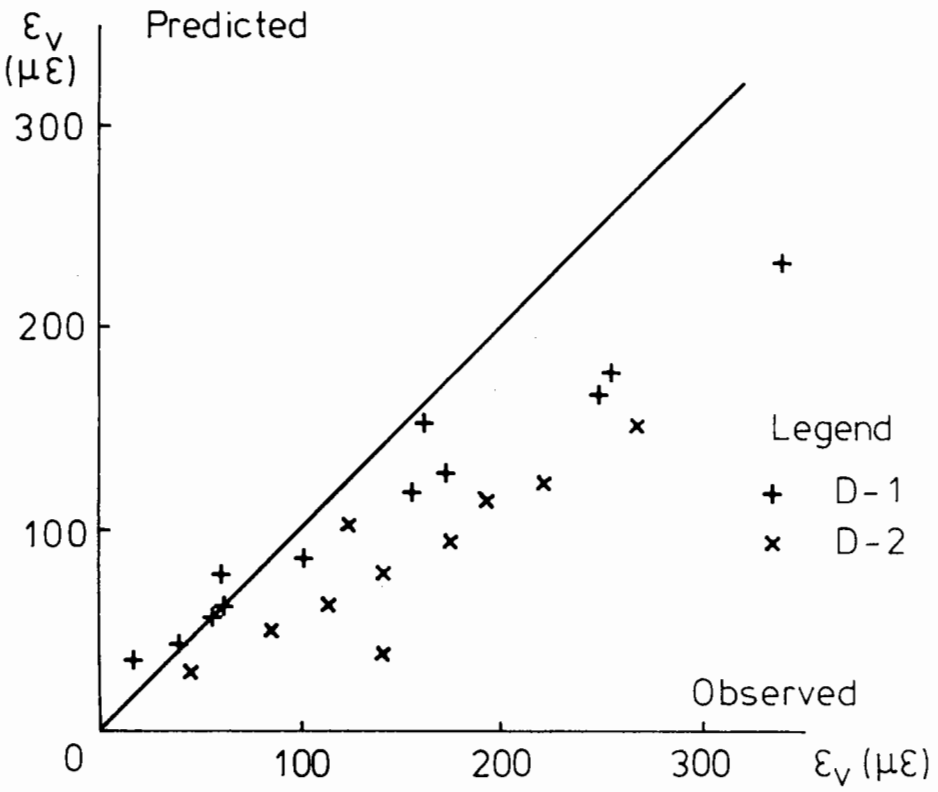

Fig.6.36 (b)

Fig. 6.36 Comparison of Predicted and Observed Resilient Volumetric Strains

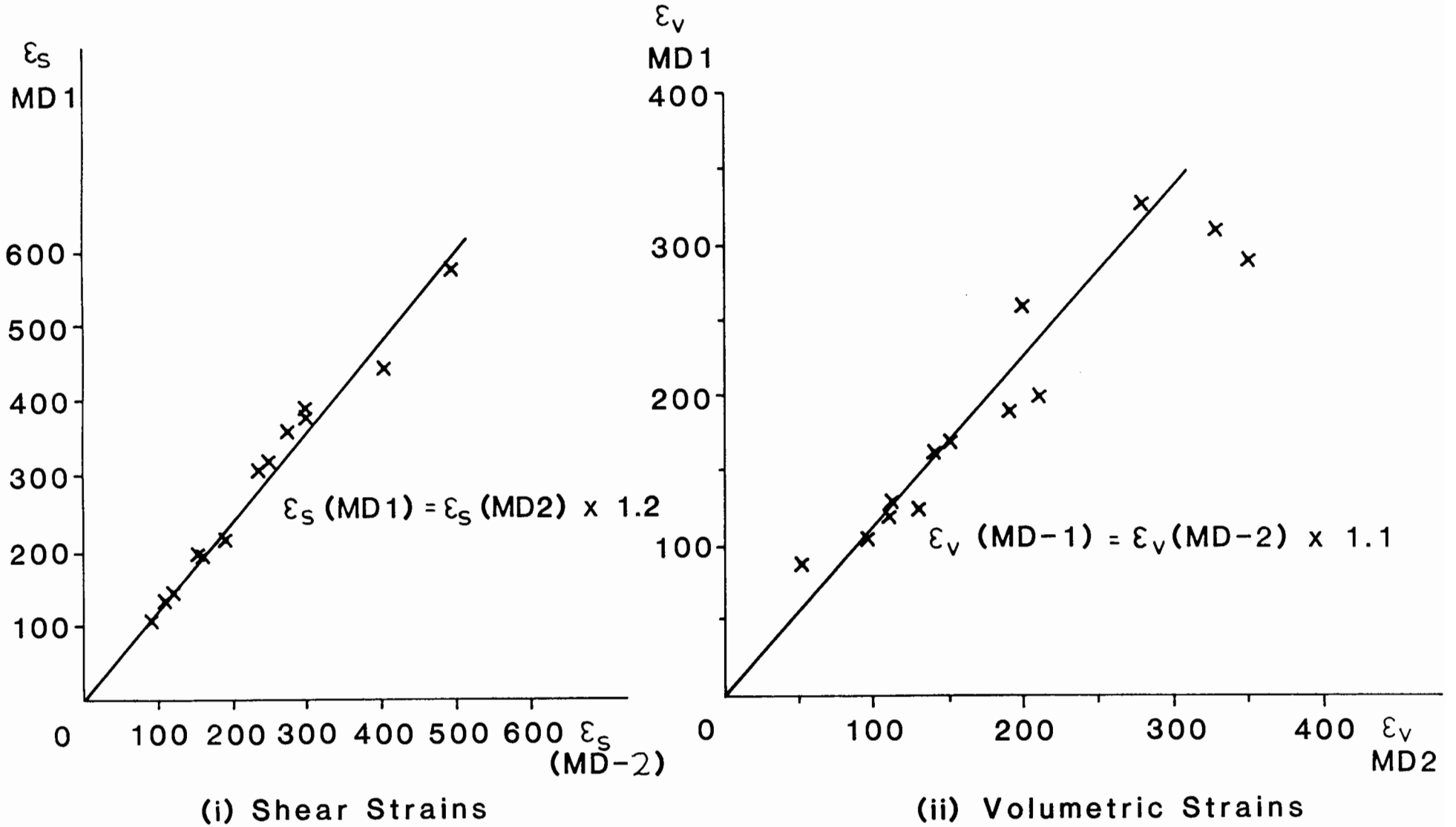

Fig.6.37(a) COMPARISON OF RESILIENT TEST RESULTS FROM TWO MODIFIED DENSTONE SAMPLES

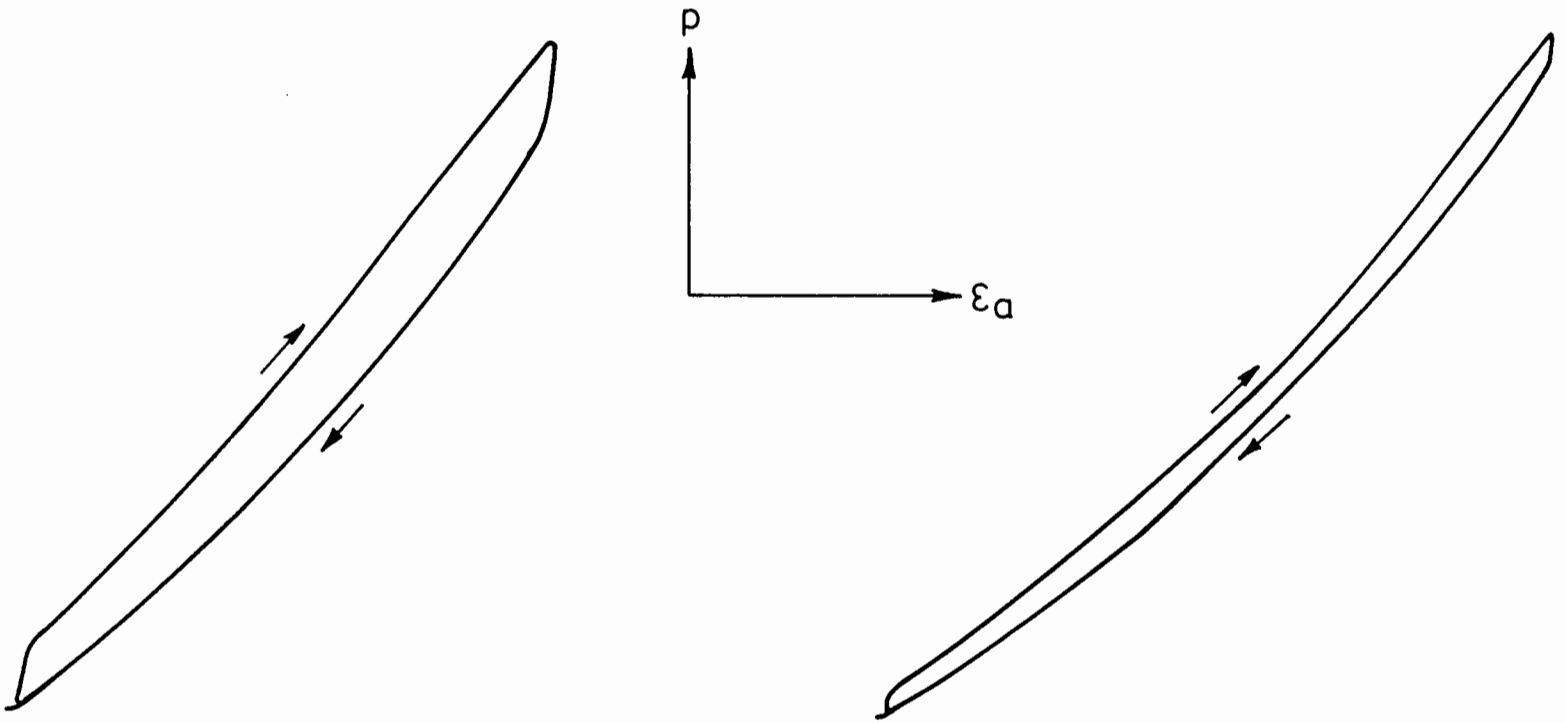

Fig.6.37(b)MEAN NORMAL STRESS vs. AXIAL STRAIN PLOTS FOR THE TWO LVDT TRANSDUCERS USED DURING TESTS ON SAMPLE MD-2

the transducer (LVDT) core and body. The effect of this will be to reduce the shear strains from sample MD-2 by a significant amount; the volumetric strains will be reduced also but not by such a great extent (because volumetric strains are far more dependent upon the radial than on the axial). This is exactly the pattern seen in the disparity between the results from MD-1 and MD-2. A further point worth noting is that the scatter of the volumetric strains is greater than for the shear strains. This is a further demonstration of the greater difficulty inherent in providing good correlation between observed and predicted results for volumetric strains.

Resilient Shear Strain Model: The model which has been derived to predict resilient shear strains occurring as a result of repeated loading along a stress path (p_1, q_1) to (p_2, q_2) is:

$$\epsilon_{sr} = 440\,(\eta_2 - \eta_1) \cdot \left[\frac{\ell r}{pm}\right]^{0.2} \cdot \left[\frac{|q_2 - q_1| + 2}{70}\right]^{0.2}$$

The correlation between predictions of this model and the observed results is shown in Fig. 6.38. A degree of scatter is evident. This is, of course, inevitable, bearing in mind the fact that the shear strains observed in tests on sample MD-1 were approximately 20% higher than those on MD-2. In view of the fact that the lower strains from tests on MD-2 were explained at least partially by transducer friction, slightly more weight was given to MD-1 results. This can be seen in Fig. 6.38 where the results of tests on the two samples are differentiated.

Comparison with Standard Denstone Resilient Shear Strain Model: The model for standard Denstone material is given by:

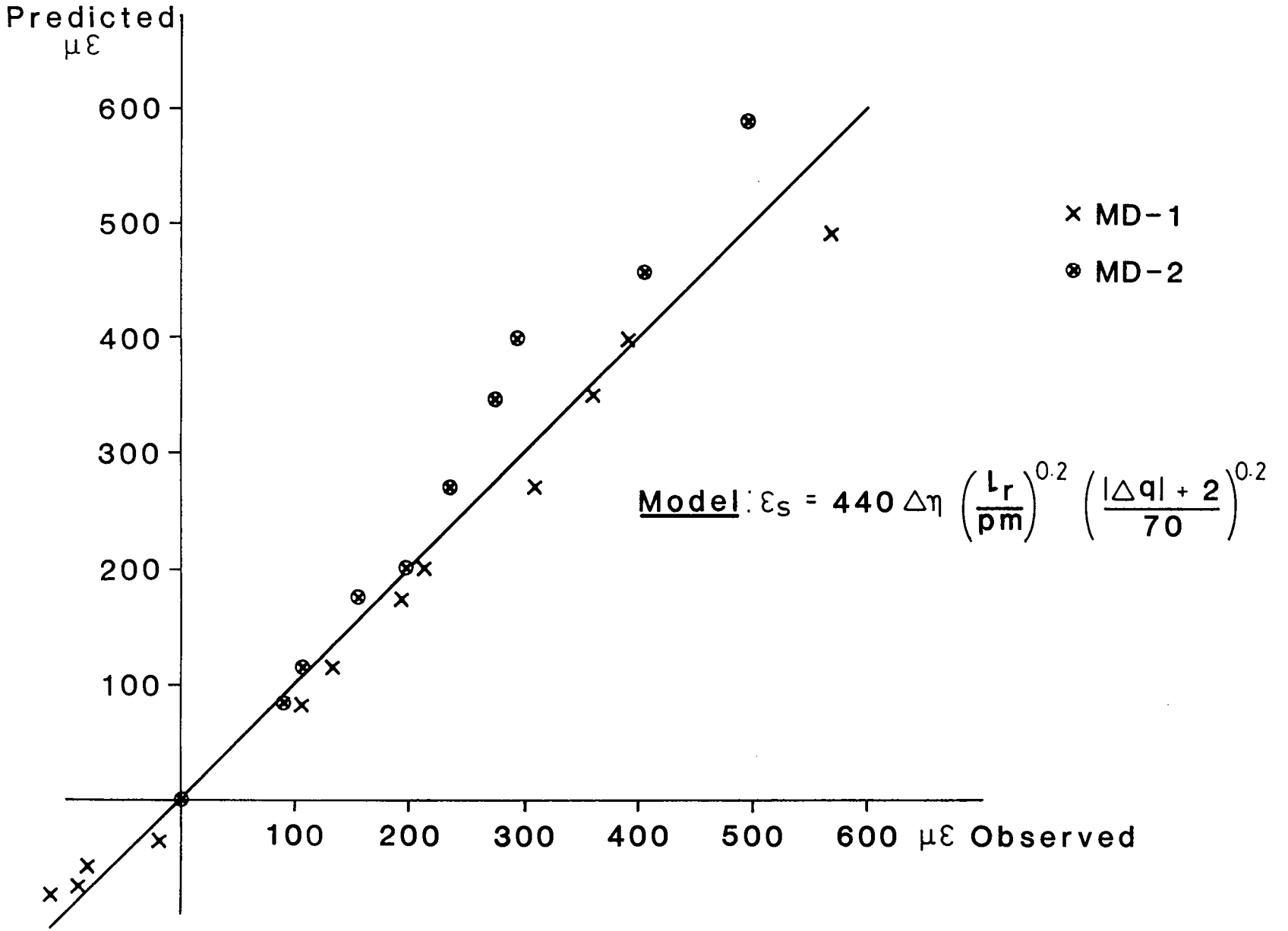

Fig. 6.38 CORRELATION BETWEEN PREDICTED AND OBSERVED RESILIENT SHEAR STRAIN

$$\epsilon_{sr} = 440\,(\eta_2 - \eta_1) \cdot \left[\frac{\ell r}{pm}\right]^{0.2} \cdot \left[\frac{|q_2 - q_1| + 2}{100}\right]^{0.2}$$

The models are almost identical. They differ only in the denominator of their second modifying factor. In fact, this difference has little effect in terms of the predicted strains. The substitution was performed mainly in advertance to the fact that this second modifying factor is partially connected with elastic deformations of the particles themselves. In isotropic compression tests (see below) the modified Denstone material was shown to be less stiff volumetrically than standard Denstone. It was therefore assumed that the shear stiffness of the particles would also be reduced. The alteration of the denominator in the second modifying factor from "100" (standard Denstone) to "70" (modified Denstone) does not have a great deal of effect on the predicted strains. Fig. 6.39 shows a range of stress paths and the strains predicted by both "standard" and "modified" models. For the stress paths shown the ratio of predicted strains from the two models is approximately constant at 1.08. This means that an equally accurate model could have been produced by changing the core expression from 440 $\Delta\eta$ to about 470 $\Delta\eta$. Changing the second modifying factor, however, is thought to show greater consistency in view of the mechanistic aspects of the model.

Resilient Volumetric Strain Model: The model which has been derived to predict resilient volumetric strains is given by:

$$\epsilon_v = 280 \left[p_2^{0.42}(1 - 0.12(\eta_2)^3) - p_1^{0.42}(1 - 0.12(\eta_1)^3) \right]$$

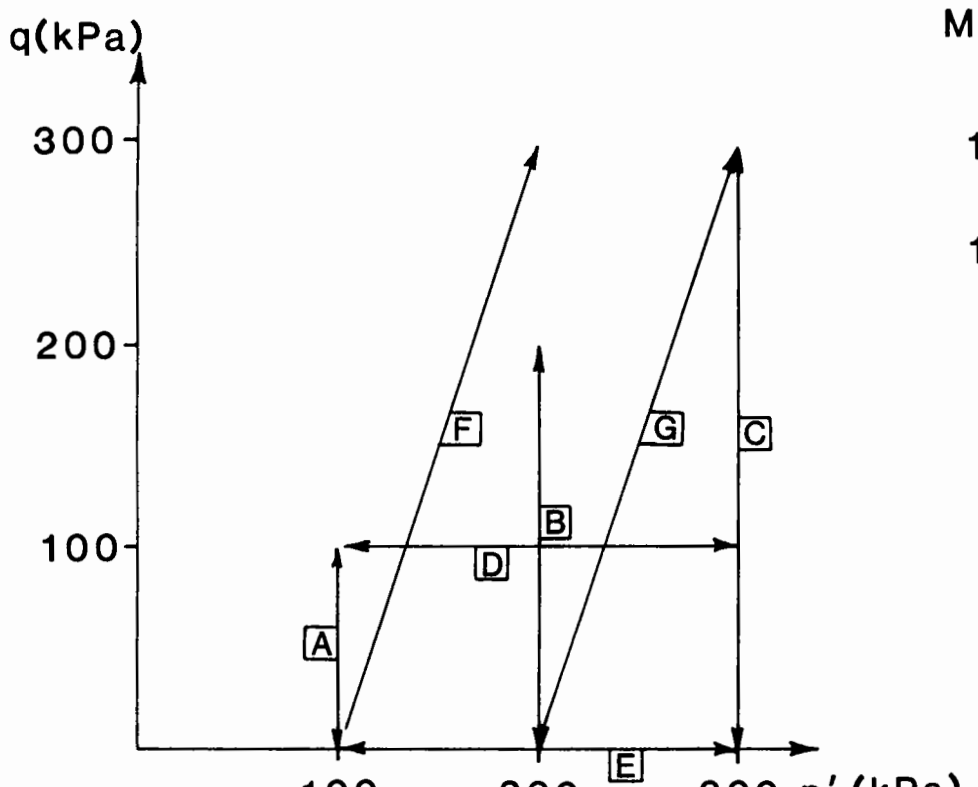

(a) Selection of Stress Paths

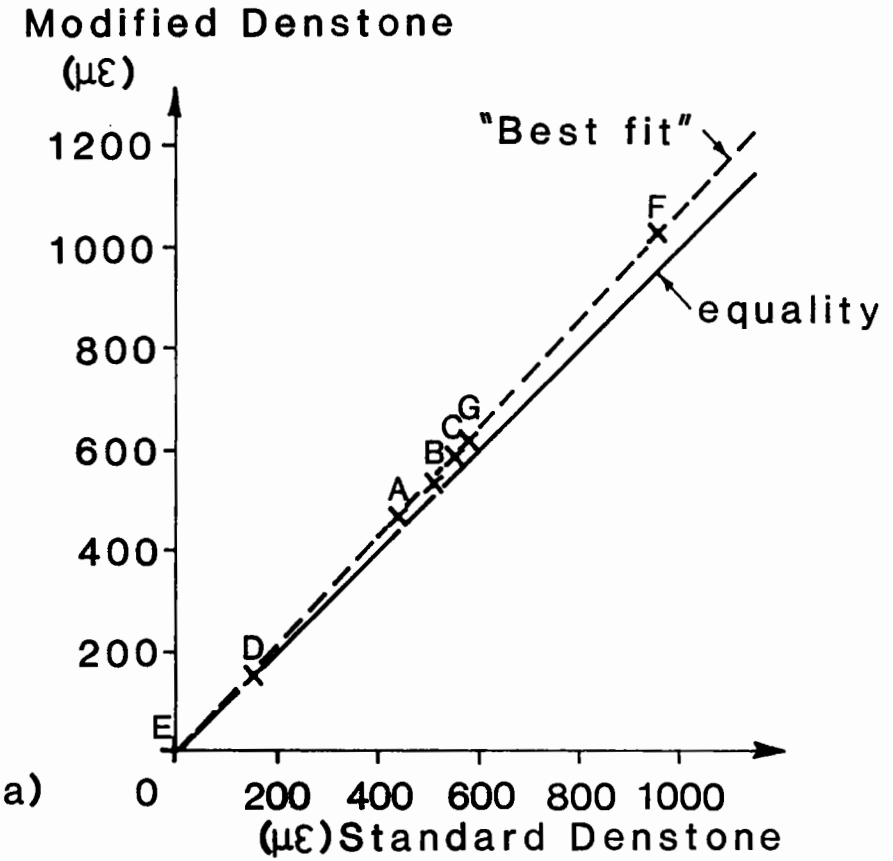

(b) Comparison of Predicted Shear Strain

Fig. 6.39 COMPARISON OF MODIFIED DENSTONE AND STANDARD DENSTONE MODELS

The correspondence between predictions and observations is shown in Fig. 6.40. As can be seen, the model predicts the strains with some success, but as with the model produced for standard Denstone, the correlation was much weaker than for the predictions of shear strains.

Comparison with Standard Denstone model: The resilient volumetric strain model for standard Denstone is given by:

$$\epsilon_{vr} = 124 \cdot \left[p_2^{0.48}(1 - 0.12(\eta_2)^3) - p_1^{0.48}(1 - 0.12(\eta_1)^3) \right]$$

The core expression of this model is 124 Δ ($p^{0.48}$). This differs substantially from the modified Denstone model. The difference can be illustrated by the fact that the volumetric strains predicted by an increase in isotropic stress at zero shear stress from 100 kPa to 500 kPa are 1318 $\mu\epsilon$ and 1871 $\mu\epsilon$ in the case of standard Denstone and modified Denstone respectively, a ratio of 0.7.

It will be noted that the factor ($1 - 0.12\eta^3$), used in the "modified" model, is the same as for the standard model. It is used to take into account the dilation due to shearing. Since the two materials had such similar shape and shear strain characteristics the modifying factor for both materials must be fairly similar.

6C.3.4 The Effect of the Intermediate Stress on Resilient Strains

The models presented above take no account of the value of the intermediate stress. Tests in extension as well as compression space were carried out and models were derived which provided good compromise predictions for both. Pappin (1979) sought to extend the triaxial (i.e. true triaxial) yield criterion to sub-failure conditions by using the

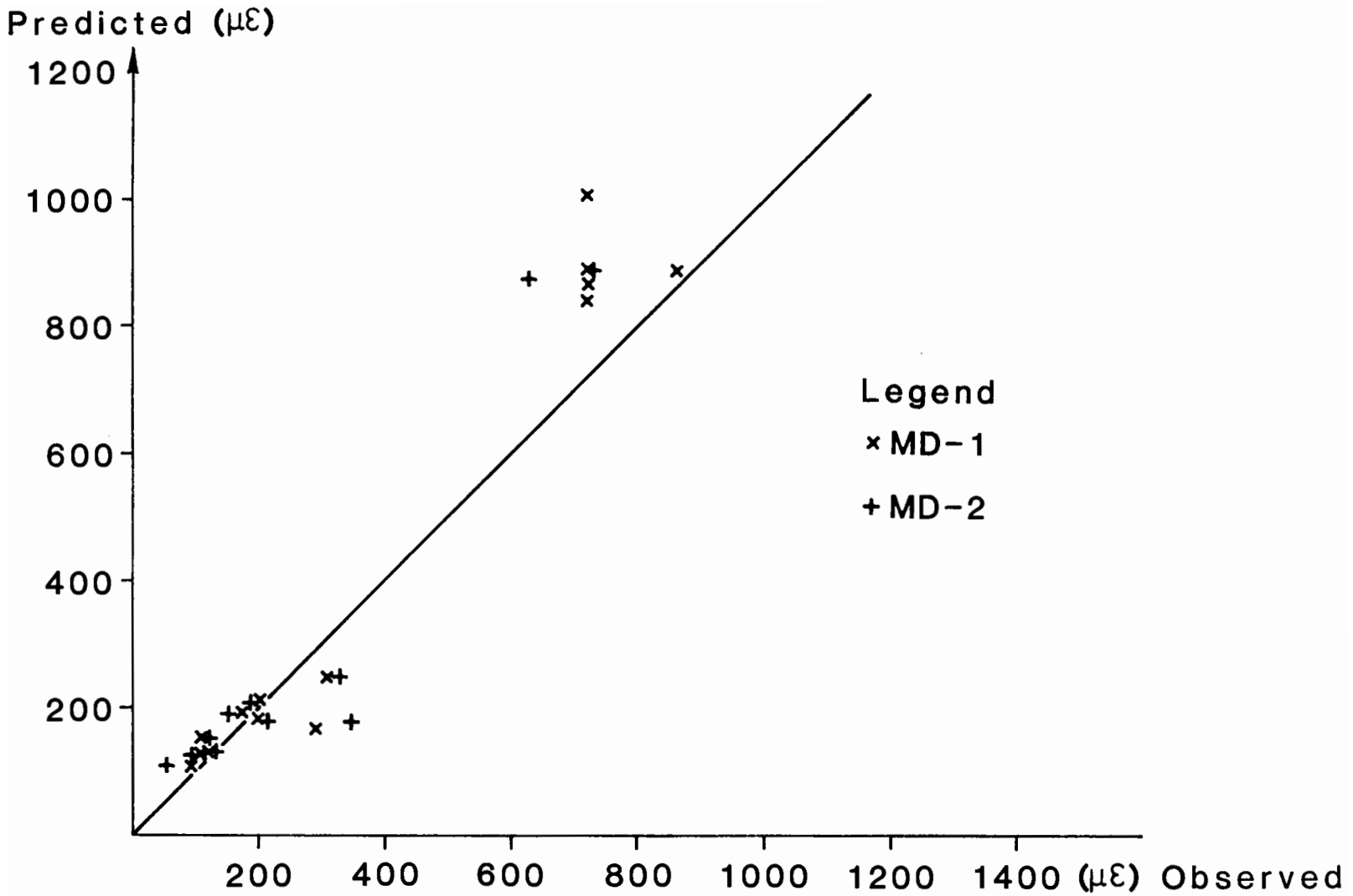

Fig. 6.40 COMPARISON OF PREDICTED AND OBSERVED RESILIENT VOLUMETRIC STRAINS

concept of an equivalent compression stress state in order to provide a resilient model which could cope with variations in the value of b (= $(\sigma_2 - \sigma_3)/(\sigma_1 - \sigma_3)$. He used the Mohr-Coulomb failure criterion as his yield model and showed that this approach provided more accurate predictions for both compression and extension testing of graded crushed rock. Shaw (1980) showed that a similar approach provided good predictions for a single-size crushed rock.

Unfortunately, not enough resilient data in the extension space was collected to prove this hypothesis for the Denstone materials. What data there is, however, indicates that resilient shear and volumetric strains observed during extension space testing were greater than those observed for an equivalent (i.e. mirrored in the p axis) path in compression space, and this is consistent with the hypothesis.

It is suggested that a more appropriate correction would be the Lade-Duncan (1975) yield criterion (see Chapter 4) rather than the Mohr-Coulomb version. It appears to agree much more closely with actual results from yield tests in true triaxial apparatuses.

Fig. 6.41(a) shows the form the modified resilient shear strain contour model might take: a constant p' slice through (η, p', b) space is shown. Fig. 6.41(b) shows a set of results for a single size crushed rock from Shaw (1980) together with Shaw's model for compression tests and also with the modification to Shaw's model i.e. the extended Lade-Duncan yield criterion.

As can be seen, good prediction is achieved. A similar correction may be applied to the volumetric model.

It may be worthwhile incorporating the intermediate stress parameter b into the stress ratio paramete η, so that Fig. 6.41(a) becomes Fig. 6.41(c). This would enable b to be eliminated as an independent parameter.

It is not certain at this stage whether the latter modification is

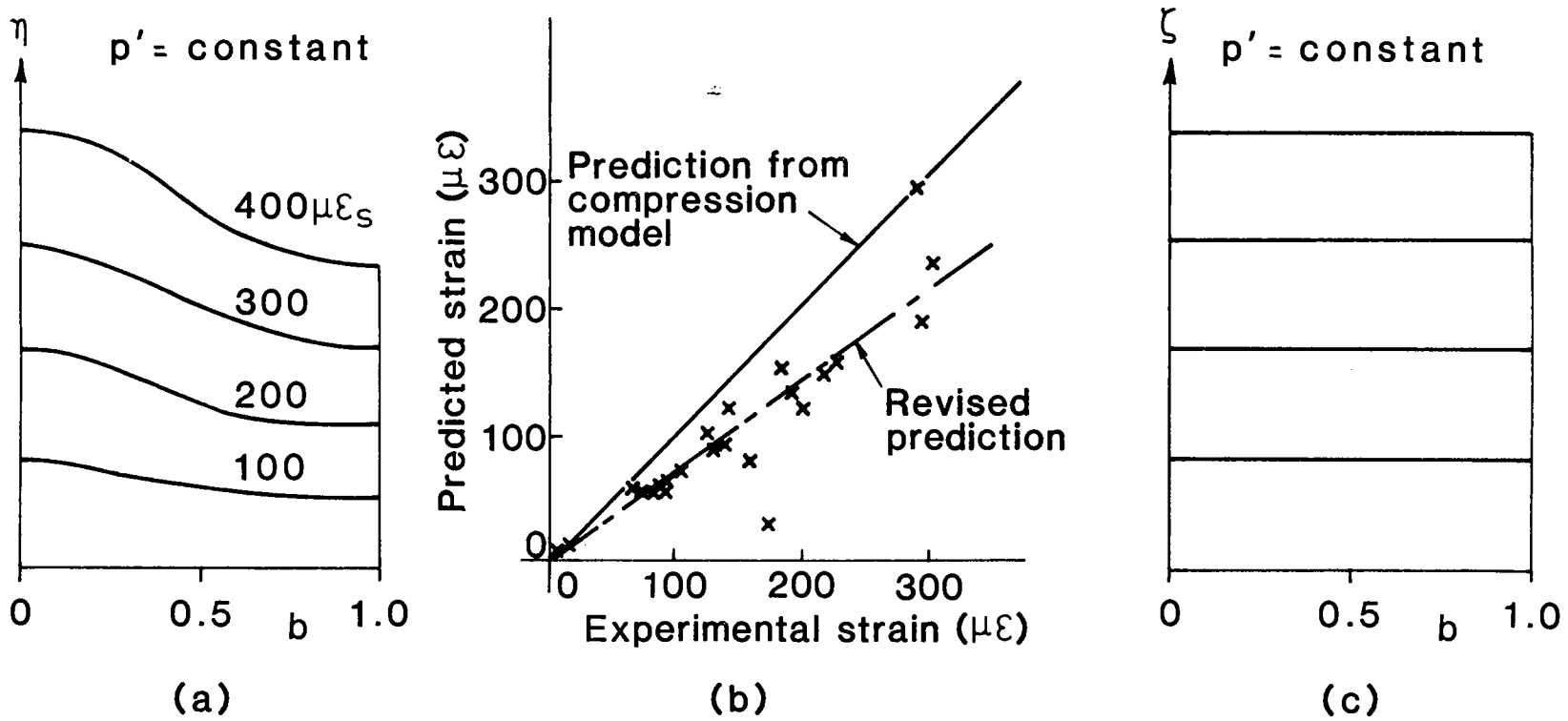

Fig. 6.41 MODELLING RESILIENT STRAINS WHEN $0 < b < 1$

appropriate when the value of b changes continuously; Chapter 8.10 contains a fuller discussion of this point.

6C.4 HYSTERESIS DURING RESILIENT TESTING

When a granular material is loaded and unloaded it exhibits hysteresial stress-strain behaviour (i.e. loaded along path p_σ in stress space it will follow path p_ϵ in strain space. If, however, it is now unloaded along path p_σ, the path followed in strain space will not be p_ϵ). Fig. 6.42 shows the stress-strain resilient behaviour during a variety of resilient strain tests, and the hysteresial behaviour is evident.

The existence of hysteresis shows that energy is dissipated during each cycle. Energy is probably lost through friction as sliding takes place at particle contacts.

Zytynski et al (1978) gave a simple sliding block conceptual model (Fig. 6.43(a)) which accounts for observed effects such as non-linearity and hysteresis. Pappin (1979) produced a theoretical model consisting of an array of contacting spheres and incorporating a block sliding system as proposed by Zytynski et al. The results which he produced compare favourably with the actual behaviour in the repeated load triaxial apparatus. Several of the theoretical model results are shown in Fig. 6.43(b) together with experimental results from the tests which the model was attempting to simulate. Below these is shown the magnitude of the strains predicted by the resilient empirical model.

Pappin (1979) originally considered that the stress path length dependency was due solely to hysteresis effects. He later stated that although it was a factor, hysteresis could not fully explain stress path length dependence. In particular, he could not show why volumetric strains (which also exhibited hysteresial behaviour) were not stress path length

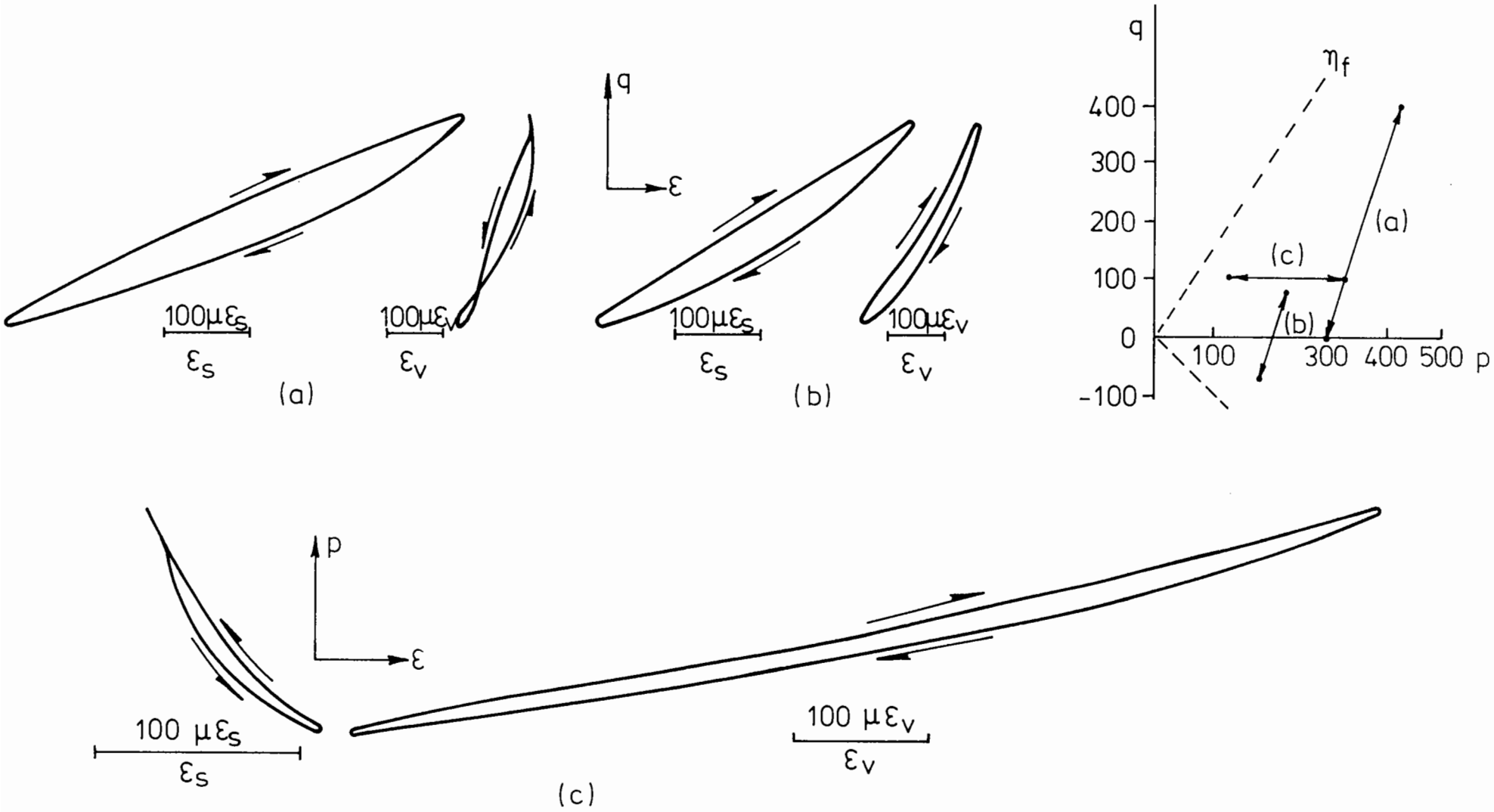

Fig. 6.42 Hysteresis Behaviour of Denstone for a Range of Tests (Sample D-4)

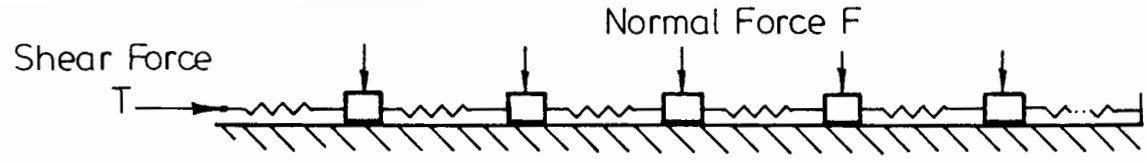

Fig. 6.43(a) Shear Behaviour Model (Zytynski et al, 1978)

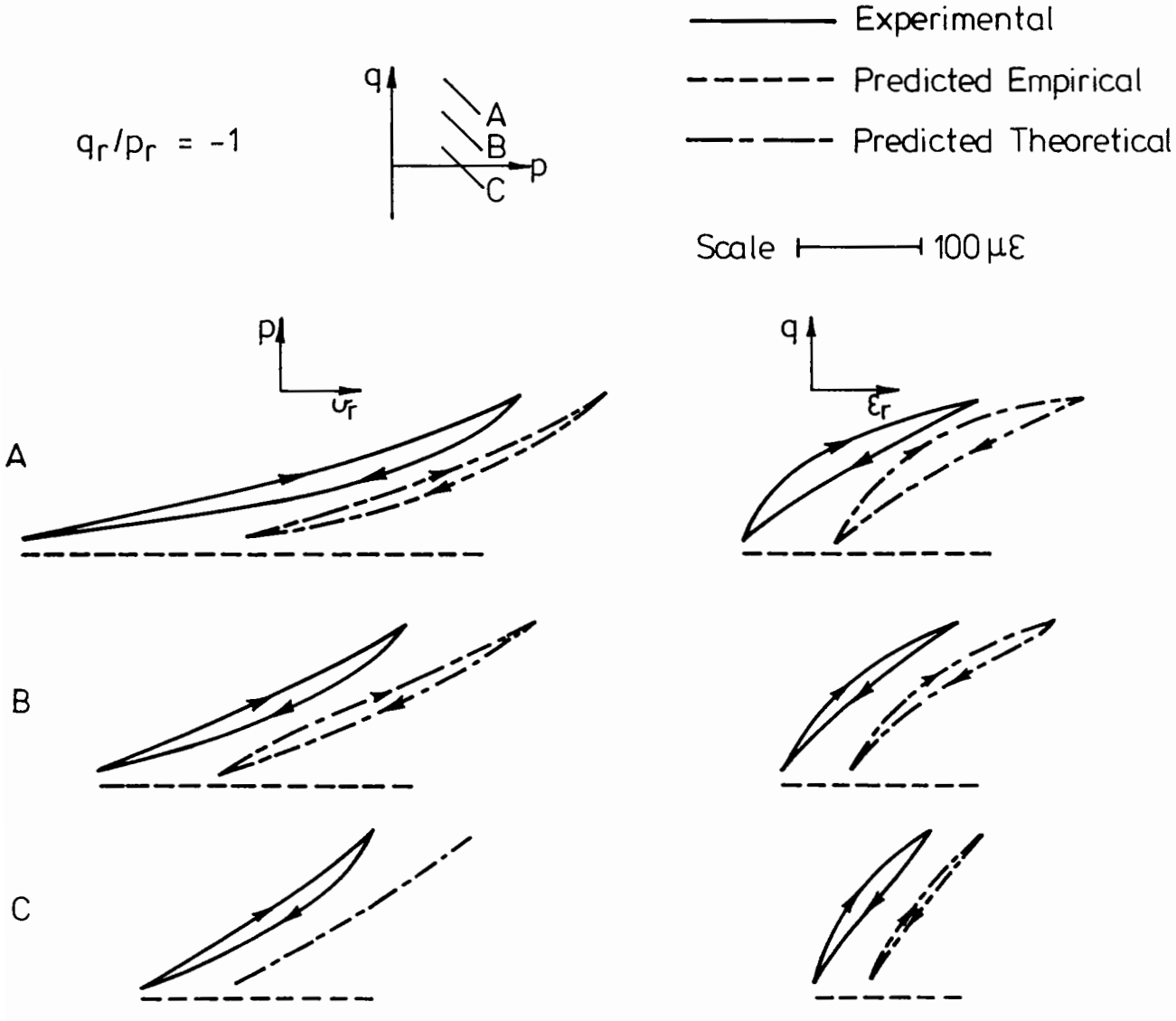

Fig. 6.43 (b) Comparison of Theoretical Granular Material Model with Experimental Results (Pappin 1979)

dependent.

The probable explanation is that volumetric strains are stress path length dependent. Research presently being conducted at Nottingham (Thom 1985) tends to indicate that this is so. Some developments of resilient strain models will be discussed later in this chapter (6C.8). These models presuppose that resilient volumetric strain is dependent, amongst other things, upon resilient shear strain. If this supposition is correct then resilient volumetric strain must be stress path length dependent.

It is likely that stress path length dependency will only occur when energy is lost during a cycle. In a granular material, most energy is probably lost in the form of irrecoverable heat as particles slide over each other. This phenomenon is not confined to granular materials however; in structural dynamics design, the phenomenon of hysteresis is often taken into account mainly because it causes damping within the structure. The fact that energy is lost means that in addition to the damping effect, the stiffness of even linear materials will become stress path length dependent under conditions of dynamic oscillation.

This seems to indicate that Pappin was correct in his initial hypothesis that stress path length dependency was due solely to hysteresis.

6C.5 DILATION DURING RESILIENT BEHAVIOUR

During the large triaxial apparatus tests discussed in Section 6A.4, the point at which the volumetric behaviour changed from compressive to dilatant was discussed. The average stress ratio at the onset of dilatancy for Denstone during monotonic loading from isotropic stress conditions was estimated from the graphed data to be $\eta_D = 1.04$. When samples B6-100-1 and B10-100-1 were loaded repeatedly, it was noted that with an increased number of cycles, the duration of the compression phase diminished. By the

fifth cycle very little compression appeared to take place before the material began to dilate (see Figs 6.21 and 6.22).

A series of tests was performed to determine the value of η_D during resilient loading. The more sophistocated instrumentation in the repeated load triaxial apparatus enabled a more detailed investigation of this aspect of behaviour than the large triaxial apparatus. The experiments involved testing a sample at constant magnitudes of repeated shear stress. The cell pressure was varied so that different stress conditions were applied during each test as shown in Fig. 6.44. Examples of the resulting $q - \epsilon_v$ plots from tests on D-4 are shown in Fig. 6.45 and from tests on MD-1 in Fig. 6.46. As can be seen, the volumetric strain behaviour changes from compressive to dilatant during loading. Fig. 6.47 shows the stress states within the sample when this change occurs plotted in q,p' space. It is clear that the points from each set of tests lie on a smooth curve. The Modified Denstone reaches η_D at higher stress ratios than the Standard Denstone. Also shown in Fig. 6.47 is the line $\eta = 1.04$ which has an estimated average value of η_D during monotonic loading. This indicates that during repeated load testing the value of η_D may reduce during successive cycles.

Wood (1982) reviews a large amount of experimental work on the repeated loading of soils. He discusses the work of Habib and Luong (1978) and Luong (1979), who introduce the concept of "characteristic state". This is the stress state in the material at which behaviour changes from compressive to dilatant - i.e. η_D used above. Wood indicates that the "characteristic state" may have similarities with the "critical state" of the Critical State Theory. Indeed, from Habib and Luong's work it appears that the characteristic state is independent of the initial void ratio, and both conditions, since they involve zero volumetric strain, imply that at neither characteristic nor critical state is any component of strength

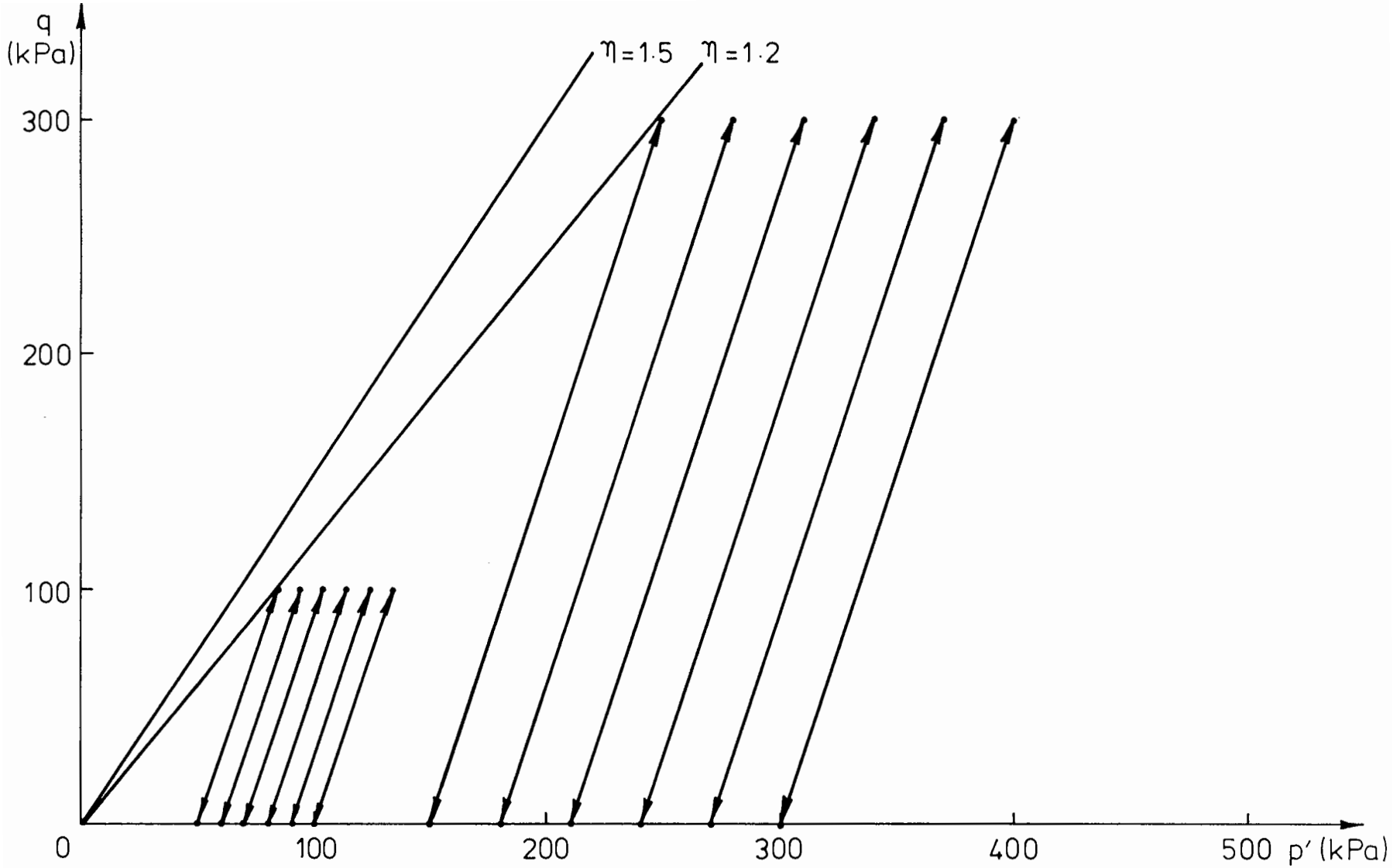

Fig. 6·44 Stress Paths Used to Determine Change from Compressive to Dilatant Behaviour

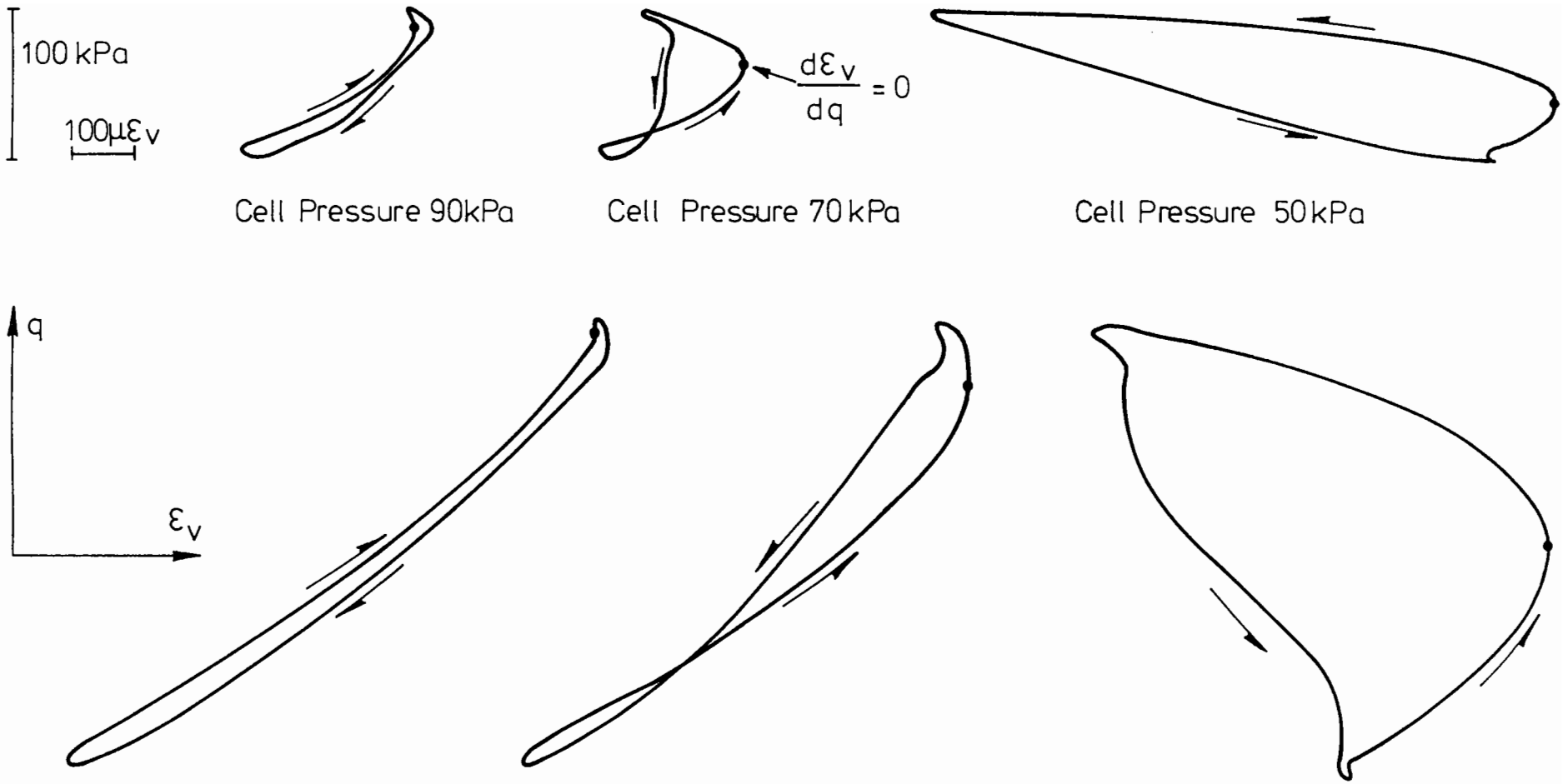

Fig. 6.45 Examples of Volumetric Strain Behaviour During Six Stress Paths Shown in Fig. 6.44

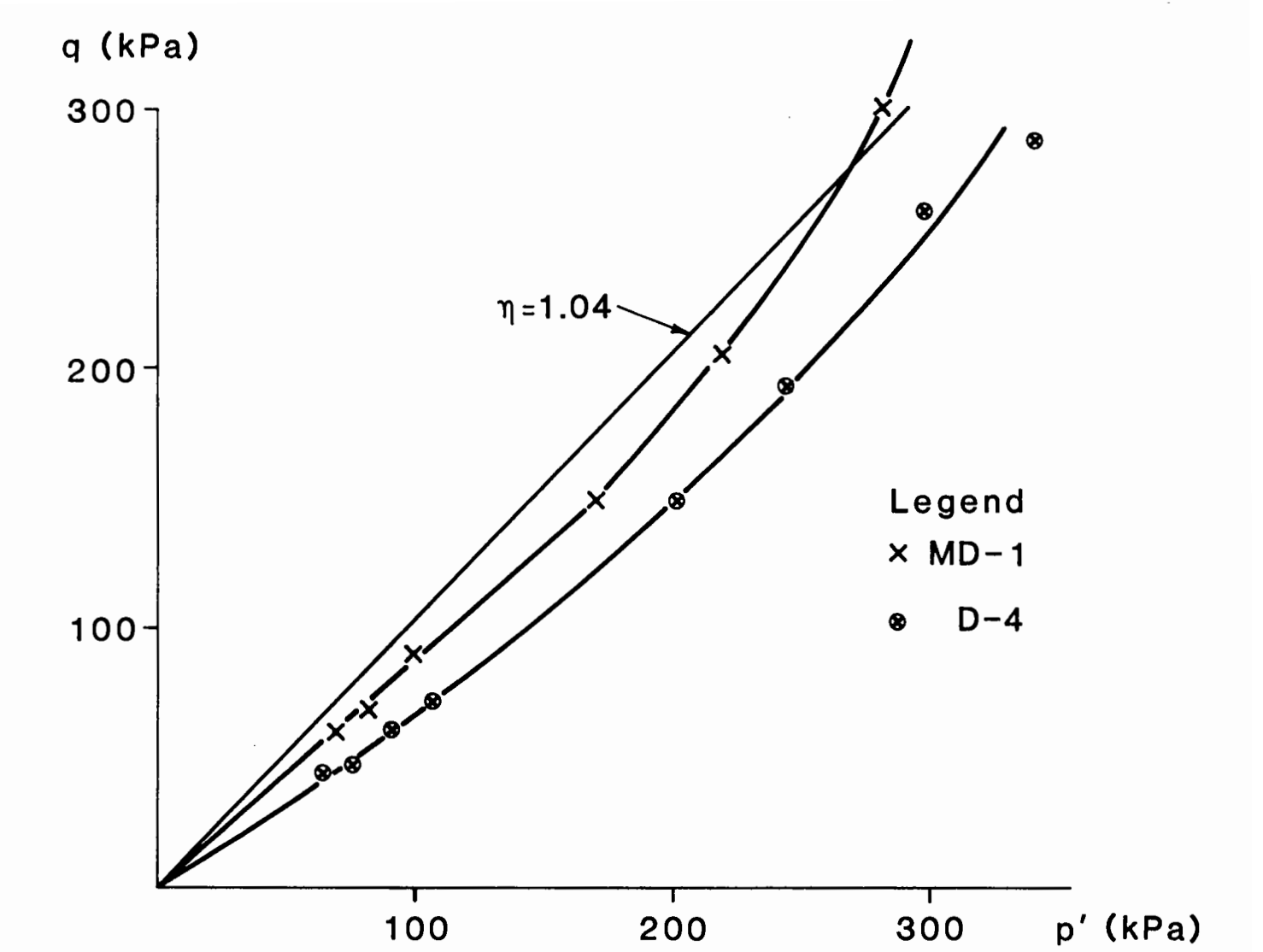

Fig. 6.47 VALUES OF η_D RECORDED DURING RESILIENT TESTING

derived from the energy involved in volumetric strain. In fact, Habib and Luong expressly make the point that determination of the characteristic state is far easier than determining the critical state.

It is not clear how a variable value of η_D (as suggested not only by the discrepancy between values recorded for Denstone during monotonic and resilient loading but also by the changes in η_D with change in mean normal stress during the resilient dilatancy tests and by the fact that η_D will depend upon the initial stress ratio value) ties in with the concept of "characteristic state" (the name surely implies that it is a constant).

6C.6 CLOSED LOOP TESTS

Resilient strain models are mainly used in computer based analyses to determine the mechanical response of pavement and railway-track structures to applied wheel loading. Several assumptions are made, including:

(a) That behaviour is elastic (within that designated portion of stress space for which the model is said to be valid), and

(b) That if the material is subjected to a closed loop stress path (eg. in order to simulate a hysteresis loop) the net strains at the end of the path will be zero.

If, however, the strains arising from a closed loop test path are considered (e.g. path ABCDA in Fig. 6.51) using resilient models of the type derived above (6C.3), then both permanent shear and volumetric strains are predicted, and this clearly violates these assumptions.

Closed loop tests were performed on samples D-4 and MD-1 to test the way in which the material actually responds to such stress paths. Four closed loops (as shown in Fig. 6.48), were used. These stress paths were followed in both the clockwise and anti-clockwise directions in stress space. The stress-strain plots, which were recorded from tests on D-4, are

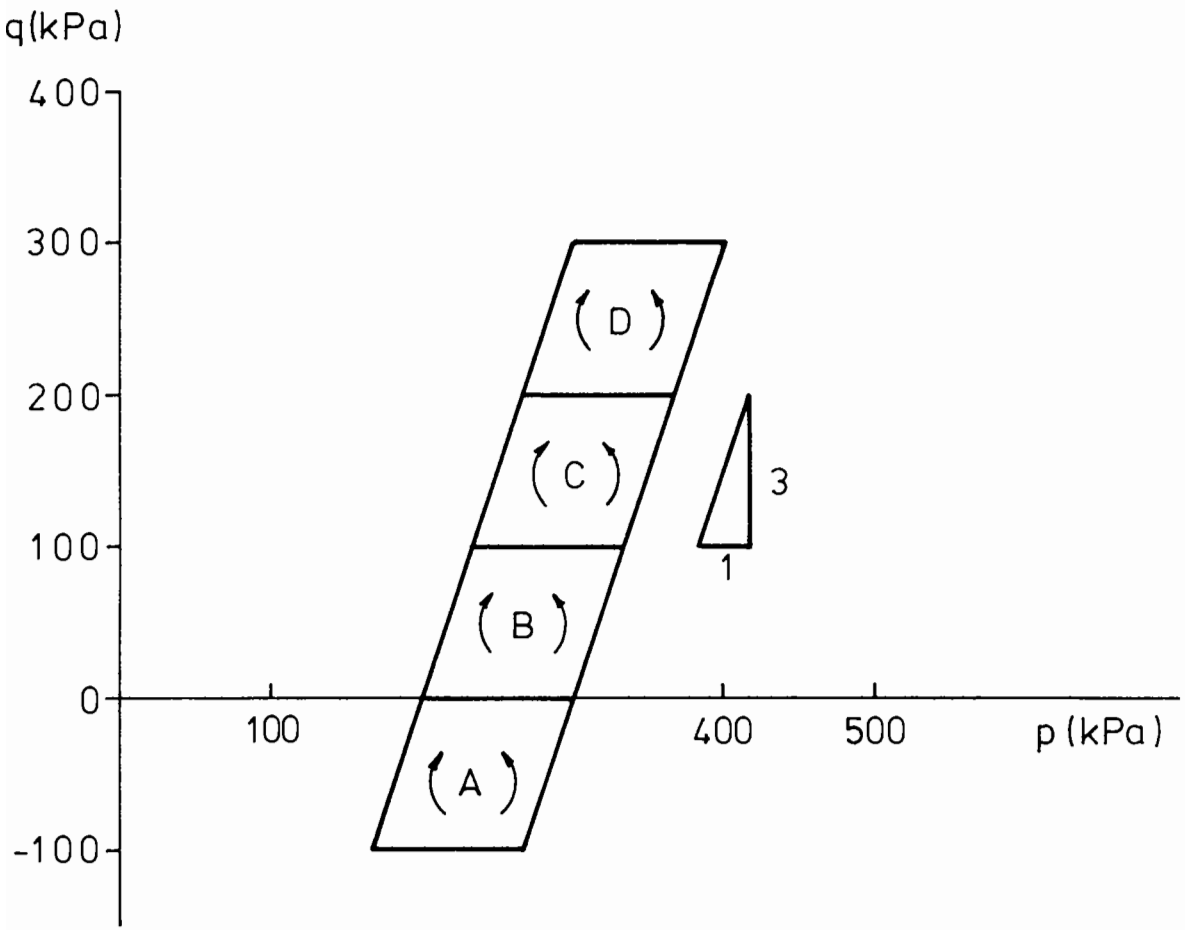

Fig. 6·48 Closed Loop Stress Paths

shown in Fig. 6.49(a)-(d) and a sample plot from tests on MD-1 is shown in Fig. 6.50. The following salient features may be noted:

(a) The material appears to reach a resilient equilibrium behaviour. After several cycles, no permanent strain was recorded at the end of a complete loop.

(b) Volumetric strain behaviour is largely independent of the direction traced around the stress loop. This fact is consistent with the finding that resilient volumetric strains are not very stress path length dependent.

(c) Shear strain behaviour is very dependent on the direction followed around the stress loop. All the plots of behaviour resulting from a clockwise path in compression space, or an anti-clockwise path in extension space have a similar characteristic shape. The plots resulting from paths traced in the opposite direction have a different characteristic shape. This stress path dependence is consistent with the finding that resilient shear strains are stress path length dependent.

It is possible to explain the characteristic shapes of the shear stress paths in the following way. Consider path BC in Fig. 6.51, for example. If the material is loaded in a clockwise direction from A, the value of η will increase until point B. As BC is then followed, the value of η will decrease. Thus point B corresponds to a change in the sign of increase in η and hence in the sign of resulting shear strains. Paths AB and BC are, therefore, separated by a fundamental divide.

If the material is loaded in an anti-clockwise direction from A, a change in the sign of increase in η occurs at point D, and the value of η increases along path DC. At point C no change in sign of increase in η takes place and the value of η continues to rise along CB.

Thus, whether the path is traced clockwise or anti-clockwise is of

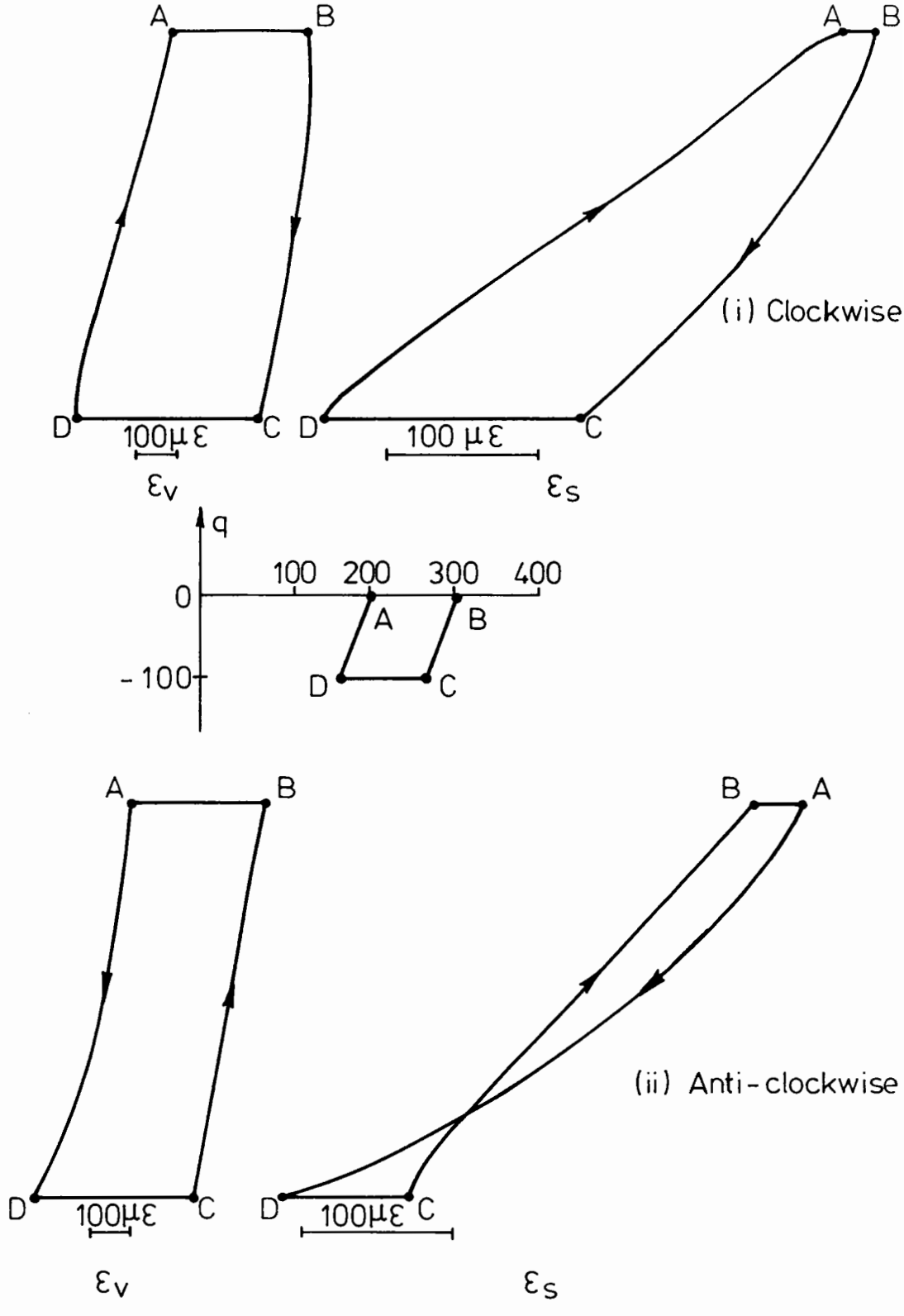

Fig. 6.49 (a) Closed Path Testing Around Loop A

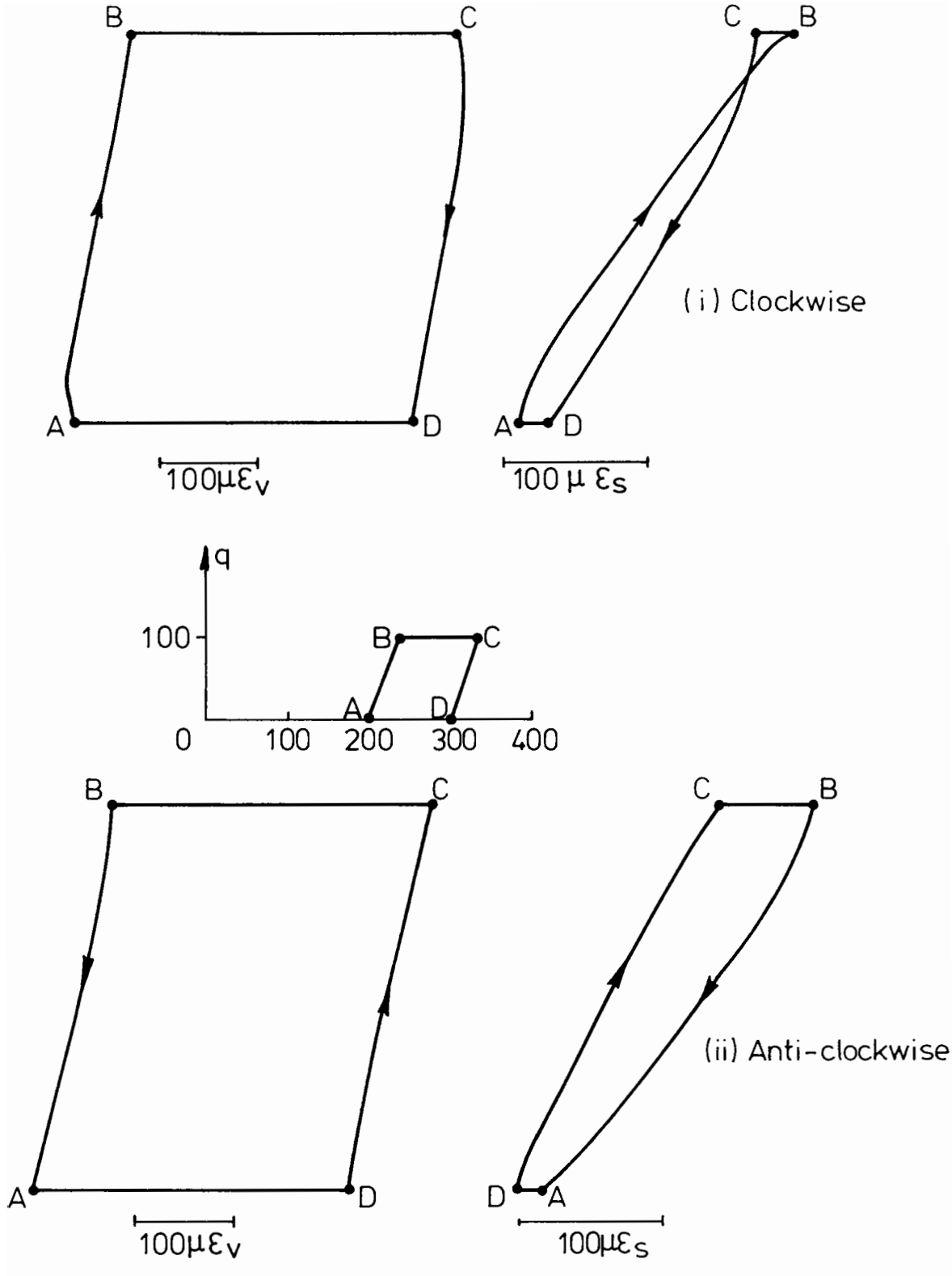

Fig. 6·49(b) Closed Path Testing Around Loop B

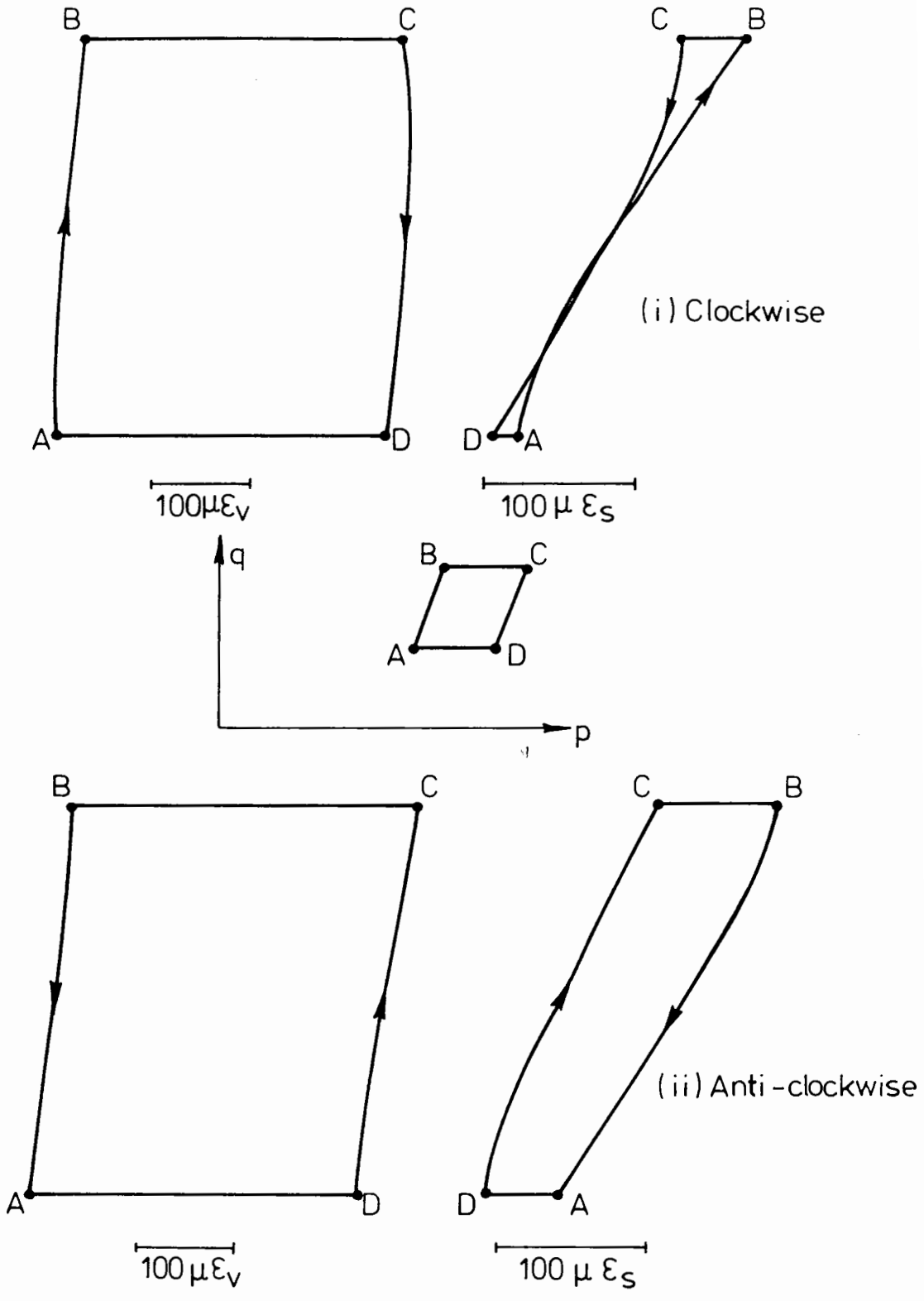

Fig. 6.49(c) Closed Path Testing Around Loop C

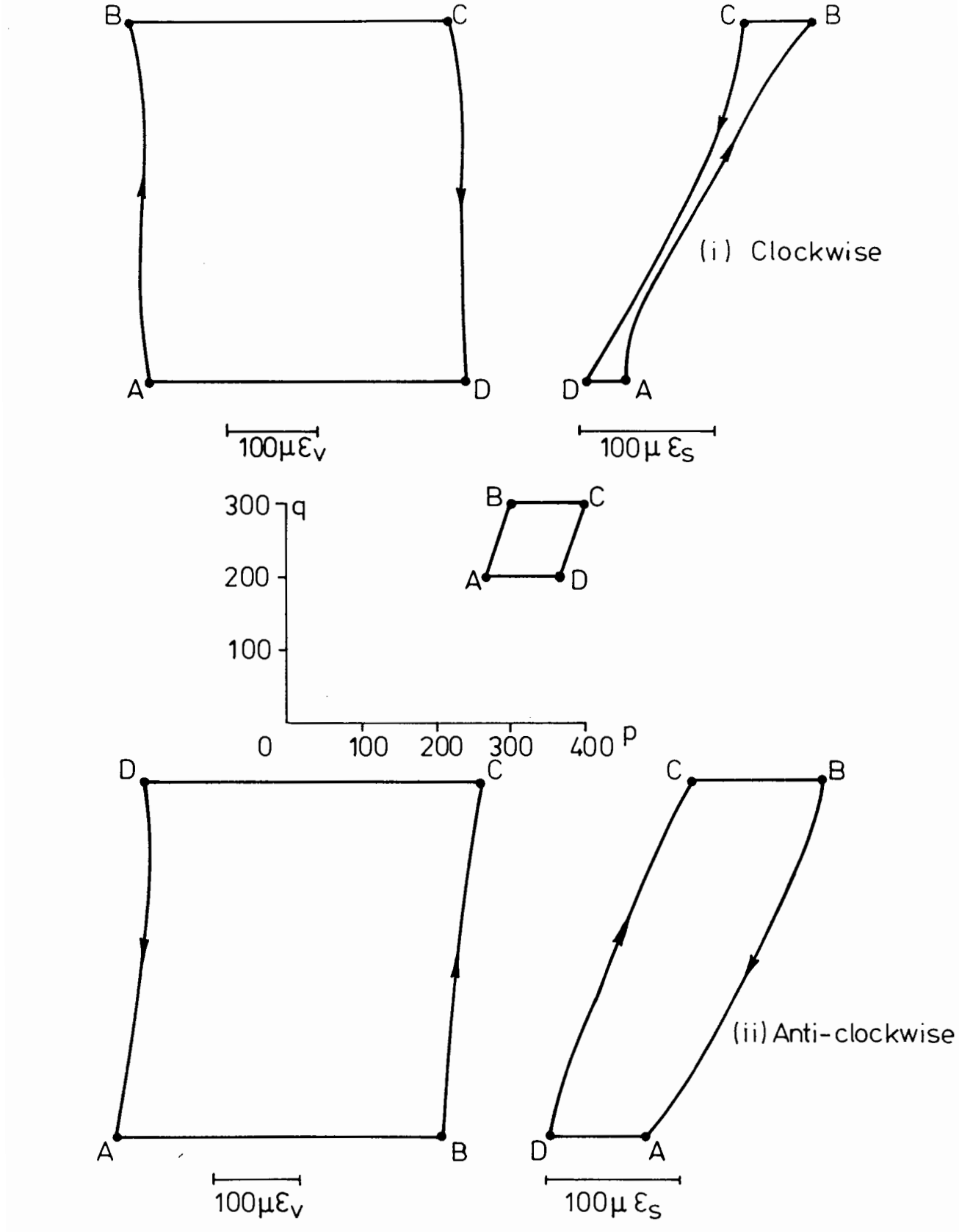

Fig. 6·49 (d) Closed Path Testing Around Loop D

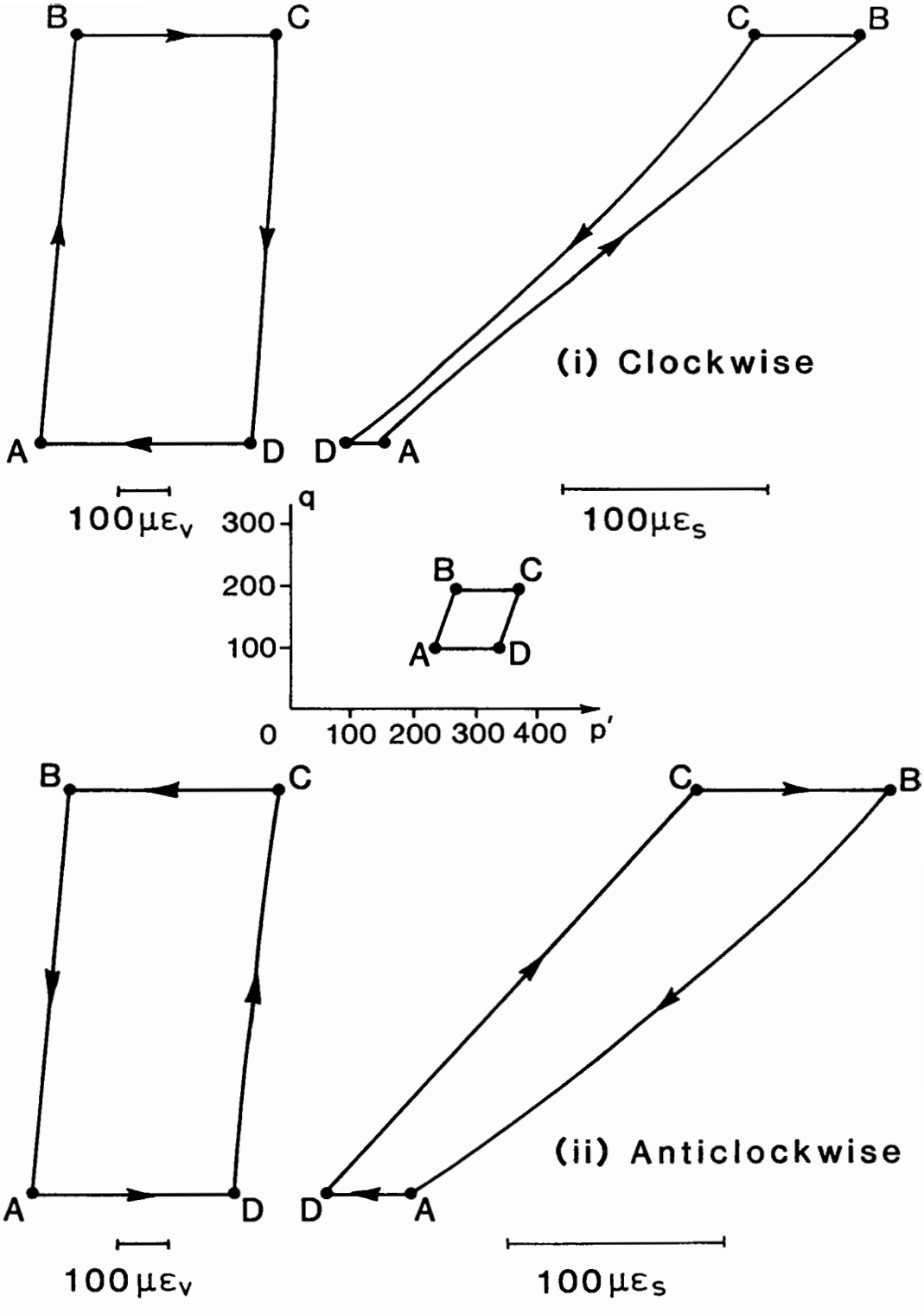

Fig. 6.50 CLOSED PATH TESTING AROUND LOOP C - SAMPLE MD-1

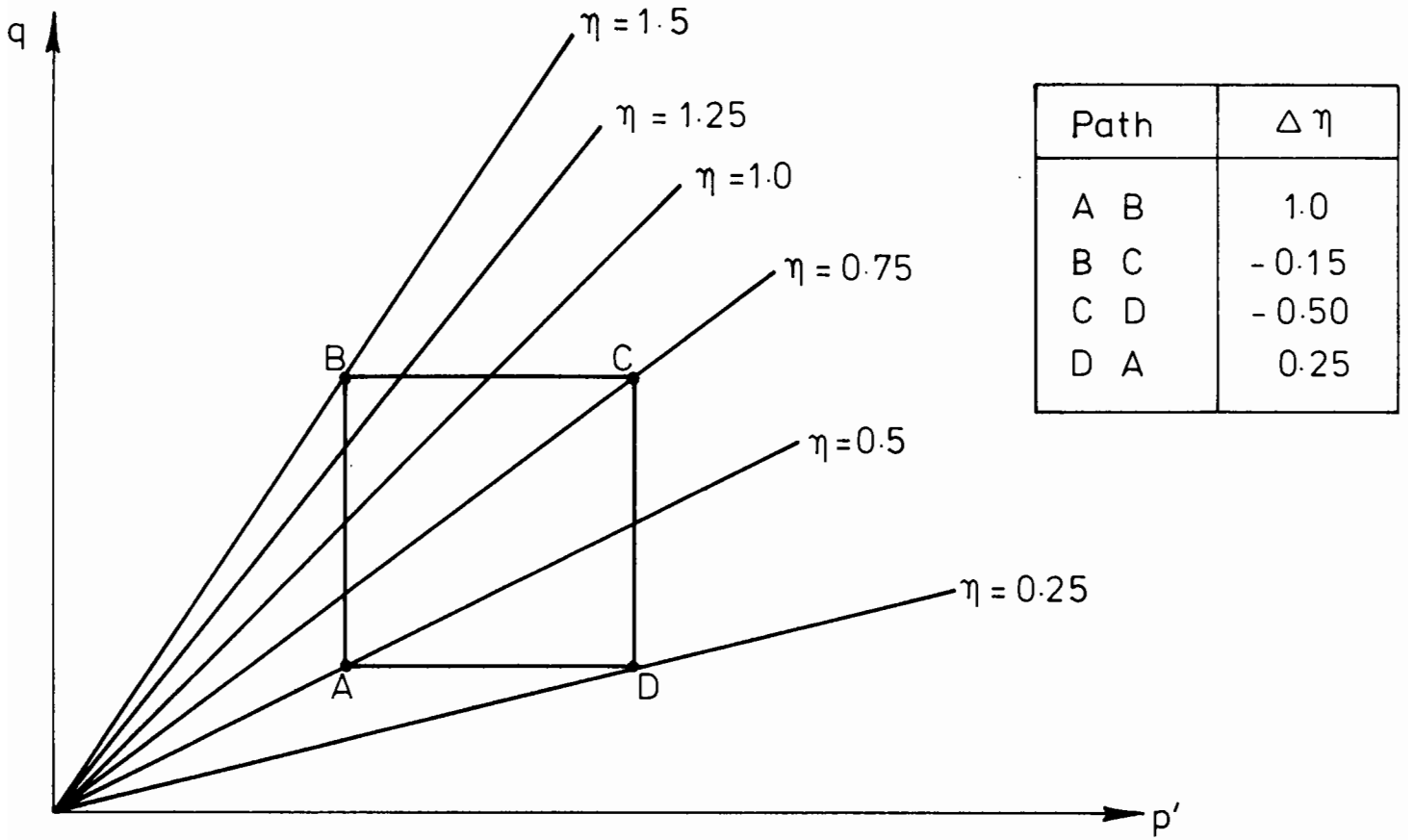

Path	Δ η
A B	1·0
B C	- 0·15
C D	- 0·50
D A	0·25

Fig. 6·51 Closed Path in q, p Space

fundamental importance to the behaviour along path BC. During clockwise loading, the embarkation upon path BC corresponds with a complete change in shear behaviour, whereas during anti-clockwise loading, path CB is merely a continuation of the shear behaviour exhibited along path DC. While an anti-clockwise path is being traced, the material "believes" that stress path CB is merely a continuation of path DC. This is, of course, important, since the material has been shown to be stress path length dependent. As a consequence of this, the prediction is that the shear strains occurring as a result of loading along BC will be greater if an anti-clockwise rather than a clockwise path is followed. The X-Y plots shown in Fig. 6.49 and 6.50 clearly indicate that this is so. The same reasoning can be applied to the other paths and the general prediction is that shear strains are greater if the preceding path has involved shear strains of the same sign.

It is hoped that further work in this direction will be carried out and that a shear strain model which accounts for recent stress history will be produced.

6C.7 BEHAVIOUR WHEN SATURATED

After extensive testing of sample D-4, several slow resilient tests were repeated and both the shear and volumetric strains were recorded. The sample was then saturated with water while being retained in its test position surrounded by cell pressure. A vacuum was applied to the sample void space from an inlet in the top platen. Water was then sucked in through an inlet in the base platen. When the sample was completely filled with water, the tests which had just been performed were repeated. Drainage was allowed, and a slow rate of loading (0.01 Hz) ensured that pore pressures did not interfere with the behaviour. The recorded $q-\epsilon_s$ and

q-ϵ_v plots are shown in Fig. 6.52. It will be seen that the difference between behaviour when dry and when saturated is small, although the material does appear to exhibit slightly higher shear stiffness when wet. This result is broadly in agreement with the findings of most researchers, who tend to state that dry and saturated drained samples exhibit the same stress-strain response (e.g. Finn and Vaid, 1977), provided comparisons are made at the same effective stress.

No tests were performed upon the Modified Denstone in a saturated condition.

6C.8 RESILIENT STRAIN MODELS - DISCUSSION AND DEVELOPMENT

The ideas presented below were formulated in the last two months of the project. The results from previous resilient testing had indicated that good agreement with experimental data could be achieved by using a model similar to that propounded by Pappin (1979). It was therefore considered more profitable to concentrate on other matters rather than producing a new model which would have only minor advantages over the existing one. Although it was realised that Pappin's model dealt only with behaviour at the "end-points" of a stress path, the errors likely to be introduced by the need to interpolate between these points had not been fully appreciated. Consider, for example, the stress-strain behaviour shown in Figs. 6.44 and 6.45. When taking into account only the "end-points" and interpolating between them, the material appears to have a very high bulk modulus. In reality the tangential volumetric stiffness changes during the cycle from a low positive to a low negative value. The problems likely to arise in attempting to produce accurate structural analyses from models based on the Pappin formulation are obvious. As ideas emerged, it became clear that the data collected during the resilient test programme

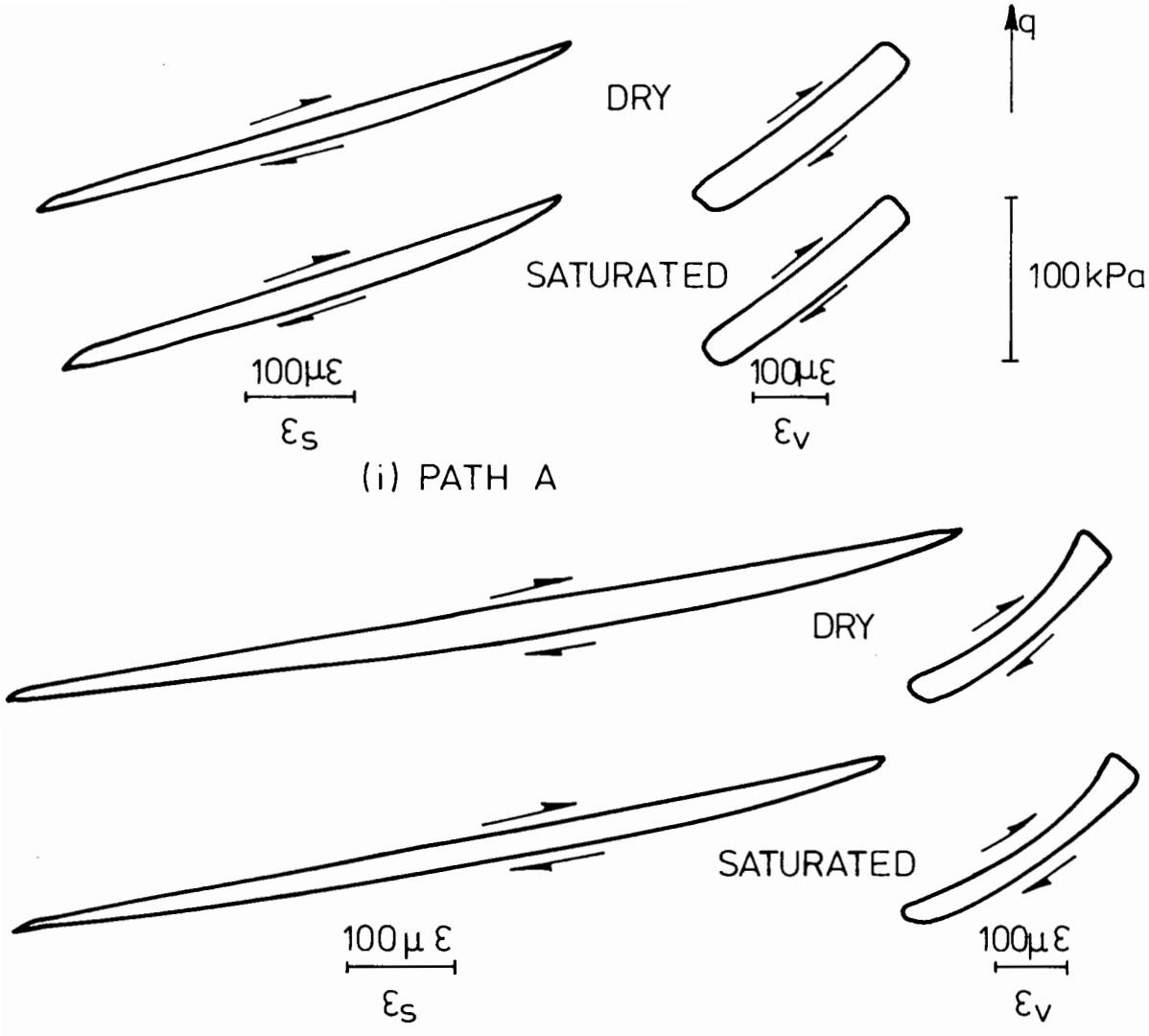

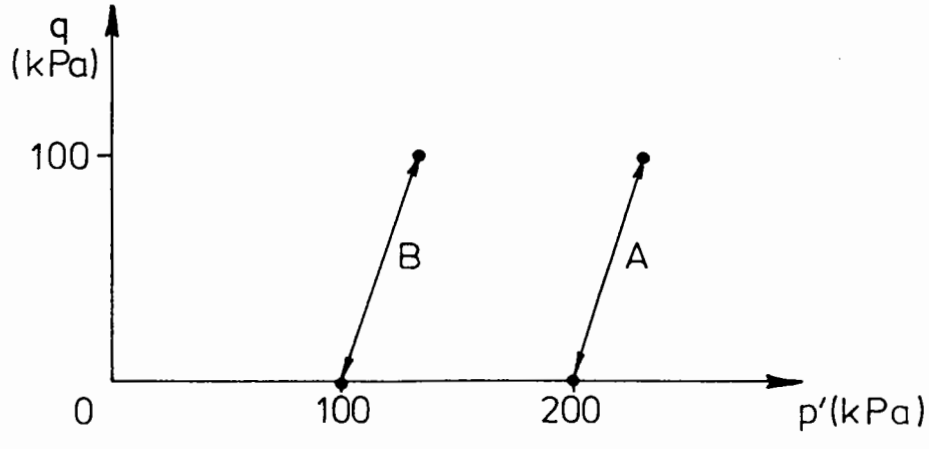

Fig. 6.52 Comparison of Dry and Saturated Behaviour

had not been varied or comprehensive enough to allow for the formulation of a full model for either Denstone or Modified Denstone.

6C.8.1 Introduction

The resilient strain models formulated by Pappin (1979) are deficient in two respects:

(1) although they take into account most of the mechanisms affecting resilient behaviour, the relationship between those mechanisms has not been fully developed, and

(2) they only relate stresses and strains at the "end-points" of the stress path.

The discussion below firstly concentrates on examining the mechanisms at work during resilient strain behaviour, and secondly attempts to use these mechanisms to predict stress-strain behaviour during the complete stress path.

It should be emphasised that the following analysis is, in places, speculative.

6C.8.2 Shear Strain

Pappin derived the following model for resilient shear strain:

$$\epsilon_{sr} = A.\ (\Delta\eta).\ \left[\frac{\ell r}{p_m}\right]^B \qquad \text{where A and B are constants}$$

The core of the model, A. ($\Delta\eta$), simply relates the shear strain to the change in stress ratio η. The modifying factor $(\ell r/p_m)^B$ takes account of stress path length dependence.

Shear Strain and Fabric: A granular material with very stiff particles

subjected to a normal stress is not truly frictional in the traditional sense; if it were, it would be capable of withstanding an increasing shear stress without deformation until some critical stress ratio η_f were reached. At η_f it would deform indefinitely without a further increase in stress ratio. An assembly of particles, of course, does not behave like this. A likely explanation is that the contact points between the individual particles are arranged randomly and the shear to normal force ratio at individual contacts, ρ, is not constant. Fig. 6.53(a) shows a typical distribution of ρ in an assembly of particles at isotropic pressure (the distribution will be affected by deposition and stress history). As the applied stress ratio η is increased, the average value of ρ also increases and some contacts fail - see Fig. 6.53(b). The failed contacts cause (1) deformation within the sample, and (2) cause load to be transmitted to other contacts (thereby making these more susceptible to failure). This process of small deformations at contacts and load shedding onto other contacts gives rise to the pre-yield stress-strain behaviour of granular materials. When the material is unloaded so that the stress ratio η returns to zero, some of the contact stresses will be "locked in" and a particle contact stress ratio distribution different from that in existence before loading will be observed (Fig. 6.53(c)). After a number of load cycles, the ρ-distributions at the maximum and minimum stress ratios will become purely resilient. Resilient behaviour only occurs when a granular material is cycling between two constant fabrics.

Shear Strain and Change in Shear Stress Ratio: Resilient shear strain is affected most significantly by changes in stress ratio. This is explained by the fact that each value of η has its own fairly characteristic ρ-distribution which is established during resilient loading. Variations in the value of b (the intermediate stress difference parameter), the mean

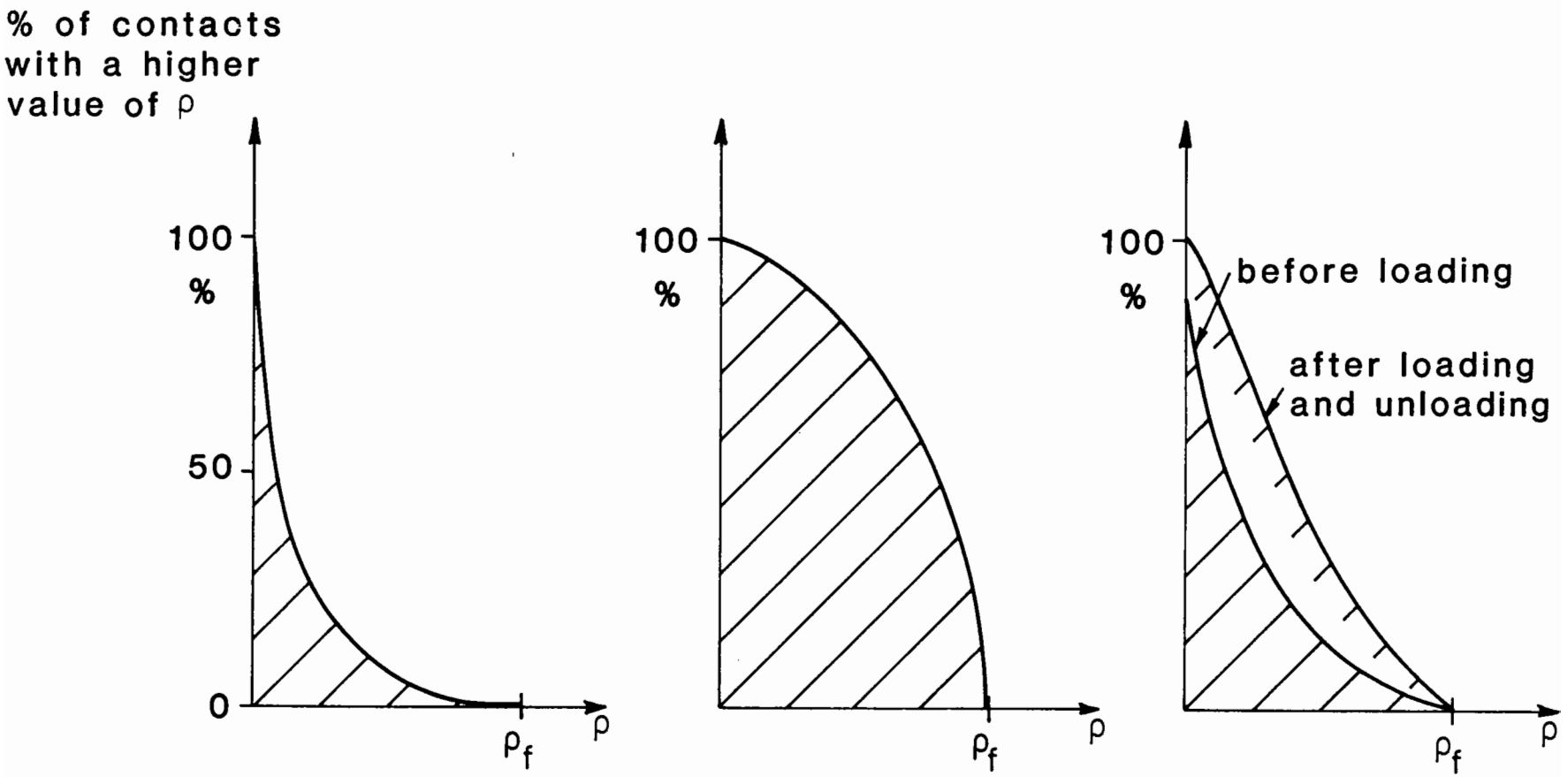

Fig. 6.53 GRANULAR MATERIAL FABRICS AT VARIOUS STAGES OF LOADING

normal stress load and principal stres rotation will, no doubt, affect this.

Since shear strains are caused primarily by changes in the ρ-distribution (i.e. by sliding at contacts and particle rotations - which are heavily influenced by the values of ρ), the strain observed during any repeated stress path will be a function mainly of the difference in stress ratio between the two end-points of the path.

Stress Path Length Dependence: If the form of the stress path length dependency factor in Pappin's model is examined it will be seen that the absolute path length (in q,p space) has been divided by p_m, the average mean normal stress along the stress path. The general effect of this is to convert a path length (in q,p space) into a stress ratio difference. (Note that in general $\ell r/p_m \neq k.\Delta\eta$, but that the difference can be positive or negative and so the use of the factor ($\ell r/p_m$) will produce a greater degree of scatter, though on average, approximately the same predictions). The phenomenon of stress path length dependency has already been discussed in this chapter (6C.4). It was shown that it occurs only when there is an energy loss. That loss, in the case of granular materials, takes the form of heat produced by interparticular contacts sliding. The sliding block and spring model proposed by Zytynski et al (1978) provides a good analogue. Fig. 6.54 shows the hysteresis loops resulting from the three stress paths AB, BC and AC. The resilient strain from the path AC is greater than the sum of the resilient strains from paths AB and BC.

This simple model illustrates that resilient strains are primarily associated with, though not directly proportional to, changes in stress ratio. It has already been shown that Pappin's "stress path length dependency factor" approximates to a "shear stress ratio difference factor". This means that a model:

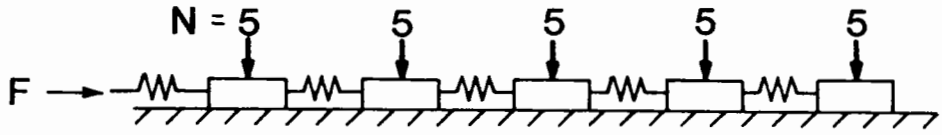

Spring stiffness = 1 : coeff. of friction = 1

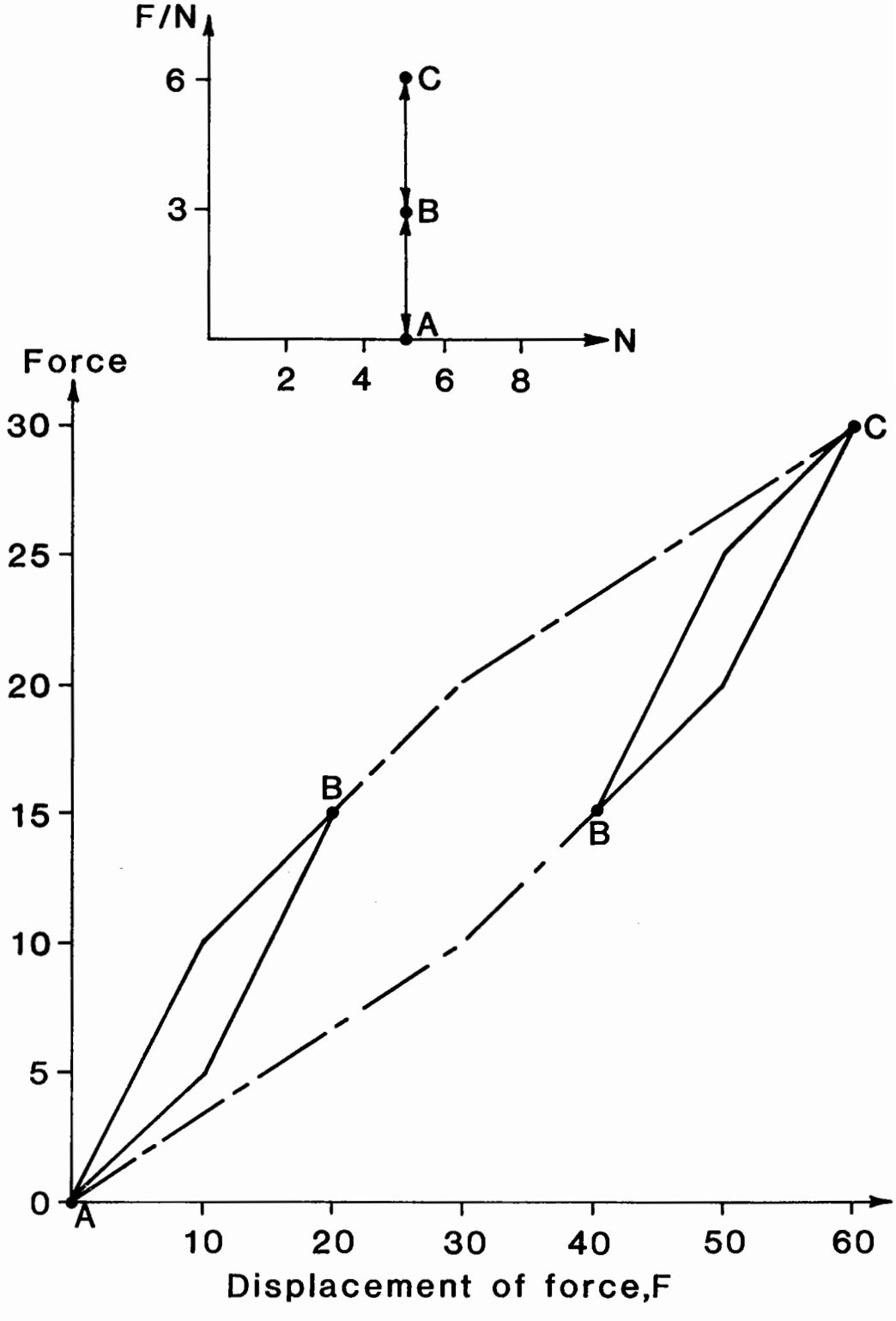

Fig. 6.54 HYSTERESIS AND STRESS PATH LENGTH DEPENDENCY

$$\epsilon_{sr} = A\,(\Delta\eta) \cdot \left[\frac{\ell r}{pm} \right]^{B}$$

would approximate to:

$$\epsilon_{sr} = A\,(\Delta\eta)^{1} + B.$$

Investigation of the spring and sliding block model with different values of normal load N reveals the pattern shown in Fig. 6.55(a). The resulting resilient strains are thus not dependent wholly upon changes in stress ratio, but also upon the mean normal stress. The reason for this is that blocks subject to different normal forces lose different amounts of friction energy through sliding and as has already been shown, stress path length dependency is associated with energy loss during the cycle. In view of this, it would be reasonable to expect that for a granular material, the two stress paths in Fig. 6.55(b) would give rise to the stress-strain behaviour shown. In fact, this is not a very marked phenomenon. The reason is probably that while the energy loss during resilient cycling (with a constant shear strain amplitude) is proportional to the mean normal stress, the secant modulus is not proportionally dependent upon the energy loss. The hysteresis diagrams in Fig. 6.54 show this: the area of the loop AC (which is a measure of the energy loss) is approximately eight times that of loop AB and yet the secant modulus is only 33% lower.

In order to incorporate this effect into the model, the normal stress during the stress path may be divided by a reference pressure (say 100 kPa), given an experimentally determined exponent (eg. 0.15) and introduced into the model as a factor as shown:

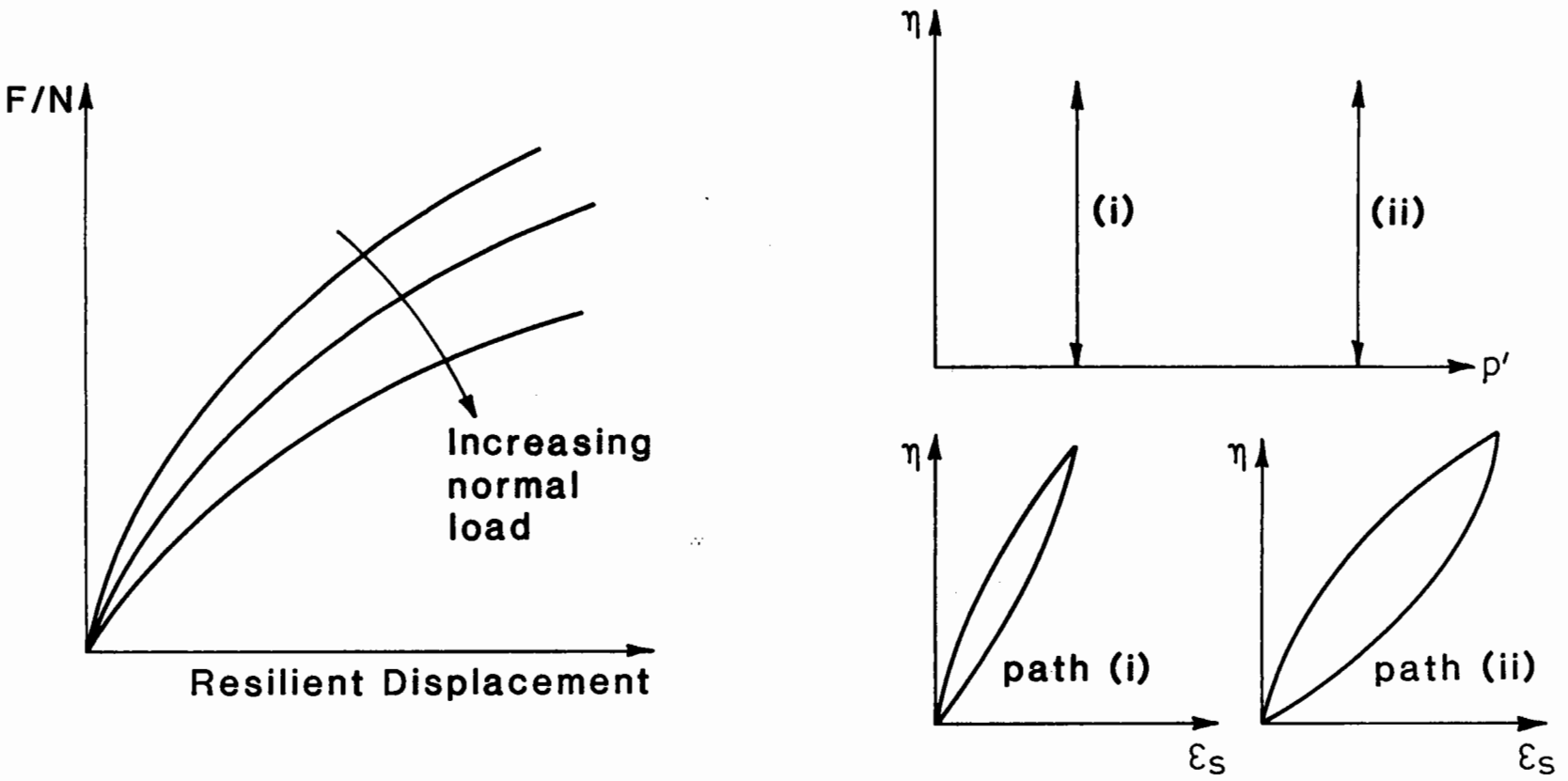

Fig. 6.55 THE INFLUENCE OF MEAN NORMAL STRESS ON SHEAR STRAINS

$$\epsilon_{sr} = A.C\,(\Delta\eta)^{1} + B.$$

$$\text{eg. where } C = \left[\frac{|p - p_o|}{100}\right]^{0.15}$$

Absolute Shear Stress Dependency: One type of behaviour noted during the testing of Denstone was that the shear strains, although predominantly affected by changes in shear stress ratio, were to some extent, dependent upon changes in the absolute shear stress. This phenomenon may be attributed to the elastic deformation of the particles themselves.

Pappin's model does not include a factor to account for this. It is possible that in a well-graded material, there would be a far greater number of highly stressed chains of particles than in a single sized material; the effect of changes in absolute shear stress would not therefore be as great.

A New Model: A shear strain model which would predict shear strains at all points along a stress path, may be written:

$$\epsilon_{sr} = A.C.\,(\Delta\eta)^{1 + B} + f\,(\Delta q).$$

Modelling hysteresis: If a series of resilient stress path tests all beginning at stress ratio η were carried out, the loading curve of the hysteresis loop would be independent of the final stress ratio (eg. in Fig. 6.54 paths AB and AC share a common loading line). Similarly, if a series of stress path tests were carried out with a common maximum stress ratio of η_2, their unloading lines would be similar (eg. in Fig. 6.54 paths CA and CB share the same unloading line). Furthermore, in (η, ϵ_s) space, the resilient loading and unloading lines are fairly similar in shape; i.e.

they are π radian rotations of each other. (Note that representations in (q, ϵ_s) space are usually distorted). Thus, if the following simplified model is to be used:

$$\epsilon_{sr} = A\,(\Delta\eta)^{1} + B$$

then the stress strain behaviour can be modelled by the following equations:

(a) increasing from η_1 to η_2,

$$\epsilon_{sr}\ (\text{at } \eta = x) = A.\,(x - \eta_1)^{1} + B$$

(b) decreasing from η_2 to η_1,

$$\epsilon_{sr}\ (\text{at } \eta = x) = \epsilon_{sr(max)} - A\,(\eta_2 - x\ )^{1} + B$$

Note that when using more sophisticated models, compatibility must be maintained; i.e. the increase in strain during $\eta_1 \rightarrow \eta_2$ must equal the decrease in strain during $\eta_2 \rightarrow \eta_1$: otherwise the model is not resilient. As long as this requirement is fulfilled, the application of a model dealing with the other forms of behaviour mentioned above should pose no problems.

6C.8.3 <u>Volumetric Strain</u>

The resilient model proposed by Pappin is: $\epsilon_v = A.\,\Delta\,[p^B\,(1 - C(\eta)^D)]$. The core of the model is the empirically derived isotropic volumetric strain model. The modifying factors ($1 - C\eta^D$) are intended to account for the observed effect of shear stresses on volumetric strains. The way in which this modification is implemented does not, however, take full account

of the mechanisms involved.

Mechanics involved during volumetric strain: When a granular material is subjected to a change in stress, the volumetric strains which result are the aggregate of two separate components: (a) the compression component, and (b) the dilation component. The former is primarily dependent upon the change in isotropic normal stress, and the latter on shear strains (which in turn depend upon the stres changes and hence can be related back to these). Pappin's model correctly identifies the role of the first component: the second, however, should be introduced as an additive component rather than as a factor.

This explains why the values of the stres ratio η_D at which the onset of resilient dilatancy occurs (see Fig. 6.47) increases with increasing mean normal stress for a series of parallel stress paths. At the higher average stresses the change in mean normal stress required to reach any ratio η is greater. The compressive component, being dependent on changes in mean normal stress, therefore, increases, although the dilatancy component, being affected primarily by changes in shear stres ratio, remains constant. The result is that the onset of dilatancy occurs at higher stress ratios at higher mean normal stresses.

Fig. 6.56 shows the relationships (a) between the compressive component and the mean stress state and (b) between the dilatant component and the shear strain. The latter relationship is shown as a curve: no data is available to confirm the shape of this. A further point for possible consideration is that the graph in Fig. 6.56(b) may be affected by the ambient isotropic stress. It is a well known phenomenon that volumetric strains at higher stresses are smaller especially in angular materials. In a strong spherical particulate material such as Denstone, the effect is likely to be much less marked.

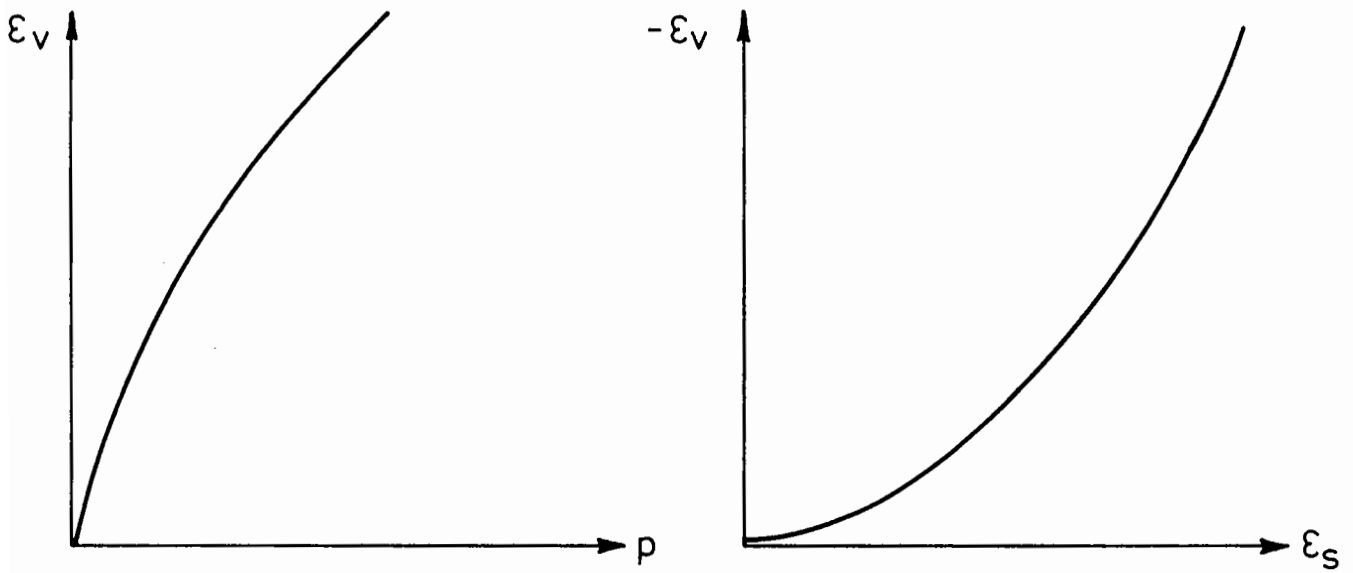

(a) compression (b) dilation

Fig. 6.56 THE COMPONENTS OF VOLUMETRIC STRAIN

A Volumetric Strain Model: A volumetric strain model which would predict volumetric strains at the end-points of a stress path is given by:

$$\epsilon_{vr} = f(\epsilon_{sr}) - A.\ \Delta(p^B)$$

where f is a function. The value of ϵ_{sr} is simply the result of the shear strain analysis (not including that part due to particle compression). Since it has been shown in experiments that there is very little hysteresis associated with purely volumetric strain, the model is satisfactory to describe the behaviour during the complete cycle.

6C.8.4 Examples of Calculations

Fig. 6.57 shows the results of a sample analysis. The stress path is defined by: p_m = 200 kPa, p_r = 100 kPa, q_m = 150 kPa, q_r = 300 kPa. The basic shear strain model was taken to be:

$$\epsilon_{sr} = (\Delta\eta)^{1.8} + \Delta q/3$$

$$\text{and } \epsilon_{vr} = 100\ \Delta.\ (p^{0.5}) - \left[\frac{\epsilon_s^2}{500}\right]$$

Both the shear and volumetric strain predictions correspond well to the type of behaviour exhibited by actual granular materials. The predictions obtained using this form of model for volumetric strains are particularly satisfactory. It has always been difficult to provide accurate predictions for changes in volumetric strains even between the end-points of the stress path. This model appears to be capable of producing reasonably accurate predictions throughout the cycle despite the large variations in bulk modulus exhibited by the granular materials.

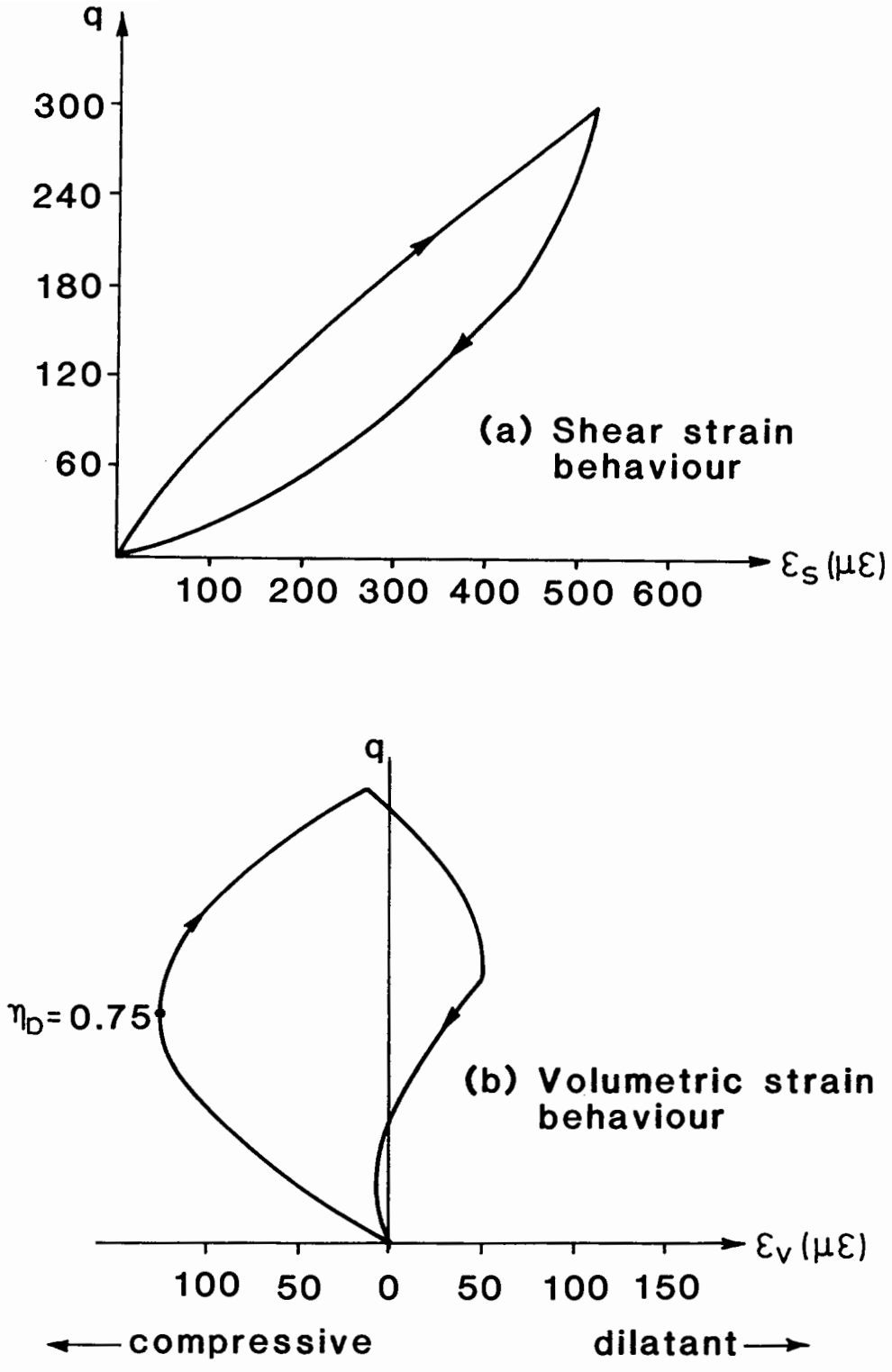

Fig. 6.57 THEORETICAL STRESS - STRAIN BEHAVIOUR

There remains, however, some differences between prediction and experiment; if ths sample analysis shown in Fig. 6.57 is compared with the experimental results in Figs. 6.45 and 6.46, discrepancies are seen to exist especially near the end-points of the stress path.

6C.8.5 Rotating Principal Stresses

While the forms of model discussed above are likely to hold for conditions of constant principal stress direction, principal stress rotation will cause the material behaviour to change. The hypothesis that behaviour depends upon changes in fabric is the key to understanding why this will be so. The fabric tensor at any stage is related to the stress and stress-increment tensors. It is obvious then, that stress rotation accompanying a change in the scalar-stress from (p_1, q_1) to (p_2, q_2) will affect the fabric "path". Since strain is affected (if not largely controlled) by changes in fabric, it follows that the strain-increments are - at least partially - related to the fabric-increments.

One practical result will be that the chord shear modulus between the scalar states (p_1, q_1) and (p_2, q_2) will decrease with increasing stress rotation amplitude. The effect upon the volumetric modulus is not so easy to predict because it has two components. The compression modulus (i.e. that part of the volumetric modulus related to changes in mean normal stress) is unlikely to be changed very significantly. The difficulty lies in predicting the dilatant component. The shear strains will be greater and it might, at first thought, be expected that the dilation component will also be greater. It must not, however, be forgotten that the particles will seek to reduce their potential energy and will consequently attempt to find themselves a "lower" place to rest. The stress rotation gives them greater opportunity to do this because each particle has a range of directions in which it might seek a potential energy reduction. This

will clearly mean that the permanent volumetric strains will be greater (i.e. more compressive), but its effect upon the resilient volumetric strain cannot be predicted with any degree of confidence.

CHAPTER 7

THERMAL ENERGY STORE DESIGN - APPLICATION OF RESULTS

The testing which has been carried out during this project has been primarily concerned with providing data for the design of thermal energy stores. This data can be used to formulate models for use in either numerical or analytical solutions. Numerical solutions will, of course, include computer techniques such as the finite element method.

Some attempts to model a TES using the SENOL non-linear finite-element program developed at Nottingham (Pappin 1979) were made, but, unfortunately, no convergence could be obtained. This may have been due to the novel load system used (i.e. strain control at the TES boundaries), which for some reason the program may not have been able to deal with. Consideration was given to hiring a commercially available non-linear package, but in view of the fact that progress in this field is continuing apace, it was felt that the expense incurred in doing this would be inappropriate at this time.

It was felt that a simplified design method which could give rough solutions for TES dimensions etc. would be useful, both in order to gain a general impression of the likely scale of the operation, and also as a starting point for more detailed numerical techniques. To this end, a simplified structural design method was developed. This method is presented below together with the results of a study in which the influence of a range of parameters is analysed.

7.1 INTRODUCTION

The problem of the structural design of a vertical axis elastic container filled with a granular material has received some consideration, notably by silo engineers (see eg. Cowin 1977). The situation where the

fill and the container are of different coefficients of thermal expansion and where the system is subject to thermal cycling has not, however, been investigated. This problem will arise, for example, when materials are stored in places where large diurnal temperature fluctuations occur (see eg. Blight 1983); a more serious and marked example of where this phenomenon may arise is a Thermal Energy Store (TES) in which heat is stored in granular materials. Large temperature fluctuations may be experienced in these TES (of the order of 800K).

The analysis presented here is aimed particularly at situations where the thermal stresses are of a much greater magnitude than the stresses due to self-weight which, in silo design for example, are normally the only ones considered.

The problem of thermal stressing in systems such as TES arises whether the coefficient of thermal expansion of either the fill or the vessel is the greater. When the coefficient of the fill is greater, the problem will arise during the heating part of the cycle: when the coefficient of the container is the greater, the stresses in the vessel wall will increase during the cooling phase.

7.2 THE PROPERTIES OF GRANULAR MATERIALS

In a container filled with a linear elastic medium, the analysis of the structure during temperature fluctuation would be very straightforward. The properties of granular materials are, however, complex, and this is what complicates the analysis. In order to proceed, it is necessary to understand some of the features of granular material behaviour.

When a granular material is loaded, both elastic (recoverable) and plastic (unrecoverable) strains will occur. During the very first cycle of load applied to any element, the plastic component will be large. With

increasing numbers of cycles, the plastic component which accrues during each cycle will reduce, so that after a large number of cycles, N, the behaviour will closely approximate to elastic conditions. This is termed resilient behaviour.

The number of cycles required to produce resilient conditions will vary from material to material. Generally speaking, however, the stress-strain relationship will become very stable within the first fifty cycles. For a very hard, rounded, single-size material, resilient conditions may be substantially formed during the first two or three cycles.

Research at Nottingham (Pappin 1979, Shaw 1980) and at TRRL (Mayhew 1983) shows that resilient strains can be predicted using a "stress-path-contour" model. The usual way of illustrating these models is to divide stresses and strains into their shear and volumetric components and to show iso-strain contours on two plots of stress spaces.

7.3 PREVIEW OF ASSUMPTIONS MADE DURING ANALYSIS

The major assumptions made during the following sections are:

(a) that the container is twice as stiff in the hoop (circumferential) direction as in the longitudinal direction.

(b) that during the phase of the thermal cycle in which the stresses increase, the coefficient of wall friction is infinity.

(c) that during the phase in which stresses decrease, the coefficient of wall friction is zero.

The corollary of the first two assumptions is that strains are purely volumetric. Volumetric strains in the granular material can be predicted by a very simple model. The possible stress states can be calculated by balancing the stresses within the granular material and the hoop stresses

in the container. The radial strain in the granular material (= 1/3 x volumetric strain) must equal the hoop strain in the container for compatibility - volumetric strains in the granular material can, therefore, be given in terms of hoop strain. Given a value for the initial volumetric stress in the container and a given temperature rise, equilibrium and compatibility considerations yield a unique solution for the internal pressure.

The third assumption above relates to the value to be chosen for the initial volumetric stress.

These assumptions ensure that the "worst case" is achieved. They are discussed and justified as they arise.

7.4 METHOD OF "WORST CASE" SOLUTION

(a) Definition of basic terms

r = radius of container

t_θ = effective thickness of vessel wall in hoop direction

E = stiffness of container

$\Delta\alpha$ = difference in coefficients of thermal expansion between the granular material and vessel

ΔT = temperature rise

p_1 = lowest volumetric stress in granular material during resilient cycle

p_2 = highest volumetric stress in granular material during resilient cycle

(b) Assume Volumetric Strains Only

If $\Delta\alpha \neq 0$, then during a thermal cycle the stress in the container and fill will increase either during the heating or the cooling phase

(depending on whether the value of α for the fill is greater or less than for the container). If the container is wide and shallow this will not lead to a very great increase in volumetric stress as the material can deform due to the nearby stress-free surface. If, on the other hand, the container is very deep, the increase in volumetric stress will be great.

In this case of a deep cylindrical bin with uniformly thick walls fabricated from an isotropic material, the hoop-stress in the wall will be given by $\sigma_\theta = p.r/t_\theta$ and the longitudinal stress by $\sigma_z = p.r/2.t_\theta$ (see Appendix C). In the interest of making the optimum use of materials, the container should have increased stiffness in the circumferential direction so that it is double the stiffness in the longitudinal direction. This, then, will cause the strains in the hoop and longitudinal directions to be equal, and so the strains in the deep container will be purely volumetric.

Note that there is, in fact, a fallacy inherent in this argument; for by increasing the hoop stiffness, we are attempting to create purely volumetric strain conditions. This is hardly in the interest of making the optimum use of materials since it is the worst condition. It is submitted however, that although this fallacy exists it does not destroy the argument, for the design will still be conservative.

So far the assumption has been that by considering the case of an infinitely deep bin, it is possible to arrive at a realistic design for a container which, obviously, will not be infinitely deep. When the container is of moderate depth (eg. depth = 2 x diameter) the use of this assumption is questionable (but at the same time conservative). How far the behaviour within such a container will approximate to that of an infinitely deep bin will depend upon:

(a) the ratio of shear to volumetric modulus - when the ratio is low, the assumption is too pessimistic. When the ratio is greater (i.e. materials with low values of poisson's ratio), the assumption may not

be very pessimistic.

(b) the coefficient of friction between the walls and the fill-wall friction "traps" stresses in the container. A reduced value will cause higher self-weight stresses to be transmitted down through the layers of granular material, but will also, during expansion of the fill, allow stresses to "escape" upwards to a stress-free surface. (NB. vibration will cause a reduction in wall-friction).

(c) Assume Stress-Strain Relationships

The vessel may in many cases (eg. if made from steel which remains at constant temperature) be considered to be linearly elastic. The granular material cannot be so easily characterised; what is known, however, is that the "worst case" is when the container is very deep, and this corresponds (in the container specified above) to the strains being purely volumetric. The volumetric strain contour model indicates that the highest volumetric moduli occurs when the stress path follows the isotropic compression line (i.e. $q = 0$). There will, obviously, be shear stresses in reality, but these will cause reduced volumetric moduli, hence representing a more favourable as well as a more realistic case. The isotropic volumetric strain expression can be expressed as:

$$\epsilon_v = ap_2^b - ap_1^b$$

where a and b are material constants, and ϵ_v is the strain which occurs during pressure change $p_1 - p_2$. Table 1 shows the values of a and b for several materials

Material	a (x 10^6)	b
Well-graded crushed limestone	190	0.33
Single-size crushed limestone	90	0.50
Denstone	124	0.48
Modified Denstone	280	0.42

Table 7.1 Material Properties

(d) Volume and Pressure Changes in the Granular Material

If an element of unrestrained granular material undergoes a temperature change such that it expands relative to the container, the expansion (relative) is given by:

$$\epsilon_v \text{ (unrestrained)} = 3.\ \Delta\alpha.\ \Delta T$$

In the case where the material is inside the container the expansion will, of course, be restrained and consequently will be reduced. The actual relative volumetric strain can be thought of as being reduced by a factor n, and expressed as:

$$\epsilon_v = \frac{1}{n} .\ 3.\ \Delta\alpha.\ \Delta T$$

The value of n depends on the modular ratio of the granular material and the container (note: this is not a constant) and also on the container radius.

The restraining effect of the wall causes an increase in the material pressure within the granular material. The volume changes due to this are directly equatable with the rise in pressure which caused them:

$$(1 - \frac{1}{n}) .\ 3.\ \Delta\alpha.\ \Delta T = ap_2^b - ap_1^b$$

or rearranging:

$$p_2 = \left[\frac{3\left(1 - \frac{1}{n}\right) . \Delta\alpha . \Delta T}{a} + p_1^b \right]^{1/b}$$

If p_1 can be estimated (see section 7.5 below) then the relationship can be given in the form:

$$p_2 = f(n)$$

(e) Strains in the Container

The strains in the container wall will be isotropic (because the stiffness in the vertical and circumferential directions have been chosen so that this is the case). These strains are given by:

$$\epsilon_c = \frac{(p_2 - p_1)\, r}{t_\theta . E}$$

(f) Compatibility of Strains

The strains in the container (ϵ_c) and in the granular material must be compatible, i.e.,

$$3\, \epsilon_c = \epsilon_v .$$

(g) Producing a Solution

Using this information a solution for the pressure rise which will occur due to a change in temperature ΔT may be obtained. A typical iterative method begins by choosing an initial value of n. Using the

equation:

$$p_2 = f(n)$$

p_2 may be calculated. This can then be used to calculate the strain in the granular material from:

$$\epsilon_v = \frac{1}{n} \cdot 3.\Delta\alpha.\Delta T$$

and the strain in the container from:

$$\epsilon_c = (\Delta p)\, r / t_\theta E$$

The ratio R, where:

$$R = 3\, \epsilon_c / \epsilon_v$$

describes the success of the chosen value of n in terms of compatibility. When R = 1 the value of n is correct. If the value of R is not equal to 1, the value of n is changed and a solution is obtained iteratively. When R = 1 (± allowable error), the value of ϵ_c can be used to determine the strain energy in the container and hence its proximity to yield.

7.5 RACHETING AND THE VALUE OF THE INITIAL PRESSURE

When a container is filled with granular materials and cycled thermally, the level of the material surface will settle especially during the first few cycles. This settlement will be accompanied by increasing

maximum pressures during the cycles. These phenomenan are termed "racheting". They are the direct result of the plastic strains developed during each cycle.

Take, for example, the case where the highest stresses occur during the hottest part of the cycle.

Assume first that the material self-weight is very small. When the container is filled, the level may be some value h above the base. During the first cycle, the container will shrink relative to the fill and the stress in the granular material will increase. At some temperature Tm where $T_1 < Tm < T_2$ the volumetric stress might be p_m. During the cooling phase the pressure at Tm will be lower than during the heating phase, $p < p_m$. The main reason for this is that a large proportion of the total strain during loading is not recoverable (plastic). At the end of the cycle, the value of p_1 will be lower than at the beginning of the cycle.

Now consider a TES filled with material with self-weight. In this case, during the cooling of the system, although the volumetric stress is being reduced, the ratio (η) is being increased (shear stress is imposed by the overburden pressure - when the value of p is large, this is largely supported by wall friction, but as the magnitude of p falls, a larger proportion is transmitted to deeper layers). The shear strain contour model indicates that the shear strain and failure condition are related to the ratio of shear stress to volumetric stress (η). The increased value of stress ratio during the cooling phase of the cycle will mean that the material will "flow" to maintain equilibrium. It is this "flowing" under self-weight which causes racheting.

The actual stresses against the container wall will, therefore, be the result of a complex interaction. Firstly, the wall, during the cooling phase, would appear to be "moving away from" the material: this will cause a reduction in stress. Secondly, however, the overburden stresses will

increase and this will cause an increase in wall stress.

Evidence from an instrumented full scale silo undergoing thermal cycling (Blight 1983) indicates that the value of p_1 will, in fact, rise with increasing cycles. The extent to which this is the case is likely to depend on the diameter of the container, the self-weight of the fill and the coefficient of friction between the fill and the container. The first two factors dictate the weight of material per unit area of wall, and the third factor determines how much of that weight is carried by friction and how much is transmitted to the underlying material.

The worst case (i.e. the one where p_1 is greatest) is the one where during the cooling phase of the cycle, the coefficient of friction is very low. In a TES vibration is a possibility and violent vibration may cause the coefficient to approximate to zero; if the value is taken to be zero, then p_1 is given by:

$$p_1 = k_o \cdot \gamma \cdot h$$

where k_o is the coefficient of lateral earth pressure. The active coefficient k_a might be more appropriate because the wall is moving away from the fill material. Vibration, however, is likely to destroy any advantage, and so it is, perhaps, more appropriate to use k_o.

There is likely to be a difference depending upon whether the coefficient of thermal expansion of the granular fill is greater than or less than that of the container. If the initial pressure (i.e. immediately after filling the container) is p, the behaviour during the first cycle will be very dependent upon whether the container expands or contracts relative to the material during the first phase of the cycle. The case where the bin contracts (relatively) has been considered above; where it expands, however, the average pressure decreases, and "flow' will occur due

to the increase in stress ratio. In order to achieve the final equilibrium during resilient cycling, however, both cases will probably tend towards the same stress regimes.

7.6 CONTAINER PROPERTIES

Though a full examination of the container properties is not within the scope of the present project, it is considered appropriate to look briefly at those properties which may affect the above analysis.

(a) Coefficient of thermal expansion

(i) Concrete

Neville (1981): "In general terms, the coefficient [of thermal expansion] of concrete is a function of the quantity of aggregate in the mix and of the coefficient of the aggregate itself."
Fig. 7.1(a) shows the effect of the quantity of aggregate in the mix and Fig. 7.1(b) shows the influence of the coefficient of the aggregate. The coefficient for concrete appears to increase slightly with temperature (Philleo 1958).

(ii) Steel

The coefficient of thermal expansion of steel is dictated mainly by its alloy components. A comprehensive list is given in Smithells Metals Reference Book (6th Ed. Section 14.10). Two examples of commonly used steels are:

1. En - 8: 11.2 x 10^{-6} k^{-1} at 100°C
2. 8% Cr - 3% Si En - 52: 13.0 x 10^{-6} k^{-1} at 100°C

Compared with Denstone (9.5 x 10^{-6} k^{-1}) the coefficient difference ($\Delta\alpha$) of the first material is 1.7 x 10^{-6} k^{-1}, and of the second is 2.9 x 10^{-6} k^{-1}.

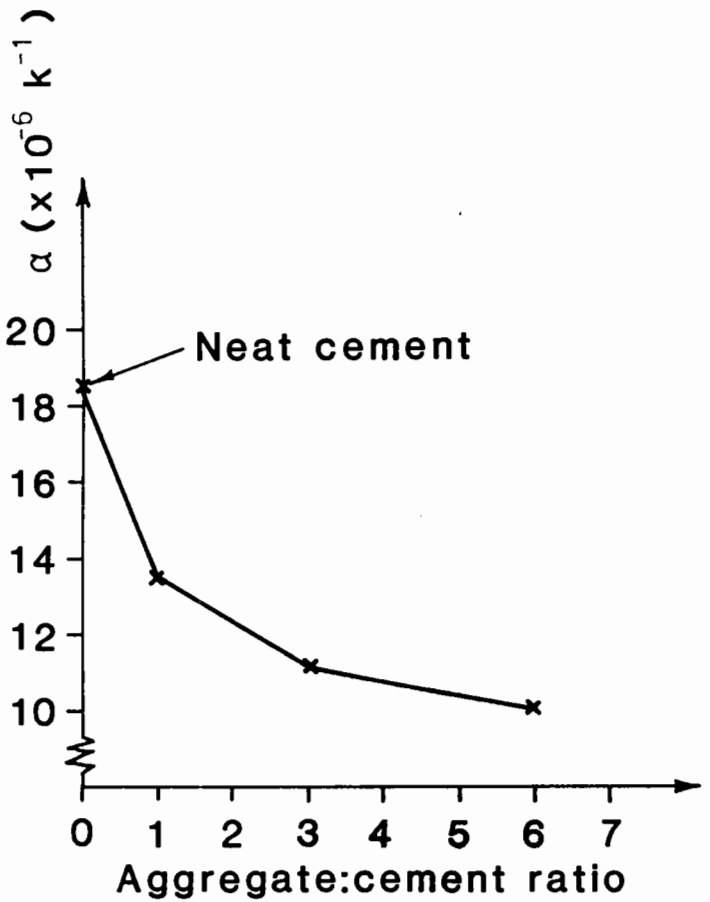

(a) Influence of Aggregate Content
(After Meyers 1940)

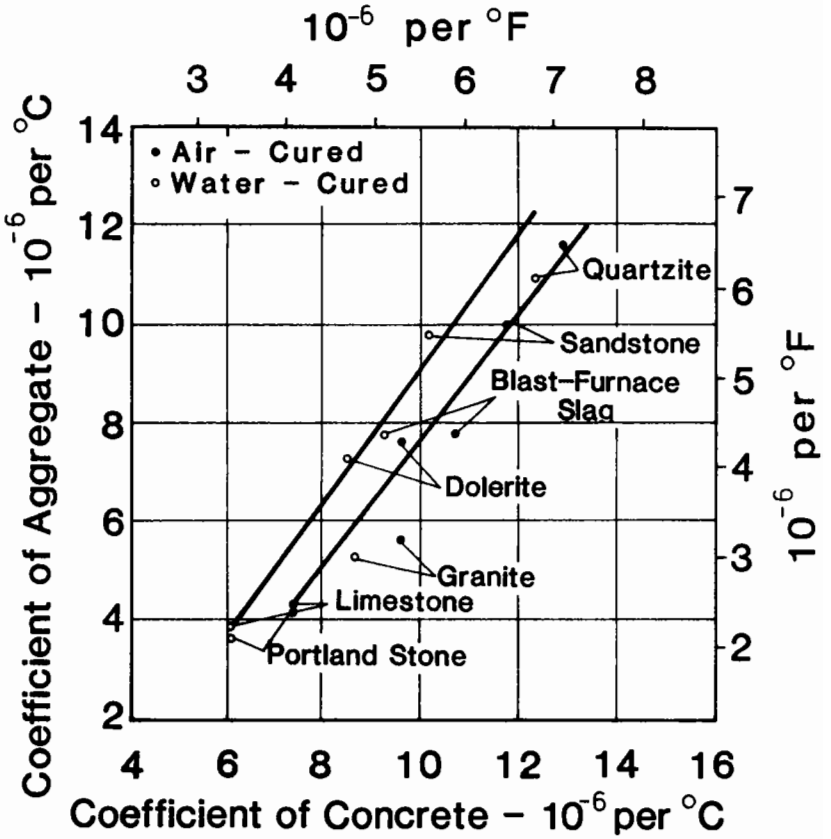

(b) Influence of Aggregate Type
(After Bonnell and Harper 1951)

Fig. 7.1 THE INFLUENCE OF THE AGGREGATE ON CONCRETE'S COEFFICIENT OF THERMAL EXPANSION

This is only true, however, at 100°C. As Fig. 7.2 shows, the coefficient of thermal expansion changes with temperature: at 500°C, for example, the En52 steel has a lower $\Delta\alpha$ value than the En8 steel.

(b) Stiffness

(i) Concrete

In a prestressed concrete vessel the stiffness of the concrete will affect the behaviour of the whole structure. Fig. 7.3 shows that the stiffness of concrete decreases rapidly with increasing temperature.

(ii) Steel

It is a well-known phenomenon that steels lose their stiffness with increasing temperature. Fig. 7.4 shows this for four steels tested by Borzdyka (1948).

(c) Strength

Both steel and concrete lose strength with increasing temperature. Fig. 7.5 shows the influence of temperature on concrete strength.

(d) Other Effects

It is necessary to take into account a range of further aspects of behaviour such as:

(i) Creep and Relaxation

See Neville (1970) for the authoritative work on concrete creep.

(ii) Thermal Stresses,

(iii) Thermal Fatigue.

An interesting introduction to the problems of thermal fatigue is

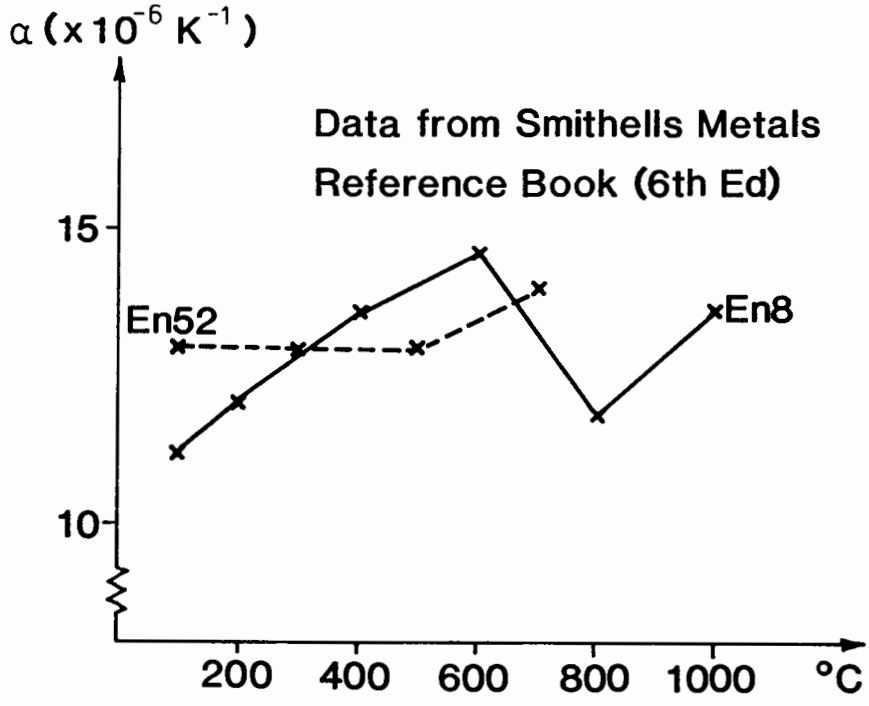

Fig. 7.2 INFLUENCE OF TEMPERATURE ON THE COEFFICIENTS OF EXPANSION FOR TWO COMMON STEELS

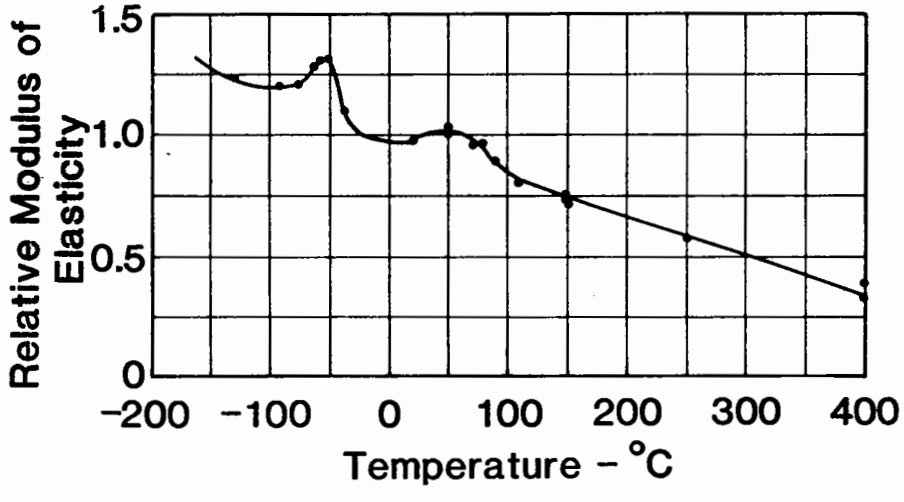

Fig. 7.3 THE INFLUENCE OF TEMPERATURE ON THE STIFFNESS OF CONCRETE (FROM MARÉCHAL 1972)

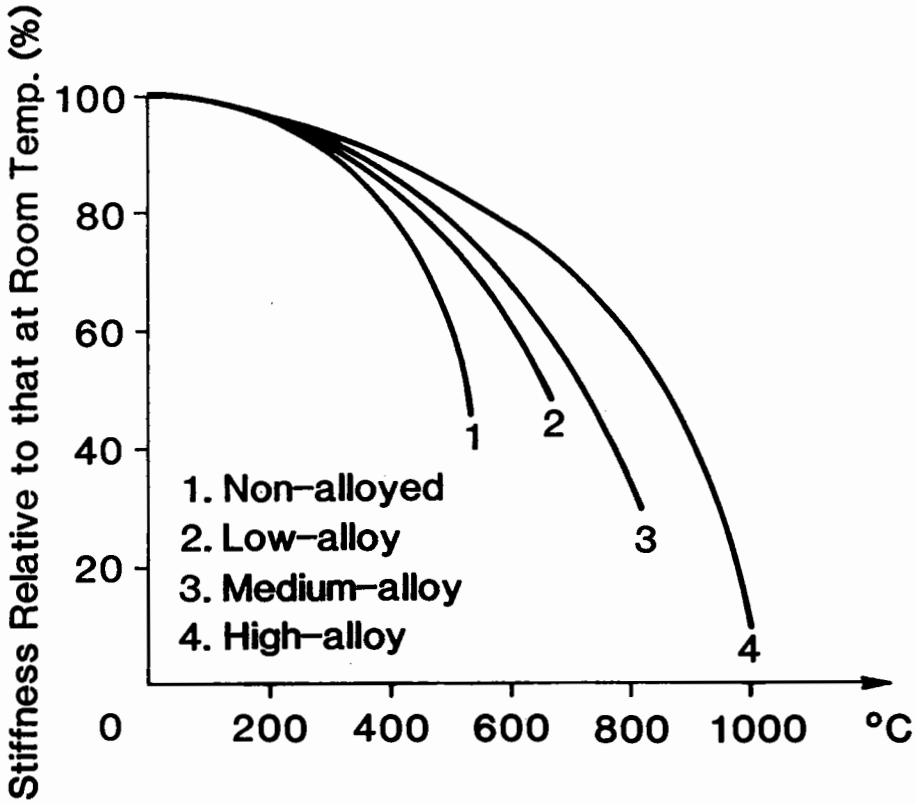

Fig. 7.4 THE INFLUENCE OF TEMPERATURE ON THE STIFFNESS OF STEELS (AFTER BORZDYKA 1948)

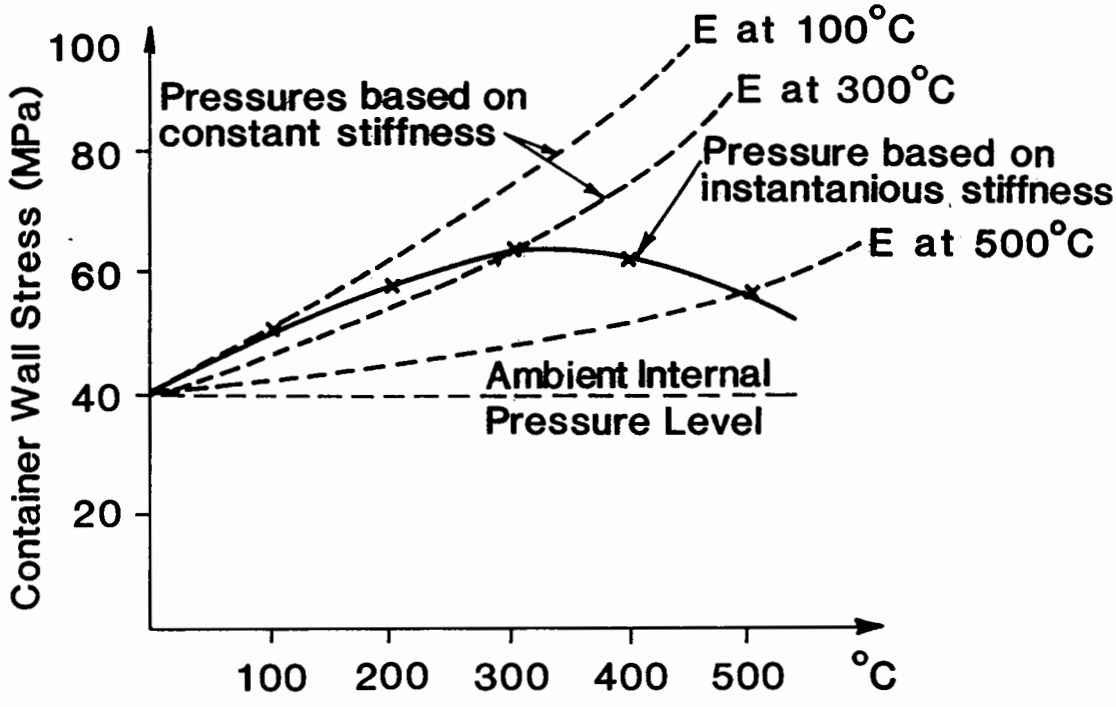

Fig. 7.6 METHOD OF SOLUTION FOR CONTAINER WALL STRESS BASED ON INSTANTANIOUS CONTAINER STIFFNESS

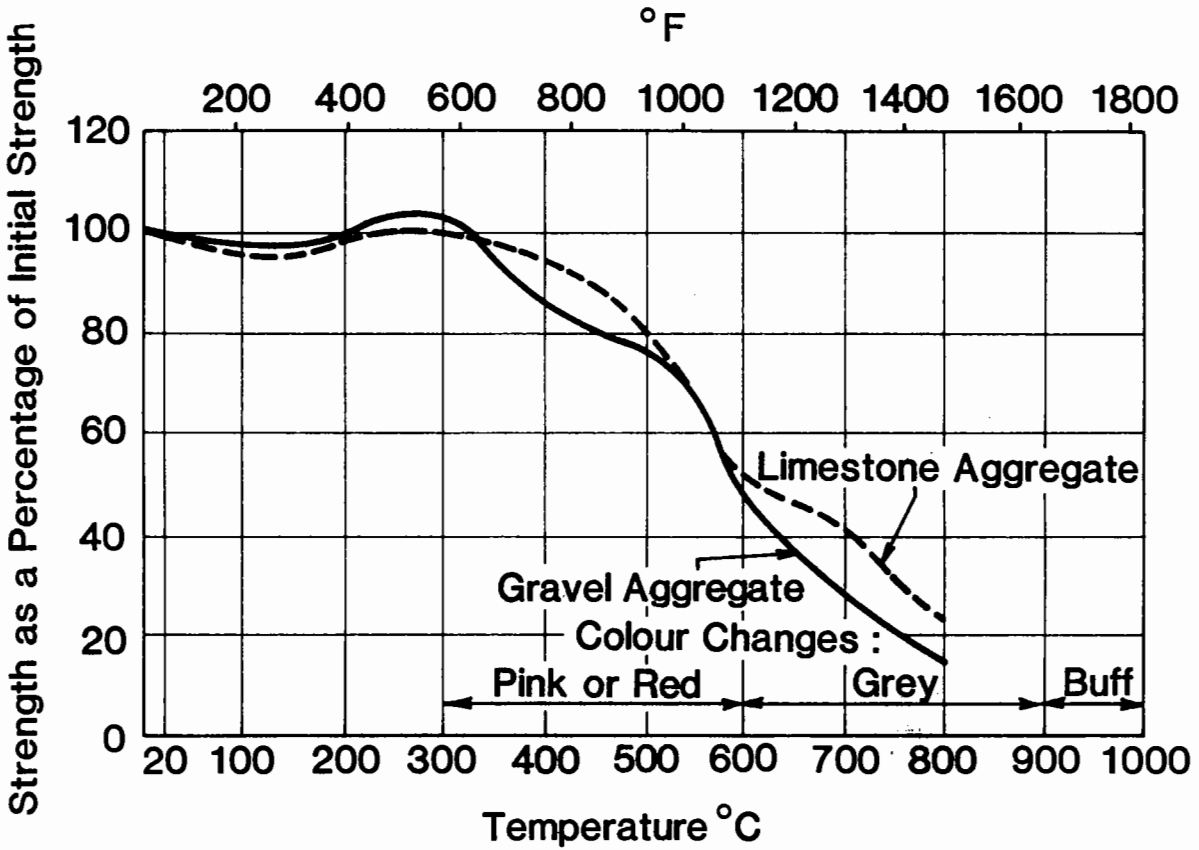

Fig. 7.5 THE COMPRESSIVE STRENGTH OF CONCRETE AFTER BEING SUBJECTED TO A RANGE OF TEMPERATURES

given in Townley and Darlaston (1969).

(e) Modelling of the Above Features

The analysis which has been developed in this project can easily be adapted to take account of the above features of behaviour:

(i) Coefficient of thermal expansion

The analysis can proceed incrementally as well as in a single step. The changing coefficient of thermal expansion can, therefore, be modelled by dividing the temperature increase into discrete rises, δT, during which the relevant coefficient, α, can be used (eg. the mean coefficient over the temperature interval). Starting at To, for example, the temperature rise δT can be modelled using the coefficient α at To + 1/2 δT. The value of p_2 calculated at To + δT, is then taken as the value of p_1 for the next increment, in which the "updated" value of α is used.

(ii) Stiffness

It is not possible to model changes in stiffness incrementally because the changes in strain due to loss of stiffness depend on the total stress, rather than on the latest stress increment. On the other hand, the stress state at temperature T can be calculated by performing the analysis in one step (from To to T) but using the stiffness at T. This method is shown in Fig. 7.6 in which a hypothetical analysis is performed on a container with an ambient internal pressure. Analyses of the behaviour for a range of container stiffnesses (corresponding to the stiffness at various temperatures) have been carried out. The dashed line shows the pressure due to the granular materials

based on the instantaneous stiffness.

(iii) Insulation

The loss of strength due to temperature rise, and the problems associated with creep, thermal stresses and thermal fatigue, may mean that insulation of the structural components is required. This can be easily modelled; if the insulation is 100%, then there will be no thermal strains in the container. The values of $\Delta\alpha$ used in the analysis will, therefore, be the absolute value for the granular fill.

7.7 PARAMETRIC STUDY

A study was carried out to identify the effects of a variety of parameters. The results are presented in terms of the container wall stress vs normalisd temperature rise. The normalised temperature rise (NTR) rise is the product of the temperature rise and the differential coefficient of thermal expansion.

(a) The Effect of Initial Granular Material Pressure

The difficulty in obtaining a value for p_1 (the initial granular material pressure) was discussed in Section 7.5 above. A study of the effect of altering p_1 was carried out based on a container filled with Denstone with a radius of 3m and a circumferential wall thickness of 0.02m. The results are shown in Fig. 7.7. As can be seen, the major effect is a vertical translation on the diagram.Therefore, a poor initial estimate of p_1 will not result in a proportionate error in the solution. This means that a value of p_1 much greater than that actually expected can be employed without drastically reducing the structure's efficiency at high

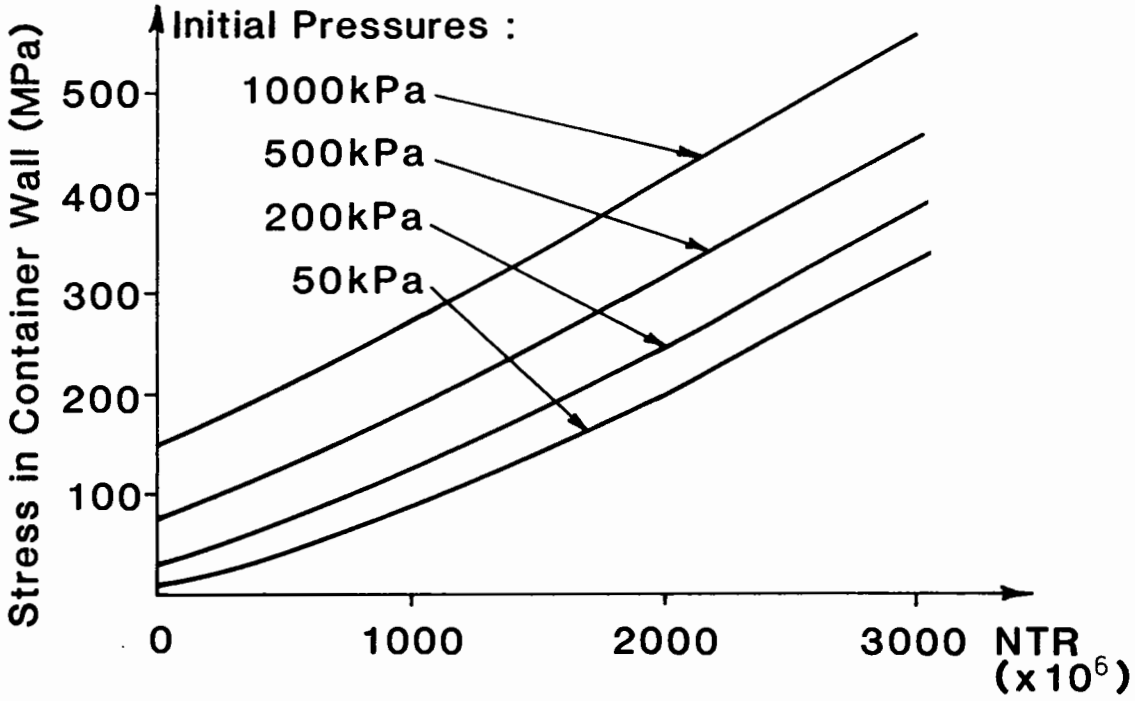

Fig. 7.7 THE INFLUENCE OF INITIAL PRESSURE ASSUMPTION ON SUBSEQUENT BEHAVIOUR

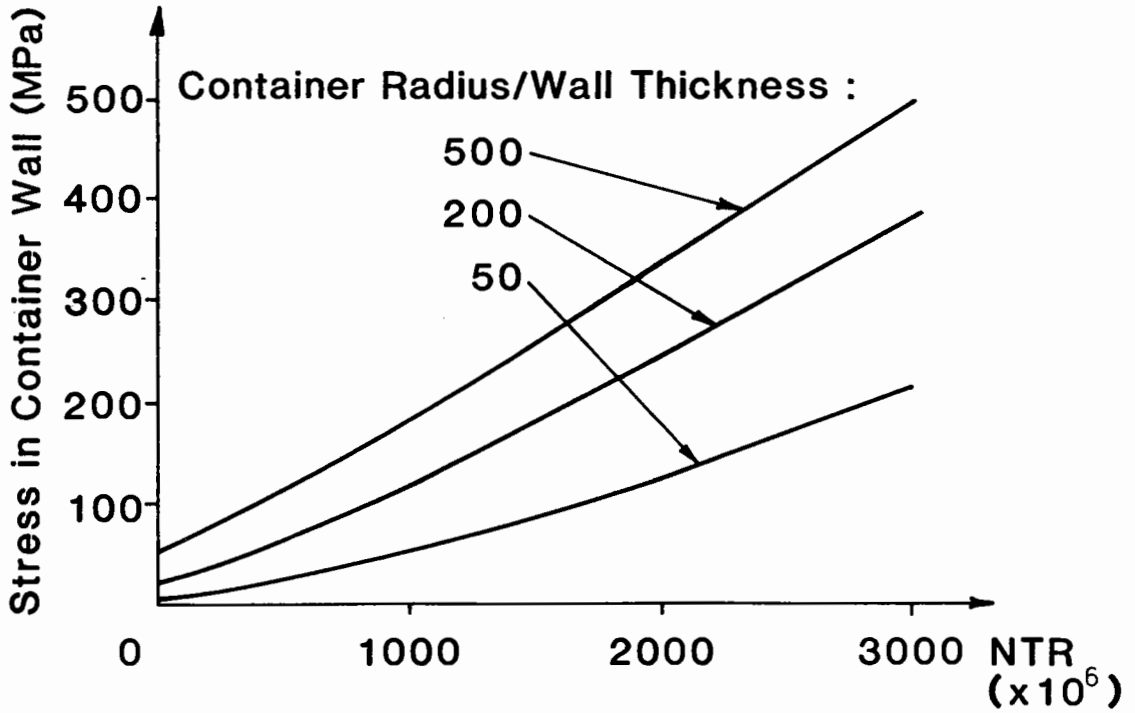

Fig. 7.8 THE INFLUENCE OF CONTAINER RADIUS/WALL THICKNESS RATIO ON CONTAINER WALL STRESSES

temperatures.

(b) The Effect of Increasing Container Radius

A study was made of a container filled with Denstone whilst its radius to circumferential wall thickness ratio was altered. The initial pressure was in all cases 100 kPa. The results are shown in Fig. 7.8. As expected, an increase in this ratio leads to an increase in wall stress. It is interesting to note that increasing the ratio by a factor of 10 (from 50 to 500) merely doubles the wall stress at a NTR of 3000×10^{-6}.

(c) The Effect of Increasing Container Stiffness

Section 7.6 above discussed the reduction in container stiffness during a temperature rise. Unless the structural components are insulated a temperature rise will occur during each cycle (eg. if a steel "fill basket" of the type advocated by United Engineers and Constructors, 1982, was to be used). A range of stiffnesses as shown in Fig. 7.3 would need to be considered for a complete analysis of such a situation. Fig. 7.9 shows the results of such an analysis. A container 3m in radius and 0.02m in wall thickness was studied. A range of stiffnesses between 50 GPa and 300 GPa was used.

(d) Calculations for a number of granular materials

In this study, the behaviour of containers in which the four different granular materials described in Table 7.1 were used as fill materials was considered; it was decided to use crushed rock as well as the Denstone and Modified Denstone in the study because of the possibility of natural materials such as crushed Dresser Basalt being used in TES. Two containers configurations were analysed; a stiffness of 200 GPa and a radius 3m were used for both. The first had an effective wall thickness of 0.02m, the

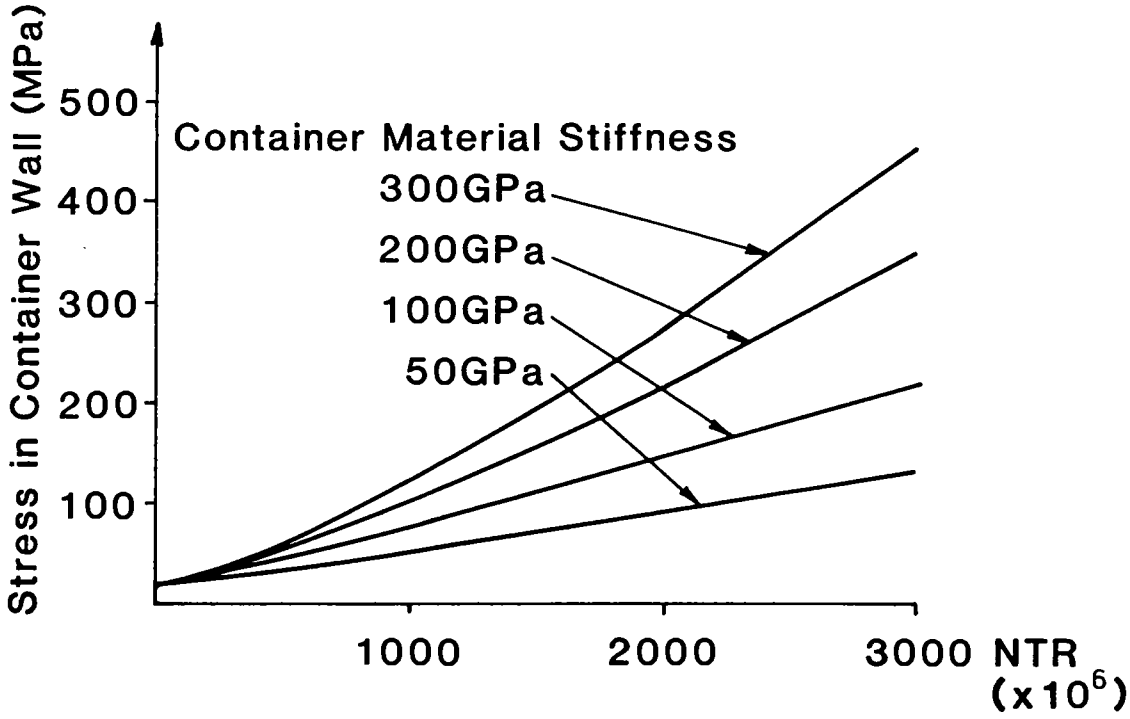

Fig 7.9 THE INFLUENCE OF THE CONTAINER MATERIAL STIFFNESS ON CONTAINER WALL STRESSES

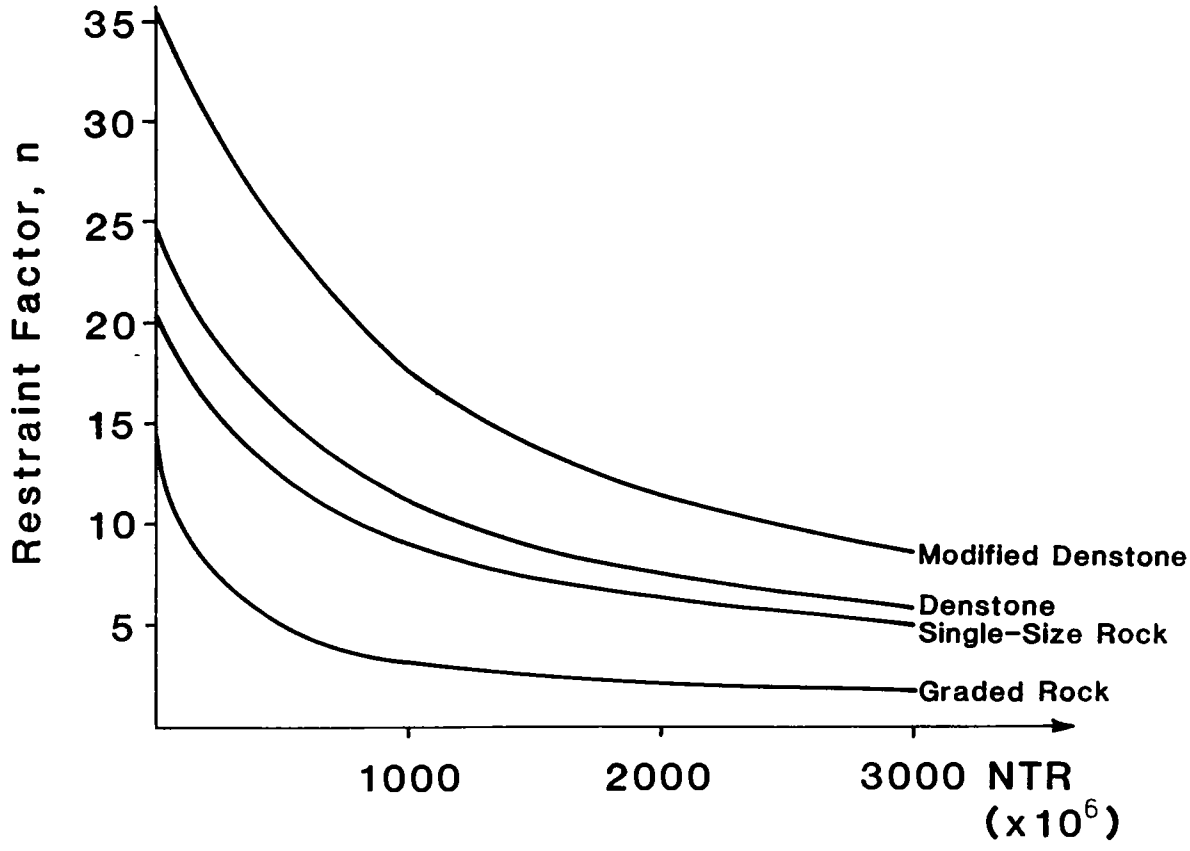

Fig. 7.11 THE REDUCTION IN VOLUMETRIC RESTRAINT DURING INCREASING TEMPERATURES

second of 0.20m.

The results of these analyses are shown in Figs. 7.10(a) and Fig. 7.10(b). Note that the increase in wall stress is smaller in the container with the greater wall thickness. The internal granular material pressures in the thick walled container, however, are much greater than in the other. Indeed they are so high (in excess of 20 MPa for the crushed rock material at NTR of 3000 x 10^{-6} that the stress-strain laws derived at pressures of less than 1 MPa may not apply.

Fig. 7.11 shows the value of restraint factor, n, against NTR for the study carried out on the thick walled container. A rapid decrease in the value of n with increasing normalised temperature can be observed. For the graded rock material, n approaches a very low value (1.9 at an NTR of 3000 x 10^{-6}). This indicates that the granular material has become very stiff; large stresses must be mobilised in the container wall in order to provide any volumetric restraint.

The Effect of very high stress on material properties

In the 1966 Rankine Lecture, Professor Bishop, (using Skinner's results), demonstrated the change in grading which occurs as a result of the application of very high pressures (4000 psi = 28 MPa). These results are shown in Fig. 4.30. It will be recalled that some particle crushing results from application of an isotropic stress. When a shearing stress is applied, further crushing takes place. This might lead one to expect that because stress relief by crushing can occur that the stresses in a closed container would be reduced. On the other hand, continued particle degradation may result in racheting. This would lead to an increase both in material density and in the number of particle contacts: consequently, the material stiffness would also increase.

The problem of degradation is likely to be greatest with an angular

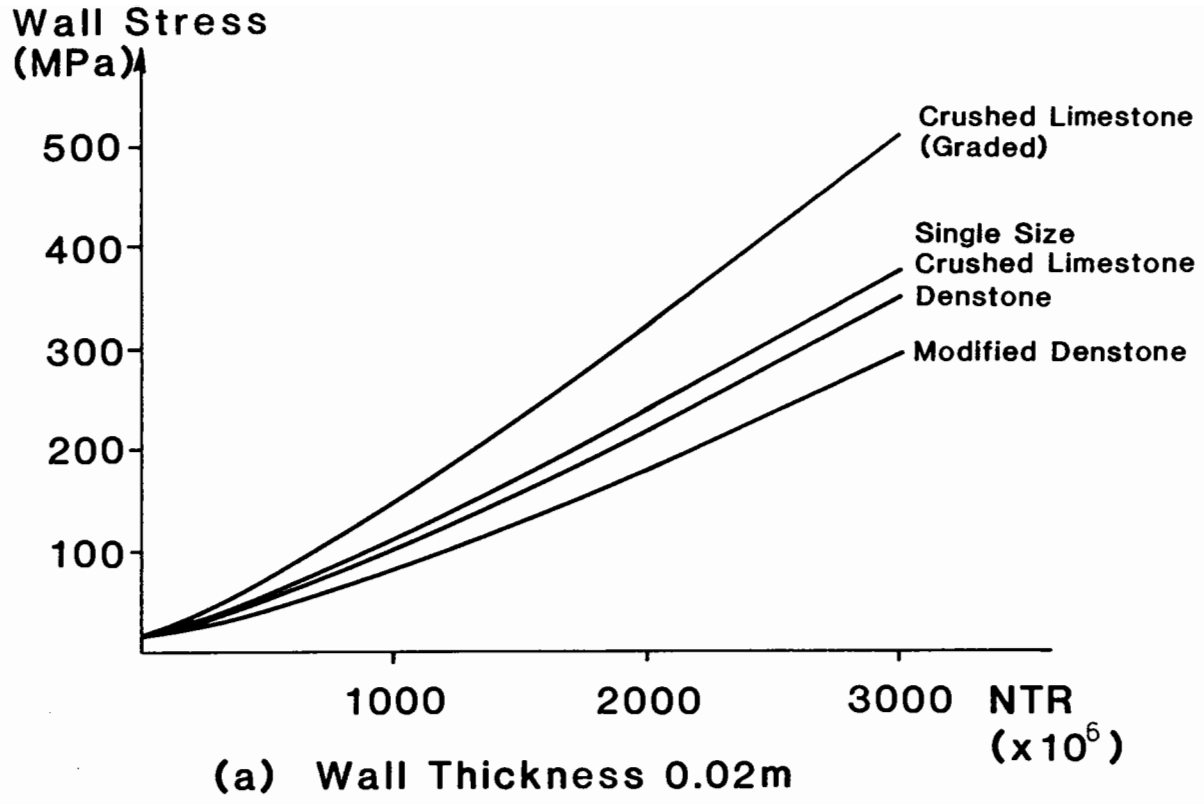

(a) Wall Thickness 0.02m

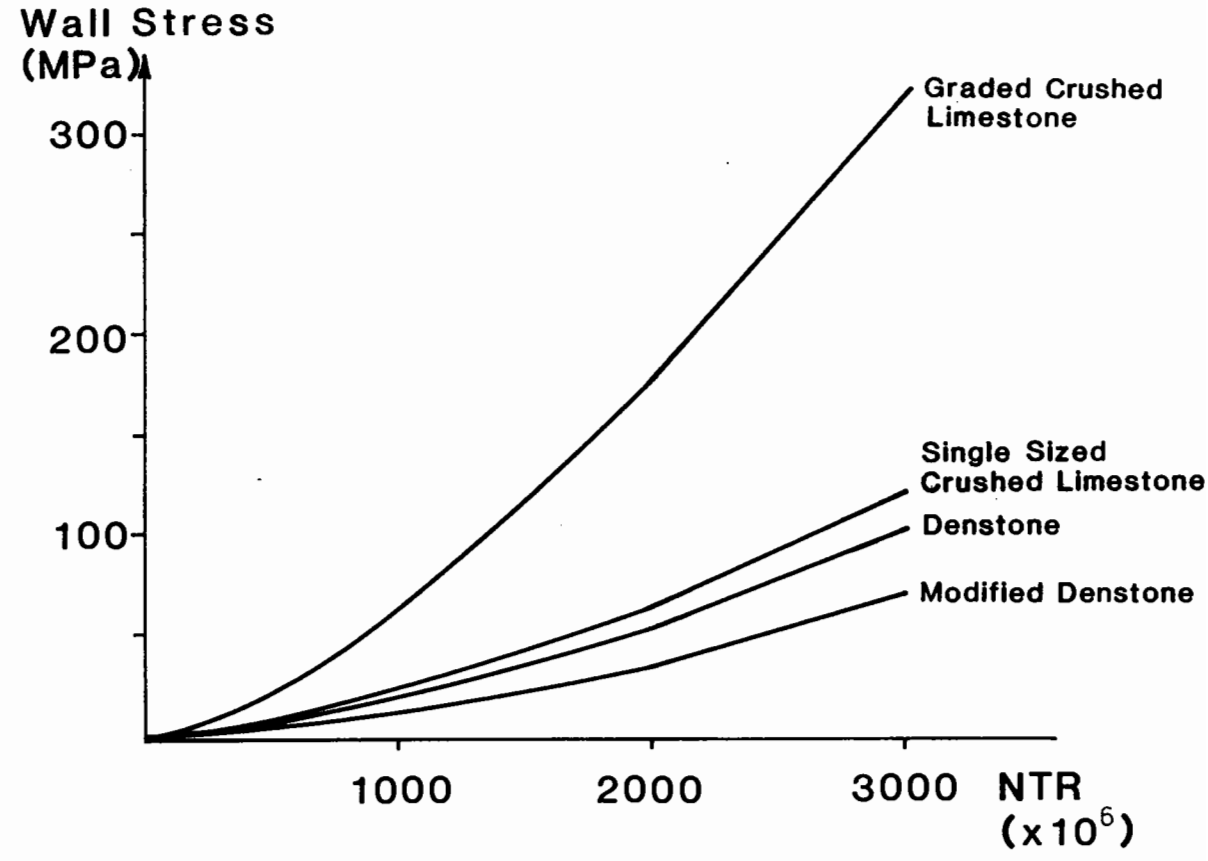

(b) Wall Thickness 0.2m

Fig. 7.10 THE BEHAVIOUR OF FOUR MATERIALS IN TWO DIFFERENT CONTAINERS

material. Note, however, that in single sized particle assemblies fracture due to intense contact normal forces may also cause degradation at high stresses. If, therefore, it is thought necessary to use a very stiff container in which very high mean normal stresses are anticipated, it may be advisable to use high strength particles.

CHAPTER 8

THE HOLLOW CYLINDER APPARATUS - DESCRIPTION AND RECOMMENDATIONS FOR FUTURE WORK

8.1 INTRODUCTION

At the outset of this project it was considered that very little apparatus development would be required since an excellent repeated load triaxial apparatus was already available for operation at Nottingham. During the project it became clear, however, that certain features of TES behaviour (notably the rotation of principal stresses during thermal cycling) could not be simulated in the standard triaxial apparatus. Research work published during the early stages of the project (especially work carried out at Imperial College) showed that rotating principal stresses might have a profound effect on material behaviour at stress ratios substantially below the failure condition. It seemed highly unlikely, then, that the tests being carried out in the triaxial apparatus were providing adequate data for TES design.

In November 1983, it was decided to give serious consideration to the construction of a hollow cylinder apparatus in order to investigate material behaviour under conditions of rotating principal stress. The equipment was expected to be in operation and to be producing results before the end of the project. Unfortunately, no testing has been undertaken, although the apparatus has now been substantially completed.

When it became evident that very little (if any) testing on this piece of apparatus would be possible, a small HCA was built in order to provide some rough supplementary results. The results obtained turned out to be very unsatisfactory and the conclusion was that no advancement in the state of knowledge of granular material behaviour had been made. The details of this testing were published in a Report to the CEGB (1985) and are

reprinted as Appendix D of this thesis. Several novel experimental and analytical devices were used.

8.2 LIMITATIONS OF THE STANDARD TRIAXIAL APPARATUS

The standard triaxial apparatus has been used extensively in laboratories for many years. Its major limitation is its inability to produce certain important stress conditions.

The axial symmetry of the equipment means that the intermediate principal stress σ_2 is equal to σ_3 (compression) or σ_1 (extension). The development of the true triaxial apparatus (e.g. Lade and Duncan, 1973) has enabled researchers to overcome this limitation. The effect of the independent intermediate principal stress (that is $\sigma_1 > \sigma_2 > \sigma_3$) has already been the subject of a considerable amount of published research.

The vertical and horizontal directions are always directions of principal stress, so intermediate positions for principal planes are not possible. In Chapter 2 the possibility of principal stress rotation in the TES was discussed. Little reliable data has been published on the effect of stress rotation, but recent research at Imperial College (Hight 1983, Symes 1983) has shown that it may be significant. It was therefore considered worthy of investigation.

8.3 APPARATUS IN WHICH PRINCIPAL STRESS ROTATION IS POSSIBLE

The Cambridge simple shear apparatus (CSSA) was developed in 1953 by Roscoe and one of its advantages was that it enabled principal stress rotation to occur. However, there are problems with this apparatus, particularly lack of stress uniformity and difficulty in obtaining accurate small deformation measurements. It is considered that its usefulness for

measuring the resilient properties of granular materials is severely limited. The directional shear apparatus (DSC), developed at University College London, appears to be an improvement on the CSSA in that much greater stress uniformity and accuracy in the determination of stress state is possible. However, this apparatus is still unsatisfactory for the type of work required in this project: friction across the "plane-strain" faces, and the inability to measure very small deformations ($\simeq 10\mu m$) accurately, are both likely to cause difficulties. Much recent attention has been concentrated on the Hollow Cylinder Arrangement, (e.g. Hight 1983), which, if well designed, has two major advantages over the CSSA and DSC. Firstly, the stress state of the sample can be more accurately determined and, secondly, deformations may be measured much more reliably since access to the sample is not via a steel box in the case of the CSSA or indirectly using X-ray techniques in the DSC.

The disadvantages of the Hollow Cylinder Apparatus (H.C.A.), which include its comparative complexity and range of particle sizes which may be tested, are also disadvantages of the CSSA. These were not, however, considered to be insurmountable problems and, consequently, a H.C.A. is presently in the late stages of construction at Nottingham.

8.4 GENERAL DESCRIPTION OF THE APPARATUS

Fig. 8.1 shows the basic arrangement of the HCA. The sample is in the form of a hollow cylinder with a large internal to external diameter ratio (80%). The external dimensions of the sample are 500mm high and 280mm external diameter. The internal voids of the sample are evacuated (either wholly or partially) and the cell pressure is, therefore, simulated by the pressure difference between the external atmospheric pressure and this negative internal pressure within the sample. This arrangement allows only

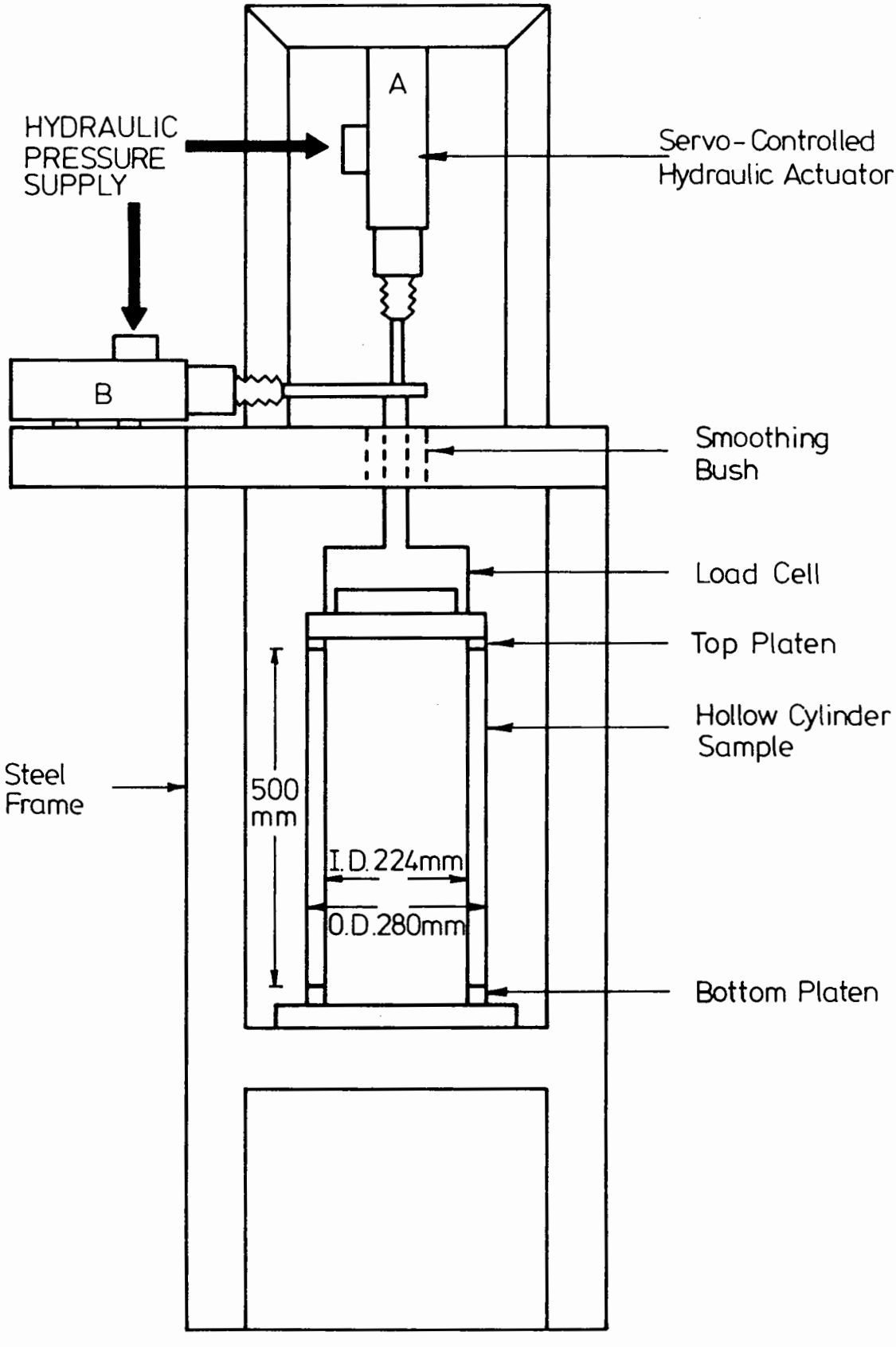

Fig.8.1 Hollow Cylinder Apparatus - Basic Arrangement

a limited range of normal pressures but, unfortunately, its simplicity was necessitated by the lack of both time and money.

With the exception of the isotropic pressure provided by the atmosphere, loads are applied by two servo-controlled hydraulic actuators. Actuator A, in Fig. 8.1, provides an axial load, and actuator B applies a torque. The sample is formed as a hollow cylinder so that when the torque is applied, the stress difference across the sample thickness is small relative to the absolute value.

Plate 8.1 shows the apparatus. The sample shown is a dummy used during proving tests. The base platen in the foreground indicates the actual sample diameter (which is larger than that of the dummy sample).

8.5 PROBLEMS ARISING FROM H.C.A. SAMPLE GEOMETRY

In order to achieve an acceptable level of stress uniformity, the thickness of the sample wall must only be a small proportion of the external diameter. In the present case the wall thickness is 28mm; 10% of the external diameter. The two main poblems associated with this are possible sample instability and the limitation on particle sizes which may be tested.

8.5.1 Sample Instability

A perfect sample under symmetric loading would not be unstable. In practice, however, sample imperfections are almost inevitable and this may lead to instability by buckling, for example. In addition, small eccentricities in the applied loads may cause or assist an unexpected mode of failure. The taller the sample, the worse this problem becomes. Unfortunately, it is necessary to produce a long sample in order to avoid end-effects due to platen friction, thus allowing measurements to be made

in a relatively unaffected zone. A conflict, therefore, arises since a lengthy sample is desirable in order to achieve uniformity, but undesirably in that it adds to instability. Hight, in a private communication (1983), has indicated that the sample height of the Imperial College H.C.A. is too low, and that it would be worthwhile investing in a greater height to diameter ratio. This recommendation is incorporated into the design of the Nottingham H.C.A with the test samples almost twice the height to diameter ratio of the Imperial College ones. If major problems of instability arise then the apparatus may be modified to produce reduced height samples.

8.5.2 Test Materials

The thickness of wall meant that it would not be possible to test any of the materials under consideration as likely T.E.S. candidates. The smallest particle diameter of the materials being tested was 6mm (Denstone). This was 25% of the wall thickness and too large to give useful results. Since smaller particles of Denstone were not available, it was necessary to choose a surrogate material. This is evidently far from ideal in producing directly applicable design data. However, the impracticality of building a H.C.A. large enough to accommodate the material under investigation, plus, again, the lack of time and money, necessitated the use of a substitute. It was considered that this would be sufficient to give an understanding of the general features of behaviour, which, after all, is better than total ignorance.

The substitute which was chosen was 1mm glass Balontini. In most respects, the glass material appears to have many similarities to Denstone. It is a single-sized hard mineral material whose particles are slightly ellipsoidal. The main respect in which Balontini differs from Denstone is in its size and, as the large triaxial tests have shown, the size of

particles has little effect on material properties. It was therefore felt that Balontini was a worthwhile and practical substitute.

8.6 SAMPLE PREPARATION

Fig. 8.2 shows the general arrangement of the sample during assembly, and Fig. 8.3 shows the sample after preparation. Sample preparation will be described referring to the components of their annotation in Figs. 8.2 and 8.3.

The inner ring (C) is bolted to the base plate (A). The internal membrane is fixed using an 'O' ring in the groove in the inner ring (C). The bottom platen (B) is then placed over the ring and bolted down to the base plate (A). The outer membrane is placed over the platen (B) and fixed with an 'O' ring.

The inner mould (D) is placed on the inner ring (C). The outer mould (E) is assembled around the platen (B).

The membranes are lifted so that they drape over the moulds (D and E). In order that the annular space accords to the design dimensions, the membranes must fit closely to the moulds (D and E). The inner membrane is formed with a smaller diameter than the mould so that it is a tight fit over the inner mould (D). The outer membrane is made close fitting by applying a vacuum to the space between the mould (E) and the membrane. The porous plastic layer (G) allows air to escape to the vacuum connectors (F). The centre rod (H) assembly ensures that moulds are fitted accurately. It serves as a datum from which deviation from the vertical can be measured and if necessary, corrected.

The sample annular space is then filled as required.

When the test material has been filled to the top of the moulds (D and E), the top platen (J) is placed on the material. The platen (J) is fitted

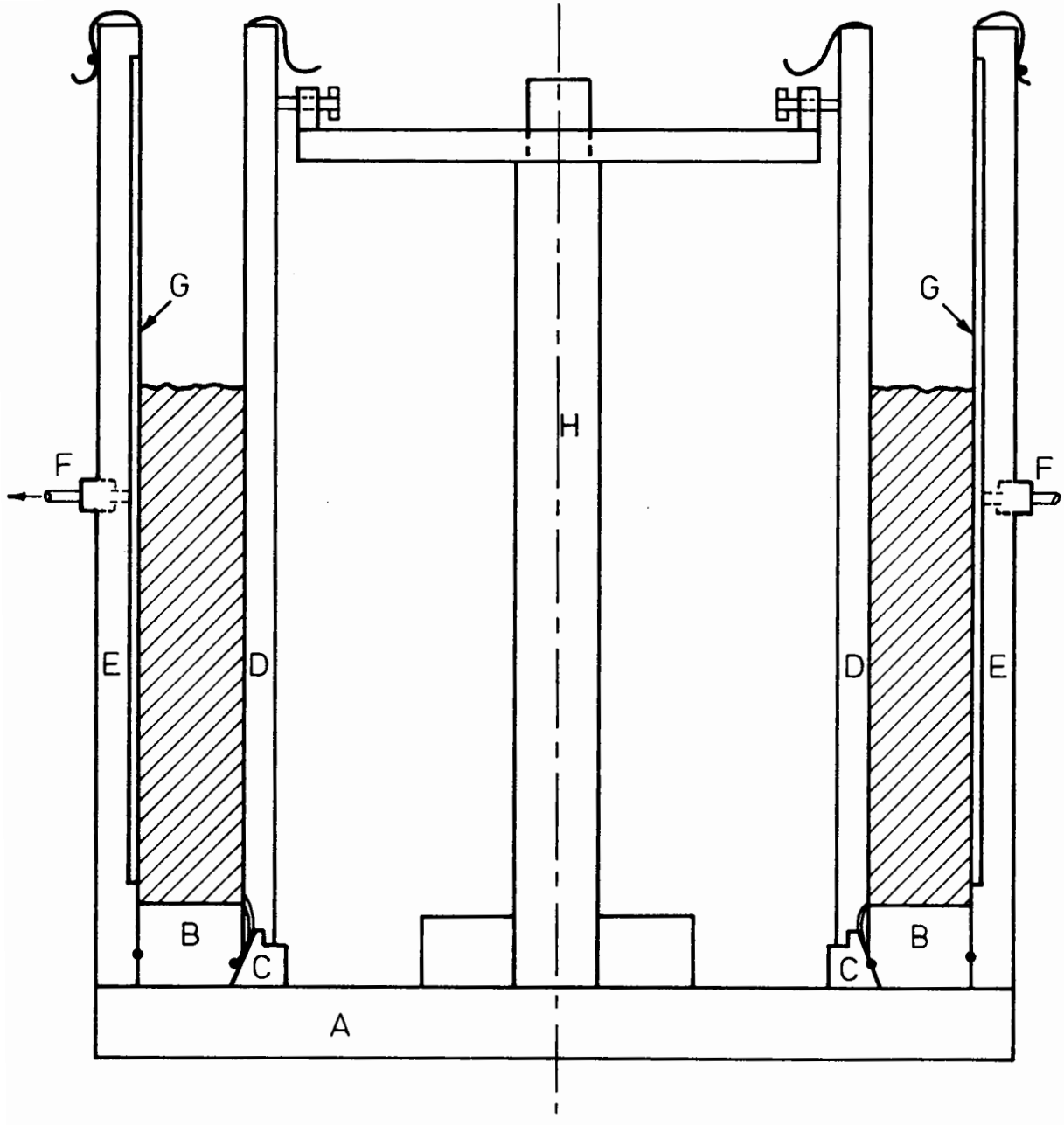

Fig. 8·2 Sample Arrangement During Assembly
(Not to Scale)

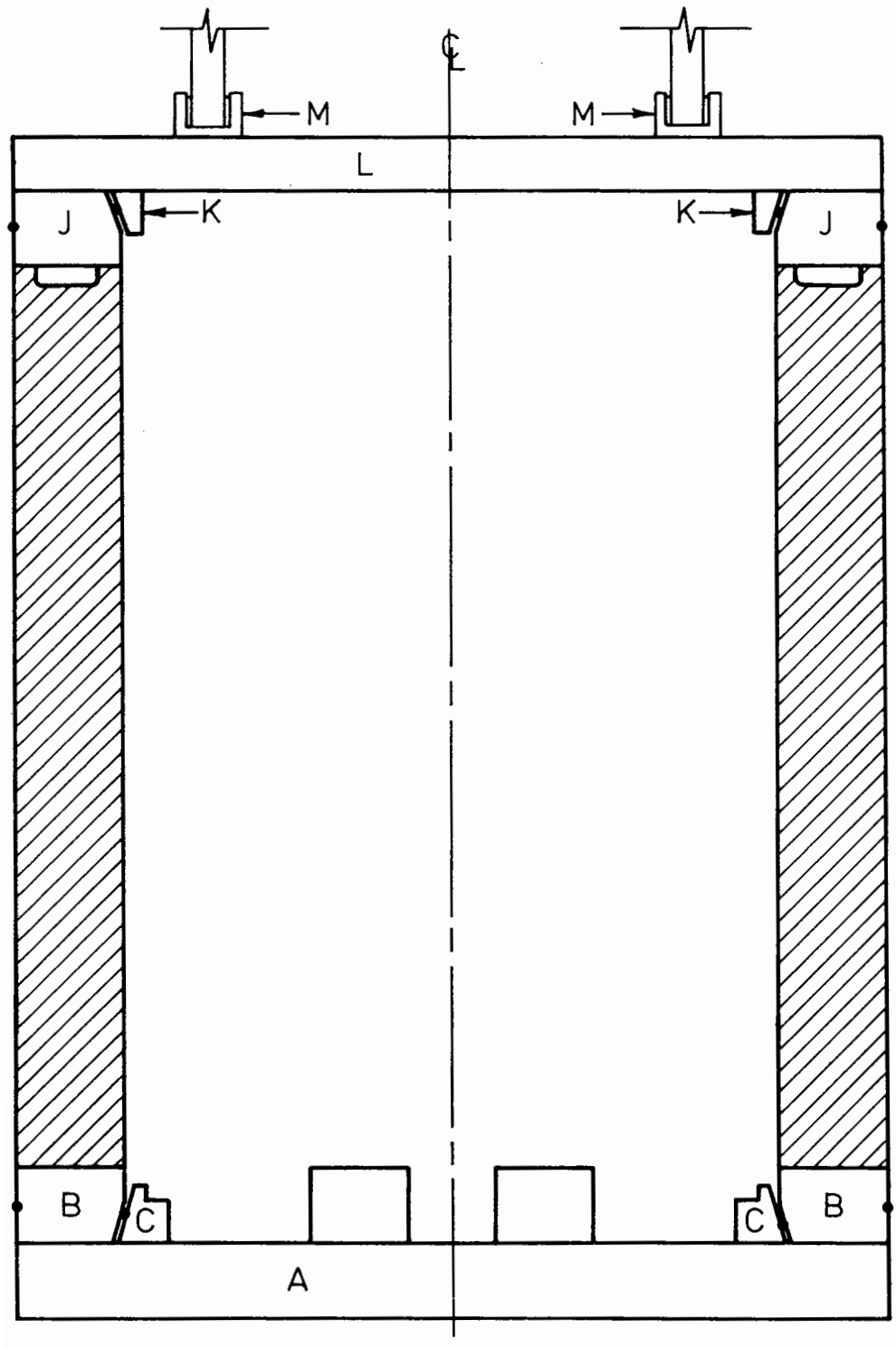

Fig. 8.3 Sample Arrangement After Assembly (Not to Scale)

with "blades" which can be pushed into the material to transfer the torsion. The outer membrane is attached by fitting it around the top platen (J) and sealing with an 'O' ring in the groove. The inner membrane is pulled up. To seal this, a top ring (K) with an 'O' ring is placed down on the platen (J) and this ring (K) is held down with three small clamps. An internal vacuum is then applied to the sample interior so that it may stand freely when the moulds are removed.

The external mould (E) may be removed simply by unscrewing the "jubilee clips" which hold it together and removing one piece at a time. The internal mould (D) is partially collapsable. Three knurled knobs hold the mould (D) in a cylindrical shape during sample assembly. By unfastening these, the mould (D) may be collapsed enough to be removed through the opening available at the top. Once the moulds have been removed, the top plate (L) is placed on the platen (J) and top ring (K) and is firmly attached by bolts.

The three connectors (M) to which the load cell will be attached and through which the loads will be applied to the sample are fixed to the top plate.

The base plate (A) is mounted on rails. Using an air pressure "hovercraft" arrangement, the sample can be moved without shock-loading to the testing position. When in position, the loading rod and load cell are lowered, so that its "feet" are within the cavities of the connectors (M) which are filled with an epoxy resin. When the resin hardens, the test may be performed.

Instrumentation is dealt with in Section 8.8.

8.7 STRESSES IN THE HOLLOW CYLINDER APPARATUS

8.7.1 General Stress States and the H.C.A.

The stress at any point has six independent components. There are two main ways of representing a state of stress. Using the first method, the normal shear stresses on three orthogonal planes parallel to an existing co-ordinate framework, are required. The second involves giving the magnitudes of the three principal stresses and their directions relative to an existing co-ordinate framework. When an increment of stress is applied which is not co-axial with the existing stress state (i.e. the directions of principal stresses in the increment are not the same as the original stress state), then the direction of the principal stress must change. A principal stress direction is one perpendicular to which there is no shear stress. If the increment is not coaxial with the initial state, then a component of shear stress acts at right angles to the initial principal stress directions. The resultant principal stress direction will consequently rotate.

Continuous principal stress rotation is not possible in the standard triaxial apparatus as there is no facility for applying non-coaxial stresses. The H.C.A. provides the cell pressure and axial stress, which are already a feature of the standard triaxial apparatus, but is also able to apply a torque which is non-coaxial with the axial load. The H.C.A. is not, consequently, subject to the same "no-stress-rotation" limitation.

8.7.2 The Principal Stress Directions in the H.C.A.

Because the rubber membranes enclosing the sample are incapable of transmitting a shear stress to the internal or external cell fluid (air in this case), the radial direction corresponds to a principal stress direction. Generally, it is found to be the intermediate principal stress,

σ_2 but may be σ_3 in some situations. With one principal stress remaining constantly in the radial direction, it is evident that to maintain mutual orthoganality of axes, the directions of both σ_1 and σ_3 must rotate by the same angle (denoted by α) in a direction perpendicular to the sample radial direction. Thus, the rotation of principal stresses in the H.C.A. is defined by a single angle α.

8.7.3 Magnitude of Stresses in the H.C.A.

Fig. 8.4 (a) shows the stresses acting on a section of wall. The average stresses acting on the element are given by:

$$\text{vertical stress } \sigma_z = \frac{W}{\pi (b^2 - b^2)} + \frac{p_o b^2 - p_i a^2}{(b^2 - a^2)} \qquad (1)$$

$$\text{radial stress } \sigma_r = \frac{(p_o b + p_i a)}{(b + a)} \qquad (2)$$

$$\text{circumferential stress } \sigma_\theta = \frac{p_o b - p_i a}{(b - a)} \qquad (3)$$

$$\text{shear stress } \tau_{\theta z},\ \tau_{z\theta} = \frac{3M_T}{2\pi (b^3 - a^3)} \qquad (4)$$

where, W = axial load

M_T = torque load

a, b = internal and external sample radii

In order to calculate principal stress magnitudes and directions it is useful to construct the Mohr Circle representation of stress. The relationship between shear and normal stress is clearly indicated in

Fig. 8.4(b). The normal stresses σ_θ and σ_z (the tangential and vertical stresses) are both associated with shear stress $\tau_{\theta z} = \tau_{z\theta}$. σ_1 and σ_3 are defined by the semi-circle which intersects both points (σ_θ, $\tau_{\theta z}$) and (σ_z, $\tau_{\theta z}$.

As has been stated already, the value of σ_2 is equal to the cell pressure. Thus the three Mohr's circles shown in Fig. 8.4(b) define the possible stress states in the HCA. The angle α is also given by the Mohr circle diagram as the angle from the normal stress axis to the point (θ_θ, $\tau_{\theta z}$). Thus when $\tau_{\theta z} = 0$ (i.e. $M_T = 0$, see equation 4 above) $\alpha = 0$, which indicates that the orientation of σ_1 from the vertical (and σ_3 from the horizontal) is 0.

In work involving three independent (or at least different) principal stresses it is useful to describe the relative proportions of the stresses by a single number. A common example of this is the use of b, where:

$$b = (\sigma_2 - \sigma_3)/(\sigma_1 - \sigma_3) \qquad (5)$$

In the standard triaxial apparatus the values of b are 0 for compression tests and 1 for triaxial extension. No intermediate values are possible. In the HCA, however, σ_2 will not in general be equal to either σ_1 or σ_3 and so the b value will lie in the region $0 \leqslant b \leqslant 1$.

8.7.4 Stress Non-Uniformity in the HCA

There are three main souces of stress non-uniformity:

(a) Sample imperfection

(b) End-restraint at the platens

(c) Variation in shear stress across the sample wall

(d) Difference in internal and external cell pressure.

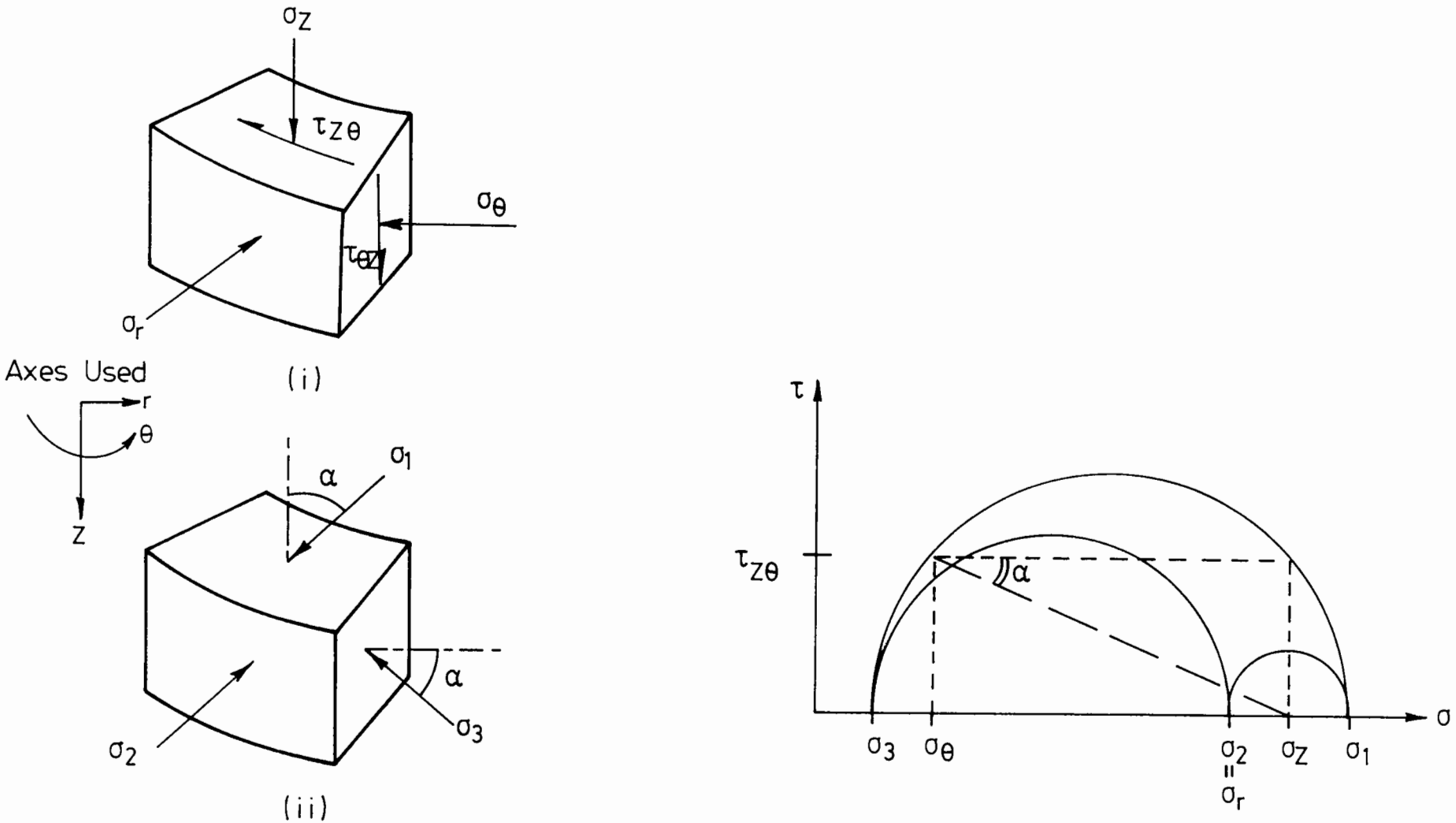

(a) Stresses Acting on an Element of Wall

(b) Mohr-Circle Representation of Stress in the H.C.A. Wall

Fig 8.4 Idealized Stress Conditions in the H.C.A.

Sample Imperfection: The degree of imperfection of any sample will depend primarily upon the quality of the sample preparation apparatus and technique. Each individual sample will also have its own unique imperfections.

When designing the apparatus, attention was paid to features most likely to affect the geometric quality of the samples.

The moulds, for example, were machined to close tolerances and the lining material for the outer moulds was chosen because of its uniform thickness. A central rod was fixed to the base plate and this serves as a datum from which deviation from the vertical can be measured and, if necessary, corrected.

End-Restraint at the Platens: In the standard triaxial apparatus, various methods are used to reduce friction and restraint at the platens. In the HCA, however, some form of restraint is obligatory, otherwise the torque cannot be transmitted across the platen/sample interface.

Hight et al (1983) describe the results of linear elastic computer analyses which model the stress non-uniformity when a hollow cylindrical sample with fixed ends is loaded. The results show that the non-unformity is largely confined to the ends of the sample. From these analyses the designers of the Imperial College HCA felt confident that a reasonably uniform stress distribution could be achieved in the central zone. By instrumenting this zone the stress distribution could be considered as relatively free from end-restraint effects. As noted in Section 8.5.1, Hight (1983) indicated that, with the benefit of hindsight, an increased sample height would have been desirable. Saada and Townsend (1981) also consider an increased sample height to be advantageous. The height to diameter ratio of the HCA under construction at Nottingham is greater than that of the Imperial College apparatus (1.8 compared to 1.0). There is one

further point to make concerning the possibility of using a friction reducing layer on the platens. The Imperial College HCA is designed for use with pore water. The porous drainage layer at the platen is fairly rough and provides a key with which the test material interlocks, thereby transmitting torque. In the HCA under construction at Nottingham, however, the platens are machined flat. The transmission of torque is made possible by radial grooves (in the case of the bottom platen) or blades (in the case of the top platen). Properly lubricated, they will allow the sample to deform radially, yet provide an effective resistance to circumferential slip, so that the torque may be applied.

Variation in Shear Strain across the Sample Wall: When a torque is applied to the sample, shear stresses will be set up in a circumferential direction. In general, if the sample remains as a hollow cylinder (i.e. does not undergo an unexpected mode of deformation), the resulting shear strain in a given element of material in the sample wall will be proportional to the distance from that element to the shear centre (i.e. the vertical axis of symmetry). This means that there will be a linear strain gradient across the sample wall. In a material with linear stress-strain characteristics this would also result in a linear stress gradient. In a non-linear material, however, the relationship between stress and distance from the shear centre will depend upon the material's constitutive laws.

The calculation of shear distribution during testing of granular materials in the HCA is further complicated by the fact that the material behaviour will be dependent upon many factors especially the mean normal stress, which increases the material stiffness. If, however, the mean normal stress (etc.) is kept constant while the torque is increased, an attempt can be made to calculate the stress distribution. Where the

material is non-linear, and where shear stress and strain are related in the following way:

$$q = a\ \epsilon_s^b, \qquad (6)$$

then it can be shown that the shear stress at a particular radius (r) is given by $q(r) = k.r^b$, where k is a constant for the sample geometry. In the case of granular materials $b < 1$, (results from triaxial tests on Denstone indicate that 0.4 might be an appropriate value) and consequently the stress distribution will be more uniforms than for a linear material (for which $b = 1$).

The Difference between the Internal and the External Cell Pressure: it has been shown (see Chapter 4) that the value of b, the intermediate stress ratio, is an important parameter. If the internal and external cell pressures are kept equal, then the value of b will change as torque is applied (b will, in fact, be $\sin^2\alpha$). In order to test at constant b value, it is necessary to introduce a slight pressure difference across the wall. This difference is normally very small: it does, however, cause a degree of stress non-uniformity.

8.8 INSTRUMENTATION

8.8.1 Measurement of Loads and Stresses

The stress state in the sample can be determined from the axial load, torque and cell-pressure. The "cell-pressure" is measured by a vacuum gauge connected to the internal void space of the sample. The load and torque are measured by a simple strain gauged load cell shown in Fig. 8.5.

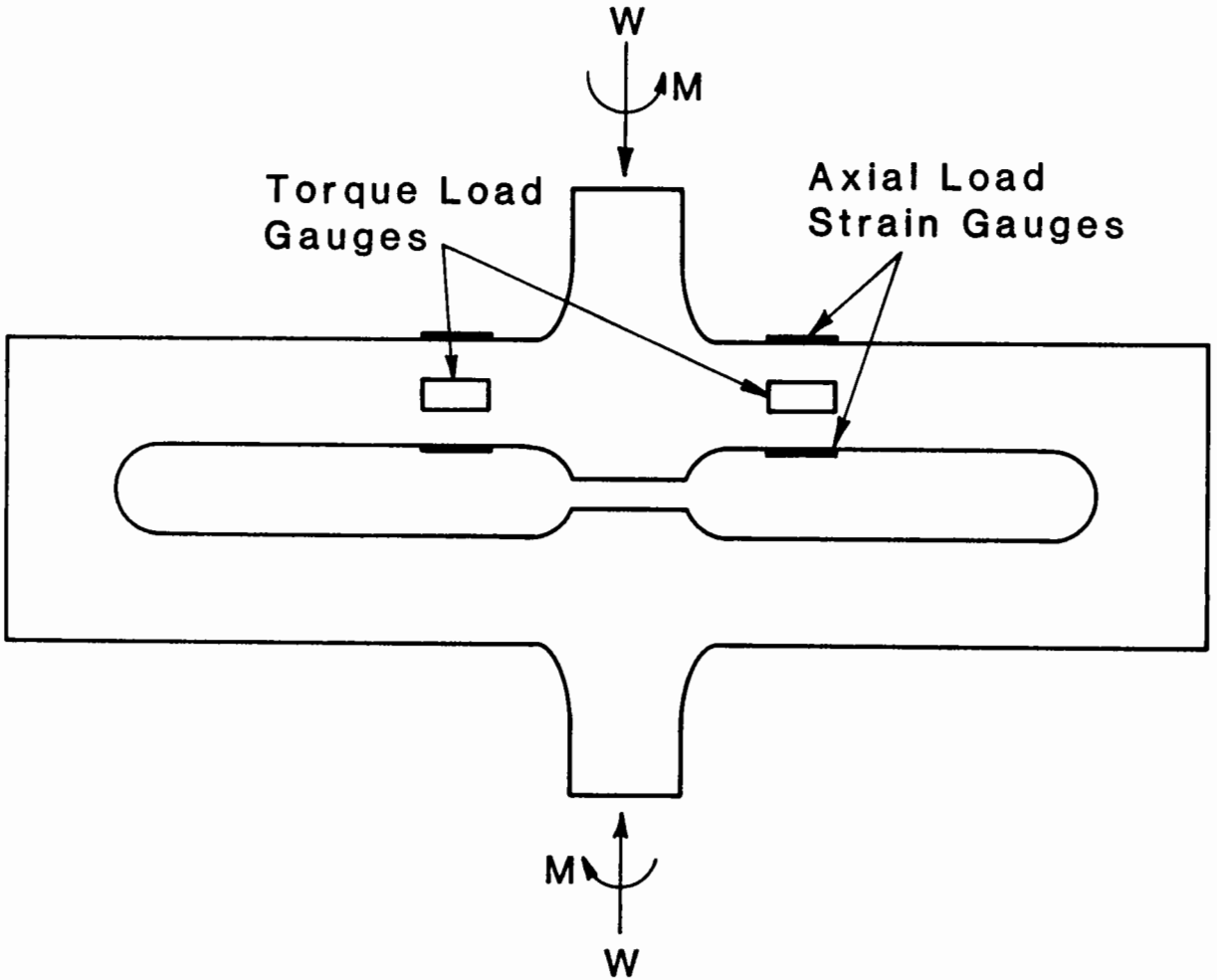

(a) Load Cell Elevation

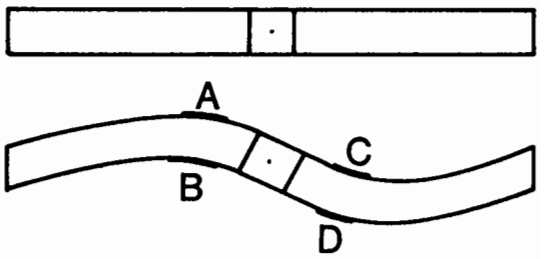

(b) Mode of Torsional Deformation

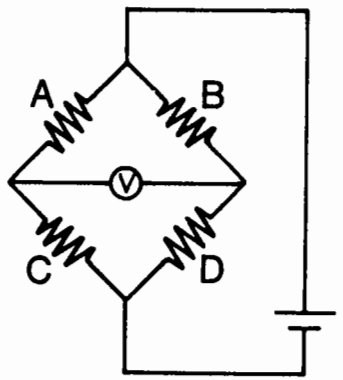

(c) Bridge Arrangement on the Torque Cell

Fig. 8.5 H.C.A. Load Cell

Axial loads are measured by the strain gauges on the top and bottom faces of the spokes. Torques are measured by the strain gauges on the sides. The load cell is made of high-yield aluminium. The advantages of using this material rather than steel include its relatively low Young's modulus and greater ease of machining. On the other hand aluminium has relatively poor fatigue properties, but this disadvantage is not considered a serious one.

Preliminary testing of the load cell indicates that "cross-sensitivity" (i.e. pure torque causing change of output in the axial circuit or vice versa) is not likely to constitute a problem.

8.8.2 Measurement of Strain

Three measurements are required to construct the complete strain behaviour:

(a) The change in sample thickness

(b) The overall change in sample diameter

(c) Axial deformation

(d) Torsional deformation

Measurement of Wall Thickness: The sample wall has an initial thickness of 28mm. Thus, to measure small strains (50$\mu\epsilon$) the measuring system must be capable of resolving to within 1.4μm. Furthermore, additional problems arise as one side of the wall is obviously isolated from the other.

At Imperial College, the system used to overcome these difficulties is shown in Fig. 8.6(a). Two inductance proximity transducers measure the distance of pieces of metal foil glued to the membrane on opposite sides of the wall. The deformation of the wall is calculated by the addition of these two measurements. The reported resolution of this arrangement (Hight et al, 1983) is 1μm. The cost of purchasing the required transducers and

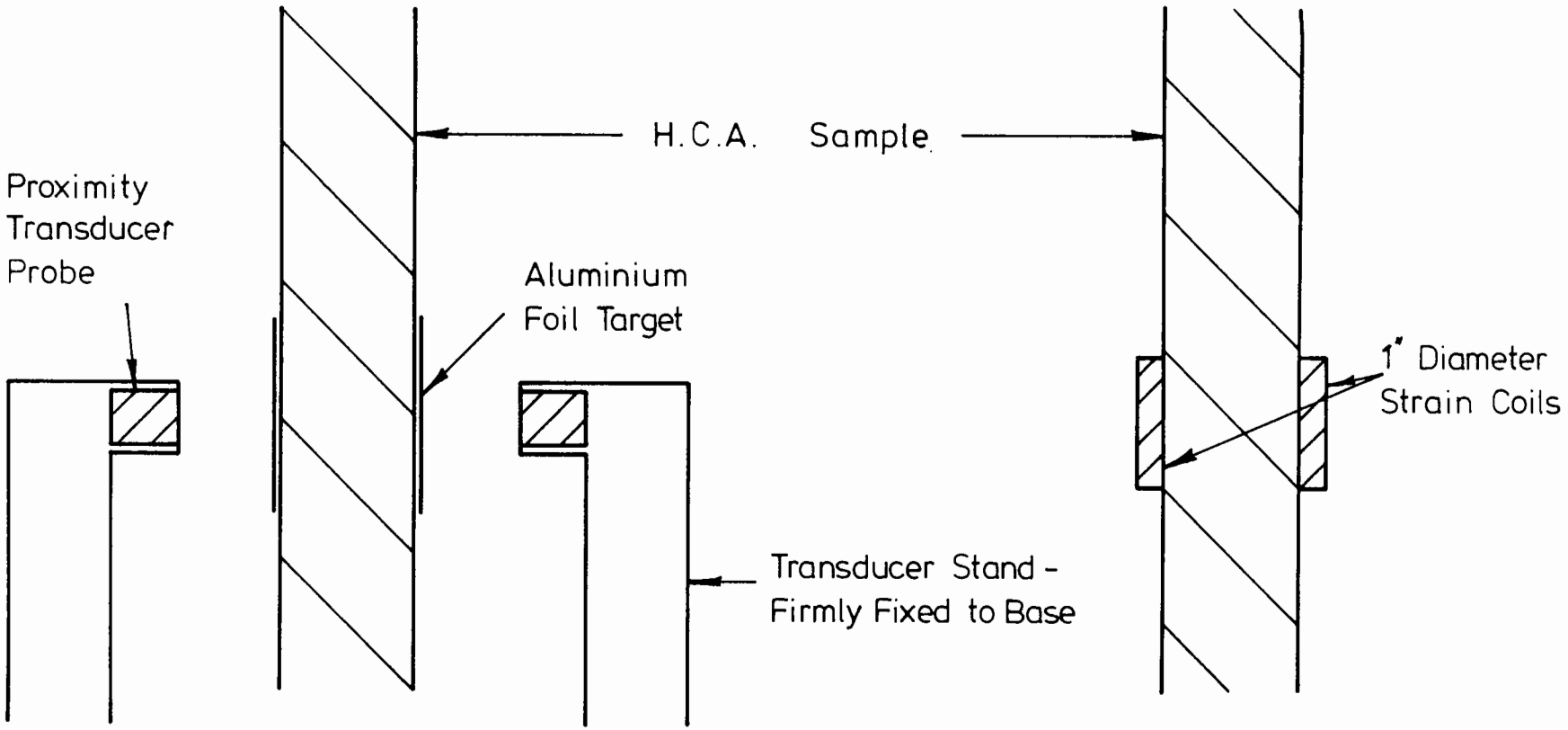

(a) Imperial College Radial Deformation Measurement System

(b) Proposed Radial Deformation Measurement System

Fig. 8.6 Radial Deformation Measurement Systems

control equipment, however, was considered to be prohibitively high.

Alternatives were investigated and the one which has been adopted is shown in Fig. 8.6(b). Two 25mm inductance coils are attached to opposite sides of the sample wall. A known current flows in one coil and this induces a current in the other. Initial tests indicate that the high resolution required is easily obtainable.

It is also considered that this system has two major advantages over the proximity transducer arrangement as used at Imperial College.

(a) The proximity transducer method requires two independent measurements to arrive at a value for the deformation. A loss of resolution and accuracy may occur in the addition circuits. Only one measurement is made in the strain coil method.

(b) In the proximity transducer method, errors may arise because of imperfections in the sample. Fig. 8.7(a) shows a section through the sample wall with an exaggerated scale in the radial direction. The distortion illustrated may be a local effect or may be due to non-concentric setting-up of the sample, as illustrated in Fig. 8.7(b). Even small distortions may give rise to appreciable errors and the apparent values of deformation may be several times the actual values as demonstrated in Appendix E. The system using strain coils mounted on the sample overcomes this problem. The coils measure the same element of material at all times and so the deformations which are measured are likely to be much more accurate, especially during small deformations.

<u>The Overall Change in Sample Diameter</u>: it is proposed that changes in the sample diameter would be measured using a system similar to that used for measuring radial strains in the large triaxial apparatus. The external pair of strain coils which monitor changes in wall thickness can be used in

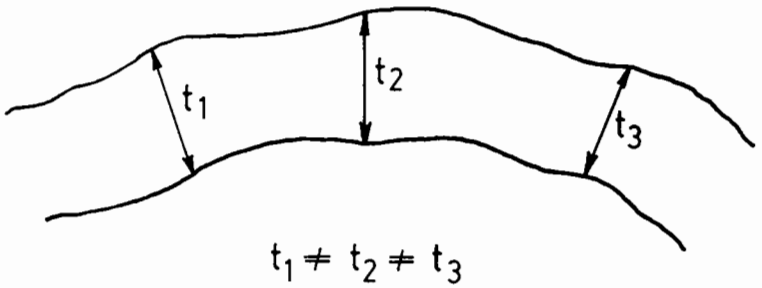

(a) Local Variations in Sample Thickness (Exaggerated)

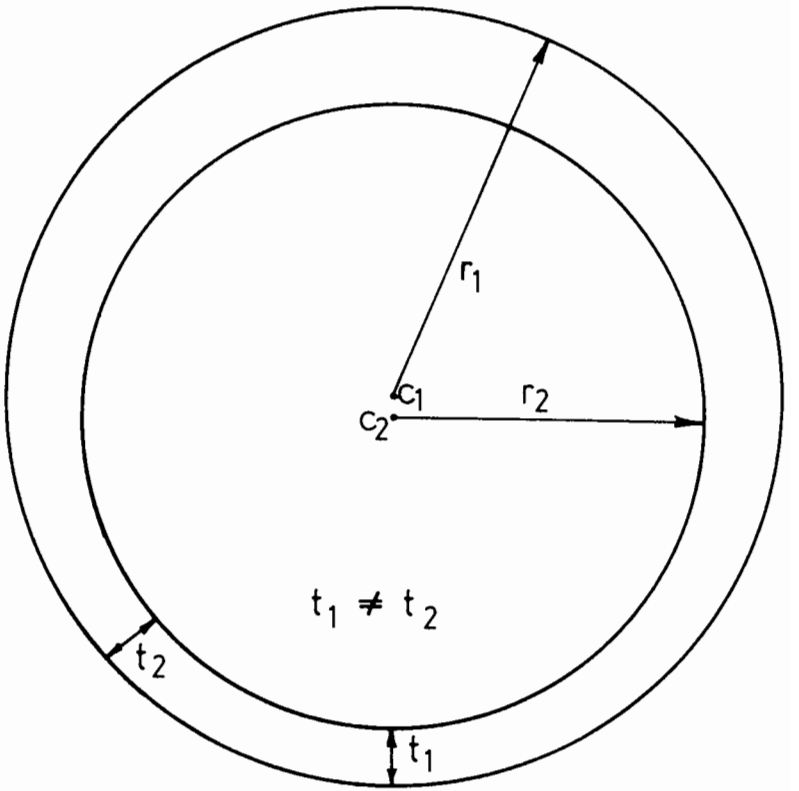

(b) Effect of Non-Concentric Setting-up on Sample Thickness

Fig. 8.7 Variation in H.C.A. Sample Thickness

conjunction with a pair of 4" diameter strain coils to determine the overall radial dimension. Like the Imperial College radial strain measuring system, this present arrangement is open to critism because of its requirement fo two independent measurements and the possibility of sample imperfections causing measurement errors. When measuring the external dimension, however, these sources of inaccuracy are not so important because the gauge length is so large - in this case ten times the wall thickness.

A Note on the Use of Strain Coils: some doubts have been expressed about the use of strain coils in dynamic testing (eg. private communication from Loach 1985). It has been suggested that dynamic calibrations may not be equal to those obtained under static conditions. It is not clear why this should be so, especially in view of the fact that these instruments operate at a frequency of 5 kHz. If, in the future, it proves to be impossible to use strain coils for measurement, they may be useful for maintaining "plane-strain" conditions. To do this, the internal cell pressure would be cycled so that the non-deformation would occur in the radial direction: the strain coil arrangement, in this case, would be used to detect rather than to measure the deformations. This is clearly not as satisfactory as keeping the b value constant.

Measurement of Axial Strain: Axial strains may be easily measured by mounting LVDT's on the sample using studs in the same way as is presently used for the repeated load triaxial apparatus.

Measurement of Torsional Deformations: The system used at Imperial College to measure torsional shear deformations involves the use of liquid level inclinometers which are unsuitable for repeated load testing except at very

low frequencies.

Several methods have been advocated as suitable for the present requirements. The most promising method at the moment appears to be use of RVDT's (Rotary Variable Differential Transformers) which would be mounted on sample studs.

8.9 CONTROL

The control system used for the HCA is similar to that used for the repeated load triaxial apparatus (see Chapter 5). It is shown in Plate 8.1. The applied loads are controlled by means of a servo-control system linked into the actuators. Feed-back is provided by the load cell shown in Fig. 8.5. A Prosser waveform generator is used to supply a sinusoidal feedback control signal.

The system which has been designed to contol the variation in internal cell pressure is simply an electric motor operating at a constant frequency which is linked to a pressure regulator. This provides pressure to a pair of small bellophrams which then apply load to a piston. This in turn causes a sinusoidal suction pressure to be experienced by the internal cell pressure. An electric motor with a frequency of about 0.3 Hz was chosen: at this frequency, it will be extremely easy to match in the sinusoidal outputs from the servo-actuators with the cyclic suction pressure.

This very simple arrangement was considered suitable for the small number of stress-controlled tests which it was hoped to carry out during this project. The complexity of the equipment, and the number of parameters that will have to be dealt with simultaneously, however, mean that the control system described above will be most unsuitable for an advanced testing programme. If strain-controlled testing were to be undertaken, for example, computer control would be almost essential.

8.10 FUTURE TEST PROGRAMME

The HCA will make it possible to investigate three aspects of sample behaviour which the standard triaxial apparatus could not. These are:

(a) the effect of principal stress rotations

(b) the effect of the intermediate stress parameter b

(c) anisotropy

The following test programme is suggested:

(a) Isotropy testing

It is important to ensure either that the sample preparation method yields isotropic samples or (if this proves impossible), that the anisotropy is quantified. The resilient models described in Chapter 6 can be derived for a number of different constant principal stress directions. This can be achieved most easily by first applying only axial loads (i.e. no torque loading), so that σ_1 is vertical (or horizontal when the axial load is negative). Tests can then be repeated using only torque loads. In the latter case, the direction of the principal stress will be constant at an inclination of 45° to the vertical.

It is important to keep α and b constant in order to isolate effects due to anisotropy. It will be seen, however, in the tests suggested above that:

b = 0 when α is 0

b = 0.5 when α is 45°

b = 1.0 when α is 90° (i.e. when the major principal stress is horizontal)

The best solution to this problem is to avoid using negative deviator stresses and to cycle the internal cell pressure so that b = 0.25 (for

example) in both of the other cases.

If a similar (or related) resilient strain model can be produced from testing in a range of directions then this will show whether or not the sample is isotropic, and if it is not, the degree of anisotropy. It will also inspire confidence in the results produced in the apparatus.

(b) The Effect of the Intermediate Stress Parameter, b

It is possible to carry out a series of very simple tests in which the values of both α and b are held constant, and where the value of b is different in each test. A model should be produced to describe the effect of the value of b (when constant) on resilient behaviour. The model proposed in Chapter 6 (the Lade-Duncan failure criterion extension) may be found adequate.

Having performed tests at constant b, it will be necessary to investigate the effect of changing values of b. It is suggested that b should be altered during the load cycle while keeping α constant. This could be done, for example, by applying only axial or torque loads, and cycling the cell pressure so that the value of α remains constant (at either 0° or 45°) while b changes from b_1 to b_2. These tests would show whether or not the model produced to describe the effect of the value of b (at constant b) was of the "contour" variety, i.e. whether or not the strain contours produced for discrete b values could be used to predict strains along a stress path in which b changes. In Fig. 8.8(a), for example, a 3-D-Constant-α "slice" from (α, b, η, p) space is shown. Two resilient shear strain contours are shown - $200\mu\epsilon_s$ at b = 1 and $200\mu\epsilon_s$ at b = 0, as well as a stress path AB between them. In Fig. 8.8(b), this can be seen projected onto b = 0. If the model derived using constant b values is of the "contour" variety, then the shear strain in the sample should not have changed between A and B.

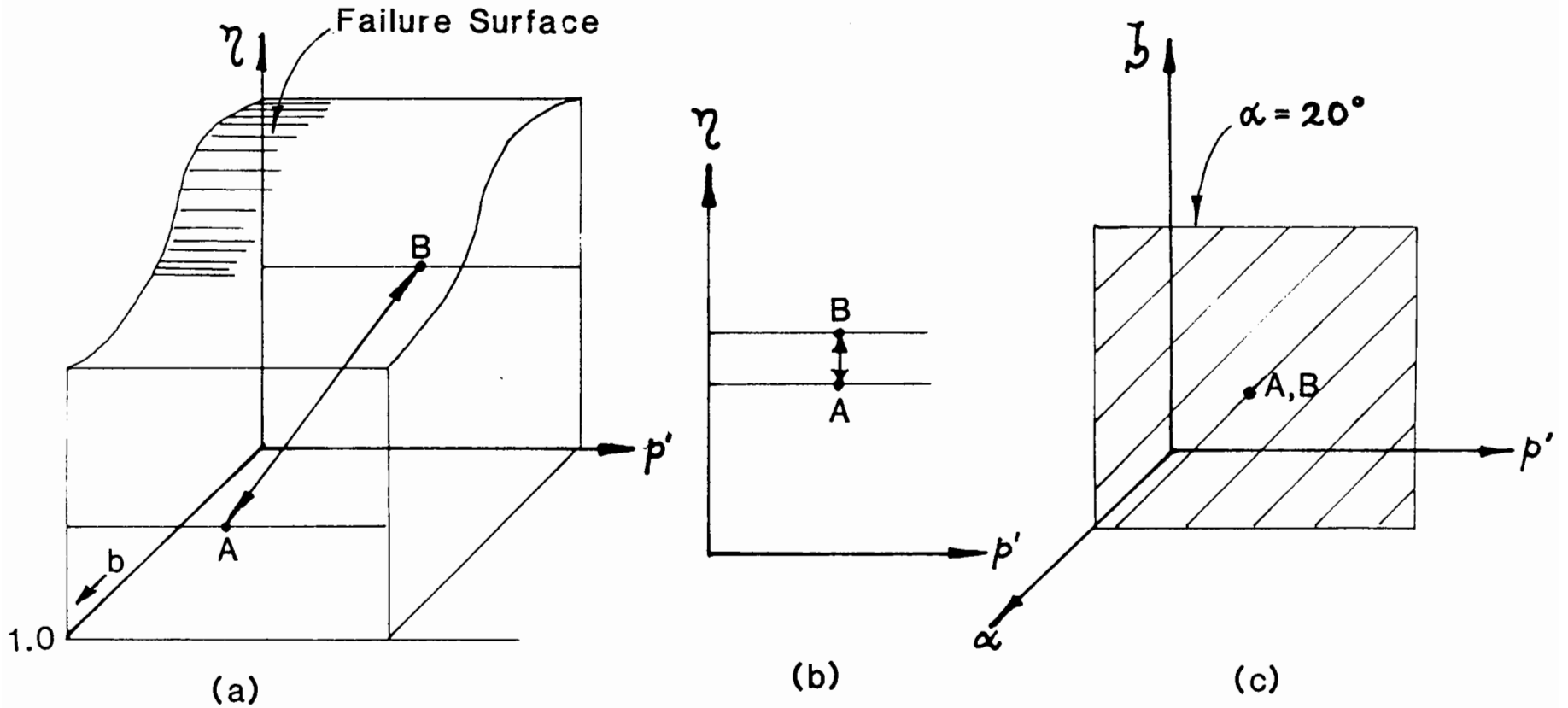

Fig 8.8 INCORPORATING THE INTERMEDIATE PRINCIPAL STRESS RATIO INTO THE RESILIENT MODELS

If the model can be extended in this way, it will be possible to reduce the 4-D (α, b, η, p) space to the 3-D (α, ζ, p) space, where is the stress ratio, modified to account for the b value. If, for example, Fig. 8.9(a) showed the $\alpha = 20°$ slice, then Fig. 8.9(c) would show the full (α, ζ, p) space with points A and B coincident.

It must be noted, however, that even if the b value model can be built into the parameter η when α is kept constant, it cannot be known at this stage whether this new model will be valid when α is changing. It is quite possible that changing b and rotating the principal stresses simultaneously will cause "cross-interference". This is discussed in (d) below.

(c) Principal Stress Rotation

The main purpose of constructing an HCA is to carry out tests in which principal stress rotation occurs.

In order to isolate the effect of principal stress rotation, b should be kept constant over a range of tests. The influence of the magnitude of $\Delta\alpha$ on stiffness and other aspects of behaviour can be calculated.

It is important to note that although in mechanics it is normally assumed that stress and strain directions coincide in a linear-elastic isotropic material, this will not generally be the case for granular materials. Work at U.C.L. (Wong and Arthur) 1985) and Imperial (eg. Symes et al 1983) shows that the direction of strain increments may lag behind that of the stress increment (see Chapter 4.3.6.2). This means that the model will now have to take into account not only the magnitude but also the direction of strain increment.

(d) Combination Stress Paths

Having independently isolated the effects of variable values of α and b, it should be possible to apply "combination" stress paths in order to

determine any "cross-influence", i.e. to discover whether a rotating principal stress system affects the influence of the b value, or vice versa. This could be tested using a series of stress paths with values of b which are fluctuating but which are all projected onto an identical path in (ζ, p) space; this series could be repeated for each of a range of different stress rotation magnitudes. If the resulting strains are those predicted by the combination of the two independent models for α and b, then it is possible to conclude that the rotation of stresses does not affect the b model, i.e. there is no cross-influence.

8.11 CONCLUSIONS

As part of this project, an HCA has been constructed at Nottingham. Although it has not yet been used for testing, it is now ready for "proving-testing".

The various problems inherent in the HCA (eg. a slight stress non-uniformity, complex control requirements etc.) have been described in this chapter. The emphasis, however, is upon the flexibility of the apparatus, and its ability to test granular materials along stress paths that no other apparatus can so far accommodate.

CHAPTER NINE

CONCLUSIONS

9.1 TES BEHAVIOUR

A simplified analysis of the sources of stress generation with a TES was undertaken. It was shown that principal stress rotation is an important factor to be taken into account. The possible problems associated with pressure loss within the TES and with racheting were also discussed.

9.2 MATERIAL TESTS

Density and water absorption tests were carried out on the Denstone and Iron Oxide materials. The iron oxide was found to be 1.6 times as dense, and approximately 15 times more absorbent than Denstone of an equivalent particle size.

A series of tests were carried out to determine the surface friction of the Denstone material. The friction coefficient appeared to be a function of both the surface conditions (wet or dry) and the normal load (although there are doubts about the experimental procedure). It appeared from the experimental tests that this variation in surface friction did not have a very large effect on the shear strength of the en masse material.

Compaction tests were performed on all materials (except modified Denstone). The results show that there are two stable random packings which may be nominated, dense and loose packing. Container surface effects proved to be of significance and the results obtained were extrapolated to give material denstities at lower surface area to volume ratios than are possible in small scale laboratory testing. It was shown that higher densities are achieved if the surface effects are reduced by a container

with an uneven surface, and in such containers densities near to the extrapolated maximum were achieved.

9.3 APPARATUS DEVELOPMENT

9.3.1 Large Triaxial Apparatus

Burrette volumetric deformation measuring system: in order to measure behaviour at large volumetric strains, a water-burrette measuring system was developed.

Reduction of platen friction: end-platen friction has been investigated with the conclusion that for large rounded particulate materials, a polythene lubricating layer gives lower friction than the traditional latex membrane, especially at higher normal loads. In an attempt to completely eliminate platen friction, coned platens were used in test series B and C.

High resolution deformation measuring systems: when it was realised that behaviour at small strains was important, new deformation instrumentation systems were installed:

(a) Axial Strains

Testing involved an on-sample system using brass location studs which had been developed for the repeated load triaxial apparatus. Initially, linear potentiometers were used to measure deformations between the location studs (series B), but these were later replaced by a LVDT system (series C).

(b) Radial Strains

A system using inductance strain coils was installed. This enabled a much greater resolution to be achieved. It was noticed, however, that there was a tendency for small random variations in output to occur. These were usually small compared to the total measured output, but at very small strains ($<100\mu\epsilon$) they became very significant.

Disruption of pebble-packing at sample wall: in order to disrupt the tendency of the pebbles to form a regular packing at the sample wall, a dimpled mould-liner was used when forming specimens.

9.3.2 Repeated Load Apparatus

Several of the above developments were incorporated in the repeated load apparatus testing procedure. These included the use of polythene membranes to reduce platen friction, and dimpled mould-liners to disrupt the packing at the sample wall.

Apart from these, and a few other minor alterations, the repeated load apparatus remained substantially unchanged.

9.3.3 Hollow Cylinder Apparatus

In order to perform repeated loading tests in which the principal stress directions would rotate, a completely new piece of equipment was designed and has been substantially completed - the Hollow Cylinder Apparatus. Axial and torque loads are applied to a hollow cylindrical sample using hydraulic servo-controlled actuators. The apparatus is discussed in detail in Chapter 8.

Unfortunately, it has not proved possible to use the HCA for testing. It is hoped that it will be used in the very near future and will produce results which will be applicable to the TES problem.

To supplement this large HCA, a small HCA was constructed and used for testing. It was considered that the results from this piece of apparatus were most unsatisfactory, and that they have not added to the understanding of granular material behaviour during principal stress rotation.

9.4 TEST RESULTS

Lists of samples tested in the large triaxial apparatus and the repeated load apparatus are given in Tables 6.1 and 6.11 respectively.

9.4.1 Monotonic Testing

Material Strength: The Series A tests indicated that the strength at failure of Denstone was η (q/p') = 1.5. Tests carried out since then have not reached this value; they were terminated before such strengths could be mobilized. The average strength at 1% axial strain was found to be η = 1.27 which is 85% of the expected maximum value of 1.5.

Testing was carried out on iron oxide pellets. The strength at 1% axial strain was recorded as η = 1.76. This is significantly higher than the strength of Denstone aggregates.

Using a sample which had been used for repeated load testing, an axial strain controlled monotonic strength test was carried out (Boyce, 1976 and Shaw 1980 have also shown that pre-failure cycling only has a slight effect on the failure strength). The maximum strength recorded was η = 1.7.

(a) Effect of Grading

Testing was performed in which equal weights of 6mm, 9mm and 19mm Denstone particles were mixed and tested. The strength of this aggregate at 1% axial strain was η = 1.32 which is 4% more than the average value for the single-size material.

(b) Effect of Particle Size

The results appeared to show a tendency for materials composed of larger particles to exhibit slightly higher strengths. It was felt that this might be connected with the inability to compact the larger particles as successfully as the smaller ones, rather than being an inherent material

property.

Dilatancy: During monotonic loading, Denstone aggregates changed from compressive to dilatant behaviour at an average value of $\eta = 1.04$ ($\Phi' = 22°$), $\epsilon_s = 2.2m\epsilon$. The values recorded during the test on iron oxide were $\eta = 1.60$ ($\Phi' = 34°$) and $2.6m\epsilon$.

When the aggregates began to dilate, the rate of dilation ($D = d\epsilon_v/d\epsilon_s$) appeared to remain fairly constant. The average value recorded for Denstone was $D = 0.58$. For the test on iron oxide a value of $D = 0.65$ was recorded.

Materials Stiffness: The tests from Series A indicated a very low initial stiffness relative to the ultimate resilient stiffness. Tests performed after the new on-sample instrumentation was installed (series B and C), however, showed much greater stiffnesses, and these could be realistically compared with the results from resilient tests.

During testing of a graded sample (an aggregate of three sizes of Denstone), a much higher initial stiffness was recorded than for single-size materials. After several millistrain, however, the disparity between mixed-size and single-size sample stiffnesses diminished considerably.

The results tend to indicate that aggregates of larger particles exhibit higher stiffnesses, particularly during the first few millistrain of loading. The explanation for this may be similar to that given for the difference in strength between large and small particle aggregates.

Only one test was carried out on iron oxide and, unfortunately, no measurements were made at very small strains. It appeared, however, to exhibit greater stiffness than the Denstone materials. In addition, the iron oxide seemed to develop a higher proportion of its ultimate strength at a given value of shear strain than Denstone.

9.4.2 Intermediate Behaviour

A range of tests was performed:

(a) Forced permanent strain tests

It was observed that the stress-strain envelope obtained from forced permanent strain tests was very similar to those obtained during monotonic tests. It also appeared that significant losses in unload-stiffnesses occurred as the magnitude of the forced strain increased.

During these tests, it was further noticed that:

$$\frac{d\epsilon_v}{d\epsilon_s \text{ (unloading)}} > \frac{d\epsilon_s}{de_s \text{ (loading)}}$$

(b) Stress and strain controlled tests

Both stress-controlled and strain-controlled tests were performed. The main observation was that the materials tended to increase in stiffness during both types of test. During the strain-controlled tests, it was observed that as the numbers of cycles increased, the radial strain had a distinctly positive (i.e. contractant) trend although the axial strain remained constant throughout.

(c) Stress history test

It was shown that the spring and sliding-block analogy advocated by Zytynski et al (1978) could be used to provide a rough model of behaviour as the material was cycled in both compression and extension space.

9.4.3 Resilient Behaviour

Empirical models were derived to predict resilient shear and volumetric strains for Denstone:

$$\epsilon_{sr} = 440\ (\eta_2 - \eta_1)\ \left[\frac{\ell_r}{p_m}\right]^{0.2} \cdot \left[\frac{|q_2 - q_1| + 2}{100}\right]^{0.2}$$

$$\epsilon_{vr} = 124\ \left[p_2^{0.48}(1 - 0.12\ (\eta_2)^3 - p_1^{0.48}(1 - 0.12\ (\eta_1)^3\right]$$

where $\ell_r = ((q_2 - q_1)^2 + (p_2 - p_1)^2)^{\frac{1}{2}}$

Similar models have been derived to predict the resilient behaviour of the modified Denstone material:

$$\epsilon_{sr} = 440\ (\eta_2 - \eta_1)\ \left[\frac{\ell_r}{p_m}\right]^{0.2} \left[\frac{|q_2 - q_1| + 2}{70}\right]^{0.2}$$

$$\epsilon_{vr} = 280\ \left[p_2^{0.42}(1 - 0.12\ (\eta_2)^3 - p_1^{0.42}(1 - 0.12\ (\eta_1)^3\right]$$

These models have been shown to successfully predict strains, although the correlation between predicted and observed volumetric strains was much weaker than for resilient shear strains.

The shear strain model derived for the modified Denstone was very similar to the Standard Denstone model. The volumetric strain model indicated that the bulk modulus of modified Denstone under isotropic mean normal stress was lower than that of Standard Denstone.

It was observed that during repeated loading dilation may occur. The stress ratio at which dilation began appeared to increase with the value of mean normal stress. At a mean normal stress of 200 kPa and with $\eta_1 = 0$, the value for Denstone was $\eta_D = 0.74$ and for modified Denstone it was $\eta_D =$

0.93.

During tests arond a closed loop, it was found that a resilient condition was achieved after a few cycles. Testing showed that the volumetric strains which occur during any part of the closed loop stress path A-B are not very dependent on the direction (i.e. clockwise or anti-clockwise) traced around the path. Shear strains were found to be affected, however, by the direction followed. This may be ascribed to stress path length dependency.

A sample of Standard Denstone was tested in both the dry and saturated conditions. The results were very similar, although shear stiffness appeared to increase very slightly when saturated. This showed that the behaviour of Denstone was not greatly affected by the presence of water.

9.5 A SIMPLIFIED DESIGN METHOD

A simplified design method for TES was developed, based on a "worst case" analysis. A parametric study was carried out to investigate the influence of a range of parameters. A large degree of interaction between the stresses in the granular material and in the container wall was shown to exist.

REFERENCES

Arthur, J.R.F., Chua, K.S. and Dunstan, T., (1977), 'Induced anisotropy in a sand', Geotechnique 27, No.1, pp.13-30.

Ansell, P., (1977), 'Cyclic simple shear testing of granular material', Ph.D. Thesis, University of Nottingham.

Bartel, J.J. and Skvarna, P.E., (1984), '10-MWE solar thermal central receiver pilot plant', Journal of Solar Energy Engineering, Transactions of the ASME, Feb. 1984, Vol. 106, pp.50-58.

Bernal, J.D. and Mason, J., (1960), 'The Co-ordination of randomly packed spheres', Nature Vol. 188, p 910.

Biarez, J., (1962), 'Contribution a l'etude des properties mechaniques des sols et des material pulverulents', D.Sci. Thesis, Universite de Grenoble.

Bishop, A.W., (1954), Discussion on Penman, A.D. (1953), Geotechnique 4, No.1.

Bishop, A.W., (1966), 'The strength of soils as engineering materials - The Sixth Rankine Lecture', Geotechnique Vol. 16.

Bjerrum, L., Landva, A., (1966), 'Direct simple shear tests on a Norwegian quick clay', Geotechnique 16, No.1.

Blight, G.E., (1983), 'Performance of a 20m diameter steel maize storage bin'. Paper communicated privately to Professor S.F. Brown.

Blight, G.E., and Midgeley, D., (1981), 'Pressure measured in a 20m diameter coal load-out bin', Journal of Power and Bulk Solids Technology, Vol. 5.

Bonnell, D.G.R. and Harper, F.C., (1951), Referenced in Neville (1981), below.

Borzdyka, A.M., (1984), 'Vestnik Mashinostroeniya' Reprinted in 'Elevated Temperature Testing of Metals', Israel Program for Scientific Translations, Jerusaleum, 1965.

Bowden, F.P. and Tabor, D., (1950), 'The friction and lubrication of solids', Oxford University Press.

Boyce, J.R., (1976), 'The behaviour of a granular material under repeated loading', Ph.D. Thesis, University of Nottingham.

Bridgewater, J. and Wroth, C.P., (1980), 'Report on mechanical problems to be expected with thermal energy storage in pebble beds'. Report submitted to the CEGB.

Bromwell, L.G., (1966), 'The friction of quartz in high vacuum', Sc.D. Thesis, MIT.

Brown, S.F., (1975), 'Sample end restraint and pore pressure measurement in cyclic load triaxial tests on Drammen Clay', University of Nottingham.

Caquot, A., (1934), 'Equilibre des Masifs a frottement interne. Stabilite des terres pulverulents et coherents', Paris, Gaunthier Villars.

Carter, J.P., Booker, J.R., and Wroth, C.P., (1982), 'A critical state soil model for cyclic loading', Soil Mechanics - Transient and Cyclic Loads Ed. Pande and Zienkiewicz, John Wiley & Sons.

Cassagrande, A. and Albert, S.G., (1930), Research on the shearing resistance of soils', MIT Report.

Charles, J.A. and Watts, K.S., (1980), 'The influence of confining pressure on the shear strength of compacted rockfill', Geotechnique 30, No. 4, pp.353-367.

Cooling, L.F. and Smith, D.B., (1936), 'The shearing resistance of soils', Proc. Inst. Civ. Eng., London.

Cornforth, D.H., (1964), 'Some experiments on the influence of strain conditions on the strength of sand', Geotechnique 17.

Coulomb, C.A., (1776), 'Essai sur un application des regles des maximis et minimus a quelques problems de statique relatifs a l'architecture', Mem. Acad. Roy. Pres. Divers. Savant, Vol.7, Paris.

Cowin, S.C., (1977), 'The theory of static loads in bins', Journal of Applied Mechanics 1977, Vol. 44, p 409.

Cowin, S.C., (1979), 'The pressure ratio in the theory of bin pressures', Journal of Applied Mechanics 1979.

Cundall, P.A., Drescher, A. and Strack, O.D.L., (1982), 'Numerical experiments on granular assemblies; measurements and observations', I.U.T.A.M. Conference on Deformation and Failure of Granular Materials, Delft.

Cundall, P.A. and Strack, O.D.L., (1979), 'A discrete numerical model for granular assemblies', Geotechnique Vol. 29, p 47.

Dantu, P., (1957), 'Contribution a l'Etude Mechanique et Geometrique des Milieux Pulverulents', Proc. 4th Int. Conf. on Soil Mechs., London, Vol. 1.

Darwin, G.H., (1883), 'On the horizontal thrust of a mass of sand', Proc. Inst. Civ. Engrs., London, Vol. 72 (1).

Drnevich, V.P. and Richart, F.R., (1970), 'Dynamic pre-straining of dry sand', Proc. ASCE, Vol. 96 SM2.

Dickey, J.W., (1966), 'Frictional characteristics of quartz', S.B. Thesis, MIT.

Finn, W.D.L. and Vaid, Y.P., (1977), 'Liquifaction potential from drained constant volume cyclic simple shear tests', Proc. 6th World Conference on Earthquake Engineering, New Delhi, 1977.

Friefeld, J.M., Moore, A.M. and Morgan, G.R., (1982), Proc. 17th Intersociety Energy Conversion Engineering Conf., L.A., Calif., August 1982.

Ghaboussi, J. and Momen, H., (1982), 'Modelling and analysis of cyclic behaviour of sands', Soil Mechanics - Transient and Cyclic Loads Ed. Pande and Zienkiewicz, 1982, John Wiley and Sons.

Gibson, R.E., Morgenstern, N., (1963), Discussion on Rowe (1963) Journ. Soil Mech. and Found., ASCE, Vol.89.

Glendenning, I., Chew, P.E., Grant, R., Glenville, R. and Moye, M.H., (1979), 'Technical and economic assessment of Advanced Compressed Air Storage (ACAS) concepts', Report to EPRI, Calif. USA.

Habib, P. and Luong, M.P., (1978), 'Sols Pulverulents sous chargement cyclique', Materiaux et Structures Sons Chargement Cyclique, Association Amicale des Inginieurs Anciens Eleves de l'Ecole Nationale des Ponts et Chaussess, 1978.

Hardin, B.O., (1965), 'The nature of damping in sands', Proc. ASCE, Vol. 91, SM1.

Hertz, H., (1881), j.f. reine v. angew, Math (Crelle) Vol.92.

Hicks, R.G., (1970), 'Factors influencing the resilient response of granular materials', Ph.D. Thesis, University of California.

Hight, D.W., (1983), 'Laboratory investigation of sea-bed clays', Ph.D. Thesis, University of London.

Hight, D.W., Gens, A. and Symes, M.J., (1983), 'The development of a new hollow cylinder apparatus for investigating the effects of principal stress rotation in soils', Geotechnique Vol. 33, 1983.

Horn H.M. and Deere, D.U., (1962), 'Frictional characteristics of minerals', Geotechnique, Vol.12.

Horne, M.R., (1965), 'The behaviour of an assembly of rotund rigid, cohesionless particles', (Parts I and II) Proc. Roy. Soc. Series A., Vol.286.

Horne, M.R., (1969), 'The behaviour of an assembly of rotund rigid, cohesionless particles', (Part III) Proc. Roy. Soc. Series A, Vol.310.

Janssen, H.A., (1895), 'Versuche vber Getreidedruck in Silozellen', Zeitschrift Verein Deutscher Inganieure, Vol. 39, 1895.

Jenike, A.W., Johanson, J.R. and Carson, J.W., (1973), 'Bin Loads - Part 2: Concepts', Journal of Engineering for Industry, Trans. ASME Series B, Vol. 95.

Josselin de Jong, G.de., (1976), 'Rowe's stress-dilatancy relation based on friction', Geotechnique Vol. 26, p 527.

Kirkpatrick, W.M., (1957), 'The condition of failure for sands', Proc. 4th Int. Conf. Soil Mech. and Found. Eng.

Kirkpatrick, W.M., (1965), 'Effects of grain size and grading on the shearing behaviour of granular materials', Proc. 6th Int. Conf. on Soil Mech. and Found. Eng. Vol.1.

Kjellman, W., (1936), 'Report on an apparatus for consummate investigation of the mechanical properties of soils', Proc. Int. Conf. Soil Mech.

Kolbuszewski, J. and Alyanak, I. (1964), 'Effects of vibration on the shear strength and porosity of sands', The Surveyor, May-June 1964.

Konishi, J., (1972), 'On the deformation mechanism of granular material', Referenced by Oda (1974).

Konishi, J., Oda, M., and Nemat-Nasser, S., (1982), 'Inherent anisotropy and shear strength of an assembly of oval cross-section rods', IUTAM Conf. on Deformation and Failure of Granular materials, Delft, 1982.

Ladd, C.C., Foott, R., Ishihara, K., Schlosser, F. and Poulos, H.G., (1977), 'Stress-deformation and strength characteristics', Proc. 9th Int. Conf. Soil Mech. and Found. Eng., 1977, Vol. 2.

Lade, P.V. and Duncan, J.M., (1973), 'Critical triaxial tests on cohesionless soil', Journal of Soil Mech. and Foundations, ASCE, Vol. 99, SM 10.

Lade, P.V. and Duncan, J.M., (1975), 'Elastoplastic stress-strain theory for cohesionless soil', Journal of Soil Mech. and Foundations, ASCE, Vol. 101, GT 10.

Leussink, H. and Wittke, W., (1963), 'The difference in triaxial and plane strain strength', ASTM, Special Technical Publication No.361.

Loach, S.C., (1985), Private Communication.

Luong, M.P., (1979), 'Les Phenomenes Cycliques dans les Sables', Journee de Rheologie: Cycles dans les Sols - Rupture - Instabilites. Publication No. 2 de l'Ecole Nationale des Travaux Publics de l'Etat, Vaulx-en-Velin, France, 1979.

Matsuoka, H., (1976), 'On the significance of the "Spatial Mobilized Plane". Soils and Foundations, Vol. 16.

Mindlin, R.D., (1949), 'Compliance of elastic bodies in contact', J. Appl. Mech., Vol.16.

Mindlin, R.D. and Deresiewicz, H., (1953), 'Elastic spheres in contact under varying oblique force', J. Appl. Mech., Vol.20.

Morgan, G.R., Cannon, I.D. and Coleman, G.C., (1984), 'Description and operation of the thermal storage system at solar one', Proc. ASME Solar Energy Div., 6th Annual Conf., Las Vegas, April 1984.

Marechal, J.C., (1972), Referenced in Neville (1981), below.

Mayhew, H.C., (1983), 'Resilient properties of unbound roadbase under repeated triaxial loading', TRRL Lab. Report 1088.

Meyers, S.L., (1940), Referenced in Neville (1981), below.

Neville, A.M., (1981), 'Properties of concrete - 3rd Edition', Pitman Publishing.

Neville, A.M., (1970), 'Creep of concrete: plain, reinforced and prestressed', North Holland Publishing Co., Amsterdam.

Newland, P.C. and Allely, B.H., (1957), 'Volume changes in drained triaxial tests on granular materials', Geotechnique Vol.17.

Oda, M., (1972), 'Initial fabrics and their relations to the mechanical properties of granular materials', Soils and Foundations, Jap. Soc. of Soil Mech. And Found. Eng., Vol.12.

Oda, M., (1972), 'The mechanism of fabric change during compressional deformation of sand', Soils and Foundations, Vol. 12.

Oda, M., (1972), 'Deformation mechanism of sand in triaxial compression tests', Soils and Foundations, Vol. 12.

Oda. M., (1974), 'A mechanical and statistical model of granular materials', Soils and Foundations, Jap. Soc. of Soil Mech. and Found. Eng., Vol.14.

Oda, M., (1977), 'Co-ordination number and its relation to shear strength of granular material', Soils and Foundations, Vol. 17.

Oda, M. and Konishi, J., (1974), 'Microscopic deformation mechanism of granular material in simple shear', Soils and Foundations, Vol. 14.

Pappin, J.W., (1979), 'Characteristics of a granular material for pavement analysis', Ph.D. Thesis, University of Nottingham.

Philleo, R., (1958), 'Some physical properties of concrete at high temperatures', O. American Conc. Inst., 54, pp.857-864.

Parkin, A.K., (1965), 'The application of discrete unit models to studies of shear strength of granular materials', Ph.D. Thesis, University of Melbourne, Australia.

Procter, D.C., (1974), 'An upperbound value for Φ_f in the stress-dilatency equation', Geotechnique Vol.24.

Procter, D.C. and Barton, R.R., (1974), 'Measurements of the angle of interparticle friction', Geotechnique Vol. 24, p 581.

Reades, D.W. and Green, G.E., (1976), 'Independent stress control and triaxial extension tests on sand', Geotechnique 36, No. 4, pp.551-576.

Reynolds, O., (1885), 'On the dilatency of media composed of rigid particles in contact', Phil. Mag. (Series 5), 20:469.

Robinson, R.G., (1974), 'Measurement of the elastic properties of granular materials using a resonance method', TRRL Supplementary Report 111 UC.

Roscoe, K.J., (1953), 'An apparatus for the application of simple shear to soil samples', Proc. 3rd int. Conf. on Soil Mech., Zurich, Vol.1.

Roscoe, K.H. and Schofield, A.N., (1963), Discussion on Rowe (1963) Journ. Soil Mech. and Found., ASCE, Vol.89.

Round, D.J., (1976), 'The solution of load/deformation behaviour of a discrete particle material by digital computer', Ph.D. Thesis, University of Nottingham.

Rowe, P.W., (1962), 'Stress-dilatency relation for static equilibrium of an assembly of particles ln contact', Proc. Roy. Soc. Series A, Vol.269.

Rowe, P.W., (1963), 'Stress-dilatency, earth pressures and slopes', Journ. Soil Mech. and Found., ASCE, Vol.89.

Rowe, P.W., (1964), Closing reply to discussion on Rowe (1963), Journ. Soil Mech. and Found., ASCE, Vol.90.

Rowe, P.W. and Barden, L., (1964), 'The importance of free-ends in triaxial testing', Journ. Soil Mech. and Found., ASCE, Vol.90.

Saada, A.S. and Townsend, F.H., (1981), 'Strength laboratory testing of soils - State of the Art', Proc. ASTM Symposium on Laboratory Shear Strength of Soil, Philadelphia STP 740.

Satake, M., (1982), 'On equivalent Mohr circle in granular materials', UNICIV Report No.R-205. The University of N.S.W., Australia.

Schofield, A.N. and Wroth, C.P., (1968), 'Critical state soil mechanics', McGraw-Hill, London.

Scott, G.D., (1960), 'Packing of spheres', Nature Vol.188.

Scott, R.F., (1964), Discussion of Rowe (1963), Journ. Soil Mech. and Found., ASCE, Vol.90.

Sharma, (1976), 'Ph.D. Thesis, University of London.

Shaw, P., (1980), 'Stress-strain relationships for granular materials under repeated loading', Ph.D. Thesis, University of Nottingham.

Shibuya, S., Hight, D.W. and Symes, M.J.P.R., (1984), 'Sand response to cyclic rotation of principal stress directions as induced by wave loads - discussion', Soils and Foundations, Jap. Soc. Soil Mech., Vol. 24, Sept. 1984.

Siebel and Pomp, (1927), Referenced in S.P. Timoshenko, 'History of the strength of materials', (1953), McGraw-Hill, p 362.

Skinner, A.E., (1969), 'A note on the influence of interparticle friction on the shearing strength of a random assembly of spherical particles', Geotechnique Vol. 19.

Smithells Metals Reference Book, 6th Edition by E.A. Brandes, Butterworths, London.

Sowers, G.B. and Sowers, B.F., (1951), 'Introductory Soil Mechanics and Foundations', Macmillan, New York.

Stroud, M.D., (1971), 'The behaviour of sand at low stress levels in the S.S.A.', Ph.D. Thesis, Cambridge University.

Symes, M.J.P.R., (1983), 'Rotation of principal stresses in sand', Ph.D./D.I.C. Thesis, University of London.

Symes, M.J. and Burland, J.B., (1984), 'Determination of load displacements on soil samples', ASTM Geotechnical Testing Journal, Vol. 7.

Symes, M.J.P.R., Gens, A. and Hight, D.W., (1984), 'Undrained anisotropy and principal stress rotation in saturated sand', Geotechnique 34, No. 1, pp.11-27.

Tatsuoka, F., (1972), 'Shear tests in a triaxial apparatus', Referenced in Nova, R., 'A constitutive model for soil under monotonic and cyclic loading', Soil Mechanics - Transient and Cyclic Loads Ed. Pande and Zienkiewicz, 1982, John Wiley & Sons.

Taylor, G.I. and Quinney, H., (1931), 'The plastic distortion of metals', Phil. Trans. Royal Soc. A230.

Terzaghi, K., (1920), 'Old earth-pressure theories and new test results', Engineering News Record, Vol.85.

Thom, N.H., (1985), Private Communication.

Tokue, T., (1979), 'A stress-dilatancy model of granular material under general stress condition', Soils and Foundations, Vol. 19.

Townley, C.H.A. and Darlaston, B.J.L., 'The CEGB research programme on thermal fatigue of structures - its background, present state and future development', Proc. Inst. Conf. on Thermal Stresses and Thermal Fatigue, Sept., 1969, Berkeley Castle, Gloucestershire.

Trollope, D.H., Lee, I.K. and Morris, (1962), 'Stress and deformation in two layer pavement structures under slow repeated loading', Proc. Australian Road Research Board, Vol.1.

Trollope, D.H. and Parkin, A.K., (1963), Discussion on Rowe (1963), Journ. Soil Mech. and Found., ASCE, Vol.89.

United Engineers and Constructors, (1982), 'Compressed - air energy storage design etc., EPRI EM-2351.

University of Newcastle-upon-Tyne, (1980), 'Thermal stressing of pebble bed heat stores', Dept. of Mechanical Engineering Design Unit, Report on Project DU 551.

Walton, K., (1978), 'The oblique compression of two elastic spheres', J. Mech. Phys. Solids, Vol.26.

Wood, D.M., (1982), 'Laboratory investigation of the behaviur of soils under cyclic loading: A review', Soil Mechanics - Transient and Cyclic Loads. Ed. Pande, G.N. and Zienkiewiez, O.C., Wiley, London.

Wood, D.M. and Budhu, M., (1980), 'The behaviour of Leighton Buzzard sand in cyclic simple shear tests', Proc. Int. Symp. on Soils Under Cyclic and Transient Loading, Swansea.

Wood, D.M., Drescher, A. and Budhu, M., (1980), 'On the determination of the stress-state in the simple shear apparatus', ASTM Geotechnical Testing Journal, Vol. 2.

Wong, R.K.S. and Arthur, J.R.F., (1985), 'Sand sheared by stress with cyclic variations in direction', as yet unpublished paper communicated to Prof. S.F. Brown.

Wroth, C.P., (1958), 'The shear behaviour of soils', Ph.D. Thesis, University of Cambridge.

Youd, T.L., (1972), 'Compaction of sands by repeated shear straining', Proc. ASCE, SM7 Vol. 98.

Zoldners, N.G., (1960), Referenced in Neville (1981), above.

Zytynski, M. and Randolph, M.F., Nova, R., and Wroth, C.P., (1978), 'On modelling the unloading - reloading behaviour of soils', Int. Journ. for Numerical and Analytical Methods in Geomechanics, Vol. 2.

APPENDIX A

RESULTS FROM THE LARGE TRIAXIAL APPARATUS

TEST B6-100-1

Stress Ratio	Axial Strain με	Radial Strain με	Shear Strain με	Volumetric Strain με
0·70	600	-85	457	430
0.82	1000	-432	955	136
0.90	1500	-272	1181	956
0·96	2000	-937	1959	122
1·01	2500	-1272	2514	-44
0·00	2000	-1000	2000	0
1·06	3080	-1604	3122	-128
1·10	4050	-2771	4547	-1492
1·135	5030	-3432	5641	-1834
0·62	4815	-3419	5489	-2023
0·00	4015	-2771	4524	-1527
1·143	5150	-3260	5606	-1370
1·19	6100	-4407	7004	-2714
1·20	7080	-5380	8306	-3680
1·20	8050	-6205	9502	-4360
1·22	9064	-7340	10935	-5616
1·22	10000	-8483	12321	-6966
0·84	10040	-8315	12235	-6590
0·62	9552	-7652	11468	-5752
0·00	7836	-5854	9132	-3892
1·12	9200	-6845	10696	-4490
1·24	11170	-8639	13205	-6100
1·27	13100	-10243	15560	-7386
1·29	15050	-12004	18034	-8958
0·84	14350	-11683	17687	-8516
0·61	11480	-11193	17114	-7906
0·00	12360	-8782	14093	-5204
1·22	14150	-10015	16108	-5880
1·31	16120	-12000	18745	-7880
1·33	18070	-14540	21738	-11010
1·32	20000	-17048	24696	-14096
1·17	20000	-17048	24696	-14096
1·01	20000	-17048	24696	-14096
0·83	20000	-16568	24376	-13136
0·61	20000	-15785	23854	-11570
0·34	18615	-14200	21874	-9785

TEST B9-100-1

Stress Ratio	*Axial Strain* με	*Radial Strain* με	*Shear Strain* με	*Volumetric Strain* με
0·00	*0*	*0*	*0*	*0*
0·85	*389*	*-184*	*382*	*21*
0·97	*780*	*-550*	*887*	*-320*
1·15	*1170*	*-730*	*1267*	*-290*
1·24	*1969*	*-1812*	*2519*	*-1657*
1·35	*3918*	*-4145*	*5375*	*-4372*
1·40	*5850*	*-6272*	*8081*	*-6694*
1·42	*7797*	*-8385*	*10787*	*-8973*
1·42	*9747*	*-9800*	*13030*	*-9853*
1·42	*11700*	*-11190*	*13258*	*-10680*
1·42	*13645*	*-12745*	*17590*	*-11841*
1·44	*15600*	*-14804*	*20267*	*-14008*
1·43	*17600*	*-17205*	*23201*	*-16810*

TEST B10-100-1

Stress Ratio	*Axial Strain* με	*Radial Strain* με	*Shear Strain* με	*Volumetric Strain* με
0·00	*0*	*0*	*0*	*0*
1·49	*507*	*-550*	*705*	*-593*
1·41	*994*	*-554*	*1032*	*-114*
1·47	*1500*	*-740*	*1493*	*20*
1·54	*2000*	*-926*	*1950*	*148*
1·56	*2500*	*-1296*	*2530*	*-92*
0·00	*1345*	*-367*	*1141*	*611*
1·42	*2020*	*-926*	*1964*	*168*
1·62	*3060*	*-1850*	*3273*	*-640*
1·64	*4110*	*-2586*	*4464*	*-1062*
1·68	*5000*	*-3132*	*5421*	*-1264*
0·00	*3411*	*-1293*	*3136*	*825*
1·46	*4152*	*-1289*	*3627*	*1574*
1·67	*5127*	*-2580*	*5137*	*-33*
1·708	*6180*	*-3501*	*6453*	*-822*
1.718	*7115*	*-4600*	*7809*	*-2085*
1·744	*8050*	*-5511*	*9040*	*-2972*
1·756	*9020*	*-6420*	*10292*	*-3820*
1·77	*10000*	*-7325*	*11549*	*-4650*
0·00	*6978*	*-3135*	*6741*	*708*
1·10	*7250*	*-3501*	*7167*	*248*
1·66	*9200*	*-5330*	*9686*	*-1460*
1·77	*11150*	*-6602*	*11833*	*-2054*
1·76	*13100*	*-8586*	*14456*	*-4072*
1·76	*15050*	*-10735*	*17188*	*-6420*
0·74	*13370*	*-8764*	*14755*	*-4158*
0·00	*10350*	*-6233*	*11054*	*-2116*
1·09	*11230*	*-6960*	*12125*	*-2690*
1·40	*12203*	*-7504*	*13137*	*-2805*
1·59	*13177*	*-8406*	*14387*	*-3635*
1·685	*14152*	*-9125*	*15516*	*-4098*
1·756	*16100*	*-11092*	*18126*	*-6084*
1·78	*18148*	*-12690*	*20557*	*-7232*
1·787	*20000*	*-14280*	*22851*	*-8560*
1·685	*20100*	*-14280*	*22918*	*-8460*
1·61	*20130*	*-14280*	*22938*	*-8430*
1·52	*20130*	*-13751*	*22585*	*-7372*
1·42	*20100*	*-13751*	*22565*	*-7402*
1·31	*20080*	*-13044*	*22080*	*-6008*
1·17	*19790*	*-12690*	*21651*	*-5590*
1·02	*19300*	*-12336*	*21089*	*-5372*
0·34	*18440*	*-11803*	*20160*	*-5166*
0·62	*17060*	*-10912*	*18646*	*-4764*
0·34	*15360*	*-10020*	*16918*	*-4680*
0·00	*13390*	*-8764*	*14768*	*-4138*

TEST C6-400-1

Stress Ratio	*Axial Strain* με	*Radial Strain* με	*Shear Strain* με	*Volumetric Strain* με
0·00	*0*	*0*	*0*	*0*
0·04	*19*	*6*	*9*	*31*
0·08	*45*	*25*	*13*	*95*
0·14	*82*	*-12*	*63*	*58*
0·17	*115*	*46*	*46*	*207*
0·21	*137*	*122*	*10*	*381*
0·31	*223*	*64*	*106*	*351*
0·39	*312*	*60*	*168*	*432*
0·48	*424*	*59*	*243*	*542*
0·55	*543*	*38*	*337*	*619*
0·61	*651*	*22*	*419*	*695*
0·67	*771*	*3*	*512*	*777*
0·74	*924*	*-75*	*666*	*774*
0·79	*1082*	*-227*	*873*	*628*
0·85	*1304*	*-227*	*1021*	*850*
0·90	*1511*	*-416*	*1285*	*679*
0·96	*1848*	*-548*	*1597*	*752*
1·00	*2165*	*-591*	*1837*	*983*
1·03	*2430*	*-813*	*2162*	*804*
1·06	*2808*	*-1002*	*2540*	*804*
1·09	*3432*	*-1247*	*3119*	*938*
1·13	*4204*	*-1842*	*4030*	*520*
1·15	*4958*	*-2328*	*4857*	*302*
1·17	*5730*	*-2851*	*5720*	*28*
1·19	*6411*	*-3450*	*6533*	*-369*
1·21	*7298*	*-4072*	*7579*	*-846*
1·22	*8018*	*-4536*	*8368*	*-1054*
1·24	*9000*	*-5220*	*9479*	*-1440*
1·24	*9635*	*-5793*	*10284*	*-1951*
1·25	*10367*	*-6545*	*11274*	*-2723*
1·26	*10883*	*-7005*	*11924*	*-3127*

TEST C9-133-1

Stress Ratio	*Axial Strain* με	*Radial Strain* με	*Shear Strain* με	*Volumetric Strain* με
0·00	*0*	*0*	*0*	*0*
0·114	*23*	*19*	*3*	*61*
0·207	*62*	*-73*	*90*	*-84*
0·32	*124*	*-73*	*131*	*-22*
0·41	*186*	*-128*	*209*	*-70*
0·55	*299*	*-202*	*334*	*-105*
0·67	*520*	*-202*	*481*	*116*
0·78	*813*	*-312*	*750*	*189*
0·87	*1243*	*-424*	*1111*	*395*
0·93	*1695*	*-609*	*1536*	*477*
0·98	*2390*	*-941*	*2220*	*508*
1·01	*2921*	*-1106*	*2684*	*709*
1·05	*3774*	*-1472*	*3497*	*830*
1·09	*4876*	*-2075*	*4634*	*726*
1·12	*5560*	*-2403*	*5308*	*754*
1·14	*6666*	*-3097*	*6508*	*472*
1·16	*7932*	*-3930*	*7907*	*72*
1·18	*8740*	*-4416*	*8770*	*-92*
1·20	*9328*	*-4968*	*9530*	*-608*
1·21	*9723*	*-5266*	*9992*	*-809*

TEST C6-133-1

Stress Ratio	*Axial Strain* με	*Radial Strain* με	*Shear Strain* με	*Volumetric Strain* με
0·00	*0*	*0*	*0*	*0*
0·073	*26*	*32*	*-4*	*90*
0·142	*67*	*-96*	*109*	*-125*
0·39	*204*	*66*	*92*	*336*
0·55	*375*	*66*	*206*	*507*
0·69	*589*	*-199*	*525*	*191*
0·83	*1083*	*-96*	*786*	*891*
0·93	*1907*	*-443*	*1567*	*1021*
1·02	*3375*	*-1504*	*3252*	*367*
1·12	*5595*	*-2016*	*5073*	*1563*
1·14	*6822*	*-2625*	*6297*	*1572*
1·165	*8260*	*-3503*	*7841*	*1254*
1·197	*9352*	*-4023*	*8916*	*1306*
0·989	*9330*	*-4023*	*8901*	*1284*
0·83	*9183*	*-3938*	*8746*	*1307*
0·68	*9031*	*-3848*	*8585*	*1335*
0·54	*8823*	*-3848*	*8446*	*1127*
0·40	*8576*	*-3588*	*8109*	*1400*
0·29	*8342*	*-3408*	*7833*	*1526*
0·14	*7904*	*-3062*	*7310*	*1780*
0·06	*7590*	*-3062*	*7101*	*1466*
0·22	*7581*	*-2881*	*6974*	*1819*
0·45	*7719*	*-2966*	*7123*	*1787*
0·68	*7937*	*-2966*	*7268*	*2005*
0·88	*8225*	*-3057*	*7521*	*2111*
1·02	*8530*	*-3142*	*7781*	*2246*
1·12	*8960*	*-3227*	*8124*	*2506*

TEST CM-133-1

Stress Ratio	*Axial Strain* με	*Radial Strain* με	*Shear Strain* με	*Volumetric Strain* με
0·00	*0*	*0*	*0*	*0*
0·07	*11*	*9*	*1*	*29*
0·21	*48*	*28*	*13*	*104*
0·342	*107*	*28*	*53*	*163*
0·46	*184*	*9*	*117*	*202*
0·53	*235*	*13*	*148*	*261*
0·64	*337*	*13*	*216*	*363*
0·75	*487*	*-124*	*403*	*239*
0·84	*644*	*-281*	*617*	*82*
0·90	*824*	*-366*	*793*	*92*
0·98	*1113*	*-451*	*1043*	*211*
1·04	*1457*	*-588*	*1363*	*281*
1·11	*2126*	*-945*	*2047*	*236*
1·14	*2635*	*-1280*	*2610*	*75*
1·17	*3142*	*-1585*	*3151*	*-28*
1·20	*3800*	*-2129*	*3952*	*-458*
1·22	*4593*	*-2697*	*4860*	*-801*
1·24	*5376*	*-3262*	*5758*	*-1148*
1·25	*6075*	*-3870*	*6629*	*-1665*
1·27	*6833*	*-4389*	*7481*	*-1945*
1·28	*7552*	*-4963*	*8343*	*-2376*
1·30	*8335*	*-5661*	*9330*	*-2987*
1·31	*8938*	*-6130*	*10044*	*-3322*
1·33	*10531*	*-7498*	*12018*	*-4465*

APPENDIX B

RESILIENT TEST RESULTS

SAMPLE D1

pm kPa	pr kPa	qm kPa	qr kPa	Es με	Er με
340	20	120	60	55	40
340	40	120	120	125	100
340	60	120	180	209	170
340	80	120	240	303	247
640	20	120	60	27	16
640	40	120	120	75	65
640	60	120	180	121	110
640	80	120	240	173	161
680	40	240	120	73	62
680	80	240	240	165	154
680	120	240	360	273	256
680	160	240	480	379	340

SAMPLE D2

pm kPa	pr kPa	qm kPa	qr kPa	Es με	Er με
100	20	50	60	175	86
100	40	50	120	340	123
200	20	100	60	109	140
200	40	100	120	251	140
200	60	100	180	390	192
300	20	150	60	80	43
300	40	150	120	167	113
300	60	150	180	277	175
300	80	150	240	391	221
300	100	150	300	534	267

SAMPLE D3

pm kPa	pr kPa	qm kPa	qr kPa	Es με	Er με
110	20	30	60	206	89
120	40	60	120	420	151
320	40	60	120	147	108
340	80	120	240	321	214
360	120	180	360	523	298

SAMPLE D4

pm	pr	qm	qr	Es	Er
117	33	50	100	302	46
217	33	50	100	154	83
317	33	50	100	110	67
417	33	50	100	92	63
233	67	100	200	341	120
333	67	100	200	224	138
433	67	100	200	197	125
533	67	100	200	169	116
367	133	200	400	554	125
467	133	200	400	437	188
567	133	200	400	374	208
667	133	200	400	325	208
183	33	-50	100	322	204
283	33	-50	100	172	108
383	33	-50	100	122	88
483	33	-50	100	97	70
367	67	-100	200	363	262
567	67	-100	200	211	163
200	200	0	0	8	729
200	200	100	0	86	758
350	300	0	0	10	833
350	300	100	0	52	800
350	300	200	0	83	813
350	300	300	0	132	894
350	300	400	0	222	980
350	300	-100	0	145	916
200	33	0	100	222	124
200	50	0	150	388	208
400	67	0	200	257	156
400	100	0	300	465	250

SAMPLE MD1

pm kPa	pr kPa	qm kPa	pr kPa	Es με	Er με
267	200	-100	0	125	860
300	200	0	0	20	740
333	200	100	0	-20	720
367	200	200	0	-80	710
400	200	300	0	-87	720
433	200	400	0	-113	730
117	33	50	100	360	125
233	67	100	200	387	200
217	33	50	100	193	120
367	133	200	400	567	290
333	67	100	200	307	190
317	33	50	100	135	105
417	33	50	100	105	88
433	67	100	200	213	170
467	133	200	400	447	310
183	33	-50	100	320	260
283	33	-50	100	190	163
367	67	-100	200	380	330
383	33	-50	100	143	130

SAMPLE MD2

pm kPa	pr kPa	qm kPa	pr kPa	Es με	Er με
267	200	-100	0	83	720
300	200	0	0	10	630
117	33	50	100	273	130
217	33	50	100	153	110
233	67	100	200	293	210
317	33	50	100	108	93
333	67	100	200	233	190
367	133	200	400	495	350
417	33	50	100	90	52
433	67	100	200	187	150
467	133	200	400	405	330
183	33	-50	100	247	200
283	33	-50	100	153	140
383	33	-50	100	118	112
367	67	-100	200	300	280

APPENDIX C

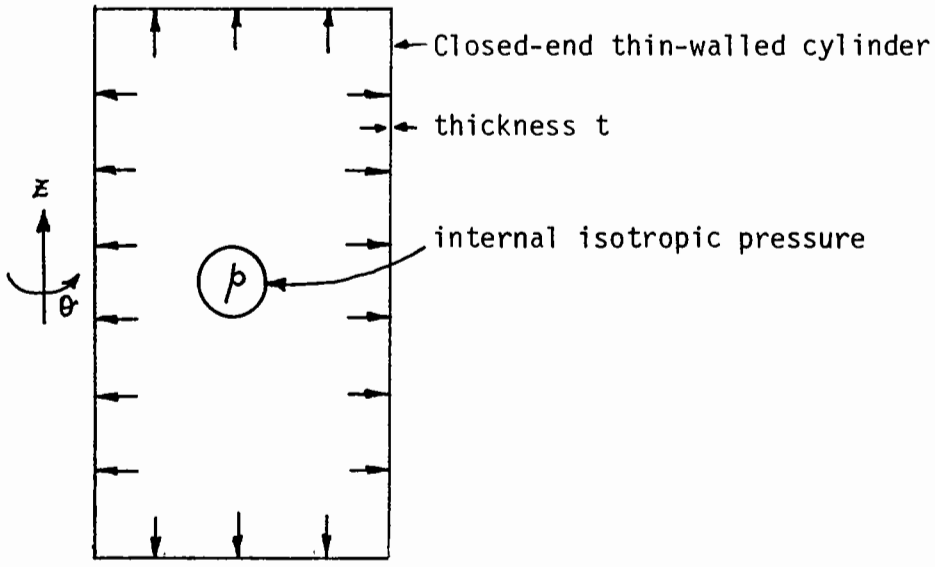

$$\sigma_\Theta = pr/t$$

$$\sigma_z = p.\pi r^2/2\ \pi rt$$

$$= \sigma_\Theta/2$$

APPENDIX D

THE SMALL HOLLOW CYLINDER APPARATUS

D.1 Introduction

The design, construction and commissioning of a large and complex piece of apparatus takes a considerable length of time, particularly when, as with the HCA described in Chapter 8, many of the principles of operation are novel. It was known from the start that there was a risk of over-running the scheduled completion date and that this might lead to a lack of time for testing. This was not thought, however, to be sufficient reason for not proceeding with development. In order to carry out at least some principal rotation testing within the project period as well as establish problem areas with this type of equipment, it was decided to build a small HCA apparatus.

Unfortunately, as will become clear, the results obtained are of little or no value. But, it must be emphasised, at the same time, that the experience gained in attempting to operate the small HCA has been of use in developing the large HCA. Furthermore, the small HCA project has highlighted certain paths which future development might take.

D.2 Description and Operation

(a) The Sample

The test sample has an external diameter of 76mm, an internal diameter of 38mm, and a height of 127mm. The internal membrane (made at the University) is closed at the lower end, and fixed to the top platen as shown in Fig. D.1. The outer membrane is of standard size and attaches in the normal way. The external mould is an aluminium three-piece split-mould. The internal mould is made from papier-mache, the advantage of which is that, when the sample has been formed and a vacuum established

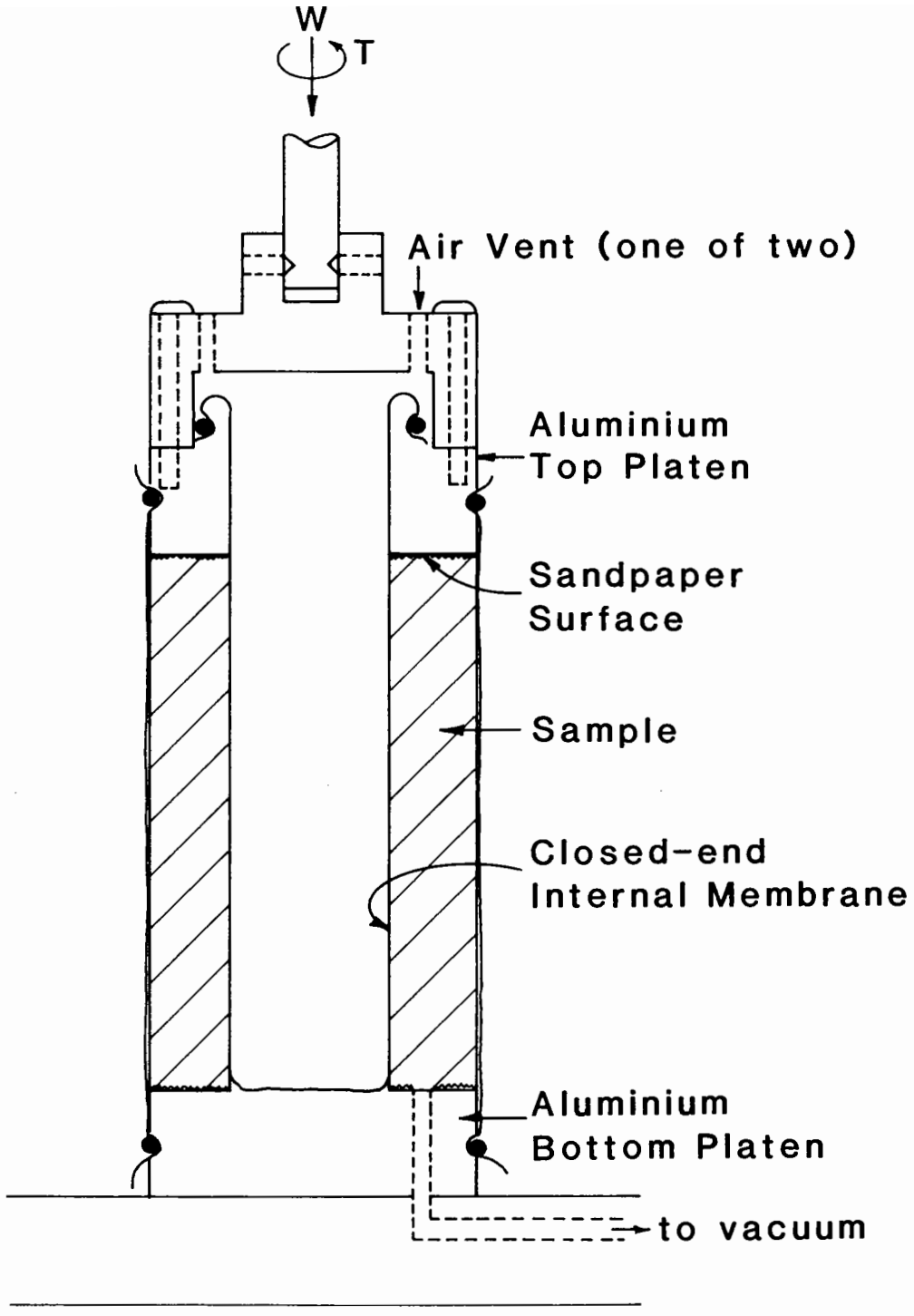

Fig. D.1. SMALL HOLLOW CYLINDER APPARATUS SAMPLE

within the pore space to enable the sample to stand unsupported the internal mould can be collapsed and extracted simply by adding water. This avoids the necessity for a complicated collapsable mould such as the one developed for the large HCA.

Loads are transmitted to the sample by two aluminium platens and sandpaper glued onto the platen surfaces provides the key to enable shear stress to be transmitted to the sample.

(b) Loading System

Three sources of load were available; atmospheric pressure, axial load, and torque. The atmospheric pressure was mobilised (as in the case of the large HCA) by evacuating the sample pore space. Axial and torque loads were applied by air-operated "bellophram" actuators. The loading system is shown in Fig. D.2. As can be seen, the axial ram bears directly down onto the sample whereas the torque ram operates through a system of pulleys and levers.

(c) Instrumentation

Loads (axial and torque) were measured using load cells positioned as shown in Fig. D.2. The axial load was measured directly. The torque load was measured indirectly as an axial load output from the bellophram which was calibrated to give the torsional stress being applied.

Axial and shear strains were measured optically. Targets were attached on each side of the sample in the positions shown in Fig. D.2. The horizontal and vertical movements of one target relative to the other indicated the axial and the shear strain, $Y_{\theta z}$. The resolution of this system was of the order of 5μm or 50$\mu\epsilon$. Unfortunately, no measurements of deformation in the radial direction were taken. To have done so would have been to greatly increase the development required.

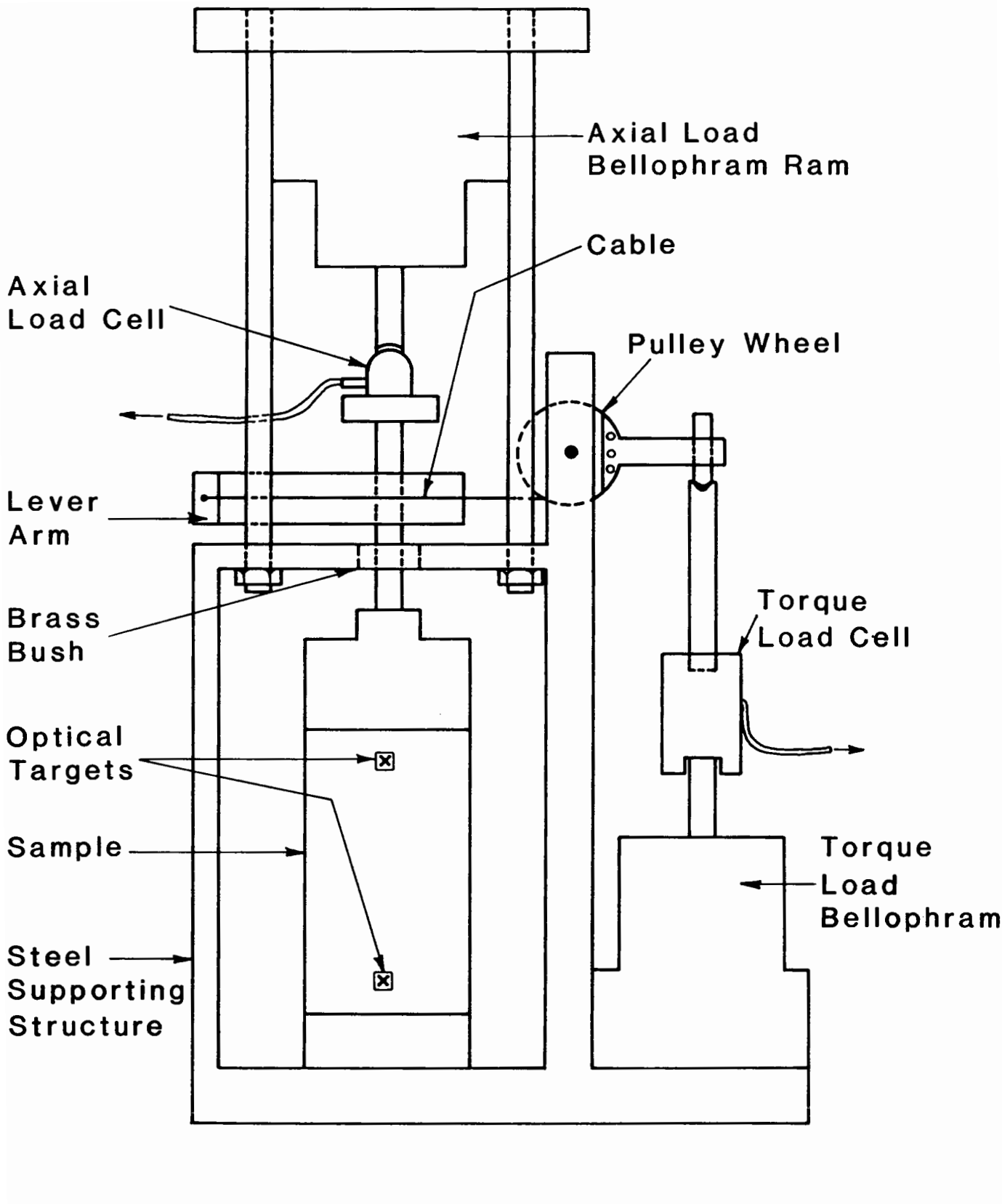

Fig. D.2. SMALL HOLLOW CYLINDER APPERATUS

D.3 Testing

(a) Stress Regimes

A range of stress paths were used during testing. A sample of five tests which are representative of the complete range of tests carried out are described in Fig. D.3. In tests 1 and 2, the initial stress state was isotropic, and only torque loads were applied ($\tau_{\theta z}$ = 20 and 40 kPa). Tests 3 and 4 were simply repeats of tests 1 and 2, but with a constant axial stress of 50 kPa (i.e. 150 kPa total) applied by the axial ram. Test 5 was, again, a repeat of test 2 but with an extra axial stress of 100 kPa applied.

Unfortunately, the apparatus could not be used for tests in which the axial and torque stresses were cycled simultaneously. The reason for this was that the pneumatic system could not cope with the discharge of air from both bellophrams simultaneously.

For these tests, the value of b (= $(\sigma_2 - \sigma_3)/(\sigma_1 - \sigma_3)$ was not held constant. The tests, therefore, involved changing two independent variables (b and α) and it was not possible to determine which effects were due to which variable (see e.g. Shibuya, Hight and Symes, 1984).

(b) Processing Strain Data

The only strain data to be collected during testing were the axial and torque deformations. A small programme was written to analyse this data into values of major and minor principal strain. It was assumed that these were in the same plane as the major and minor principal stresses, (i.e. the circumferential "plane").

It was assumed that the mean circumferential dimension of the sample was constant during testing. This is a valid assumption in a sample which is unaffected by end-restraint providing that the internal and external

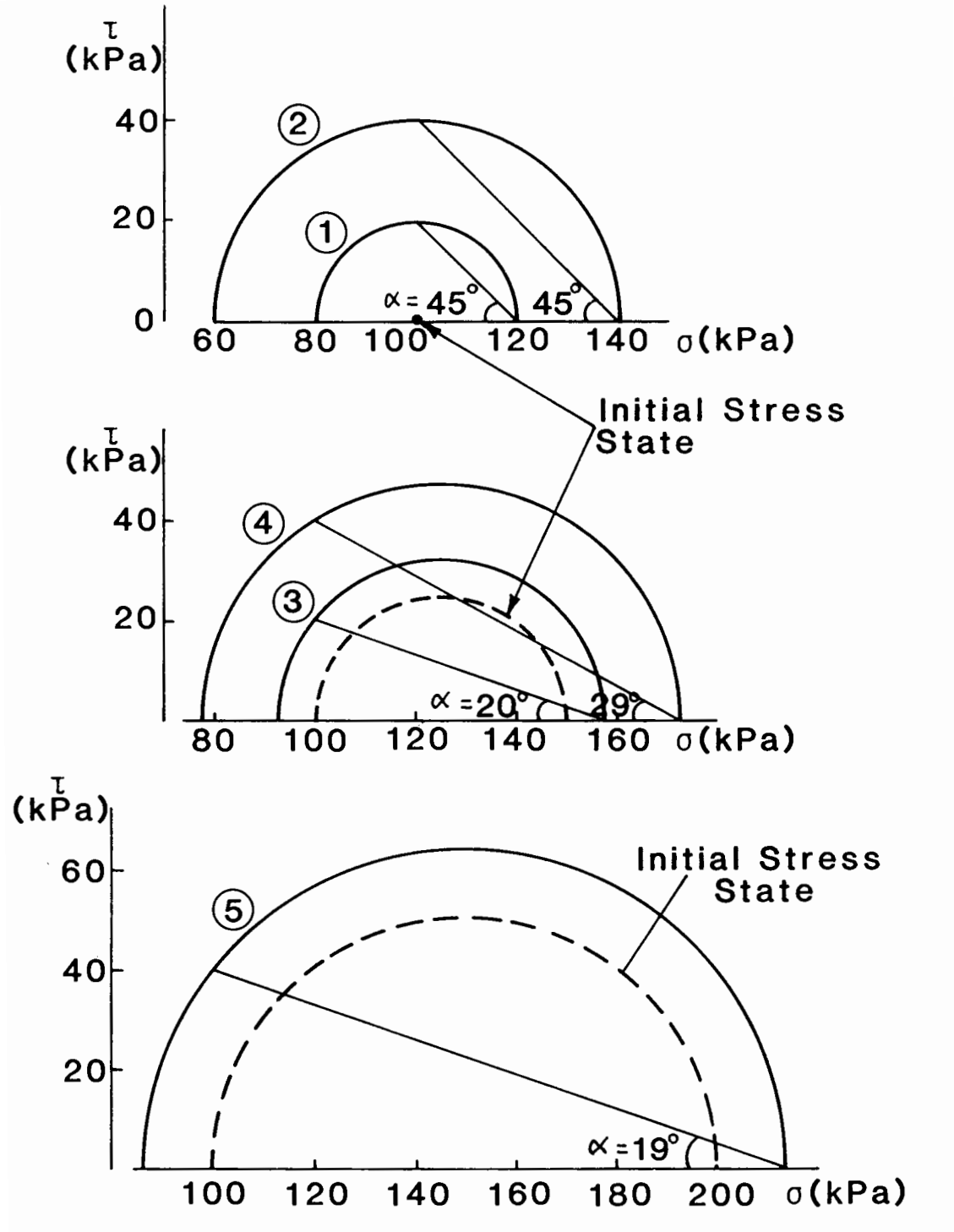

Fig. D.3. INITIAL AND FINAL STRESS STATES FOR 5 TESTS

cell pressures are constant. As the deformation measurements were made away from the sample ends, this assumption was considered reasonable.

As mentioned above, no data was gathered from which the intermediate principal strain could be calculated. It was considered initially that it might be possible to make use of the elasticity equation:

$$\begin{bmatrix} \epsilon_1 \\ \epsilon_2 \\ \epsilon_3 \end{bmatrix} = \frac{1}{E} \begin{bmatrix} 1 & -\nu & -\nu \\ -\nu & 1 & -\nu \\ -\nu & -\nu & 1 \end{bmatrix} \begin{bmatrix} \sigma_1 \\ \sigma_2 \\ \sigma_3 \end{bmatrix}$$

and to solve for ν_{13} using:

$$E.\delta\epsilon_1 = \delta\sigma_1 - \nu.\delta\sigma_3$$

$$E.\delta\epsilon_3 = \delta\sigma_3 - \nu.\delta\sigma_1$$

and then to make the assumption $\nu_{12} = \nu_{13}$. This method failed to provide a value for ν_{13}, firstly, because $\delta\sigma_1$ was equal to $(-\delta\sigma_3)$ in every case, thus producing only one equation with two unknowns; and, secondly, because in general, $\delta\epsilon_1$ was not equal to $-\delta\epsilon_3$ although $\delta\sigma_1 = -\delta\sigma_3$. This implies that either stiffness or poisson's ratio (or both) must be variable in order to solve the simultaneous equations. This being the case, the set of solutions is infinite.

In order to use the data, some other way of calculating ϵ_2 had to be developed. It was eventually decided to calculate ϵ_2 using a method based on the average b value during the test. If b = 0, then generally $\epsilon_2 = \epsilon_3$ (e.g. triaxial compression test). If b = 1, then $\epsilon_2 = \epsilon_1$ (e.g. triaxial extension test). If b $\simeq$ 0.3, then $\epsilon_2 = 0$ (e.g. plane-strain test, Wong and Arthur 1985). A smooth curve was drawn through the points (0, ϵ_3), (0.3, 0), and (1, ϵ_1) on a graph of strain against b value. ϵ_2 was then read off as being that strain value corresponding to the average b value during

the test. It was, therefore, possible to obtain an estimate for ϵ_2. This method is shown in Fig. D.4 for a test in which the average b value is 0.15.

(c) Results

Table D.1 gives details of Tests 1 to 5 together with the estimated values of ϵ_2 and the calculated shear and volumetric strains.

The shear strains might be expected to correspond, at least roughly, to the predictions of the model:

$$\epsilon_s = A \cdot \Delta\eta, \qquad \text{where A is a constant}$$

The values of A calculated for Tests 1 to 5 are shown in Table D.2.

Test	Value of A
1	190
2	520
3	340
4	745
5	1225

TABLE D.2 CALCULATED VALUES OF A

The inconsistency in the value of A observed in Table D.2 is too great to be due solely to the inability to measure the value of ϵ_2 (which, as long as it lies between ϵ_1 and ϵ_3, cannot affect the calculated value of shear strain by more than about 15%).

It is possible that stress rotation is partly responsible for the large range of values of A. The graph of the change in principal stress direction, $\Delta\alpha$. vs. A, however, shows no coherent pattern (Fig. D.5(a)). The graph of maximum value of η vs A does, on the other hand, show a good correlation (Fig. D.5(b)). It seems likely, therefore, that the inaccuracy

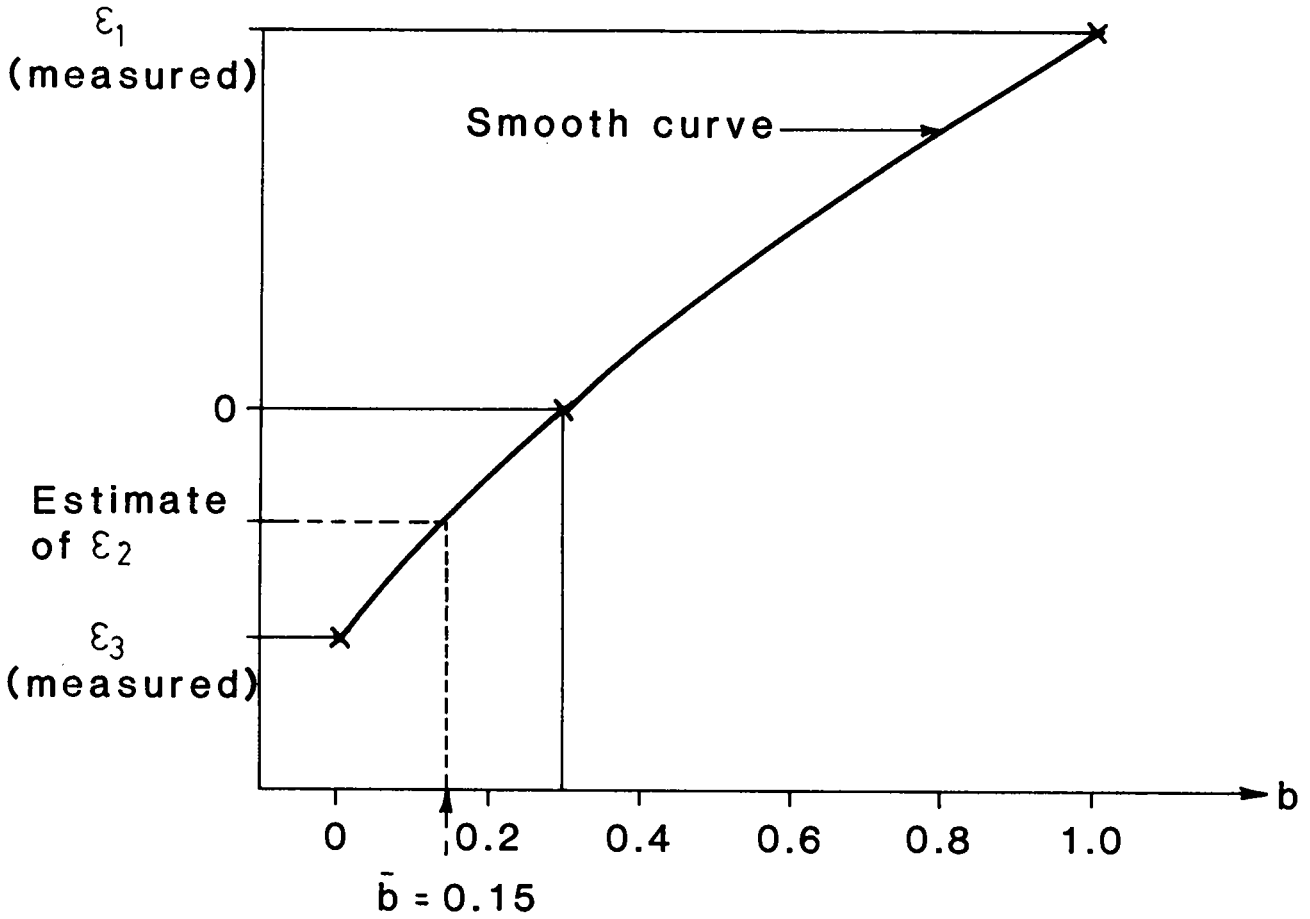

Fig. D.4. METHOD OF ESTIMATING THE VALUE OF THE INTERMEDIATE PRINCIPAL STRAIN

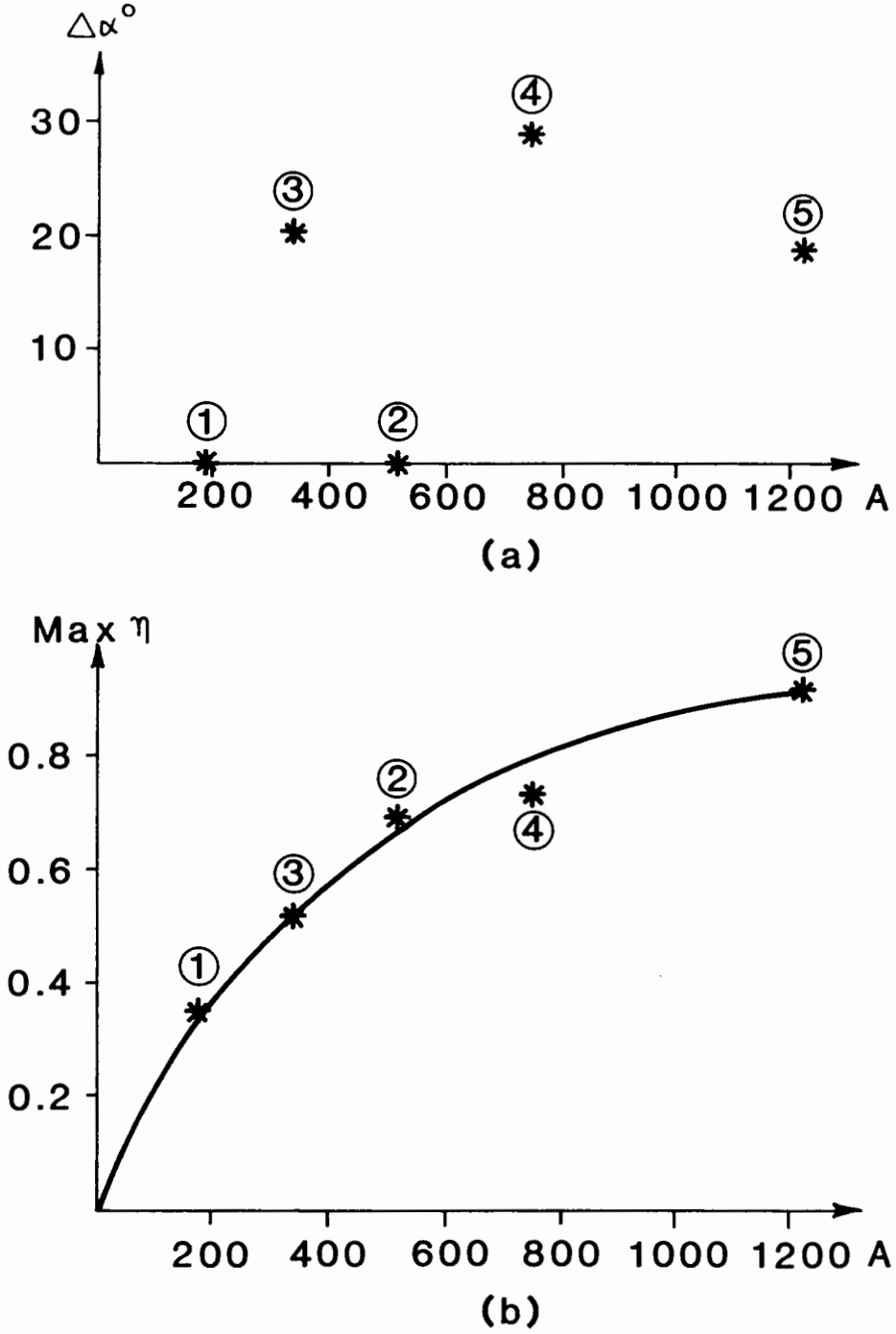

Fig. D.5. THE CORRELATION BETWEEN SHEAR STIFFNESS PARAMETERS A AND
(a) STRESS ROTATION AMPLITUDE
(b) MAXIMUM STRESS RATIO DURING STRESS PATH

Table D.1 Data from Five Representative Tests carried out in the Small Hollow Cylinder Apparatus

Test	η_1	η_2	$\Delta\eta$	$\Delta\alpha$	$\bar{b}$	ε_1	ε_2	ε_3	ε_s	ε_v
1	0	0.35	0.35	0	0.5	55	30	-55	66	30
2	0	0.69	0.69	0	0.5	260	115	-340	360	35
3	0.42	0.52	0.10	20°	0.05	27	20	-27	34	20
4	0.42	0.73	0.31	29°	0.12	170	-105	-220	231	-155
5	0.75	0.91	0.16	19°	0.05	140	-120	-180	196	-160

may be due to errors in the experimental technique (e.g. a reduction in the level of friction in the bearing as the torque load becomes greater) and in the assumptions used in stress calculations (e.g. the assumption of a linear stress distribution across the sample wall).

The assumption of a linear stress distribution is reasonable when the wall is thin compared with the sample diameter but, in the present case, the deviation from the assumed distribution is large. Material non-linearity will lead to a reduction in the radius of torsional resistance. Higher strains will, therefore, need to be mobilised in order to maintain equilibrium. As the total torsional resistance required increases in magnitude, this affect increases also. This explains, at least partly, the behaviour observed in Fig. D.5(b).

D.4 Conclusions

A small HCA was constructed and used for testing . A method for estimating the values of radial strain was developed and applied.

The results from testing appear to depend more upon the maximum value of η reached during any stress path than upon either the change in shear stress ratio $\Delta\eta$ (which is the result predicted by triaxial testing) or the magnitude of principal stress rotation $\Delta\alpha$, (which was the effect it was hoped to measure). A possible explanation is given for this.

The conclusion, therefore, is that these results have not added to the understanding of granular materials during principal stress rotation.

APPENDIX E

Errors in Radial Strain Measurements due to Sample Imperfection

The H.C.A. sample will deviate slightly from the ideal hollow cylindrical form. This deviation may be characterised by the angles θ_1 and θ_2 shown below in Fig. D.1.

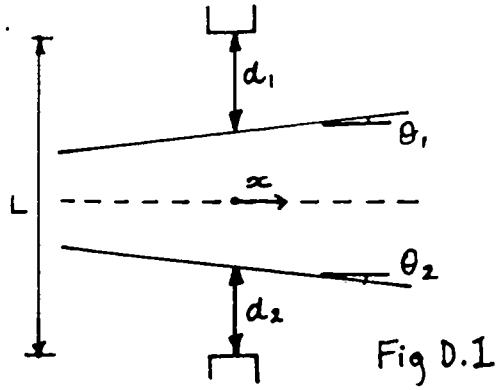

Fig D.1

The measured thickness t is given by:

$$t = L - (d_1 + d_2)$$

If the sample section translates a distance x (as shown in Fig. D.1) due to torsion stresses, then the change in measured thickness, Δt, is given by:

$$\Delta t = -(\Delta d_1 + \Delta d_2)$$
$$= \delta - (x \sin \theta_1 + x \sin \theta_2)$$

where, δ is the actual differential radial deformation due to the applied stresses

Two components may contribute to translation, x, at the section in question.

1. torsion shear in the sample

2. slip at interfaces and torsional compliance of test equipment

A typical expected deformation is shown below in Fig. D.2.

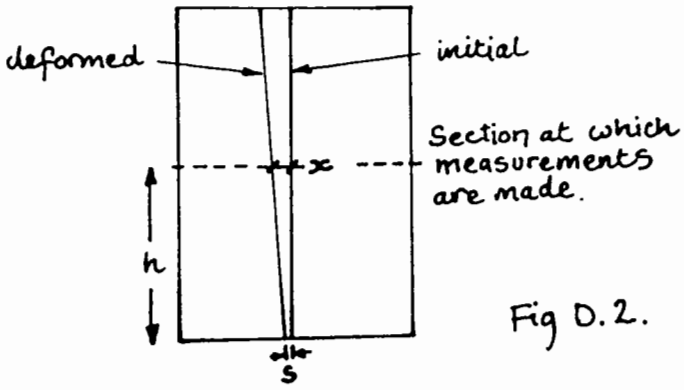

Fig D.2.

If the torsion shear strain in the sample is φ and the total slip and equipment deformation is s, then the tangential translation of the measured element is given by:

$$x = h.\varphi + s$$

If, say, $\theta_1 = \theta_2 = 1°$ and $\varphi = 500\mu\epsilon$, h = 250mm, and substituting eqn. (3) into eqn. (2),

$$\Delta t = \delta - 2(h.\varphi + s) \sin \theta$$

$$= \delta - 2(250 \times 500 \times 10^{-6} + s) \sin 1°$$

$$= \delta - (4.4\mu\epsilon + 3.5 \times 10^{-2}\ s)$$

As the sample thickness t is 28mm, then the error term due to torsion shear strain is given by:

$$\frac{4.4 \times 10^{-6}}{28 \times 10^{-3}} = 160\mu\epsilon$$

The error term due to slip and equipment compliance is given by 3.5×10^{-2} s. If s is (say) 0.25mm, then the error term to this source is given by:

$$\frac{3.5 \times 10^{-2} \times 0.25 \times 10^{-3}}{28 \times 10^{-3}} = 312\mu\epsilon$$

Thus, using these hypothetical (although it is submitted that they are realistic) figures, we arrive at an equation:

$$\Delta t = \delta - 472\mu\epsilon$$

As δ might be expected to have a value somewhat less than the torsion strain, it is clearly seen that the error term has assumed an over-riding significance in the measured value.